THE STRENGTHENING AND "SOFTENING" OF LOW-CARBON STRUCTURAL STEELS BY SILICON

by

Chinasa Chukwuemeka Anya MSc

A thesis submitted to the University of Strathclyde in fulfilment of the requirements for the award of the degree of Doctor of Philosophy

Division of Metallurgy & Engineering
Materials (Department of Mechanical
& Process Engineering)
University of Strathclyde

October 1989

CONTENTS

ACKNOWLEDGEMENTS

I wish to thank Dr. T. N. Baker, the chairman of the Div. of Metallurgy & Engrg. Materials, University of Strathclyde, for making facilities available for conducting this research project, and also for the support and advice he readily availed to me, as my supervisor, during this period. My special thanks go to Professor Alan Hendry, of the same address, for helpful discussions on the thermodynamics of silicon-interstitial compound formation.

I also wish to thank Dr. W. B. Morrison of Swinden Laboratories, British Steel plc, Rotherham, for gifting the steel plates used for this study, his personal interest in the work and for helpful discussions. My thanks are due to Professors N. J. Petch (retired) and R. W. Armstrong of University of Maryland, U. S. A., for very useful discussions. Iam very grateful to Dr. H. S. Ubhi, now at University of Nairobi, Kenya, for his practical help in electron microscopy and useful discussions.

I am grateful to the technical staff of the Metallurgy & Engrg. Materials Div., University of Strathclyde, for maintaining the equipment and instruments in a good working condition throughout the duration of the project.

I wish to acknowledge the Association of Commonwealth Universities in London for financial support.

Finally, many thanks go to my sons, Chima, Ikechi and of course to my lovely wife, Mariana, for their daily patience, waiting for me to come back,often very late, from the laboratories throughout the duration of this project.

ABSTRACT

The variation of tensile properties and grain sizes, on adding silicon, up to 1.03 wt% in five grades of low carbon structural steel was studied. The reduced sensitivity of the lower yield stress, σ_y, at sub-zero test temperatures, otherwise called "softening", of these steels with reduced grain sizes, brought about by the silicon additions was also investigated.

Optical and transmission electron microscopes were used to characterize the ferrite-pearlite structures, decarburized layers, random interlamellar spacings in the pearlite constituent, slip line, twin and dislocation structures. The precipitates observed were studied qualitatively with the transmission electron microscope, and microanalysis was carried out by using the dispersed energy of the X-rays (EDAX). Dilatometric studies were done to establish the critical temperatures of the steel grades. Uniaxial tensile tests were carried out at between 77 and 350 K, with strain rates of 1.7×10^{-4}, 3.3×10^{-4} and 0.33 s^{-1}. The data from these tests were analyzed in terms of the contribution silicon and nitrogen make to the tensile properties, and were used to determine the thermal activation parameters, hence "softening".

It was found that silicon additions beyond 0.31 wt% in these steels inhibit grain growth, due to the effect of silicon on the grain nucleation kinetics. In conformity to previous reports, the Hall-Petch slope, K_y was reduced

to a limit, on the initial additions of silicon, but further to this observation, it was found that low silicon steels, below 14 μm possess higher strength than high silicon steels, within 0.31 to 0.78 wt% Si. In contrast with previous reports, in which SiN precipitates were identified in similar steel grades, under aged conditions, low temperature (∝) Si_3N_4 precipitates were observed in both the annealed and the aged samples of the steels in the present study. It was also found that reduced grain sizes increase the "softening" tendency of these steels.

These results were correlated with those from limited reports found in the literature, regarding the effect of silicon (above 0.7 wt%) on the impact behaviour of these grades of steel. From the correlation, it is suggested that a new theory should be sought to explain how the initial additions of silicon, with reduced grain sizes, improve the impact behaviour. Hypotheses are advanced linking the improvement of impact behaviour with the "softening" phenomenon. It is also suggested that a higher silicon to manganese ratio, with silicon not exceeding 1 wt%, may improve not only the strength and the impact behaviour, but also the cost indices of these grades of steel.

INTRODUCTION

The role of silicon in steels has been controversial for as long as a century now. Thus, its content in structural steels used to be limited to about 0.3 wt%. From about two decades ago, it was increased to 0.5 wt%. The wariness has been due to the well established solid solution strengthening capacity of silicon, which, it is believed could provoke an embrittling effect at higher silicon levels. Again, the effect of silicon on the grain size is much less known; infact, previous reports have indicated that silicon additions have no effect on grain size, or even lead to coarser ferrite grains. However, some reports have also shown a possible ease of deformation of low carbon steels, with silicon content greater than 0.5 wt% , through the reduction of the value of the Hall-Petch slope, K_y, of this grade of steels, up to 0.7 wt% Si.

It is well known that silicon additions reduce the sensitivity of the lower yield stress to sub-zero test temperatures; i.e. these additions promote "softening". Some work has also shown that the initial additions of silicon in low carbon steels, with small grain sizes, favour lower values of the impact transition temperature, T_c. Nonetheless, there is no work linking the impact behaviour with the "softening" phenomenon. A review of the literature, on the effect of grain size on "softening" does not give a clear picture of the situation. It was rather suggested by some authors that the effective stress (the

component of the lower yield stress, principally responsible for the "softening" phenomenon) is independent of grain size.

Explanations of the reduction of K_v and the increased tendency to "softening" of these steels, for low levels of silicon, are mostly based on the pile-up and ledge theories for the former, and silicon-interstitial interaction for the latter. Nevertheless, pile-ups and ledges are rarely found in alpha-iron, and some reports have shown that the experimental results of "softening" are not entirely compatible with the silicon-interstitial interaction model. Similarly, silicon-carbon interaction, which has been used by some authors to explain the improvement of the impact behaviour by silicon additions, has been found unsatisfactory.

Therefore, this work studies the effect of silicon on the grain size and the tensile properties, with a view to resolving some of the aforementioned controversies. By equating the "softening" phenomenon with the impact behaviour, both being governed by the same thermal activation processes, the work suggests a link between the two phenomena.

CHAPTER ONE

THE SOLID SOLUTION STRENGTHENING OF STEELS

There are various ways[1] of strengthening iron and its alloys; some of which are:

a) solid solution strengthening by substitutional and interstitial atoms.

b) precipitation and dispersion strengthening: nitrides, carbides or intermetallic compounds could be precipitated in steels. Depending on the shapes and the dispersion of such precipitates in the matrix, strengthening could be achieved.

c) refinement of grain sizes.

d) work-hardening: consequent upon deformation, dislocations interact with themselves or other obstacles.

The "a" and "c" points are of interest in this work.

The solid solution strengthening of iron and steels could be interstitially[2] or substitutionally[3] achieved.

1.1 Underlying Causes of Solid Solution Strengthening of Steels.

For the substitutional solid solution, the essential[4] factor is the size misfit parameter, ξ_s given as:

$$\xi_s=(1/a_o)(da/dc) \quad \ldots\ldots\ldots\ldots\ldots\ldots\ldots\ldots\ldots\ldots (1.1)$$

where a_o is the lattice parameter of pure iron [illegible] and c is the concentration of the substitutional solute atoms.Zwell et al[5] found that for silicon ,this leads to a compression of the iron lattice parameter by 0.0003 Å per one atom per cent silicon(in a dilute solution of $\leq$ 3 at% solute). This is,because whereas the atomic radius[4] of silicon is 1.18 Å,that of iron is 1.23 Å.It is this compressional tendency of the iron lattice,which is believed[4] strengthens the steel.

In the case of interstitial solid solutions where the interstitial atoms are far smaller[1] than the alpha-iron atom(eg: C=0.77 Å and N=0.72 Å), the strengthening could be due to dynamic processes such as:

i) short-range,stress-induced migration of the interstitial atoms: this short-range migration leads to an internal friction in the alloy lattice,

ii) Cottrell atmospheres[2]: here the interstitial atoms concentrate randomly (Fig.1.1a) or in a condensed form(Fig.1.1b) in the immediate neighbourhood of the dislocations. The interstitials concentrate around the dislocations because by so doing, a minimum energy state of the interstitial-dislocation system is achieved.This concentration of the interstitial atoms around the dislocations invariably locks the latter,thereby increasing the stress required for dislocation movement,

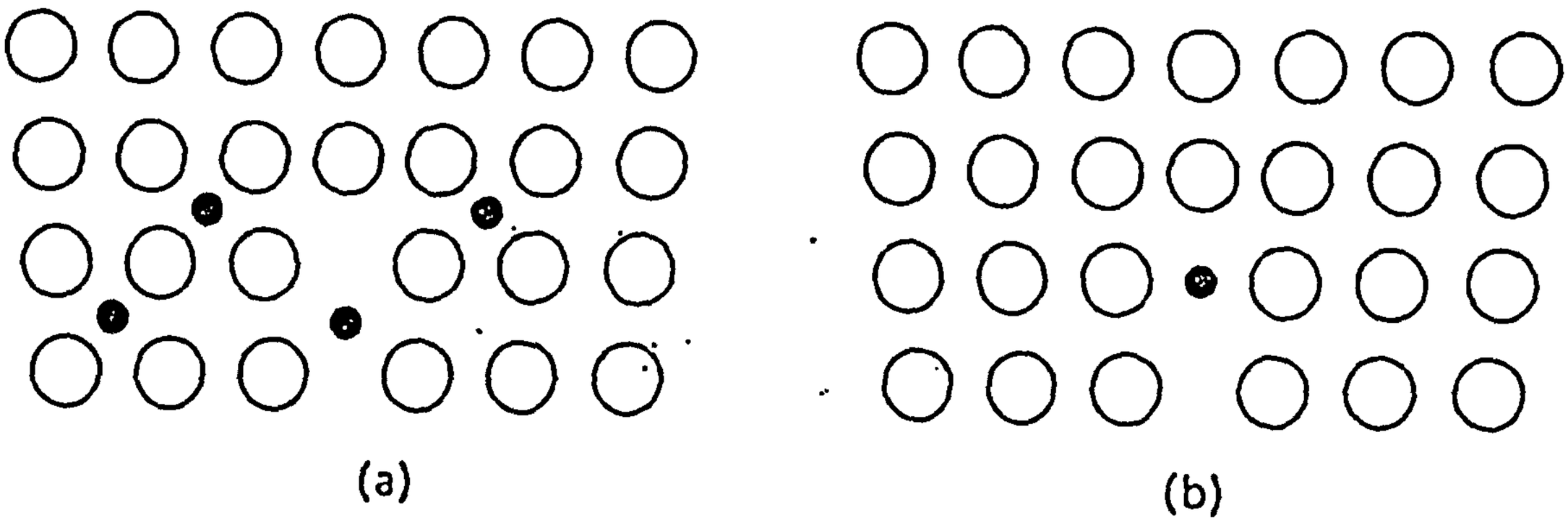

Fig 1.1: Interstitial atoms in the immediate neighbourhood of an edge dislocation: a), random atmosphere; b), condensed atmosphere,(Ref 1).

iii) pinning[8] of the dislocations by these interstitial atoms: whereas the first two(i and ii) are of a dynamic nature,the pinning is of a static nature.

There are other indirect ways through which the substitutional and interstitial atoms could affect the strength of the steels.As an example, the addition of a substitutional element could push up the transformation temperature of the steel. This in turn could lead to an inhibition of grain growth. The substitutional atoms could at the same time precipitate out the interstitial atoms, which, depending on the volume fraction,distribution and form of the precipitates,could affect the strength.These indirect ways are reviewed in subsequent sections.

1.2 Concepts of Grain Boundary Strength: Strengthening by Grain Refining

The grain boundaries are a misfit to the rest of the grain structure and therefore present a departure[9] from the single crystal. Owing to a higher dislocation density at the grain boundaries[10], the atoms associated with the grain boundary have a greater total energy than the grain interior.

It has been demonstrated[11] that grain boundaries can pose obstacles to deformation processes in polycrystalline materials.Grain boundaries, as obstacles dislocations build up forming pile-ups at them,Fig.1.2. If the deformation is to continue,additional external stress

would be required to overcome this barrier.

The role of this high energy/barrier region plays very much determines the strength of polycrystalline materials and as such,has attracted different theories.

1.2.1 Pile-up Theory

Hall[12] and Petch[13] measured at ambient and liquid nitrogen temperatures,respectively the values of lower yield stress(σ_y) for alpha-iron polycrystals with different grain sizes and thence formulated the well established Hall-Petch relationship:

$$\sigma_y = \sigma_o + K_y d^{-1/2} \quad \ldots\ldots\ldots\ldots\ldots\ldots\ldots\ldots (1.2)$$

where σ_o refers to the frictional stress within the grain,d is the average grain size and K_y is the Hall-Petch slope, otherwise known as the intensity of stress at the tip of the deformation band.

Hall[12] suggested that this stress(σ_y) is the external stress which with the help of the pile-up(Fig.1.2), would give birth to a critical stress concentration within a certain distance ahead of the pile-up,to oppose the grain boundary strength,if yielding is to occur.Petch[13], however modified this view by proposing that the stress concentration is rather at the grain boundary.Yielding takes place when this stress concentration matches the strength of the grain boundary.

Cottrell[14], in his contribution, proposed that the critical streess concentration is that which can unlock a Frank-Read dislocation source near the grain

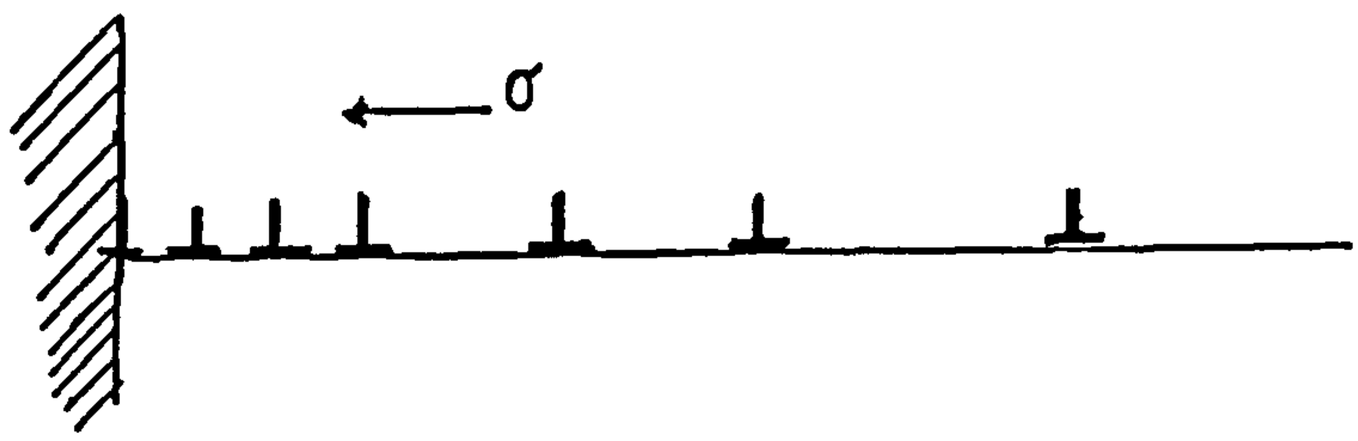

Fig 1.2: A pile-up of dislocations at the grain boundary.

boundary.When this source is unlocked,there would be mobile dislocations to continue the plastic deformation of the material.

Still emphasizing the importance of the grain boundary strength, Li and Chou[15] demonstrated that irrespective of type of pile-up and the distribution (continuous or discrete) of dislocations within the former,the stress concentration was found to be a function of the grain boundary strength. To this end, they formulated an expression for the stress concentration(σ_{tip}) for single-layer, single-ended pile-ups(both of discrete and continuous dislocation distributions) as:

$$\sigma_{tip} = n\sigma \qquad (1.3)$$

where n is the number of free dislocations and σ is the applied external stress.

According to Petch[13], during yielding,this stress concentration(σ_{tip}) would equate to a critical stress, σ_c required at the grain boundary in order to release a blocked glide plane; in other words,this stress concentration is synonymous with the strength of the grain boundary.

For a large number of dislocations, n, Li and Chou[15] found that the grain size, d could be given as:

$$d = 2nA/\sigma \qquad (1.4)$$

$$A = \mu b/2\pi \text{ (for screw dislocations)} \qquad (1.4a)$$

$$A = \mu b/2\pi(1-\nu) \text{ (for edge dislocations)} \qquad (1.4b)$$

where μ is the shear modulus of the material, b is the Burger's vector of the dislocations and ν is Poisson's

ratio. From eq. 1.3, $n = \sigma_i/\sigma$ ($\sigma_{i,p} = \sigma_i$), substituting for n in eq. 1.4, solving for σ and introducing a possible frictional stress σ_o, Li and Chou[15] obtained the expression:

$$\sigma = \sigma_o + (2A\sigma_i)^{1/2}d^{-1/2} \quad \text{.....(1.5)}$$

Eq. 1.5 is similar to eq. 1.2 in which σ from eq. 1.5 represents the lower yield stress, σ_y and the Hall-Petch slope, K_y is given as $(2A\sigma_i)^{1/2}$, in which A for mixed dislocations is given as $ub(2-\nu)/4\Pi(1-\nu)$.

However, Chou[16] further developed the foregoing by considering the situation where the locked dislocation at the grain boundary has a different Burger's vector(defined as mb, m being a positive real number) from that of the grain interior dislocations and therefore suggested that K_y is equal to $(2Am\sigma_i)^{1/2}$. This treatment made it evident that the phenomena that take place at the grain boundary(which would affect m) very much affect the magnitude of K_y.

1.2.2 Inconsistencies of the Pile-up Theory

While the pile-up theory seems to explain the onset of yield satisfactorily, it has always been deficient[15] in explaining the various stages and types of plastic deformation of metals and alloys.

Another limitation of the theory is that of the lack[17] of direct observation of pile-ups in pure metals,though they are found in alloys of low stacking fault energy. Yet,the Hall-Petch relation holds reasonably

well for both cases.

Chou and Louat[10], considering the effect of a non uniform stress field on a single-layer,single-ended pile-up,found that the stress concentration equally depends on a constant, λ and thus suggested that the stress concentration, σ_c is given as:

$$\sigma_c = \sigma^2 d(\lambda+2)^2/8A \qquad \ldots\ldots\ldots\ldots\ldots\ldots(1.6)$$

where σ is the external applied stress and the other symbols are as already defined. Solving for σ, which at yielding is equal to σ_y, gives $K_y = (8A\sigma_c)^{1/2}/(\lambda+2)$.

Li and Chou[15] using the non-uniform stress field[18] approach concluded that the Hall-Petch relation becomes inexact if the product,$\sigma\lambda$ is independent of grain size and can be exact if only λ is independent of grain size. This inexactitude is the case in work-hardening processes. Work-hardened materials do obey the Hall-Petch relation,but on applying the pile-up theory,the relation becomes inexact due to the birth of non-uniform internal stresses arising from the formation of subgrains or cells.

From a study on a 3% Si steel,it has been reported[19] that dislocations are emitted from grain boundaries(Fig.1.3) at stresses much below the yield stress,without the help of pile-ups.The work also showed that the stresses for moving the dislocations are not grain size dependent. The study on a similar steel composition by Carrington and Mclean[20] has shown slip lines originating from grain boundary sources(Fig.1.4) at microstrain regions;i.e.,at stresses defined as $\sigma_o < \sigma < \sigma_y$.The

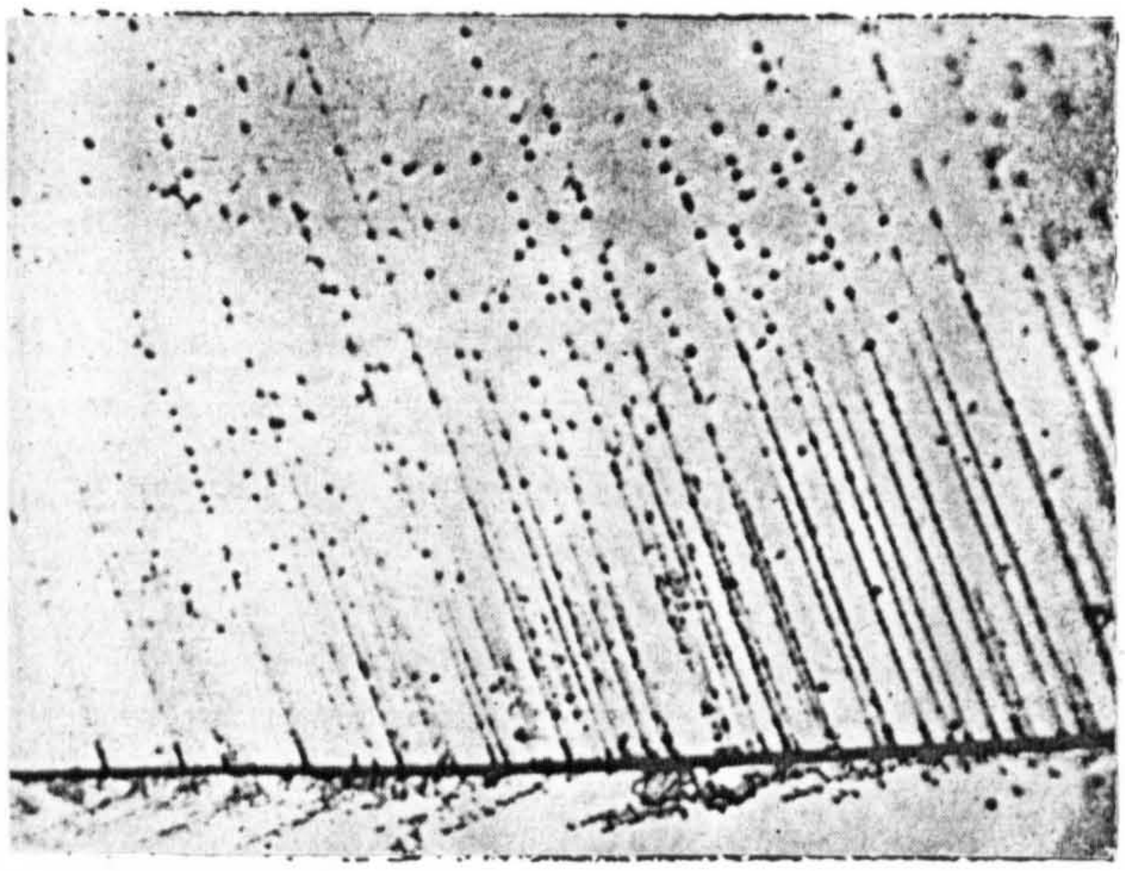

Fig 1.3: Emission of dislocations from a grain boundary, (Ref 19).

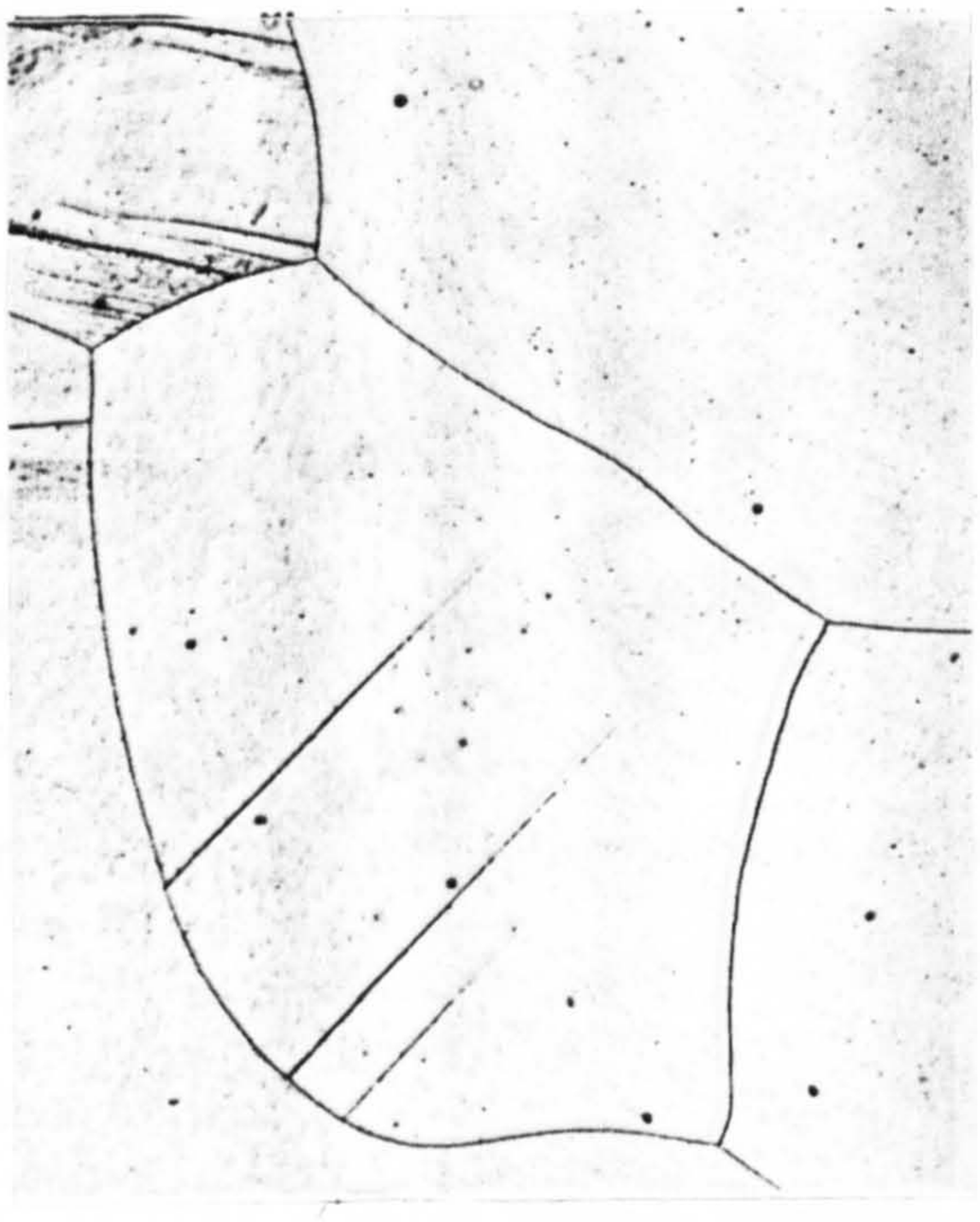

Fig 1.4: Slip lines originating from grain boundaries, (Ref 20).

inconsistency of the pile-up theory has also been reported by Margolin and Stanescu[21] on a 9.8% Mn-titanium alloy.

To circumvent the inconsistencies of the pile-up theory, the work-hardening theory[15] was developed. In this theory, the role of the grain boundary strength(critical stress), σ_c is de-emphasized, and K_y is given as:

$$K_y = \mu b \epsilon^{1/2}/(b\beta)^{1/2} \quad \ldots\ldots\ldots\ldots\ldots\ldots(1.7)$$

where ϵ is the plastic strain and β is a coefficient of direct proportionality to the ratio of the average distance the dislocations slip and the grain size of the material. But the work of Carrington and Mclean[20](in which the grain boundary role was very evident) does suggest that the work-hardening theory may not be applicable to Fe-Si system.

1.2.3 Grain Boundary Source

In the search for a more satisfactory theory, Li[22], using the angle of misorientation between grains, θ, proposed that the stress, σ_y required to move dislocations in a Taylor-type forest(parallel dislocations of opposite sign) is given as:

$$\sigma_y = \sigma_o + (\mu b/2\,\Pi\,(1-\nu))\,(8\theta/\Pi\, b)^{1/2} d^{-1/2} \quad \ldots(1.8)$$

According to this model, a partially locked tilt boundary can supply mobile dislocations by any of the following mechanisms:

i) when the angle, θ is small, the free dislocations can be separated from the locked dislocations.

ii) when the angle, θ exceeds a critical[23] value of b/h(b is Burger's vector and h is the distance separating two adjacent parallel edge dislocations),the locked dislocations can break free,and

iii) the tilt boundary having all its dislocations free or they have just become free.

When the stress in eq. 1.8 exceeds any of the stresses arising from the three mechanisms above, a comparable Hall-Petch relation with a slope comparable to that of a pile-up theory is produced. By this approach, Li[22] concluded that the pile-up theory could be dispensed with. The implication of eq. 1.8 is that at high values of θ (as met at grain boundaries),the stress becomes so large that the unlocking of dislocations gives way to the mechanism of dislocation generation.

Li and Chou[15] found that the capacity of grain boundaries to emit dislocations may change with the structure and the composition of the grain boundary, independent of the grain size.

1.3 Mechanisms Through which the Yield stress and K_y are Affected.

The previous sections reviewed the underlying mechanisms of strengthening and the associated theories.How these mechanisms achieve the strengthening is now reviewed.

1.3.1 Dislocation Locking

As was highlighted in section 1.1,Cottrell and Bilby[2] proposed that interstitial atoms would form atmospheres around dislocations,because the strain energy of the crystal is lowered by so doing. A relatively high applied stress is needed if the dislocations are to be liberated from these atmospheres, because the atmosphere produces a stress concentration. Cochardt et al[24], in their work on body centred cubic metals,found the energy of this dislocation-interstitial atom interaction(i.e., the atmosphere) to be about 0.75 eV, and the saturation concentration of the solute atoms near the dislocation to be about 6 atom percent.

Locking of dislocations is essentially[23] the action of interstitial atoms. As far as iron is concerned, the commonest interstitial atoms with a significant locking strength are carbon and nitrogen. Nevertheless, Codd and Petch[25] found that if boron is present in the iron,its locking strength supersedes that of carbon or nitrogen.They also showed that a semi-killed mild steel has a higher K_y value(more locked dislocations) than a fully silicon killed steel.There tends to be a divided opinion about which of the two interstitial atoms-carbon or nitrogen, is respons-ible for the variation of K_y, i.e.,which of the two has the higher locking strength. Probably based on the level of the content of the respective interstitial elements in the steel,some authors[15,26,27] have suggested that carbon is dominant. However,Heslop and Petch[28], testing alpha-iron

at 73 K, found that deoxidizing the steel with 0.07% Al reduced K_y. They concluded that since aluminium combines with nitrogen as well as oxygen,it is rather more probable therefore that nitrogen locking is stronger.Codd and Petch[25] suggested that if nitrogen is a stronger locking element, it would have a more concentrated atmosphere,which would necessitate a larger activation energy to unlock. Thus, nitrogen locking may be expected to be less temperature dependent;however,nitrogen locking was found to be very temperature dependent[25]. Nonetheless, nitrogen has been demonstrated to have a high propensity[29] to lodge at the grain boundary sites(higher dislocation density region of the crystal),probably because of its lower activation energy for diffusion[30] and its higher solubility[31] in alpha-iron relative to carbon.

There is therefore this contradiction of the temperature dependence of nitrogen locking vis-a-vis its experimentally demonstrated[25] stronger locking ability, even with a higher carbon concentration in the steel, Fig. 1.5. An explanation of this experimental observation was offered by Petch[32]; based on the results from denitrided and decarburized steels, which were subsequently recarburized(to achieve pure carbon locking) and renitrided(to achieve pure nitrogen locking) he concluded that nitrogen locking of dislocations is stronger than carbon locking. This, he argued is because the locking of dislocations by carbon or nitrogen is energy related rather than concentration related.

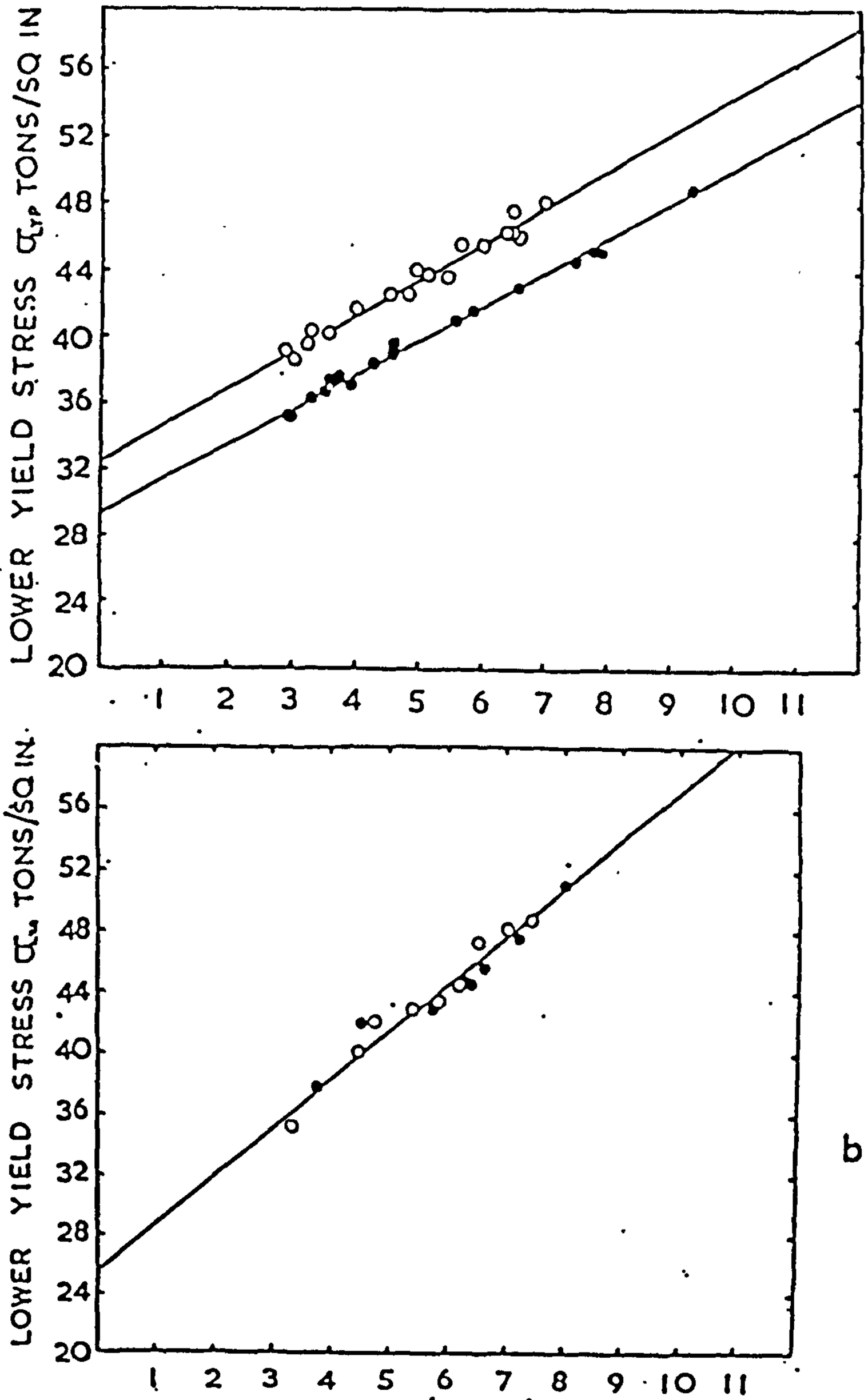

Fig 1.5: The higher locking strength of nitrogen, relative to carbon in a steel of composition (wt%):0.45C, 0.006N, and 0.47Mn; a), σ_y Vs grain size at -196° C for a pure carbon locking, o-quenched from 650° C, ●-annealed. K_y=33.9 MPamm$^{1/2}$; b), same as (a) for a pure nitrogen locking, o-annealed.●-quenched from 650°C. K_y=48 MPamm$^{1/2}$. (Ref 25).

The higher solubility of nitrogen made most of the nitrogen in (b) to be already in solution on annealing,thus making no difference to the σ_o on quenching; But in (a), the increased concentration of carbon retained in the ferrite on quenching led to an increase in σ_o[23].

1.3.2 Segregation and Precipitation(Effect of Cooling Rate)

Wilson[33] showed that the K_v value of a slowly cooled annealed steel is higher than that of the steel quenched from 700° C. On ageing the quenched steel at 90° C however, the K_v value of this quenched steel recovered to the as-annealed value after 10^3 minutes,Fig.1.6. It has been reported[9] that during the ageing of a prior quenched steel, the dislocation pinning process is expected to take far less time to complete than grain boundary locking. Thus,the time factor, Wilson[33] rationalized, is an indication that it is grain boundary locking that determines the magnitude of K_v. Hence, he concluded that the recovery of K_v during ageing was probably controlled by the extent of solute segregation to the grain boundary.

Mintz[158] has also suggested that the precipitation of the excess carbon produced at grain boundaries as carbides could lead to a reduction of the K_v value of low carbon steels. The precipitation, he argued, would be favoured by holding the steel specimen for a sufficient time at below the transformation temperature. Nevertheless, he further suggested that for low carbon steels of about 0.045% C, a slow cooling rate could infact raise the K_v, through the segregation of excess carbon interstitial atoms to the grain boundary.

The concept of segregation nonetheless, was opposed[15] on the grounds that if it were the mechanism, carbon atoms would segregate to the grain boundary during

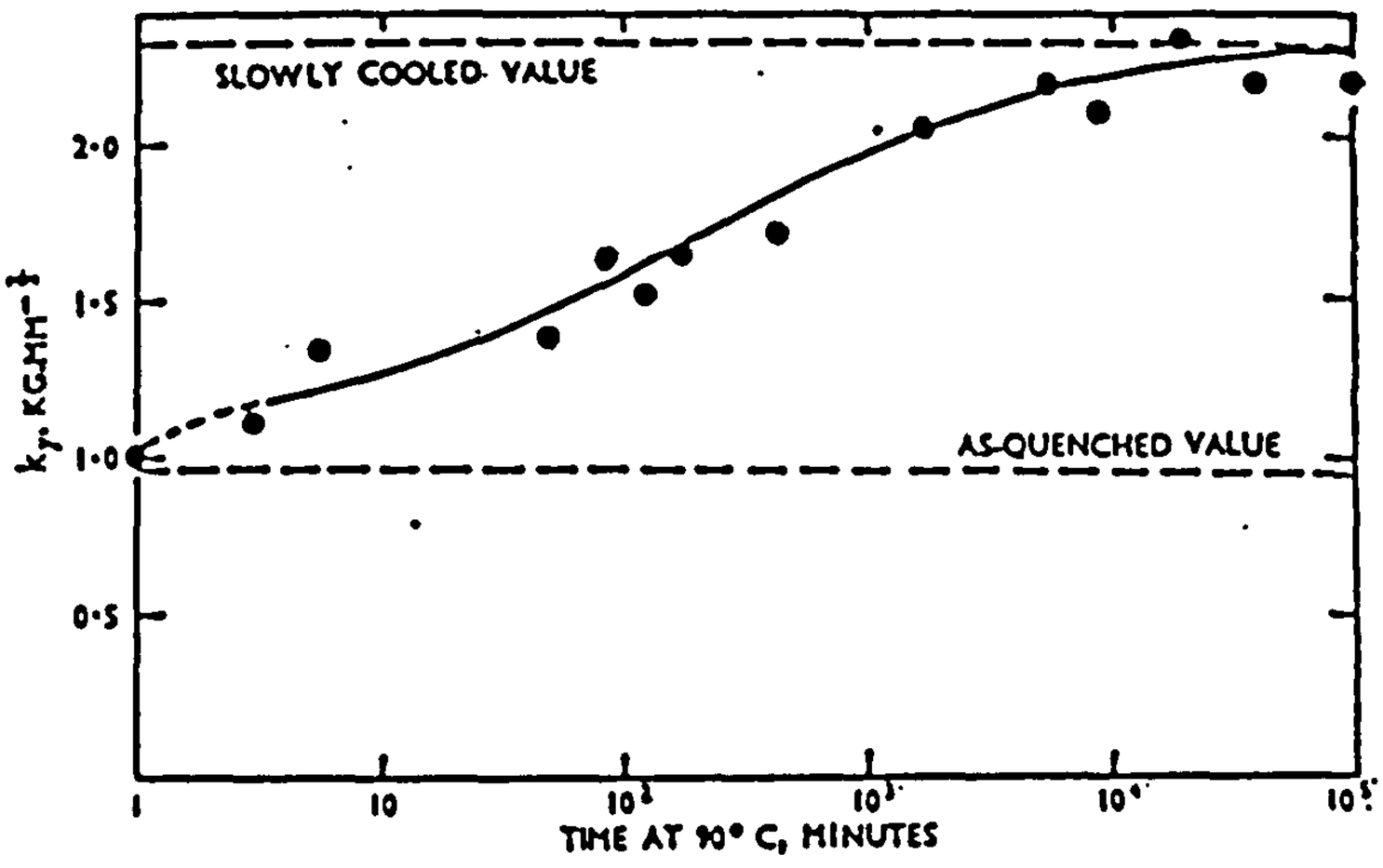

Fig 1.6: Recovery of K_y during ageing at 90°C of a (wt%) 0.003C-0.34Mn steel, quenched from 700°C, (Ref 33).

ageing. The carbon segregation would have increased the proportionality coefficient, β in eq. 1.7, and this in turn should have decreased the K_y value rather than increase it.

Sibley and Breyer[26] have suggested that a reduction in value of K_y on the initial additions of silicon, may be due to carbide precipitation around or near the grain boundaries. The precipitation of carbides therefore depletes the carbon atoms that should have locked the dislocations, thus the dislocations are freed and K_y is therefore reduced. However, there is no report so far identifying carbides(of silicon or manganese) in low carbon steels with silicon $\leqslant$ 2 wt%, but rather reports of silicon nitride precipitation in this grade of steels abound. Baker[34] identified silicon nitride in the form of SiN(c=5.05±0.07Å and a = 3.17±0.05Å), with some manganese in the precipitate. Arrowsmith[33] also identified the same SiN. There are reports of unidentified manganese-silicon nitride[36] and Si_3N_4[37].

1.3.3 Ledges.

The objection of Li and Chou[15] to the segregation theory advanced by Wilson[33], concerned the way the solutes segregated to the grain boundaries affected the dislocations in the latter,and not the segregation per se. Contrary to Wilson's[33] approach, they suggested that the solute which diffused to the grain boundary during the ageing could increase the ledge density in the grain boundary.

On the basis of these ledges in the grain boundaries, Fig.1.7, Li[22] proposed that yield may be controlled by the displacement(say by straining) of the ledges. The ledges on being displaced,generate dislocations in the matrix.These ledges are considered to be adsorbed dislocations on the grain boundaries[38]. However, Li[22] pointed out that this theory is intended only to apply at the initial yielding stage when the dislocation density is still very low. This source of dislocations is not quite a dislocation mill, in the Frank-Read sense, but rather he considered the grain boundary source as a "donor" of dislocations. As more dislocations are generated, the donated dislocations can multiply, say by the cross-slip mechanism.

Li[22] pointed out that the stress to generate a dislocation out of a forest of ledges is dependent on the ledge density. The ledge density increases with decreasing grain size, since dislocation density per unit volume increases inversely with grain size. The free energy of formation of a grain boundary ledge may be lowered by impurity atoms,thus more impurities(at low impurity content level) can increase the ledge density,which in turn implies more generated dislocations(dislocation density). Using a thermodynamic model, he calculated that at low impurity levels,the square of K_y value should vary linearly with solute impurity content at the grain boundary.

Mintz et al[39] observed that a 0.3% Si steel had a higher ledge density than had a 0.03% Si steel, Fig 1.8. This may be in line with Li's[22] theory of the stability

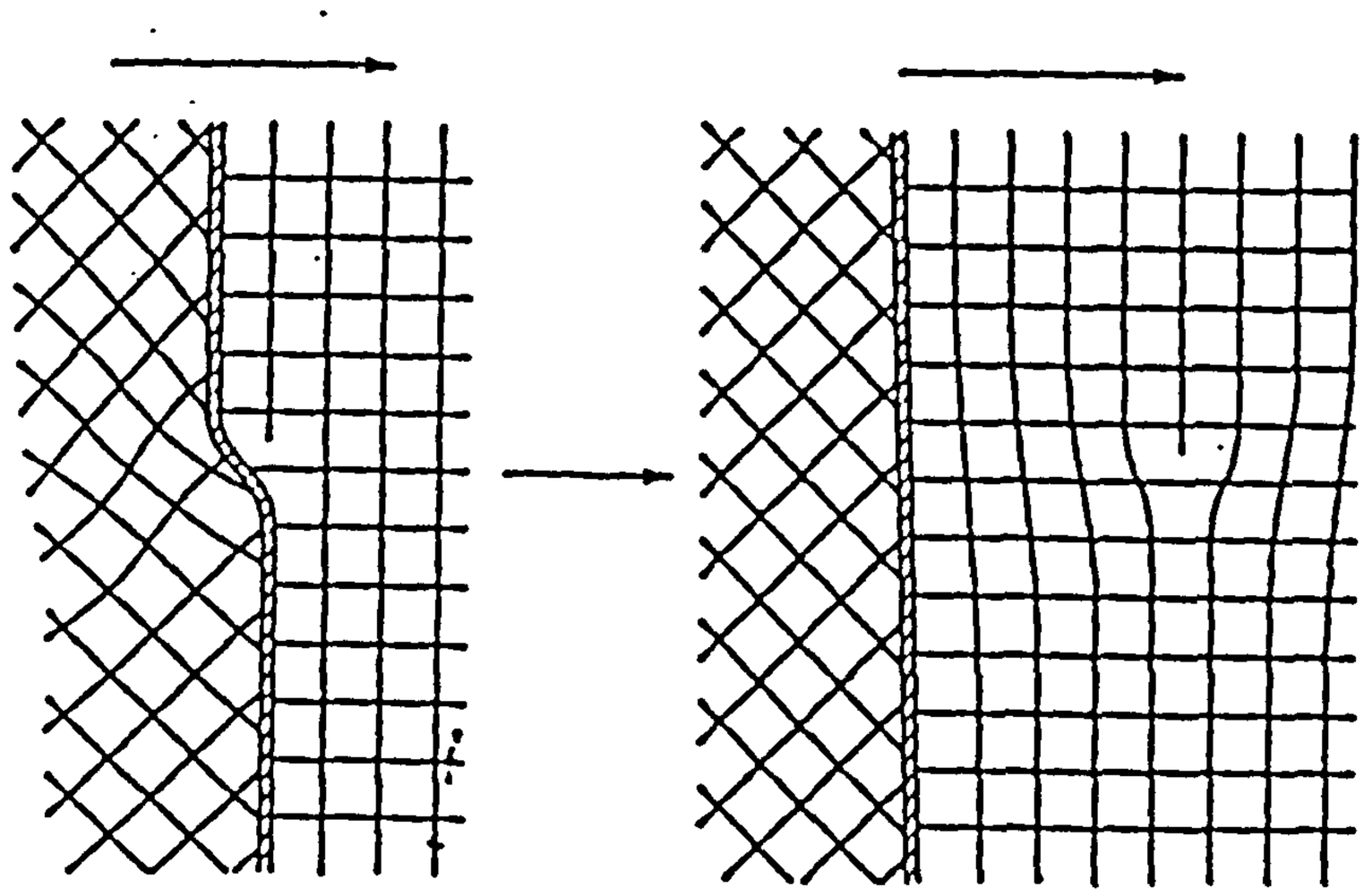

Fig 1.7: Grain boundary ledge, acting as a donor of dislocations,(Ref 22).

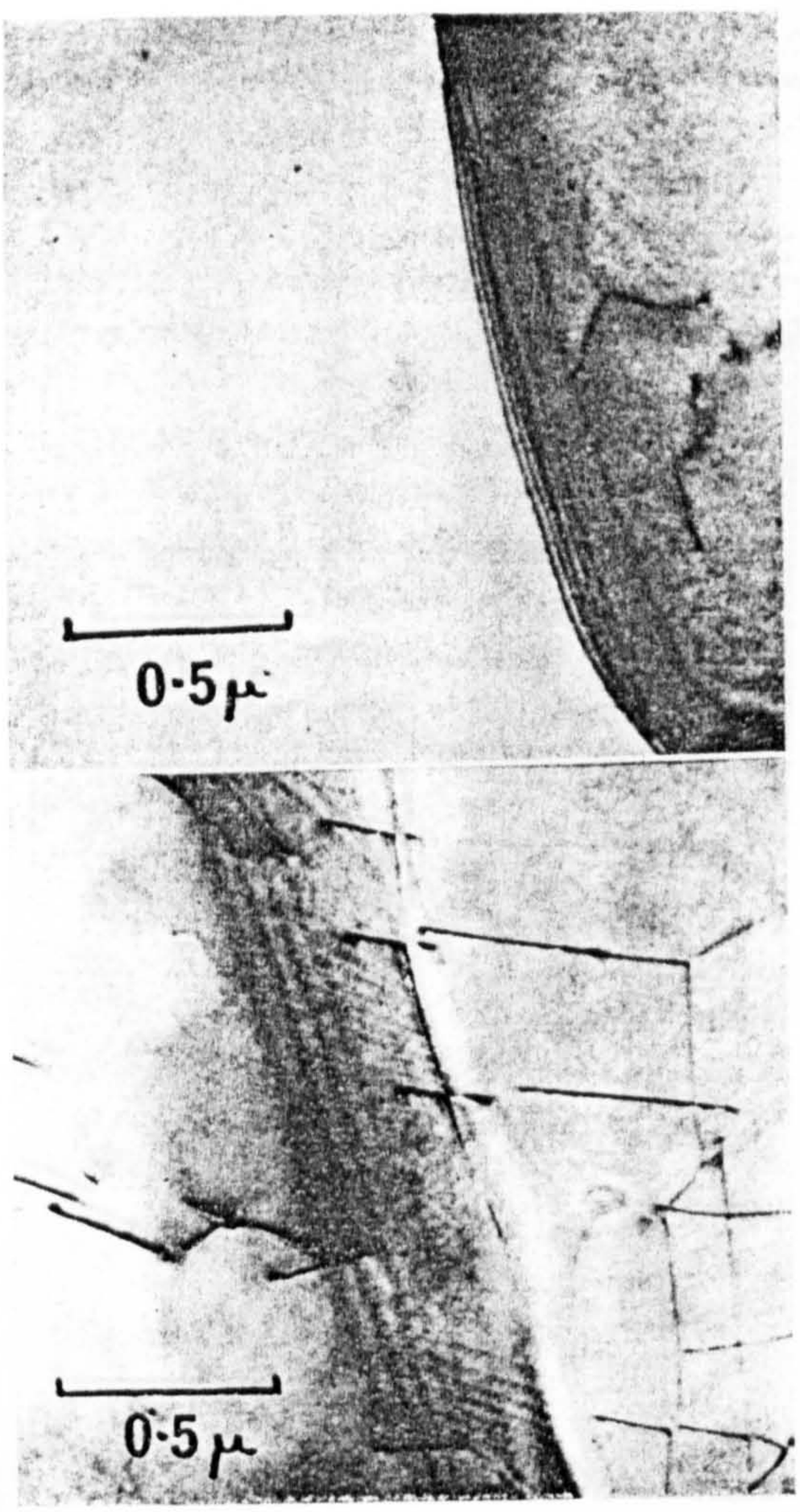

a

b

Fig 1.8: Thin foil electron micrographs of grain boundaries showing some dislocations in 0.6% M steels containing 0.005% free nitrogen, with:
a), 0.03% Si, showing a low incidence of ledges
b),0.3% Si,showing a high incidence of ledges (Ref 39).

of ledges. However, they also observed that the 0.03% steel had a higher K_y value, which therefore seems contradictory to Li's[22] thermodynamic calculations. Nonetheless, Ishida et al[40] have demonstrated that features like ledges, when present in high density, could have a poor resolution of individual ledges in the transmission electron microscope. Hence, Mintz et al[39] suggested that this may be the reason for Li's[22] thermodynamic theoretical calculations not conforming to experimental observations. They further suggested the possibility that of even more importance in the effect of ledges on K_y, could be the degree of pinning of the ledges by impurities,rather than the ledge density itself.

1.4 Effect of Pearlite on the Tensile properties of Low Carbon Steels.

In ferrite-pearlite steels, Petch[13] suggested that the yield stress, σ_y, should be independent of the pearlite content,when ferrite has the greater volume fraction. This, he argued, is because σ_y is the stress needed to propagate the Luders-band through the ferrite.Petch found that increasing the carbon content in the steel from 0.04 to 0.16% had no appreciable effect on σ_y or the frictional stress, σ_i. Gladman et al[41] observed that pearlite does not have any effect on σ_y,while Karlson et al[42] have also shown that initial yielding is almost entirely confined to the ferrite phase.

Preston[43], however found that increasing the

carbon content of a steel from 0.067 to 0.21 wt% increased the K_y value from 12.6 to 14.5 MPa $mm^{1/2}$. This he argued, is understandable since any carbide situated on the grain boundary would make it more difficult for arriving dislocations(to this portion of the grain boundary) to initiate yield in an adjacent grain.

The pearlite constituent has been shown[41,44] to affect the ultimate tensile strength(UTS), due to the greater work-hardening of pearlite relative to ferrite. Irvine and Pickering[44] have suggested that a decreasing interlamellar spacing leads to a pronounced increase in the tensile strength,though in low-carbon steels, this effect is relatively small.

1.5 Effect of Silicon on the Tensile properties of Low Carbon Steels at Room Temperature.

Several reports[24,44-46] have noted the solution hardening effect of silicon on ferrite resulting from the size misfit parameter(see section 1.1). One thing common to all the reports is the non-uniformity of base compositions of the steels either within a given report,or between the different reports. This may be responsible for reports of an increase of frictional stress,σ_i as low as 25[44] to as high as 117[24] MPa per one wt% Si.

These reports also show that the yield stress, σ_y is increased by the addition of silicon. Most authors, in quoting the level of strength increase brought about by the addition of silicon, neglected the effect of grain size.

However, Mintz[15] found a rate of increase of yield strength of approximately 77 MPa per 1% Si at a grain size of $d^{-1/2}$ = 8 $mm^{-1/2}$. Preston[47] has also observed that increasing the silicon content in the steel from 0.2 to 0.5 wt% led to an increase in yield stress of 34 MPa at about 20 um($d^{-1/2}$ = 7 $mm^{-1/2}$), but at 10 μm($d^{-1/2}$ = 10 $mm^{-1/2}$), this increase in the yield stress reduced to 18 MPa.

Silicon has also been reported[24,47] to lower the Hall-Petch slope, K_y, at the initial additions of silicon(up to 0.71 wt%), followed by an increase in K_y with higher levels of silicon. The work[24] speculated that the mechanism involved was that of carbide precipitation in the presence of the silicon atoms. Morrison and Leslie[48] observed a low value of K_y of about 5.8 MPa $mm^{1/2}$ for a 0.7 wt% Si steel(at room temperature tests), relative to the K_y value of about 18 MPa $mm^{1/2}$ for a Ferrovac iron. They also observed that the K_y value for room temperature tests increased beyond the 0.7 wt% Si content up to 1.43 wt% Si. The K_y value beyond this 1.43% Si level was found to be constant. They rationalized their experimental results on the basis of ledge theory(see section 1.2.3).

It has been reported[45,47] that silicon additions up to about 1 wt% do reduce the ratio, σ_y/σ_{UTS}. The ultimate effect of silicon on the tensile properties of steels has always attracted divided opinions. As far back as 1891, Howe[49] expressed the opinion that silicon up to 0.7 wt%, in the great majority of cases, may directly or indirectly(by restraining the formation of blow holes and

reducing iron oxide) increase the tensile strength and even the ductility of steels. He concluded that the deleterious effect of silicon on the mechanical properties is particularly associated with high carbon steels.

1.5.1 Effect of Silicon on the Austenite to Ferrite/Pearlite Transformation Characteristics.

Since strengthening very much depends on the transformation characteristics of a steel, it is necessary to review some of the work relating to the effect of silicon on the $\gamma \longrightarrow \alpha$ and pearlite transformation.

Aaronson et al[50] have suggested that any alloying element that raises A_{e3} and raises the activity of carbon in austenite, increases the rates of nucleation and growth of ferrite allotriomorphs. Kinsman and Aaronson[51], in their work, confirmed this theory for silicon additions. Irvine and Pickering[44], studying low carbon steels with $0.42 \leqslant Si \leqslant 2.93\%$, confirmed that silicon additions increase the transformation temperatures(at $0.6 \leqslant Mn \leqslant 1.6\%$). On this basis they suggested that silicon produces coarse ferrite and less pearlite.

Ferrite formers, like silicon(though to a lesser degree,relative to chromium or molybdenum),at critical concentration, partition[1] when intercritically annealed from high temperatures, and could lead to a change in the composition of the cementite, with still the same crystal structure, but could affect the pearlite interlamellar spacing, and the tendency of the cementite to spheroidize.

CHAPTER TWO

"SOFTENING" OF STEELS

2.1 Definition of "Softening"

The yield and flow stresses increase with the lowering of test temperatures[52-54] and increasing strain rate[52,55,56]. This interrelationship of strain rate and temperature has led to alloy "softening" being essentially studied under the concept of a thermally activated process(TAP)[57]

During a plastic deformation process, outside the inherent resistance of the lattice(Peierls-Nabarro,P-N stress), a dislocation may encounter other obstacles as it moves through the crystal. Conrad[58] has categorized these obstacles to be:

i) temperature independent: these arise out of long range stress fields; i.e. stress fields of the order of $\geqslant 10$ atomic diameters, eg: grain boundaries, other dislocations and large precipitates.

ii) temperature dependent: these are due to short range stress fields, of the order of < 10 atomic diameters, eg: P-N stress, forest dislocations, screw dislocation jogs, cross-slip of screw dislocations and climb of edge dislocations.

Conrad[58] pointed out that thermal fluctuations play no

role in overcoming the long-range obstacles, hence the stress required by the dislocations to overcome this type of obstacle constitutes the athermal component, σ_{ath} of the applied stress. However, thermal flutuations can assist the applied stress to facilitate the overcoming of the short-range obstacles by the dislocations. Therefore this stress constitutes the thermal component, σ_{th} (σ^*) of the applied stress.

The athermal component, generally is increased through alloying. Alloy "softening" is manifested through the thermal component (also known as the "effective" stress), and it is quantified[57] in terms of the rate of change of the yield stress, σ_y with respect to the change in test temperature, T ($d\sigma_y/dT$). Alloy "softening" normally occurs (though not exclusively) at temperatures $\leqslant$ 0.15T_m, where T_m is the absolute melting temperature of the alloy.

Under normal circumstances, a steel, X, by virtue of the level of the alloying element (say silicon) content in the steel, would possess a higher yield stress, σ_y than another steel,Y which has a lower level of silicon. The general condition, thus for alloy "softening" is that $(d\sigma_y/dT)_x < (d\sigma_y/dT)_y$. When this condition is fulfilled, two situations (see Fig 2.1a) exist and are defined[57] as:

a) apparent (true) "softening"; the yield stress of steel X now becomes smaller than the yield stress of steel Y.

b) pseudo-"softening"; the yield stress of steel X is still larger than that of steel Y

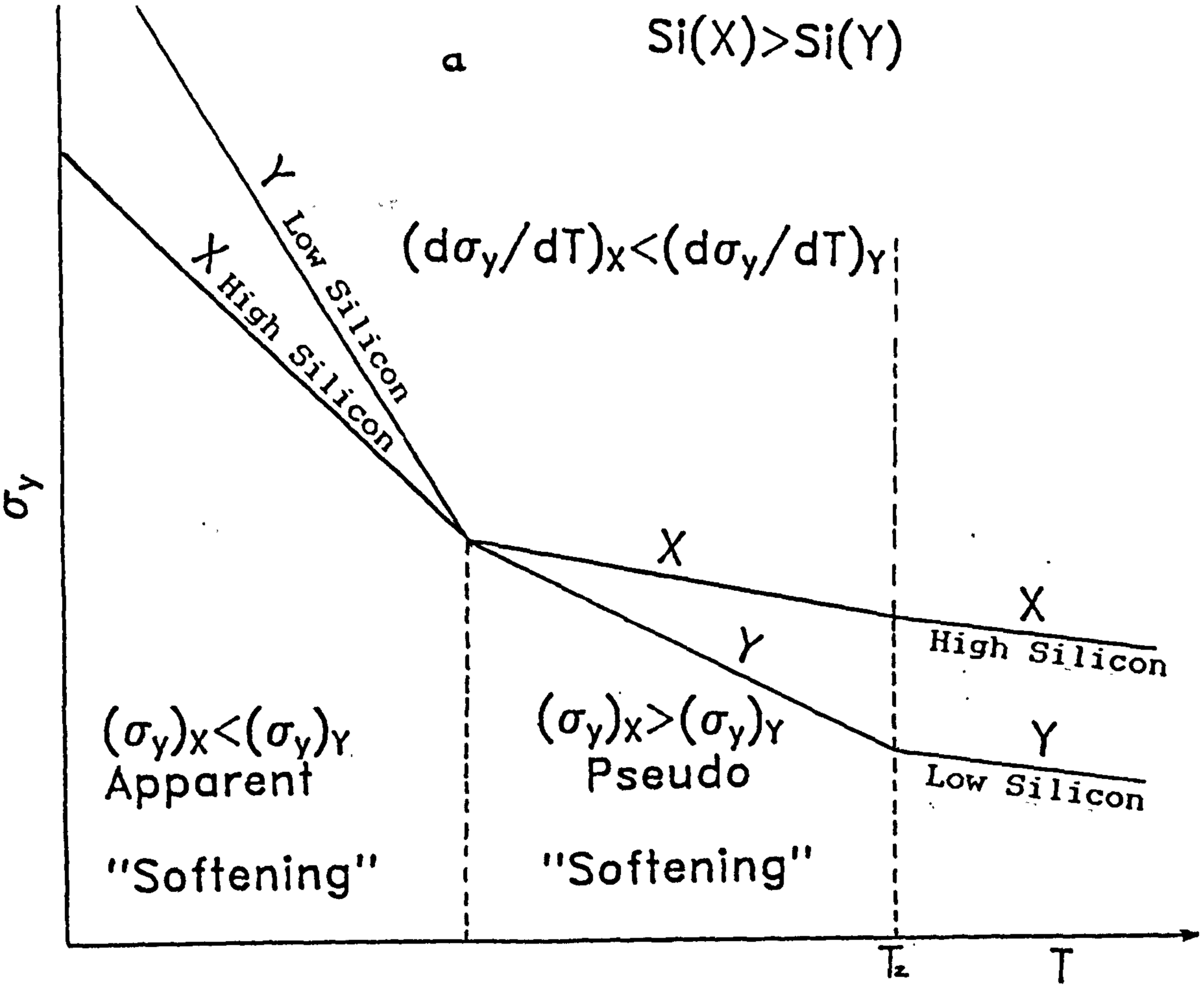

Fig 2.1: Schematic temperature dependence of the applied stress,defining "softening" for steels with silicon; a),total yield stress Vs temperature b),effective stress Vs temperature.

However, if the "effective" stress is plotted against the test temperatures, alloy "softening" (both apparent and pseudo) would lead to the yield stress (i.e. thermal) of the X steel to be always smaller than that of the Y steel, Fig 2.1b.

Alloy "softening" has also been defined as "reduced hardening"[59]. This has been demonstrated by Stephens and Witzke[60], who working on Mo-Re alloys, observed a reduction in hardness at Re concentrations < 7 at% for test temperatures < 300 K, Fig 2.2.

2.2 Theories of Alloy "Softening"

2.2.1 General

Pink and Arsenault[57] have suggested that alloy "softening" is associated with body centred (b.c.c.) lattices. The b.c.c. lattice, they pointed out, can be shown to possess a larger lattice resistance (i.e. Peierls stress) than is found in either face centred cubic (f.c.c.) or hexagonal close packed (h.c.p.) lattices. This has led to most theories of alloy "softening" to be related to the intrinsic b.c.c. lattice. However, they also pointed out that one single model can not satisfactorily explain alloy "softening" in all the b.c.c. systems.

Some authors[61-64] have demonstrated that alloy "softening" could also depend on the interstitial solute content in the steel, particularly at the low interstitial atom content range.

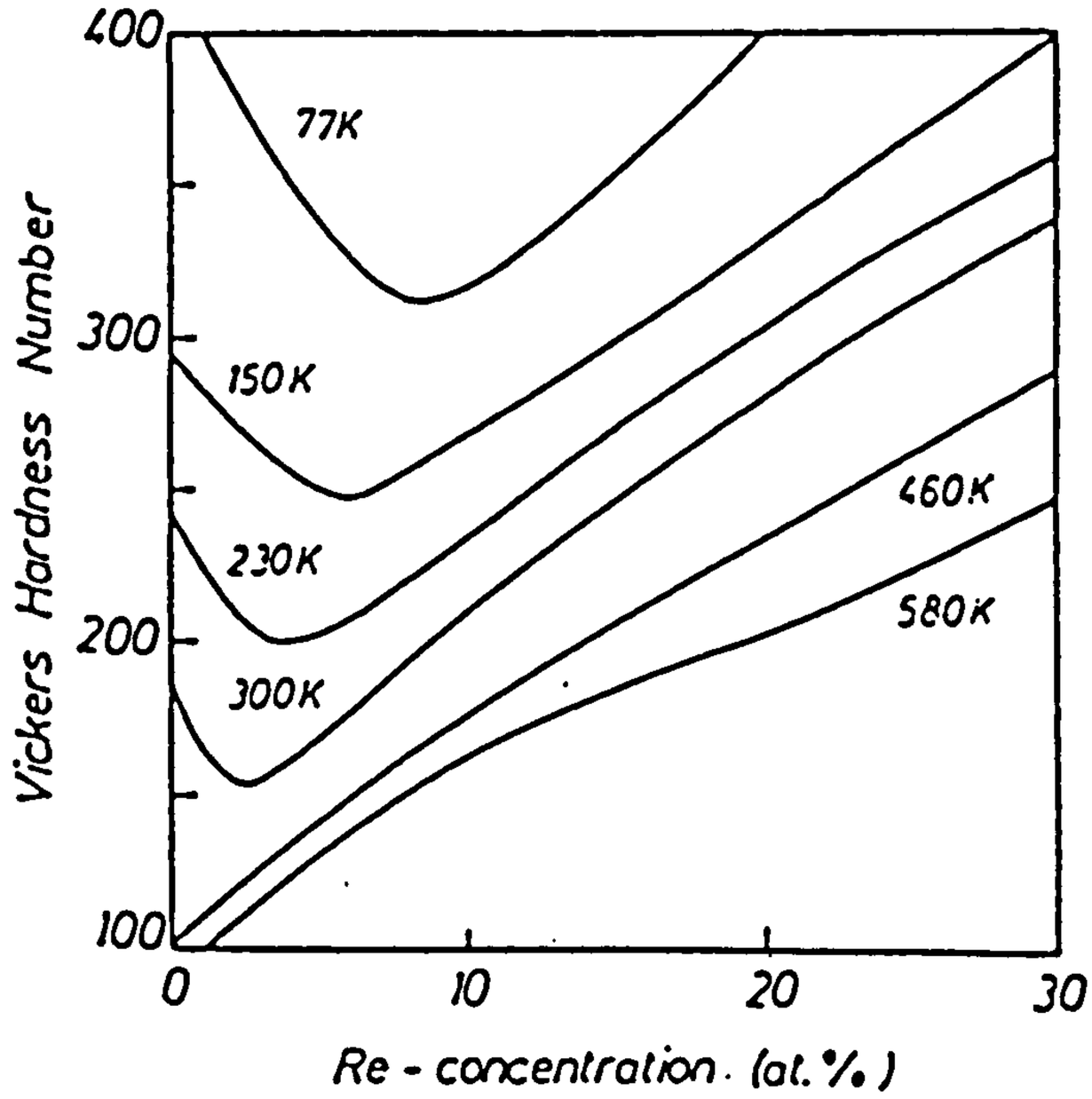

Fig 2.2: Hardness Vs Rhenium concentration, illustrating alloy "softening", (Ref 60).

Consequent upon the above considerations, the theories of alloy "softening" are mainly advanced along two directions- extrinsic ("scavenging") and intrinsic. These two approaches are the most probable and accepted models[57]. However, there are other theories which have been used to describe or explain alloy "softening":

2.2.2 A Unified Model of Low-temperature Deformation

This model was initiated by Frank and Sestak[45] who suggested a combination of the extended core model of the screw dislocation and the linear elastic effect of solute atoms. The length,l of a glissile dislocation segment, that is newly nucleated, is related to the distance L between impurity points[57]. Above approximately 100 K, l would be equal to L and the deformation proceeds by the transformation of sessile dislocations into glissile, thus accounting for the "softening". This model suggests that alloy "softening" should vanish below 77 K.

2.2.3 Changes in Deformation Mechanism

Brown and Ham[46] proposed that the yield stress resulting from the action of the edge dislocations penetrating weak particles is greater than that of the screw dislocations. On this basis, Tuominen and Koss[47], working on a Si-Ti b.c.c. lattice suggested that at low temperatures, only screw dislocations control deformation, while both edge and screw dislocations may be operative at high temperatures.

2.2.4 Internal Stress Fields

Takeuchi[66] proposed that the intrinsic lattice resistance to a lateral motion of kinks, assumed to be very small, should permit the possibility of a dislocation line having some of its length in this region. This would facilitate the formation of a double kink.

Arsenault and Li[69] observed an increase of activation enthalpy and volume at small values of the effective stress due to the large value of the ratio, σ_{eth}/σ_y. Since σ_{eth} of alloys is quite high, as a result of periodic internal stresses, Roberts and Bergström[70] suggested that an increase in a periodic internal stress (as in alloys) may give rise to a pseudo-alloy "softening".

However, it has been pointed out[57] that these models are not compatible with experimental results.

2.2.5 Increase in Dislocation Density and Activation Parameters.

Johnston and Gilman[71] gave the velocity of mobile dislocations, v for an effective stress, σ^* as:

$$v = v_o(\sigma^*)^m \quad \text{.....2.1}$$

where v_o is a constant, and m^* is the dislocation velocity exponent. The general expression for strain rate, is:

$$\dot{\epsilon} = \rho_m bv \quad \text{.....2.2}$$

where ρ_m is the density of mobile dislocations and b is the Burger's vector. The model, which is dependent on an increase in dislocation density, assumes that under a given operating strain rate, when the thermal stress is reduced

("softening"), there must be an increase in the density of mobile dislocations to maintain the given strain rate[43]. In support of this model, Christ[72] proposed that stationary impurities could exert forces which push screw dislocations away from the primary glide plane into a cross-slip plane. This should lead to a dislocation multiplication process, as described by Low and Guard[73]. Christ[72] further suggested that a maximum "softening" effect should occur within the range of 0.04 to 0.06 at% interstitial content in the alloy, and that a critical temperature exists,above which the interstitial solute atoms again lead to hardening.

Conrad[74] has evaluated the activation parameters for yielding and flow. These parameters are, the activation energy (enthalpy), H, the activation volume, V* and the frequency factor of mobile dislocations, υ during the deformation process. H is given as:

$$H = kTLn(\upsilon/\dot{\gamma}) \quad \ldots\ldots\ldots\ldots\ldots\ldots\ldots\ldots\ldots\ldots 2.3$$

where k is Boltzman's constant, T is the absolute temperature at which the deformation is taking place and is the shear strain rate, given as $0.7\dot{\varepsilon}$[52], $\dot{\varepsilon}$ being the tensile strain rate. V* is given as:

$$V^* = kT(\partial\dot{\gamma}/\partial\gamma^*)_T \quad \ldots\ldots\ldots\ldots\ldots\ldots\ldots\ldots\ldots\ldots 2.4$$

where γ^* is the thermal shear stress defined as $\sigma^*/2$, provided the Tresca's yielding criterion is obeyed. υ is given as:

$$\upsilon = \rho_m bsf, \quad \ldots\ldots\ldots\ldots\ldots\ldots\ldots\ldots\ldots\ldots 2.5$$

where f is the frequency of vibration of the dislocation

segment involved in the activation process and s is the average distance a dislocation moves after every successful thermal activation.

Some authors[63,75] have used the increase in these activation parameters to explain the "softening" of alloys. However, Sakuma and Karashima[74] found virtually no change in the values of the frequency factor and the mobile dislocation density between a "softened" and an "unsoftened" molybdenum steel. It is believed that an increase in the activation enthalpy is a result of alloying additions[75]. Pink[77] has suggested that the high activation enthalpies found in alloys (which supposedly contain "inclusions") are due to non-conservative motion of jogs. These jogs are assumed to develop on the screw dislocations, which overcome incoherent obstacles by cross-slip.

2.2.6 Extrinsic Theories (The Scavenging Model)

Authors of earlier papers[78-80] on the subject of alloy "softening" had thought that a possible chemical interaction between impurities (such as interstitial atoms) and the alloying solute atoms was responsible for the "softening" observed. Some reports were made based on this concept: Ravi and Gibala[81] extrapolated stress-concentration diagrams to zero alloy concentration, and found stresses comparable with the shear stress of a high purity material. Substitutional atom-interstitial atom clusters were identified[82] to have been the cause of the

appearance of high temperature internal-friction damping peaks, Fig 2.3. These peaks developed with an increasing level of the substitutional element, replacing the original Snoek peak due to dissolved interstitials.

Where the affinity of the matrix to the interstitial is larger than that of the solute, the "scavenging" of the interstitials by the solute alloying element still takes place, but the nature becomes geometric[63]. The presence of the substitutional atom is said to reduce the tetragonal strain usually linked with the interstitial atom in the matrix lattice[64]. This is because energy wise, the interstitials prefer the sites around the substitutional solute atoms. Thus, the interaction between the interstitial and the substitutional atoms is accomplished by the local reorientation of the former in the vicinity of the latter.

A higher concentration of free electrons in certain alloys has been found concomitantly with reduced solubility of interstitial elements in the matrix material[78]. This, it has been suggested[57], could contribute to alloy "softening".

Ravi and Gibala[81] have proposed that the scavenging mechanism is "non reversible"; i.e. alloy "softening" can be observed when interstitials are added to the metal, but no stress minimum would be observed when interstitials involving the same composition range are removed by means of consecutive zone-refining.

The validity of the "scavenging" model has been

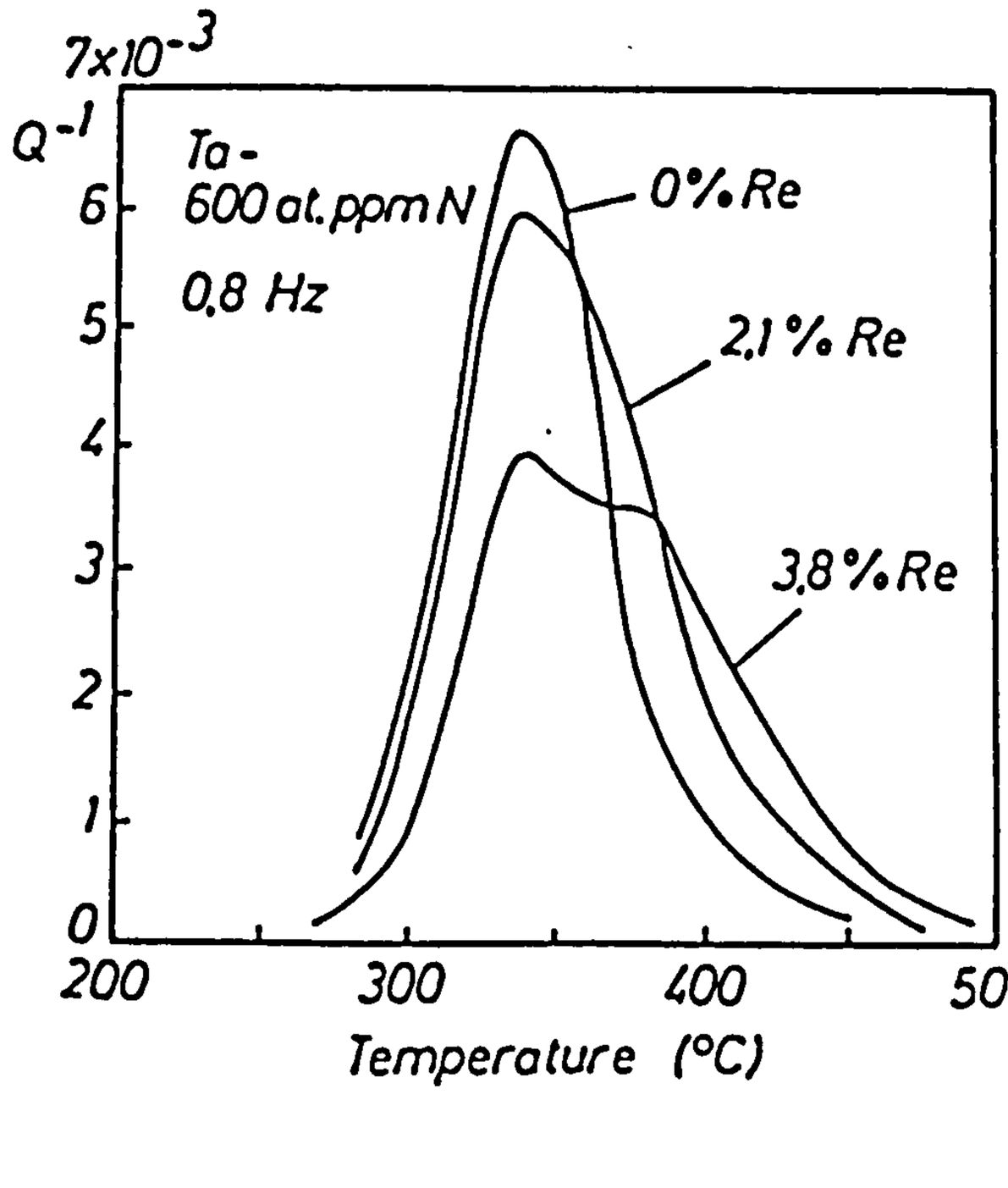

Fig 2.3: Effect of Re on the Snoek peak and high-temperature anelasticity in a Ta-N alloy,(Ref 81)

questioned by the results of some authors[65-67], particularly the non-reversibility condition of alloy "softening". They found that the yield stress of carbon and nitrogen alloyed iron increased after hydrogen purification. Crowe and Arsenault[66] have tried to relate the changes in stress and activation parameters to the interstitial atoms concentration, but the experimental data do not fit the theory. Tanaka and Watanabe[62] have also demonstrated that a carbon steel, in which the interstitial carbon atom concentration level in the lattice was reduced by annealing, showed a lower tendency to "soften" than the same steel with a higher concentration level of carbon atoms in the lattice (produced by quenching).

It has been suggested by Pink and Arsenault[57] that scavenging is not a mechanism per se,but that it creates the conditions which may be prerequisites for alloy "softening".

2.2.7 Intrinsic Theories

The term "intrinsic" is rather literary, because in reality, foreign atoms are still necessary for "intrinsic" alloy "softening" to take place[57]. Whereas in the extrinsic model,the "softening" is brought about by the alloying solute atoms ridding the matrix of the foreign atoms, the intrinsic model envisages the presence of the foreign atoms and considers how their presence reduces the lattice resistance.

Some authors[69,70] have related alloy "soften-

ing" to changes in the shear moduli and the atomic radii on alloying. Thus,only solute atoms of smaller sizes than the matrix atoms were suggested to be capable of initiating alloy "softening"[91,92]. The work by Stephens and Witzke[93] tends to suggest that it is then the atomic size that is of relevance to "softening". Therefore they suggested that every alloying substitutional element,with its atomic radius fulfilling the Hume-Rothery's 15%-rule for solid solutions, can initiate alloy "softening". However,if the atomic radius exceeds the 15%-limit, it may not initiate alloy "softening" in iron base alloys.

Intrinsic theories could further be classified into two parts; namely, those that predict changes in the intrinsic lattice resistance, and those where the overcoming of the intrinsic lattice resistance by the dislocations is facilitated by the solute atoms.

2.2.7.1 <u>Changes in the Intrinsic Lattice Resistance (Peierls Stress).</u>

Weertman and Weertman[94] have demonstrated that the Peierls stress of a lattice, σ_p is related to the spacing of the constituent atoms, c thus:

$$\sigma_p = \alpha(\mu b/2c)\exp(-2\pi\gamma/c), \quad \ldots\ldots\ldots\ldots\ldots\ldots 2.6$$

where α is a constant related to the variation of the force with distance in the lattice and $\gamma = a/2$ ("a" being the lattice constant) is the width of the dislocation. α can vary between 0.5 to 1. Thus, a variation of , u or "a" could lead to a variation of σ_p. Changes inα[95] have been

reported on alloying. The lowering of σ_p due to changes in "a"[74] or reduction of μ[44,77] (relative to the matrix value) have also been reported.

It has been argued that on the application of an external stress, the motion of a screw dislocation is determined by two components[57] of the Peierls stress: the first component gives rise to a small translation that would be maintained, even after the removal of the applied stress. This stress and its nature depend very much on the width of the core of the screw dislocation. The second stress component leads to free dislocation motion and seems to be relatively insensitive to the width of the core of the dislocation. Hence, changes of the core structure of the screw dislocations could change the Peierls stress[78].

These atomistic conclusions were derived from the interpolation of the interatomic potential with the elastic constants. On this basis, Pink and Arsenault[57] argue that the part of the potential that may determine the Peierls stress could be completely unrelated to the part of the potential which determines the elastic constants.

It has also been suggested[78] that the Peierls stress of a material could be correlated with the electronic configuration of the alloying solute atom. Thus, transition metals with unfilled and non spherical d orbits bring about covalent bonding which can give rise to large Peierls stresses; however, filling the d orbit with electrons is considered to decrease the stresses.

2.2.7.2 Solute Atoms and Double-Kink Formation

Solute atoms can form dilute random or concentrated solid solutions. In the former, a given segment of dislocation line is affected only by a single solute atom, but in the concentrated solution, the given segment is affected by many solute atoms[57].

The self energy of screw dislocations is lower than that of the edge or mixed dislocations[74]. As such, the lattice resistance to the motion of screw dislocations is much higher in the b.c.c.lattice. A double kink is the lowest energy mechanism through which the dislocation can overcome such a large resistance. The alternative mechanism is dependent on the constriction of the extended core of the screw dislocation. Essentially, constriction requires about the same energy value as kink formation[57].

The solute atoms affect the nucleation of these double kinks through the type of interaction existing between the solute atom and the dislocations. The interactions could be penetrable (surmountable by thermal fluctuations) or impenetrable (can not be overcome by just thermal fluctuations) obstacles[78].

An increase in the number of impenetrable barriers leads to increased athermal internal stress. Tuominen and Koss[47] observed that this increase in athermal stress ultimately leads to a decrease in the thermal stress- a situation which would equate to a "pseudo-softening". Arsenault[78] demonstrated that for a given distance between barriers, a finite stress is required to

form a double kink. This stress is reduced as the distance between the barriers is increased.

For the penetrable barriers, Urkami and Fine[99] have suggested that a spherical defect could exert a torque on a screw dislocation and form a kink .

The cases above assume that the solid solution is dilute. If the solid solution is concentrated, the strain fields of the solid atoms overlap at concentrations above 0.1 at%[100]. This overlapping makes the study of double-kink formation more complicated[57]

2.3 Miscellany of Alloy "Softening"

2.3.1 Temperature Range of Occurance of Alloy "Softening"

Jolley[101] observed a merging of the yield stress of a pure iron with that of a 3.3% Ni iron (the latter was "softened" appreciably relative to the former) at about 77 K. This tends to the suggestion that the "softening" vanished below 77 K, but Jolley explained the merging on the basis that the pure iron (which was coarser in grain size) showed a higher incidence of twinning, thus reducing the yield stress of the pure iron.

Pink and Arsenault[57] advanced some arguments to invalidate any such suggestion that below a critical temperature,alloy "softening" ceases. The arguments are: once solute associations have been formed at some time during the preparation of the alloy, with the scavenging model, it is highly improbable for a drastic change from

this state below say,77 K. The second argument considers that the low-temperature effective stresses of impure metals (that show alloy "softening") never return to the original values of the impurity-free condition of the same metals.

2.3.2 Microscopic Aspects of Alloy "Softening"

Hildebrandt and Dickenshield[102],in their study of the Fe-Ni system, found that alloying increases the number of slip planes. It has also been found that alloying increases the tendency for alloys to form wavy slip lines (during deformation) in a wider range of temperatures, in comparison with pure metals[101-103]. Wavy slip lines in alloys after low temperature tests are said[101,103] to be a consequence of cross-slip. Cross-slipping results in dislocation tangles and cells; thus, wavy slip lines, observed optically, were associated with dislocation tangles and cells observed in the transmission electron microscope[103]. Pure metals, which after low temperature deformations revealed planar slip lines under the optical microscope, showed[101] a dislocation structure of relatively shorter segments and reduced density under the transmission electron microscope. Michalak[104] has suggested that a reduced dislocation density and short segments are consequences of dislocation cutting, which arises during very low temperature tests or very high dislocation velocities. These short segments are less effective in the thermal activation processes. Jolley[101] observed long dislocation

segments (without cells and tangles) of a relatively higher density in a "softened" 3.3% Ni steel; the associated optical microstructure was of wavy slip lines. He argued that the absence of cells is not an indication of the absence of cross-slip, and justified this by citing the presence of long dislocation segments which, it has been suggested[103], result from the lower mobility of jogged screw dislocations. It has also been explained[71] that the jogging of screw dislocations results from dislocation-multiplication by the cross-slip mechanism.

Some authors[104-108] have suggested that twinning preceeds yielding wherever both phenomena are possible. Hence twinning could reduce the yield stress. On the basis that twinning could reduce the yield stress, Jolley[101] rationalized the decrease of the yield stress of pure iron relative to 3.3% Ni iron, both tested at 77 K. Alloy "softening" has also been observed by other authors[109,110] simultaneously with twinning in b.c.c. alloys.

However, the work of Anderson and Spread-borough[54] tends to suggest that alloy "softening" may not be related to twinning. Some reports[111,112] have indicated that a crystalographic slip is necessary if twinning is to be initiated. Price[113] and Bell and Cahn[114] related twin formation to grain sizes. Their[113,114] work suggested that grain sizes larger than a critical size strongly favour the formation of twins. In the grain sizes smaller than this critical value, twins,

they suggested, may form if there are inhomogeneities in the grain size ditribution, or stress concentrations due to slip dislocation reactions.

2.3.3 Grain Size Effect on Alloy "Softening"

It has been reported[113] that in the Fe-Cr system, alloy "softening" occurs in single crystals, but not in polycrystals. While Keh et al[114] observed that alloy "softening" is more intense in polycrystals, Spitzig[117] observed that alloy "softening" is greater in large-grained specimens. Kelley and Stoloff[109], working on the same Fe-Cr system as Leslie et al[118],but with a grain size of 20 μm,observed an alloy "softening" effect at the low temperatures for chromium contents up to 2.8 wt%. However, Leslie et al[118], using grain sizes of 30 to 70 μm, only observed an increase of yield stresses for chromium levels up to about 3.2 wt% at the low temperature tests,Fig 2.4.

Pink and Arsenault[57] tried to rationalize, in terms of the scavenging model, the idea that a large grain size favours alloy "softening" more than does the small grain size. The small-grained specimen has far more grain boundaries than the large-grained specimen. These grain boundaries can also be viewed as "sinks" for impurity interstitials. Thus, the alloying solute has less impurity interstitial to scavenge from the matrix of the small-grained lattice. Therefore, the small-grained specimen should show less tendency to "soften" than the large-

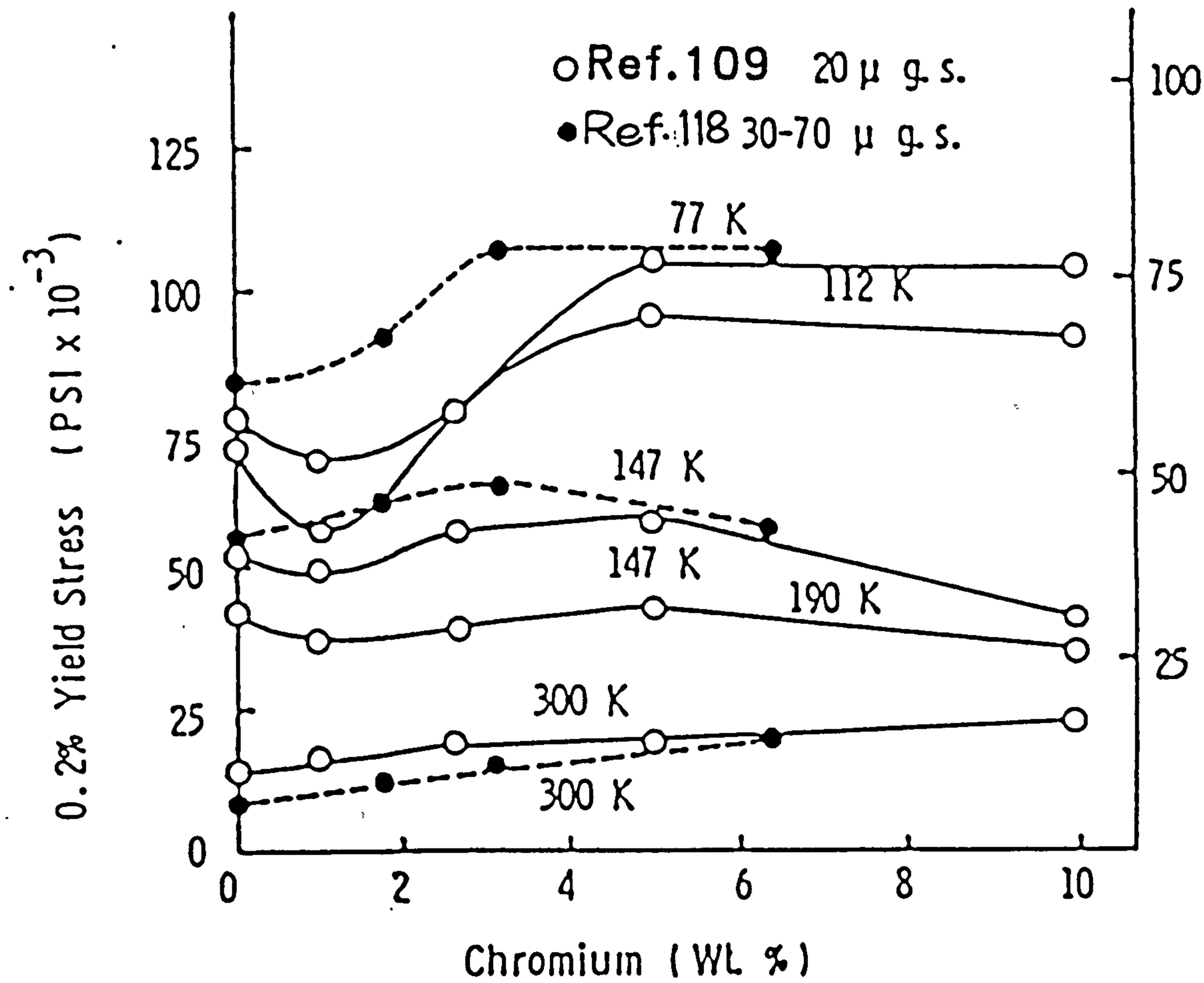

Fig 2.4: Effect of grain size on alloy "softening" in Fe-Cr system, (Ref 109).

grained specimen.

Christ[72] invoked the pile-up theory to explain a possible nucleation of new dislocations, which can facilitate alloy "softening". However, a pile-up of screw dislocations is not viewed to be stable, and therefore, the probable theory to explain the effect of grain size on alloy "softening" would be the model based on the dislocation density[57]

2.4 Alloy "Softening" and the Impact Transition Temperature, T_c

Petch[32] indicated that a ductile fracture will change to a cleavage fracture when the fracture stress, σ_f, is given as:

$$\sigma_f \geq 4\mu\gamma'/K_y d^{-1/2} \quad , \quad \ldots\ldots\ldots\ldots\ldots\ldots\ldots\ldots 2.7$$

where μ is the rigidity modulus of the material and γ' is the effective surface energy associated with the growth of a crack. Dieter[11] has suggested that a metal is brittle at temperatures below which the fracture stress, σ_f is defined as:

$$\sigma_y \geq \sigma_f \quad \ldots\ldots\ldots\ldots\ldots\ldots\ldots\ldots\ldots\ldots\ldots 2.8$$

On the basis of equations 2.7 and 2.8, Pink and Arsenault[57] have argued that, depending on the fracture mode (resulting from alloying), "softening" could affect the ductile-brittle (impact) transition temperature, T_c. Thus, if the alloying is such that a transcrystalline fracture is favoured, γ' is raised. Under these circumstances, the lowering of σ_y (simulated by the alloy

"softening") would lead to a further lowering of temperature, if the above conditions (eqs. 2.7 and 2.8) for a brittle fracture are to be satisfied. However, if the alloying is such that an intercrystalline fracture is developed, γ' would decrease. Thus, σ_f would also decrease, and the alloy "softening" may not be sufficient to mask the deterioration of the fracture stress. If only alloy hardening is present (at higher alloy concentrations), T_c should increase. They[57] pointed out that it is the co-relationship of the fracture stress with the apparent "softening" (see section 2.1, Fig 2.1a), and not with the "pseudo-softening" that would determine the variation of T_c. Thus, the reduction of T_c can manifest itself in two ways: if the T_c of the unalloyed metal (in practical terms, this would equate to metals already devoid of embrittling agents) is well situated in the apparent "softening" domain, and secondly, if the alloying element plays the dual role of scavenging the crystal (thereby increasing the fracture stress), and at the same time, "softening" the crystal.

Some experimental results[28,54] seem to confirm that a minimum in T_c is associated with apparent "softening", while others[53,120] showed an increase in T_c, though apparent "softening" was exhibited. The non-conformity of the latter group may be due to the embrittling precipitates at the grain boundaries[121], resulting from such alloy additions (for example,Al), which therefore reduces the fracture stress. However, it has also

been suggested[54] that whether a certain alloy addition (which leads to a "softening" tendency) reduces or increases the T_c may depend on the grain size of the alloy.

2.5 Survey of some Experimental Work on the "Softening" of Steels by Silicon.

"Softening", due to an increase of silicon content in steels has been reported[79,122] for room temperature tests. For steels however, room temperature is very likely to be above T_z (where the thermal component of the applied stress is zero); thus, this is not a typical situation of the alloy "softening", as defined in section 2.1[57].

Most of the experimental reports are for steels with silicon contents significantly greater than one weight percent and with grain sizes between 30 to 500 μm. Nunes[53], and Anderson and Spreadborough[54], however did consider steels with less than one weight percent silicon content. The study of "softening" by silicon discussed in most of the reports separated the two components of the applied stress- thermal and athermal. The explanations used the strain rate sensitivity and/or the activation parameters (equations 2.3 to 2.5) involved in the deformation process,since the thermal component is very much affected by temperature and strain rate[58].

An index of the strain rate sensitivity is found in the dislocation velocity exponent, m^*, defined[54], for

a given test temperature, T, as

$$m' = [\delta(Ln\dot{\varepsilon})/\delta(Ln\sigma^*)]_T, \quad \ldots\ldots\ldots\ldots\ldots\ldots 2.9$$

provided $\Delta\dot{\varepsilon}$ is not so large. m' is reported[54,123] to increase with silicon content (within 2,5 to 4.5 wt% Si).

Spitzig and Leslie[97] suggested that silicon additions decrease the change in activation enthalpy, ΔH^* (for a given value of σ^*) and the thermal stress for a given temperature, due to kink formations on the screw dislocations. These kinks in turn are due to the solute-atom dislocation interactions. They argued that cross-slip is insignificant in alloy "softening". This hypothesis, they based on the work by Barrett et al[124], which demonstrated (with silicon greater than 1.13%) that silicon additions favour the formation of planar slip lines. Spitzig and Leslie[97],however, do not support the increased dislocation frequency-factor model, but rather favour the increased dislocation model.

Some authors[42,123] do not support the scaveng-ing model, but rather suggest that it is the inherent lattice friction to the dislocations that is responsible. Any change in the dislocation properties could facilitate the reduction of this friction. Other reports[110,123] suggest that the "softening" by silicon may be due to a decrease in the stacking fault energy, SFE, of ferrite as a result of the movement of dissociated screw dislocations. The reduction of the SFE is due to a reduced twinning stress with the addition of silicon[110]. Zarubova[124] suggested that it is the co-operative glide of parallel

screw dislocations that appears to control the plastic deformation.

CHAPTER THREE

EXPERIMENTAL PROCEDURE

3.1 Material and Analysis

The steels used in this study were vacuum-melted and controlled-rolled by the British Steel Corporation, Swinden Laboratories, Rotherham. They were supplied as 15 mm gauge, 150 mm wide plates. The rolling schedule of the 15 mm plates, as provided by the manufacturer is shown in Table 3.1. The manufacturer also undertook a chemical analysis of the steels. Each steel grade was subsequently analyzed for solid elements with an emission spectrometer, "PV 8020" manufactured by Philips in the Metallurgy and Engineering Materials Division of this University.

The equipment was first calibrated with a plain carbon spectroscopic steel specimen, mechanically ground perfectly flat (so that no ingress of air takes place when placed over the aperture of the spark chamber). Several sparks on the flat test sample were made,each time ensuring that the burns do not overlap. The software offered the opportunity of rejecting burns that seemingly did not correspond to expectations,and calculating the average of accepted burns. Five burns were made for each sample, out of which one or two was rejected. The accuracy of the analysis by the spectrometer was ± 1%.

The oxygen and the nitrogen in the steels were determined with St. Joseph M1 (Leco Corporation) nitrogen-

Table 3.1: Rolling schedule* of the 15mm guage plates

Soaking time:1hr; T_{AUST}:1200° C;weight of vacuum melts:40 Kg

Pass no.	Guage mm	Aimed Temp. ° C	Actual Temperature, ° C Steel Grades (wt% Si) 0.156	0.31	0.53	0.78	1.03
Start	100		1185	1171	1174	1197	1190
1	85	1120	1120	1118	1115	1170	1118
2	75	1100	1089	1099	1084	1098	1099
3	65	1080	1082	1081	1080	1079	1082
4	55	1070	1069	1073	1070	1073	1067
5	50	1060	1059	1062	1066	1060	1058
	HELD,	TILL	DOWN	TO		1000° C	
6	40	1000	997	1000	999	992	1000
7	30	970	965	969+	969	970	971
8	25	940	932	905	940	927	939
9	20	920	910	888	918	911	916
10	15	900	894	837/807	885	901	897

* As prepared by BSC,Swinden Laboratories

\+ Mill broke down for this grade at this 7th pass.Rolling continued for the stock in the forward direction.

oxygen determinator, model 784-300 which uses fusion-extraction technique. The maximum reading of the equipment is 5000 parts per million (ppm) for nitrogen, and 3000 ppm for oxygen. The machine has an accuracy of ± 5%.

A calibration of the oxygen-nitrogen determinator was made, 0.3 t0 0.4 grams of the test specimen was placed in a graphite crucible and this was introduced into the vacuum furnace of the machine. The nitrogen was read out before the oxygen.

The analysis of the materials is shown in Table 3.2. From the manufacturer's and the University's analyses, cumulative errors were determined and are indicated in the table.

3.2 Dilatometry

Transition temperatures, A_{c1} and A_{c3} of each steel were determined by differential dilatometry using a Linseis dilatometer.

A heating rate of 10°C/min, corresponding to the maximum heating rate recommended by the manufacturers of the Linseis dilatometer was chosen. The cylindrical test-piece of a cross sectional diameter of 8mm had a length of 35 mm.The recording chart was temperature based and the amplifier rating used was 500 times. Above this value, the dilatometer's function became non-linear. Three samples were used for each determination.

Table 3.2: Chemical composition of the steel grades (wt%)

Steel code (VS)	C+	Si++ x10^{-1}	Mn+++	Al x10^{-3}	Ni x10^{-3}	P x10^{-3}	S x10^{-3}	B x10^{-4}	N x10^{-4}	O x10^{-2}
248	0.12	1.56	8.25	<0.5	27	<5	4	<5	2.3	4.1
249	0.12	3.1	8.25	<0.5	28	<5	3	<5	2.3	7.8
250	0.13	5.3	8.25	<0.5	25	<5	4	<5	2.3	8.5
251	0.13	7.8	8.3	5	28	<5	3	<5	2.3	7.0
252	0.13	10.3	8.37	11	28	<5	3	<5	2.5	4.0

Errors:- +: ±15%; ++: ±2%; +++: ±1%.

3.3 Heat Treatments

3.3.1 Heat Treatments to vary the Grain Size

Tensile blank specimens of 20 mm width and 120 mm in length were made from each grade. Each blank specimen was made with the long axis parallel to the rolling direction. The specimens of the five different grades were always simultaneously heat-treated.

Electrically heated room furnaces were used for reaustenitizing treatments. For an accurate reading of the temperature of the specimens,a Chromel-Alumel insulated thermocouple was imbedded in the specimens. The thermocouple had a tested accuracy of ± 3% above 400°C. It was connected to a digital millivoltmeter, from which the actual specimens' temperature was read.

The specimens were reaustenitized as shown in Table 3.3. Various cooling times achieved in the heat treatment codes A to D were possible through the use of the variable rheostat of the room furnace. Thus, depending on the position of this rheostat, the furnace could be made to heat and cool in cycles. For the shorter values of cooling time, the position was chosen so that a cooling cycle took three times that for a heating cycle. The position of the rheostat was changed at the highest value of cooling time in such a way that the time lapse for a cycle at the initial cooling period was rather short (about one-third the heating-cycle time). Subsequently, the cooling cycle time lapse was increased.

Table 3.3: Heat treatments used to produce grain sizes.

H.T code	T_{AUST} ±8° C	Tim.at T_{AUST} min.	Cool.tim.to lower temp. min.	Frnce.Temp.bef. spec.removal† ±8° C
A	955	45	160	719
B	1053	80	250	719
C	1115	360	420	710
D	1216/1083*	150/30*	990	684
E	910	60	Cooled with compressed air to Room Temperature.	
F	900	30	Transfered to a Sn bath at 553° C,waited 3 mins.,quenched in cold water.	

* Transfer to a lower temperature furnace.

† Aircooled to room temperature

Increasing the undercooling, ΔT of an austenite to ferrite transformation leads to finer ferrite allotriomorphs[30]. This is because ferrite mostly grows by the diffusion of carbon into the austenite[127]. Hence, the undercooling reduces the tendency of the carbon atoms to diffuse into the austenite.

To this end, the finer grain sizes were realized by a rapid cooling of the specimens from 900°C and 910°C, as indicated in heat treatment codes E and F (Table 3.3). However, the interest was to produce the smallest possible grain sizes with a ferrite-pearlite structure, so the need arose to use a tin bath. To determine the temperature of the molten tin to avoid a martensitic or a bainitic transformation, use was made of an empirical formula[128] relating the Ms (martensitic transformation start temperature) to the alloying elements (in weight percent) as:

$$Ms=561-474(\%C)-33(\%Mn)-17(\%Ni+Cr)-21(\%Mo) \quad ...3.1$$

Silicon is not included in this empirical formula, but in terms of its contribution to the hardenability of steels (through the formation of martensite), its effect has been described[128] as moderate. Thus, the Ms of the steels should be about 472°C. Hence,the choice of 553°C as the temperature of the molten tin to avoid the formation of martensite. There was also a requirement to avoid the formation of bainite. Therefore, the specimens (introduced into the bath through a nichrome wire) were held in the bath only for the uniformization of the temperature of the specimens with that of the bath. There was also the need to

repress any growth of the unstable austenite. So, the shortest incubation time range of the TTT curve, Fig 3.1, was aimed at, and was found to be 3 to 5 minutes. Time intervals above this did not lead to a bainitic transformation, but however led to slightly coarser ferrite allotimorphs than those obtained within the 3 to 5 minute-hold. Subsequently, the blanks were quenched in cold water.

A batch of these specimens was aged for 30 minutes at 550°C

The tensile blanks were not heated under vacuum, but their dimensions were such that all the decarburized layers were more than compensated for, and did not constitute a problem, even at the highest austenitizing temperature.

3.3.2 Heat Treatment to Determine the Prior-Austenite Grain Size (Oxidation Procedure). Aging of the 0.78 and the 0.31 wt% Si Steels.

Following the ASTM standards[129] from which Bepari[130] demonstrated that the oxidation technique is quite satisfactory for determining the prior-austenite grain sizes in 0.15% carbon steels, an oxidation technique was used in this study. 20x20x15 mm specimens from the five steel grades were polished by conventional metallographic methods on one side and heated at 900, 955 and 1053°C respectively in an argon atmosphere. They were austenitized and soaked for the times corresponding to heat treatment codes A, B and F respectively, exposed to the air for about

one minute before being quenched in iced brine.

Some of the 0.78 and 0.31 wt% Si steels, prior annealed according to heat treatment code C,were aged under a vacuum of 10^{-4} torr at 595±10°C for 72 hours.

3.4 Metallography

Metallographic specimens were prepared from the heat-treated samples by mechanical grinding and polishing. Those used for the study of the ferrite-pearlite structure were etched in 2% nital, while those used for the prior austenitic grain size determination were etched in a 4% picral solution by immersion for about 40 seconds. The specimens for the slip-line studies were chemically polished with a solution of 80% hydrogen peroxide (30% w/v), 5% hydrofluoric acid and 15% water. The fractured round specimens (in the tests at 77 K, with a strain rate of $3,3x10^{-4}$ s^{-1}) for the twin study were sectioned longitudinally. They were ground, polished and etched in Fry's reagent, made up of 5g $CuCl_2$ in 40 cm^3 HCl, 30 cm^3 water and 25 cm^3 methanol.

The optical microscope, "Leitz Wetzlar 3745" (which allows the measurement of grain sizes and micro-hardness) was used for the quantitative aspects of the optical study. It has a micrometer which was read off after a number of grain boundaries were traversed within a field of view; thus the magnification value is only necessary for the vizual counting of the traversed boundaries. Triple boundary intersections were counted as two intersections.

The optical micrographs were taken using a "Nikon Epiphot" inverted metallurgical microscope.

3.5 Carbon Extraction Replicas

The aged 0.78 and 0.31 wt% Si steel samples were more deeply etched in 2% nital to facilitate the extraction of the particles. Carbon was evaporated on to the specimen in a Balzers High Vacuum Coating unit, "Mikro BA3",with a vacuum status of about $5x10^{-5}$ torr. The aimed thickness of the carbon film was 200 to 400 Å. This was estimated using the colour-change (of the specimen's surface) guide provided in the equipment's manual, of which the colour could be Indigo red (200 Å), blue (240 Å) or blue-green (350 Å) from interference fringes developed during the build up of the carbon film.

The coated specimens were scored to produce sections of the replica small enough to be lifted on to the copper grids. The replica was etched out using 9% perchloric acid in 91% acetic acid, for about 30 minutes. The replica sections were twice washed in methanol before being transfered into a beaker of distilled water. Under the surface tension of the water, the sections unroll themselves. They were collected on to the grid and dried.

3.6 Thin Foil Preparation

The annealed, aged and the 8% tensile strained flat samples were cut into about 2 mm slices, using the diamond saw. Then, 3mm discs were made from the slices

using a Metals Research Servomet Spark Machine.

The discs were subsequently manually ground on the emery papers down to between 80 to 110 μm.

A Struers "Tenupol" equipment was used to electropolish, with 5% perchloric acid (70%) in 95% acetic acid as electrolyte,at a temperature between 13 and 15°C. The optimum current was 200 mA and the corresponding voltage (between 85 to 110 volts) was found to depend on the thickness of the prior-manually ground specimen, the temperature of the electrolyte and the thickness of the stainless steel anode (strip); the thicker the stainless steel strip or the lower the temperature of the electrolyte, the higher the voltage. Depending on the thickness of the prior-ground specimen, the time lapse for the hole to appear was 50 to 70 seconds. Successive washing in acetic acid and methanol was employed to eliminate the contamination of the specimen on completion of thinning.

3.7 Transmission Electron Microscopy

The thin foils and replicas were examined in a "Philips" EM 400T operated at 100 KV. A camera length of 800 mm was usually chosen for the diffraction studies. This was because the calibration of the microscope with MoO_3 crystals (made for determining the angle of rotation of a bright field image, with respect to the diffraction pattern) was made for this camera length at 100 KV.

3.8 Energy Dispersive Analysis of X-Rays (EDAX)

The transmission electron microscope is furnished with a detector to collect the X-rays from thin specimens. These rays are analyzed by the machine based on their energies. A qualitative examination was carried out on the replicas using a beam, with the microscope's spot size knob at the number three position (corresponding to 0.4 μm probe size), and adjusting the intensity of the beam with the knobs of the second condenser, till an acceptable count rate, but less than 6000 counts per second- pink colour, was attained.

Following the observations made by some investigators[131,132] regarding the reproducibility of EDAX results, the following procedures were adopted during this qualitative analysis:

i) a compromise between the beam time and the X-ray count level was made. A higher X-ray count leads to a lower counting error, but this demands a longer beam-time which allows the possibility of a serious sample contamination by "spurious" radiation.

ii) a reduction in the degree of absorption of the radiations and fluorescence from areas of the specimen, away from the electron probe. This may be facilitated by tilting the specimen towards the detector. Absorption may lead to errors in the analysis. Checks were made to ascertain if there was any change in the

analysis between the 0 and the 20° tilts,but there was no significant change.

iii) a small probe size reduces the effect of beam broadening (beam broadening could introduce "spurious" radiation), but leads to a long counting time. Therefore, an optimum probe size was used which did not require an excessively long time to build up a significant count.

iv) a repetition of the analysis for at least five times, out of which no consistent variation occured.

3.9 Tensile Testing

Rounds of 6.40 ± 0.02 mm diameter, (the average from 3 readings,along the parallel length of the piece), Fig 3.2a, were made from the blanks.Flat tensile pieces of 5 x 3 mm^2 cross section, Fig 3.2b, were made from the large and small-grained 0,156 and 1.03 % Si steels.

The low temperature tests were carried out at 77, 153 and 223 K. For the tests at 77 K, liquid nitrogen was used as the medium, while petroleum ether (with 40 to 60°C boiling point) was used as the medium,cooled with liquid nitrogen for the tests at 153 K. The tests at 223 K were done in methanol (as the medium) and liquid nitrogen (as the coolant). A temperature variation of ±5°C was maintained in the tests at 153 and 223 K. The medium and the coolant were held in a stainless steel bath, made

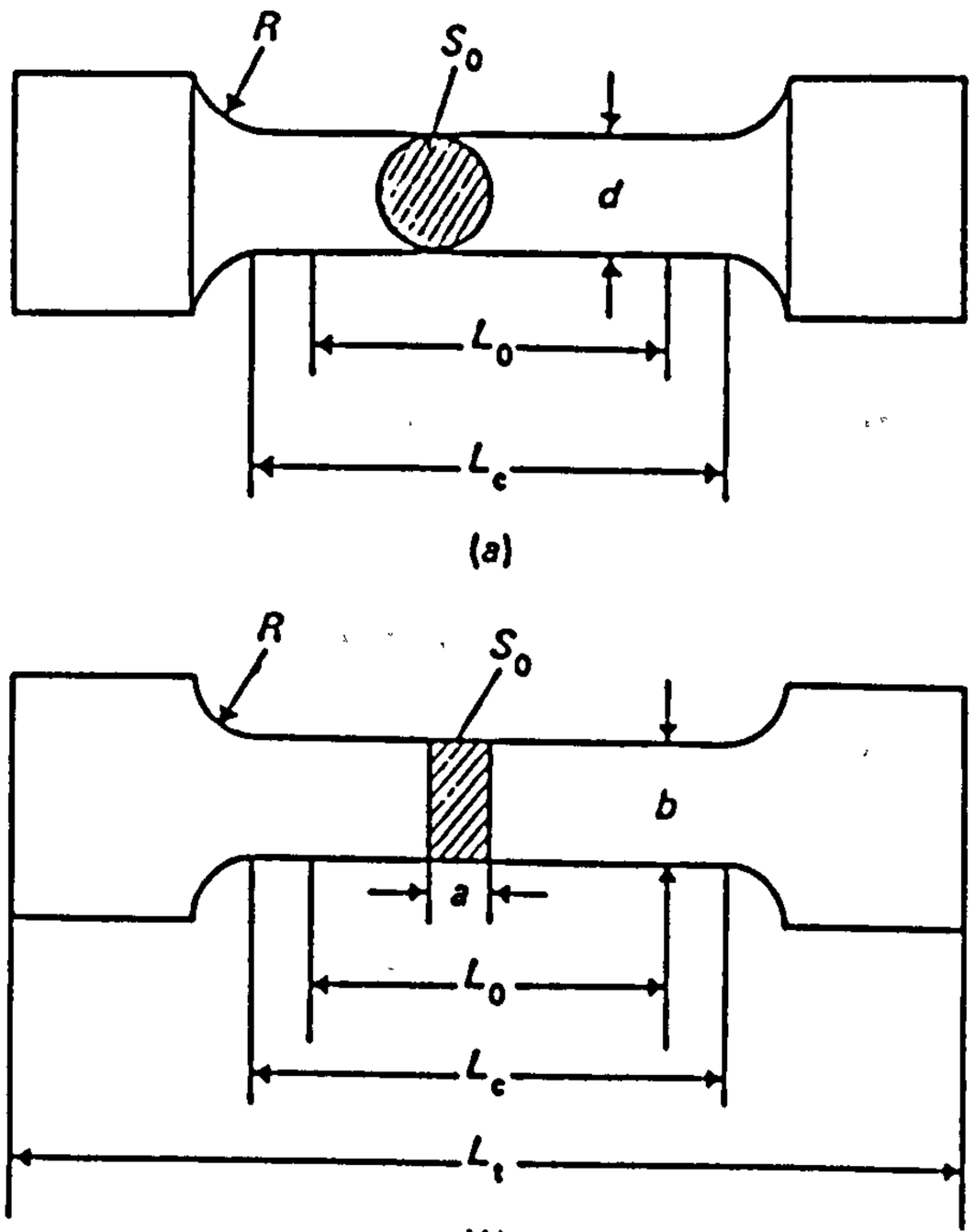

Fig 3.2: Schematic diagrams of the tensile pieces, a), round piece; b), Flat piece.

Dimensions, mm	Round	Flat
R	1.2	6
a	-	3
d/b	6.4	5
L_o	23	22
L_c	26	28
L_t	-	42
S_o (sq)	32	15

specifically for this study. The flat specimens were only tested at room temperature and 77 K. For the tests at 77 K,the gauge length of the flat pieces was covered with glass wool and liquid nitrogen was continuously poured on to the wool. In each low temperature test, the specimen was allowed up to 10 minutes in contact with the medium, to ensure that it had cooled down to the aimed temperature.

Each test was repeated for the rounds of all the steel grades, and the average value was taken. The tests were done on an Instron Universal Testing Machine- model 1114, with a load weighing accuracy of ±0,5% of the indicated load or ±0.25% of the recorder scale, whichever was greater, for all the range of loads. The cross-head speed is synchronously controlled to an accuracy better than ±0.1% for all the specified cross-head speeds and loads. Prior to the tests, the machine was calibrated with a full-scale-load of 25 KN and 30 KN, depending on the anticipated strengths of the samples to be tested.

A strain rate of $3.3x10^{-4}$ s^{-1} was used for the testing of the rounds and flats at room and sub-zero temperatures. The prior chemically polished flats were only 8% tensile strained, while the rounds were tested to fracture. A batch of the rounds, for all the steel grades, was tested with a strain rate of 0.33 s^{-1} at 153 K. Another batch of the rounds for all the steel grades was tested at 350 K, with a strain rate of $1.7x10^{-4}$ s^{-1}.

Total elongation and reduction of area (after the fracturing of the specimens) were measured, using standard

fracturing of the specimens) were measured, conform to ASTM standards[173], using standard tensometric instruments.

CHAPTER FOUR

EXPERIMENTAL METHOD

4.1 γ/Ferrite Grain and Pearlite Colony Size Measurements

The mean intercept length method has been used by some authors[133,134]. This is a method whereby the grain boundaries are counted upon being traversed by a line in a field of view, using an optical microscope. In the past, there was always the need to divide the final result by the magnification used, but with the microscope used in this study, this practice was not necessary. Thus, a number of grains, N, of the constituent of interest was traversed in many fields of view and the sensitive micrometer, attached to the stage,which measured the actual length of the traversed grains was read directly.For the ferrite/pearlite structure, it was necessary to subtract the length of the constituent that was not of interest from the entire traversed length. Therefore, while the counting was in progress, a record of the individual lengths of the constituent not of interest was kept. After the desired number, N of grain /colony boundaries was counted, the recorded individual lengths were summed up and subtracted from the entire length read on the micrometer.Six different fields,i,of 100 boundaries of interest were made;i.e. a total number of 600 grains or colonies were intercepted for each specimen.

There is a problem with the mean lineal intercept method: most of the time, within a field of view, the

segments of the grain/colony cut by the line range from zero to the maximum dimensions, with very few constituents being actually cut through the maximum dimensions[135]. However, Underwood[134] pointed out that the important parameter in randomly orientated grains, is the average distance across the grains,rather than the maximum dimensions.

It was necessary to determine the standard deviation, σ_{n-1} of the values of the grain/colony sizes so obtained for an estimation of the statistical error. To this end, an approach similar to Abram's[137] was used in this study. If all the steel specimens, after a particular heat treatment, are of a fairly uniform grain/colony size distribution, the ratio, $\sigma_{n-1}/\bar{X}$ (known as the coefficient of variation, C.V., $\bar{X}$ is the average grain/colony size) should be constant. Assuming that the average grain/colony size from a field of view is $\bar{q}$, the average grain/colony size, $\bar{X}$ for the six fields of view would be:

$$\bar{X} = (\bar{q}_1 + \bar{q}_2 + \ldots\ldots + \bar{q}_6)/6 \quad \ldots\ldots\ldots\ldots\ldots 4.1$$

The standard deviation, σ_{n-1} would be:

$$\sigma_{n-1} = [\sum_{i=1}^{i=6}(\bar{q}_i - \bar{X})^2/(i-1)]^{1/2} \quad \ldots\ldots\ldots\ldots\ldots 4.2$$

In this work, the coefficients of variation for the two heat treatments (codes C and D) were found to be fairly constant, with a value of 0.07.

Chatfield[138] has defined the 95% confidence limit as:

$$\bar{X} + t_c(\sigma_{n-1}/i^{1/2}), \quad \ldots\ldots\ldots\ldots\ldots 4.3$$

where t_c is a statistical constant varying from 1.96 (for

i=20 to infinity) to 3.18 (for i=4). In this study, i=6, and t_c was taken to be 2.77. The term, $t_c(\sigma_{n-1}/i^{1/2})$ can be denoted as $\triangle\bar{X}$, and it is the statistical error of the evaluation. This was found by Lapointe[134] to be equal to $1.3\bar{X}/N^{1/2}$. In this work, $\triangle\bar{X}$ was found to be:

$$\triangle\bar{X} = (1.9\pm0.2)\bar{X}/N^{1/2} \quad \text{.....4.4}$$

Lapointe had a $\triangle\bar{X}$ value of less than 6% fitting into his 95% confidence limit, with a total number,N of traversed grains as 500. However, in this work, the $\triangle\bar{X}$ was found to be 8.7±0.7%, with a total of 600 grains/colonies traversed. The slightly higher error value in this work may be because of the wide range of grain sizes (7 to 76 μm) used; for example, the error of the 76 μm grain size sample was 6.7%, while the 7 μm grain size sample had an error of 12.5%.

The viewing (under the optical microscope) of the very small-grained samples of the 0.78 and the 1.03% Si steels, treated according to the heat-treatment code F was eye-straining. To improve the reliability of the results therefore, the transmission electron microscope was used to recount the grains in these samples (Appendix A), and their sizes were corrected by about-8% and-4% for the 1.03 and the 0.78 wt% Si steels respectively. The samples of the other steel grades did not require such a correction.

4.2 Pearlite Volume Fraction Determination

If the constituent of interest is randomly distributed, and its volume fraction is low, Hilliard and Cahn[13] suggested that the volume fraction can be

expressed from a lineal analysis as:

$$(1/N)[(\sigma_{n-1}/\bar{t})^2+1], \quad \ldots\ldots\ldots\ldots\ldots\ldots\ldots 4.5$$

where σ_{n-1} is the standard deviation of the intercept lengths of the constituent, N is the number of intercepts the constituent makes within a traverse of a given length. $\bar{t}$ is the average intercept length. The error by this method, they suggested, is given as $1/N^{1/2}$, excluding the experimental error.

Their method was used to evaluate the volume fraction of the pearlite constituent in the steels under study. The intercepts across the pearlite were three hundred; i.e. the number of intercepts within a given length read on the micrometer was far more than three hundred. The error, with three hundred intercepts, as proposed by Hilliard and Cahn[139], would be ±5.8%, but it was found to be ±8.6% (95% confidence limit) in this work.

4.3 Determination of Slip Band (Line) Spacings

Slip-band spacings have been used[21,140] to characterize the yielding behaviour of metals. In their[21,140] approach, visible slip-band spacings were related to stress and strain. The average slip-band spacings of interest were those at the grain boundary, S_{gb}, in the body of the grain, S_g and for the entire grain volume (i.e. grain boundary and the grain interior), S_{av}.

Margolin and Stanescu[21] gave various relationships for these quantities, but for the purpose of this work, the average slip-band spacing per grain, S_{av} was

of interest. S_{Av} is defined as:

$$S_{Av} = D/n_{gb}+n_b, \quad \text{.....4.6}$$

in which D is the average grain diameter (i.e. the grain containing the slip-bands; in a ferrite-pearlite structure, this is the ferrite grain), n_{gb} is the average number of slip bands in the grain boundary deformation region, and n_b is the average number of slip bands within the grain.

A differentiation of n_{gb} from n_b was not made in this work, so the average number of slip bands, within the grain (both at the grain boundary region and the interior of the grain) was used to study a number of samples strained 8% in tension at 77 K.

4.4 Determination of the Interlamellar Spacing of Cementite

A method similar to that used by O'Donnelly[41] was used. However, instead of using the scanning electron microscope, the transmission electron microscope was used.

Micrographs of the pearlite colonies (from different steel grades that underwent the same heat treatment) were taken at a suitable magnification, M. These micrographs were further magnified by N times on being printed.

The random intercementite spacing, l_r was then measured in the pearlite by a linear intercept technique. This was done in twenty fields for each micrograph. Thus, the average interlamellar spacing, $\bar{l}_r$ was found using the

relationship:

$$\bar{l}_r = \sum_{i=1}^{i=20} l_{r,i}/20NM \quad \text{.....4.7}$$

The error (95% confidence limit) determined in the study was ±20%

4.5 Identification and the Estimation of the Volume Fraction of Precipitates

Selected area diffraction technique was used to obtain the diffraction spots of both the matrix and the precipitates.

Agar[142] demonstrated that for a fairly accurate use of this technique, the correct optical conditions must be met. Thus,an intermediate image was obtained with the objective aperture removed, then the selector diffraction aperture was introduced. At the correct focussing of the intermediate image, the selector aperture appeared clean and sharp. The objective aperture was replaced, and a final focussing was made, to ensure that the intermediate image coincided with the selector aperture. The objective aperture was now removed, and the microscope put into the diffraction mode.

Even with the correct optical conditions, errors are still very likely in the identification of small crystals. These errors are due to the spherical aberration of the objective lens, and an incorrect focussing of the objective lenses[142,143]. The error due to the spherical aberration, Δr of the objective lens is given as:

$$\Delta r = C_s \alpha^3, \quad \text{.....4.8}$$

where C_s is the spherical aberration constant, and α is the angle the diffracted beam (hkl reflection) makes with the transmitted beam. The error, Δr for incorrect focussing is given as:

$$\Delta r = D\alpha, \quad \text{.....4.9}$$

where D is positive and negative for overfocussing and underfocussing respectively. Thus, the major error comes from the spherical aberration, where the error is proportional to α^3. The interplanar spacing measurements very much depend on the camera constant, λL, which is given as:

$$Rd = \lambda L, \quad \text{.....4.10}$$

where R is the distance from the central (transmitted) spot to the (hkl) reflection, d is the interplanar spacing of the crystal diffracting, λ is the wavelength of the electron beam and L is the distance of the specimen from the screen or plate (also called the camera length). Phillips[143] showed that the camera constant decreases slightly with an increasing order of reflection.

In view of this strong interrelationship of the accuracy of identification with α, reflections of lower order (reduced value of α) were used wherever possible. The camera lengths, which very much depended on the specimen height, was determined with the known alpha-iron reflections. This was then used to identify the precipitates.

The nature of the crystal could lead to complex diffraction patterns. Thus,very thin precipitates could

lead to the streaking, broadening[144] and/or splitting[145] of the precipitate spots. The broadening leads to the extension of the reciprocal lattice points perpendicular to the plane of the film[144]. The curvature of the reflecting (Ewald) sphere implies therefore that those reflections with angle, α (which is now relatively large,due to broadening) would have an interplanar spacing, d_α given as:

$$d_\alpha = d(1-\alpha^2/2), \quad \text{.....4.11}$$

where d is the real interplanar spacing value.

To minimize these effects, the d spacings were measured from the brightest parts of the broadened or split spot.

Outside these optical and crystallographic limitations, De Jong[146] has reported that errors also do arise in the reproducibility of magnifications in transmission electron microscopy (TEM) due to the magnetic hystereses in lenses. Thus, the reproducibility of results is reduced to not less than $\pm$1.5% in the TEM. In this work, the error involved in the measurements of the interplanar spacings was 2$\pm$0.7%.

The crystallographic relations that were observed between the cubic alpha-iron matrix and the hexagonal precipitates, the latter being for c/a ratio of 0.73, were verified by preparing a stereogram, with $001_{\alpha\text{-Fe}}$ // 0001_{hex} in the centre of the projection, Fig 4.1. The stereogram was rotated and found to agree with the orientation relations observed experimentally, thence the consistency

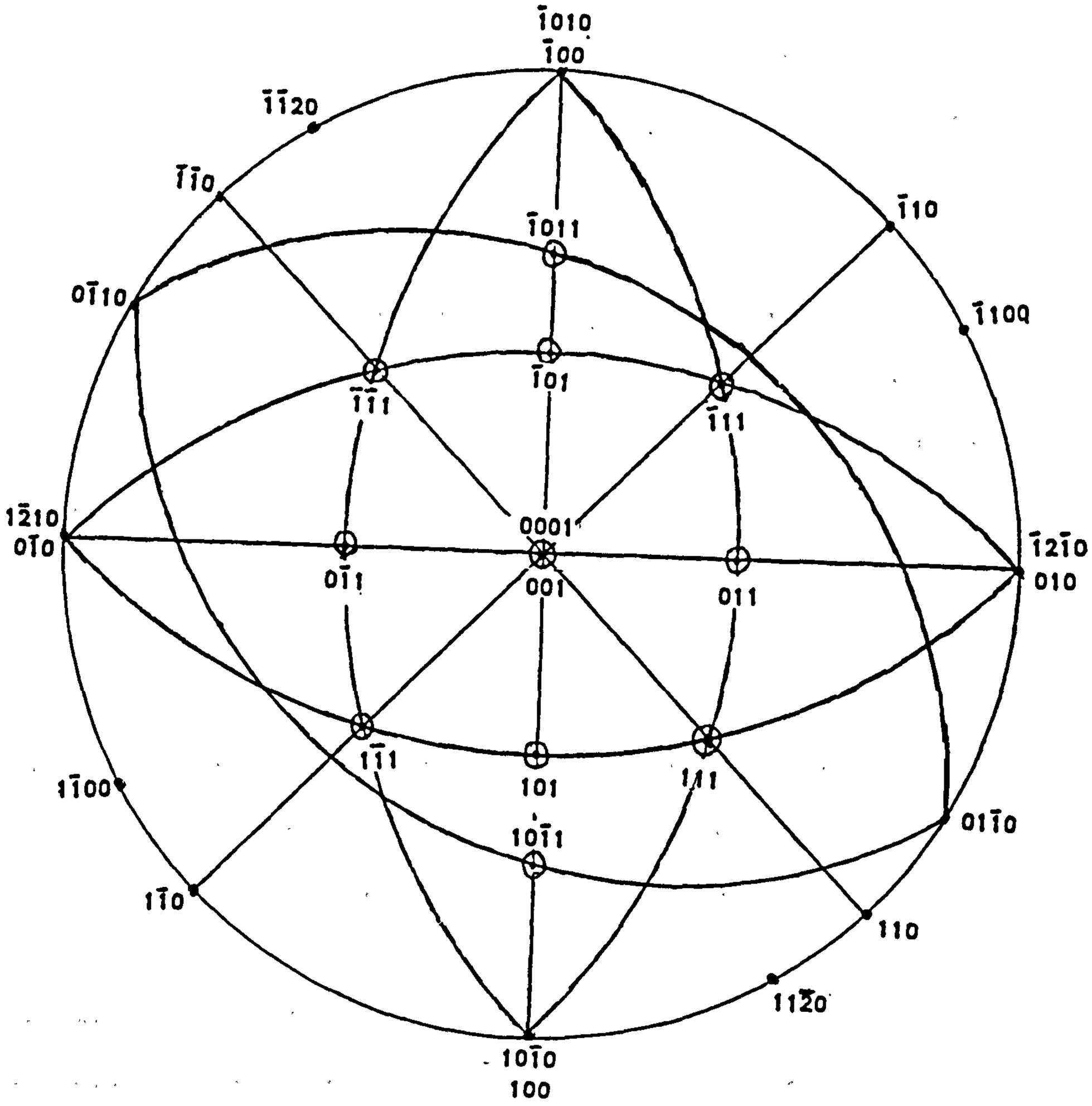

Fig 4.1: Stereogram from the cubic and hexagonal (latter being for c/a=0.73, α-Si_3N_4) systems, with $001_{cub}//0001_{hex}$ in the centre of the projection.

of the relations was proven. The volume fraction of the precipitates was calculated stoichiometrically, and found to be a maximum of 5.8×10^{-3} (see Appendix B).

4.6 Thermal Activation Parameter Studies

Most studies[52,55,56-58,42] of thermal activation parameters utilized the effective (thermal) stress. The effective stress, σ^* at a given strain rate and test temperature is defined[55] as:

$$\sigma^* = \sigma_y - \sigma_a, \quad \text{.....4.12}$$

where σ_a is the athermal stress of the material. The choice of the athermal stress amongst authors has always been arbitrary, but the basic reasoning behind the choice is that the thermal stress should be zero. Conrad[74] suggested that the athermal stress is the yield stress of the material tested at 300 K, with a time of yielding of approximately one second, or the yielding stress in a test at 300 K, with a strain rate of 10^{-1} s^{-1}. It has been indicated[147] that the athermal stress can also be the yield stress in a test at 350 K, with a strain rate of 10^{-4} s^{-1}. Tanaka and Watanabe[42] considered as athermal stress, the yield stress of the steels tested at 318 K with a strain rate of 4.2×10^{-4} s^{-1}.

In this work, the athermal stress was determined following the indication made by Conrad and Hayes[147]. Thus, a special tensile test at 350 K, with a strain rate of 1.7×10^{-4} s^{-1} was carried out to determine the athermal yield stresses. The athermal stresses were then evaluated

for various grain sizes.

Sandström and Bergström[55] considered the dislocation dynamics of a thermally activated process, and related the effective stress, σ^* constitutively to other parameters thus:

$$\sigma^* = \sigma_a^*(\dot{\varepsilon}/\upsilon)^{T/T_o}, \quad \ldots\ldots\ldots\ldots\ldots\ldots\ldots\ldots 4.13$$

and

$$T/T_o = 1/m', \quad \ldots\ldots\ldots\ldots\ldots\ldots\ldots\ldots 4.14$$

where T is the absolute testing temperature. T_o is a constant relating to the kink energy[148] of the material, its unit is in degrees K. $\dot{\varepsilon}$ and υ are as defined in equations 2.2 and 2.5 respectively. σ_a^* is the effective stress of the material at 0 K, and it is obtained by extrapolating[147] a semilog graph of Ln σ^* versus test temperature to 0 K. It is a constant which does not depend on the state of the material or the conditions of the test.

In this work, from the data of the two strain rates for the test temperature of 153 K, the m' values were evaluated using equation 2.9. Thus, it was possible to evaluate the values of the dislocation frequency factor, υ, for the respective grain sizes.

The activation energy (H) and volume (V') for the various grain sizes were then evaluated using equations 2.3 and 2.4 respectively.

CHAPTER FIVE

EXPERIMENTAL RESULTS

The results are presented in subject areas of grain size and strengthening, "softening" and thermal activation parameters. The tables and figures refered to in the presentation are at the end of this chapter, in the numerical order of presentation.

5.1 Grain Size and Strengthening Studies

5.1.1 Measured Ferrite Grain Size

The ferrite grain sizes produced by the heat treatments (Table 3.3) used in this study are as in Table 5.1. Also in this Table are the values of the tensile properties of the room temperature test with a strain rate of 3.3×10^{-4} s^{-1}. The error margins indicated for these tensile properties are within the 95% confidence limit of the statistically processed errors of individual tests. Owing to some unavoidable experimental circumstances (for example, owing to poor machining of certain samples, such samples presented rather unusual results; or, sometimes it was forgotten to note down the average cross sectional diameter of the guage length), some grades ran short of specimens for tensile testing. Thus, in some cases, a second batch (single asteriks in Table 5.1) of the grade (heat treated under the same conditions of the stipulated

code) was necessary.

5.1.2 Measured Prior Austenite Grain Size

Similar heat-treating conditions as used in codes A, B and F (excluding the cooling times) were used to produce the prior austenite grain sizes shown in Table 5.2. The need for this study arose out of the observation (from the ferrite grain study) that silicon additions may be inhibiting grain growth.

The ratios of the prior austenite grain size to the ferrite grain size (d_γ/d_α) were computed from Tables 5.1 and 5.2 (in the case of the 0.53 wt% Si steel, this computation was done with the first batch of code F, Table 5.1). These values were plotted against the silicon content in the steel for the different solutionizing temperatures, Fig 5.1.

The interpretation of Fig 5.1 is specifically for the individual temperatures. Following the time differentials from one temperature to another,as in Table 3.3, the ratio at one temperature for a given steel does not necessarily compare with the ratio from another temperature.

5.1.3 Dilatometry

Consequent upon the observation regarding a possible inhibition of grain growth by the additions of silicon, a dilatometric study was carried out. The results are as shown in Table 5.3 and Fig 5.2, the latter being the

actual curves obtained from the experiment. The initial additions of silicon, infact, reduce the transformation temperatures. From Table 5.3 and Fig 5.2, it is evident that it is from the 0.53% Si content level that an increase in the transformation temperature started to occur.

5.1.4 Microstructures and Room Temperature Tensile Properties

All the grades of steel in the as-received condition had the same grain size of 15±2 μm, Fig 5.3.

In Fig 5.4 are the optical micrographs of the grain sizes produced from heat treatment codes A and D. The corresponding (to ferrite grain sizes produced from codes A and B) prior austenite grain sizes are in Fig 5.5. Note the decreasing trend in grain sizes of both the ferrite and the prior austenite, as the silicon level was increased. Note also the extent of oxidation in the prior austenite micrographs of the B code.

A low volume fraction of Si_3N_4 precipitates were observed in all the steels in the annealed condition. In Fig 5.6 are examples of such precipitates, observed in the thin foil specimens of the 1.03% Si steel,heat-treated according to the A code.

Fig 5.7 shows the electron micrographs of the 1.03, 0.78, and 0.31% Si steels (heat-treated according to the F code),in the 30 minute—550°C aged (only the 1.03% Si steel) and unaged conditions. The structures are the same; however, the unaged specimens had some extremely fine

grains (for the 1.03% Si steel in particular, and to a less extent, for the 0.78% Si steel too) as a result of the quench. On ageing (subsequently refered to as "short-ageing",because it was at 550°C for 30 minutes;thus differentiating it from the main ageing treatment that would be reported later), it would appear that they showed a small increase in size. This short-ageing was necessary, for all the steel grades, but particularly for those under the heat treatment codes with relatively short time durations, to enhance a further segregation of solutes to the grain boundary. As already mentioned in section 4.1 (appendix A), the grain sizes determined from the optical micrographs for the 1.03 and 0.78% Si steel grades were recounted using the transmission electron microscope, and had to be corrected by about -8 and -4% respectively. The rest of the steel grades did not need any such correction,as the quench did not produce very fine grains in them.(example, the 0.31% Si steel,Fig 5.7c).

The room temperature tensile properties of the steels in an unaged condition are in Table 5.1.The σ_y values were plotted against grain size ($d^{1/2}$),and are shown in Fig 5.8a (with the regression equations inserted) This same figure is reproduced in multiple slope, Fig 5.8b, to emphasize the start of the tendency of K_y to assume lower values,for steels that showed very fine grain sizes.Fig 5.8c is the graph of σ_y versus $d^{-1/2}$ of the short-aged steel grades. It can be seen that the short-aged specimens normally gave a lower value of K_y. Owing to the general

tendency of the K_y value to be reduced with the addition of silicon to the steel (up to 0.78% Si), below a certain grain size, about 8.8 $mm^{-1/2}$ (13μm) and 11.2 $mm^{-1/2}$ (8 μm) in Fig 5.8 (a and c respectively), the lower silicon steels had higher strength values than the higher silicon steels.

Consequent upon the reduction of K_y at higher silicon levels (up to 0,78 wt%) in the steels, the degree of strengthening due to Si additions (expressed as the change in σ_y, $\triangle$LYS, obtained from regression equations in Fig 5.8a), decreased with a reduction in grain size, Table 5.4.

Attempts were made to rationalize the reduction of the K_y value in terms of the observed ledges in the steels. The very rarely observed ledges in the 0.31 and 0.78% Si steels are shown in Fig 5.9. It is noteworthy the fact that the density of rezolvable ledges was higher in the 0.78% Si steel, Table 5.5.

The immediate observation, from the steel grades treated according to the heat treatment, code D, viewed under the optical microscope, Fig 5.10, was that the higher silicon steels showed thicker decarburized layers. Thence, a study of the data from the pearlite in three of the grades (0.31, 0.78 and 1.03% Si steels) was undertaken, Table 5.6. From this table, it can be seen that above 0.78 wt% Si content in the steel, the volume fraction of the pearlite decreased, but the colony size increased. At all silicon levels, a higher silicon content in the steel led to a thicker decarburized layer, A-B in Fig 5.10.

There was the risk that the regime of treatment

of the F code of heat treatment, which involved a large undercooling could create a situation favouring the creation of transformation dislocations[30]. Such a risk,when rife,could lead to the dislocation structure of the unaged steel grades,differing amongst them or from that of the short-aged specimens. However, this was not the case, as the structures of the short-aged and the unaged specimens were similar in all the steel grades, Fig 5.11. The 1.03 wt% Si steel grade that showed the finest grain size (code F), thus had the highest probability of such a risk, and the more slowly cooled 0.31 wt% Si steel grade (code D),which gave the coarsest grain size, were used for this demonstration.

The same precipitates as observed under the annealed condition (Fig 5.6), but with a higher volume fraction, were also observed on ageing at 595 ± 10°C for 72 hours under a vacuum, of the prior-annealed 0.31 and 0.78% Si steel grades, heat-treated according to the C code of the heat treatments, Fig 5.12. This ageing treatment was used to investigate if the Si_3N_4, precipitated in the annealing treatment would transform to SiN, Mn-Si nitride or another form of silicon nitride (different from that precipitated in the annealing treatment). The precipitates in the aged 0.78% Si steel were extracted onto a carbon replica. This is shown in Fig 5.12c. The fact that some of the diffraction spots from the precipitates, shown in the thin foil micrographs, Fig 5.12a and b, are co-linear with those of the alpha iron is noteworthy. These precipitates

were identified as low temperature (α) Si_3N_4, with c = 5.617 Å and a = 7.748 Å. Table 5.7 is the summary of the identification, using the diffraction patterns from the thin foils. In this table, column 1 contains the ASTM standard[149] interplanar spacings, in Å; column 2 gives the corresponding (hkil) values. Columns 3 to 8 contain the data from the six different patterns used in the identification of the precipitates found in the annealed batch of specimens. The letter "A" has been used to indicate the data related to the ageing condition. In total, ten diffraction patterns were used for the identification. The identification procedure is given in appendix C.

A qualitative microanalysis of the extracted precipitates on the replica was made using the EDAX facility attached to the TEM. This is shown in Fig 5.13, from which it can be seen that silicon was the only substitutional element in the precipitate. It was not possible to detect nitrogen, as the noise peak of the EDAX machine interfered with the reading of the interstitials' spectra.

The reciprocal of inter lamellar spacings of the pearlite constituent in three of the steel grades (0.31, 0.78 and 1.03% Si), heat treated according to codes A and D has been plotted against the silicon content in the steel, Fig 5.14.It can be seen that at the lower austenitizing temperature, the general tendency for the reciprocal of the spacing was to increase with the silicon content. However, at the highest austenitizing temperature, beyond a critical

concentration of silicon in the steel, the tendency was for a decrease of the reciprocal of spacing.

The typical structures of pearlite in the respective steels, following the D code of heat treatments is shown in Fig 5.15. Note the fragmentation and spheroidization of the cementite phase at the 1.03 wt% Si level.

5.2 "Softening"

5.2.1 Low Temperature Tensile Tests

The linear regression equations resulting from the plot of σ_y against grain size ($d^{-1/2}$) are given in Table 5.8 for the different test temperatures, at the strain rate of 3.3×10^{-4} s^{-1} and 0.33 s^{-1}. For the latter strain rate, tests were done at only one temperature, 153 K.

5.2.2 Athermal Yield Stress

In Fig 5.16 is shown a graph of the athermal yield stress (test temperature of 350 K, with a strain rate of 1.7×10^{-4} s^{-1}) of the steels versus the grain size. The regression equations are inserted in this figure.

5.2.3 Effective (Thermal) Stress

From the regression equations (section 5.2.1), it was possible to compute the lower yield stress, σ_y of a particular grain size, i at a test temperature, T. The athermal stress for the corresponding grain size, i was

also computed from the regression equations, obtained from the graph of athermal yield stress versus grain size (section 5.2.2).

Using equation 4.12, it was possible to evaluate the effective (thermal) stress for a given grain size, i at any given test temperature,T. The effect of grain size, strain rate and test temperature on the effective stress is shown in Fig 5.17. Only two steels- those with 0.156 and 1.03% Si, are represented for the sake of clarity of the figure. Fig 5.17a emphasizes to what extent this effect depends on the chosen strain rate.

Regression equations from the graphs of effective stress versus the grain size of steels (similar to Fig 5.17a) were obtained at different test temperatures for a strain rate of $3.3 \times 10^{-4}\ s^{-1}$. Hence, it was possible to evaluate the effective stress due to silicon alone (the intercepts of the effective stress axis) at various silicon levels in the steel, for different test temperatures. Thus, quantitative estimates of "softening" per one weight percent silicon were made for silicon alone, function of a given grain size, i with the equation:

$$[(\sigma_{Yi}^{*}-\sigma_{Xi}^{*})/\sigma_{Yi}^{*}]114.4,\ \%, \qquad \ldots\ldots\ldots\ldots\ldots 5.1$$

where X and Y are the 1.03 and 0.156 wt% Si steel grades respectively, and 114.4 is a factor with which the "softening" between the 0.156 and the 1.03% Si levels in the steel is converted to percentage "softening", per one weight percent silicon addition.

The various degrees of "softening" per one weight

percent addition of silicon, derived using equation 5.1, are plotted against grain size (Fig 5.18a) and test temperature (Fig 5.18b) for a strain rate of 3.3 x 10^{-4} s^{-1}. From Fig 5.18a, it is noteworthy that grain sizes above 58 μm (less than about 4.2 $mm^{-1/2}$) would not "soften" at 223 K. In Fig 5.18b, the effect of just silicon, has been separated from the combined effect of silicon and grain size, on the degree of "softening". The facts worthy of note here are: there is a critical temperature at which the degree of "softening", which initially increased with the reduction of test temperature, starts to fall, and this fall is limited by the "softening" guaranteed by the silicon effect alone.

The lower yield stresses of the steels for four grain sizes (55, 36, 20 and 8 μm) were computed from the regression equations (Table 5.8) for all the steels at each test temperature. These have been plotted against test temperatures, Fig 5.19 (a to d). It can be observed from the figure that apparent "softening" (see section 2.1) set in at much higher temperatures as the grain size was reduced,Fig 5.19 (153 K and 175 K in c and d respectively).

5.2.4 Microstructural Features of "Softening"

In this area, the study used only the 0.156 and the 1.03% Si steels. The specimens were grouped into two categories, namely a large-grained group, with grain sizes $\geq$ 20 μm, and a small-grained group, with grain sizes $<$ 20 μm. In some cases, where the feature was the

same for the two groups, a steel grade has been used to represent both groups. Otherwise, the large-grained group is represented by the 0.156% Si steel, while the small-grained group is represented by the 1.03% Si steel.

The slip lines or bands, present in the large-grained specimens, strained 8% in tension at room temperature, are shown in Fig 5.20. Of importance here is the observation that the lines were mostly wavy in nature for the two groups (steel grades).

In Fig 5.21 is shown the slip lines in the 8%-strained small-grained samples, tested at both room temperature and 77 K. The structure contained very short wavy lines and was similar for both grades of steel. The samples tested at 77 K (Fig 5.21b) tended to have a higher density of lines than those tested at room temperature (Fig 5.21a).

The large-grained samples of the steels, 8% tensile strained, and the slip lines they produced in the tests at 77 K, are shown in Fig 5.22. Of significance here are the observations that the 0.156% Si steel (Fig 5.22a) showed preponderantly long planar slip lines, with the incidence of secondary slip lines in the region marked S-S, and that the slip lines crossed the grain boundaries. In contrast, the 1.03% Si steel, with a relatively smaller grain size than the 0.156% Si steel,showed shorter and more wavy slip lines, Fig 5.22b.

The average slip line or band spacing, S_{Av} (see section 4.3) was evaluated for the steel grades that were

tensile strained by 8% at 77 K. This is given in Table 5.9. In this table, n_s represents the average number of slip lines per grain of sample. It can be seen from the table that small grain sizes favour large slip line spacings.

The cellular dislocation structures of the specimens, for the two grain-groups, strained 8% at room temperature, are shown in Fig 5.23. The steels presented similar structures in each grain-size-group; the small-grained samples showed smaller cell sizes (of 0.28±0.02 μm, Fig 5.23a) than the large-grained samples (Fig 5.23b) that showed cell sizes of 0.84±0.3 μm.

The small-grained samples, strained 8% at 77 K still maintained a fairly cellular structure, with rather lengthy dislocation segments, Fig 5.24a. But the large-grained specimens showed a reduced density and short dislocation segments, Fig 5.24b.

The structures of the round specimens, fractured in the tests at 77 K, with a strain rate of 3.3×10^{-4} s^{-1} from the two grain groups, which were etched with Fry's reagent for the study of twins, are shown in Fig 5.25. In Fig 5.25a are shown the structures of the 0.156% Si steel. Note the high incidence of twins in the large-grained specimen (ai) and the virtual absence of twins in the small-grained specimen (aii). Similar structures were obtained for the 1.03% Si steel, Fig 5.25b.

5.3 Thermal Activation Parameter Studies

In Fig 5.26 is a semilog graph of effective

stress versus test temperature, at a strain rate of 3.3 x 10^{-4} s^{-1} for the 0.78% Si steel. Similar graphs were plotted for the other four steel grades. Following the suggestion of Conrad and Hayes[147], the value of the effective stress at the intercept of the Ln σ^* axis was adopted as the material constant, σ_o^*.

Introducing the differentials (between the two strain rates used, and between the effective stresses of a particular grain size at these two strain rates) into equation 2.9 (section 2.5), the values of the dislocation velocity exponent, m^* were determined for the five steel grades at 55, 36, 20 and 8 μm grain sizes. Having all the terms in equations 4.13 and 4.14 (section 4.6) now known, with the exception of the dislocation frequency factor, υ, it was possible to evaluate (from equation 4.13) the latter for the steel grades at these grain sizes. Table 5.10 gives the determined values. It can be seen that silicon additions reduce the σ_o^*. The general tendency was for m^* and υ to increase with silicon additions and reduced grain sizes, provided there was an apparent "softening". Another fact worthy of note from this table is the constant nature of υ, irrespective of the strain rate. This is a proof that the condition (section 2.5)[56,104] which makes the determination of m^* with equation 2.9 valid, was fulfilled.

The thermal activation parameters were then evaluated using equations 2.3 and 2.4. The graphs of activation energy, H or volume, V^*/b^3 (where b is the dislocation's Burger's vector) against effective stress

have always shown[52,58,74] the activation parameters to increase with the reduction of the effective stress. Since the effective stress was observed to be reducing with the reduction of the grain size in this work, the activation parameters, H and V^*/b^3 of the steels were plotted against the grain sizes. The data for the graphs were generated from the two strain rates- 3.3×10^{-4} s^{-1} and 0.33 s^{-1} at the test temperature of 153 K. The graph is shown in Fig 5.27. It can be seen that in the large-grain-size region, $\geqslant$20 μm, $\leqslant$ 7 $mm^{-1/2}$, changes were small, except for the 1.03% Si steel which showed the least value. However, in the small-grain-size region, it is evident that the activation parameters appreciated in value, particularly for the activation energy, where even the 1.03% Si steel showed a higher value than those of the 0.156 and 0.31% Si steels.

Table 5.1: Ferrite grain sizes produced from the H.T. used and their room temperature tensile properties in an unaged condition.

Steel wt% Si	H.T. code	Grain size µm	σ_{UTS}** ±6MPa	σ_y** ±6MPa	Total** ε ±1.5%	Ψ
0.156	A	32±3	399	230	42	68
	B	47±4	387	214	40	67.5
	C	64±4;53±5*	385	208	41	70
	D	73±6;65±6*	419	204	39	59
	E	19±1;14±1*+	404	253	42	73
	F	12±1	450	326	40.5	75
0.31	A	35±3	413	240	41	68.5
	B	48±4	402	225	41	68
	C	66±5;59±3*	400	220	41	70.5
	D	76±5;68±4*	436	208	39.5	59
	E	20±2;15±1*+	427	270	45	74.5
	F	13±1	468	339	41	74
0.53	A	30±2	439	255	44	70
	B	45±4	436	240	40	67
	C	50±5	424	233	38	67.5
	D	67±5;61±3*	462	227	39	57.5
	E	17±1;14±1*+	445	284	41	72
	F	11±1;10±1*	494	354	40	75
0.78	A	19±2	460	270	41	69
	B	39±3	460	249	40	67
	C	47±4	454	242	38.5	63.5
	D	58±4;60±2*	497	239	39	57
	E	16±1;11±1*+	493	317	40.5	73
	F	7±1	624	381^	34	58
1.03	A	17±2	496	313	40.5	69
	B	32±3	484	279	38	65
	C	43±4	477	278	39	62
	D	58±4	503	270	36.5	56.5
	E	15±1;10±1*+	517	346	40	73
	F	7±1	667	431^	35.5	54

* : second batch under the same heat treatment conditions.
\+ : the compressed air jet was more forceful
**: average of two tests from the first batch
^ : 0.2% proof stress

Table 5.2: Measured prior austenite grain sizes

Steel wt% Si	Heat Treatment* code	Grain Size μm
0.156	A	50±4
	B	57±4
	F	23±2
0.31	A	55±4
	B	62±5
	F	25±2
0.53	A	44±3
	B	52±4
	F	20±1
0.78	A	27±2
	B	44±3
	F	13±2
1.03	A	23±2
	B	34±3
	F	12±1

* excluding the cooling time

Table 5.3: Critical temperatures of steels

Steel wt% Si	A_{c1} ° C	A_{c3} ° C
0.156	740±2	822±1
0.31	733±1	814±3
0.53	748±2	833±1
0.78	748±2	851±6
1.03	754±1	861±2

Table 5.4: Strengthening degree (ΔLYS) by silicon

Si step wt%	$d^{-1/2}$ $mm^{-1/2}$	ΔLYS,MPa Short-aged	Unaged
0.31-0.53	5	12	1
	10	3	-4
	16.76	-16	-17
0.31-0.78	5	22	1
	10	9	-12
	16.76	-20	-42
0.31-1.03	5	44	33
	10	37	27
	16.76	21	12

Table 5.5: Determined ledge properties.*

Steel wt% Si	K_v MPamm$^{1/2}$	Area examined mm^2	Av.no of ldg. μm^{-1}	Ldg.height (95% confid.) nm
0.31	22.5	0.84	2.8	35±2
0.78	19	0.65	5.8	40±10
* A similar determination was made by Mintz et al[3]:				
0.02		0.81	8.3	3(smallest)
0.3		0.91	11.4	10(smallest) >50(freqnt)

Table 5.6: Optical metallographic data of pearlite produced from H.T.code D.

Steel wt% Si	Vol.fract. %	Colony size µm	Dcarb. Layer mm
0.31	16±2	19±2	1.74±0.25
0.78	16±1	18±2	2.16±0.24
1.03	14±1	22±3	2.38±0.22

Table 5.7: Diffraction patterns' data of identified Si_3N_4

1 Std."d" Å	2 (hkil)	3 Å	4 Å	5 Å	6 Å	7 Å	8 Å
	UNAGED		BATCH				
2.32	$21\bar{3}1$	2.32					
2.28	$11\bar{2}2$	2.28	2.29		2.32		
	$11\bar{2}\bar{2}$				2.32		
1.49	$32\bar{5}1$	1.49					
1.94	$22\bar{4}0$		1.98		1.96		
....	$33\bar{6}2$		1.19*				
4.32	$10\bar{1}1$			4.33			
2.16	$\bar{2}022$			2.19			
1.81	$\bar{1}013$			1.81			
2.55	$21\bar{3}0$					2.57	2.55
1.6	$2\bar{2}02$					1.61	
1.3	$4\bar{1}\bar{3}2$					1.31	
2.6	$10\bar{1}2$						2.61
1.55	$31\bar{4}2$						1.6
	AGED		BATCH				
1A	2A	3A	4A	5A	6A		
2.55	$21\bar{3}0$	2.5					
2.16	$20\bar{2}2$	2.12					
1.30	$41\bar{5}2$	1.28					
2.6	$10\bar{1}2$		2.55				
1.884	$21\bar{3}2$		1.88				
....	$31\bar{4}4$		1.16*				
4.32	$10\bar{1}1$			4.31			
	$\bar{1}011$			4.31			
2.82	0002			2.8			
3.37	$20\bar{2}0$				3.20		
2.599	$10\bar{1}2$				2.59		
1.75	$30\bar{3}2$				1.70		

* The interplanar distance,"d" values are given down to d=1.155Å,but the (hkl) equivalents are given down to d=1.213Å.

Table 5.8 : Linear regression equations of yield stress versus grain size of steels tested at low temperatures

Test temp. K	$\dot{\varepsilon}$ $s^{-1}, x10^{-4}$	Steel wt% Si	Lin. reg.equation	R
77	3.3	0.156	$\sigma_y=636.8+19d^{-1/2}$	0.98
		0.31	$\sigma_y=616.4+19.8d^{-1/2}$	0.95
		0.53	$\sigma_y=602.2+18.3d^{-1/2}$	0.95
		0.78	$\sigma_y=585.3+16d^{-1/2}$	0.96
		1.03	$\sigma_y=571.7+16.1d^{-1/2}$	0.97
153	3.3	0.156	$\sigma_y=291.5+17.6d^{-1/2}$	0.97
		0.31	$\sigma_y=289.8+17.7d^{-1/2}$	0.97
		0.53	$\sigma_y=287.9+17.5d^{-1/2}$	0.98
		0.78	$\sigma_y=307.6+14.8d^{-1/2}$	0.97
		1.03	$\sigma_y=309.6+15.1d^{-1/2}$	0.99
223	3.3	0.156	$\sigma_y=162.9+19.4d^{-1/2}$	0.97
		0.31	$\sigma_y=169.7+19.9d^{-1/2}$	0.97
		0.53	$\sigma_y=206.6+17.4d^{-1/2}$	0.98
		0.78	$\sigma_y=208.9+17.2d^{-1/2}$	0.99
		1.03	$\sigma_y=215.6+18.1d^{-1/2}$	0.96
153	3300	0.156	$\sigma_y=487.8+8.9d^{-1/2}$	0.99
		0.31	$\sigma_y=454.8+11.2d^{-1/2}$	0.99
		0.53	$\sigma_y=466.8+6.5d^{-1/2}$	0.98
		0.78	$\sigma_y=482.2+4.1d^{-1/2}$	0.97
		1.03	$\sigma_y=484.2+4.8d^{-1/2}$	0.95

Table 5.9 : Average Slip-line spacings, S_{Av} of steels 8% tensile strained at 77 K with a strain rate of 3.3×10^{-4} s^{-1}

Steel wt% Si	Grain size μm	n_b grain^{-1}	S_{Av} ± 0.4 μm
0.156	66	17±3	4
	15	3±1	5
1.03	43	11±2	4
	12	2±1	6

Table 5.10 : Values of σ_o's, m's, and υ's.

Steel wt% Si	σ_o's, MPa	Grain size μm	m at T=153°K	υ, s^{-1} at $\dot{\varepsilon}$ = 3.3×10^{-4}	υ, s^{-1} at $\dot{\varepsilon}$ = 0.33
0.156	1375±40	55	11.7±0.5	2.0×10^{6}	2.1×10^{6}
		36	12.0±0.5	4.6×10^{6}	4.8×10^{6}
		20	12.5±0.5	2.9×10^{7}	3.0×10^{7}
		8	14.4±0.6	6.7×10^{9}	7.0×10^{9}
0.31	1254±9	55	12.3±0.5	6.9×10^{6}	6.7×10^{6}
		36	12.3±0.5	1.1×10^{7}	1.2×10^{7}
		20	12.6±0.5	5.4×10^{7}	5.2×10^{7}
		8	13.0±0.5	1.6×10^{9}	1.6×10^{9}
0.53	1175±8	55	12.0±0.6	4.2×10^{6}	4.2×10^{6}
		36	12.5±0.6	1.6×10^{7}	1.6×10^{7}
		20	13.8±0.7	3.7×10^{8}	3.9×10^{8}
		8	19.3±1.0	6.9×10^{14}	6.9×10^{14}
0.78	1170±50	55	12.1±0.5	5.4×10^{6}	5.5×10^{6}
		36	12.5±0.5	2.1×10^{7}	2.1×10^{7}
		20	13.5±0.6	4.5×10^{8}	4.4×10^{8}
		8	18.4±0.8	9.8×10^{14}	5.8×10^{14}
1.03	802±40	55	11.5±0.3	4.1×10^{4}	4.2×10^{4}
		36	11.8±0.3	1.1×10^{5}	1.1×10^{5}
		20	12.4±0.4	9.7×10^{5}	1.0×10^{6}
		8	15.4±0.4	1.1×10^{10}	1.1×10^{10}

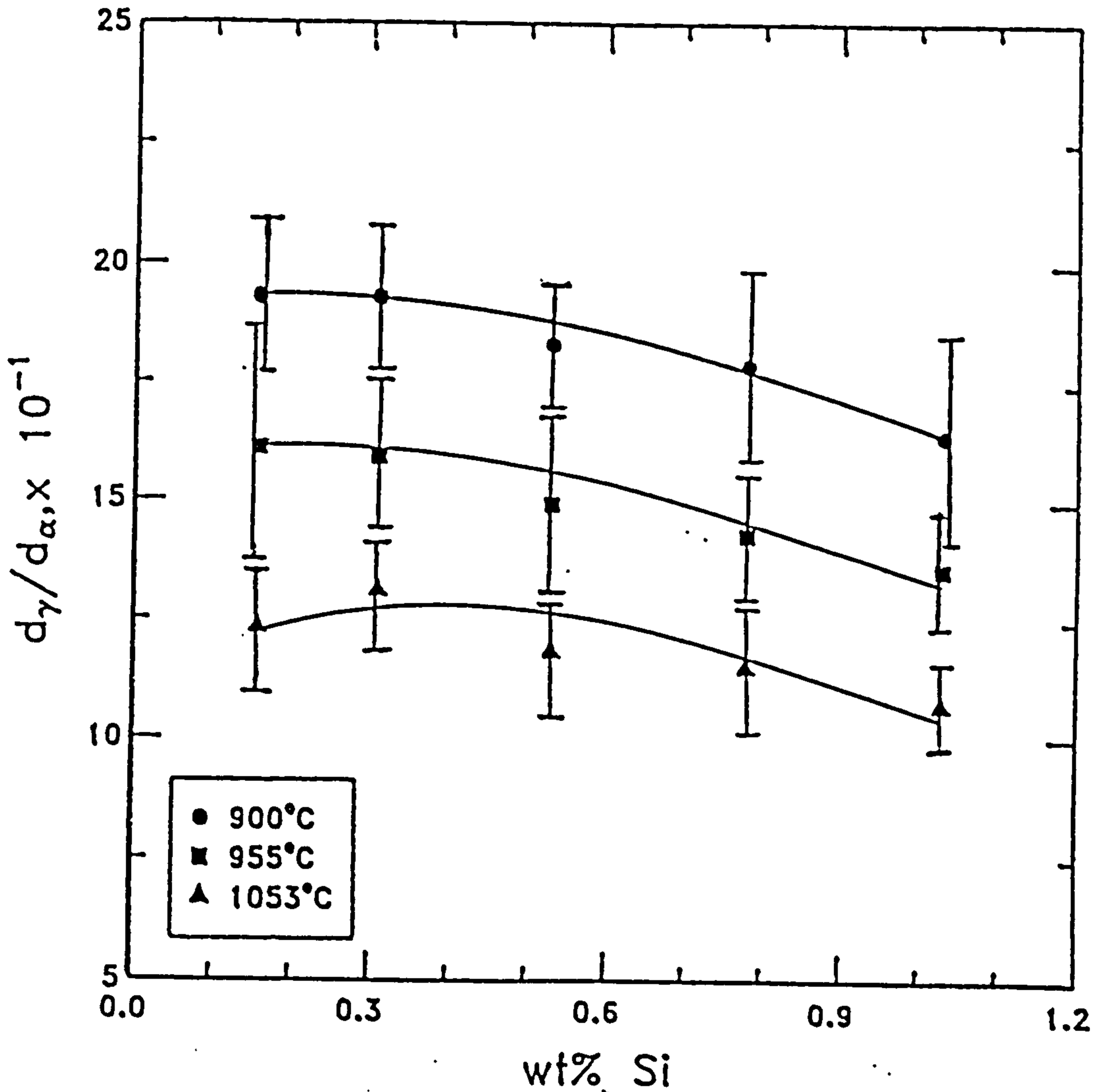

Fig 5.1: Effect of silicon on the prior austenite to ferrite grain size(d_γ/d_α) ratio.

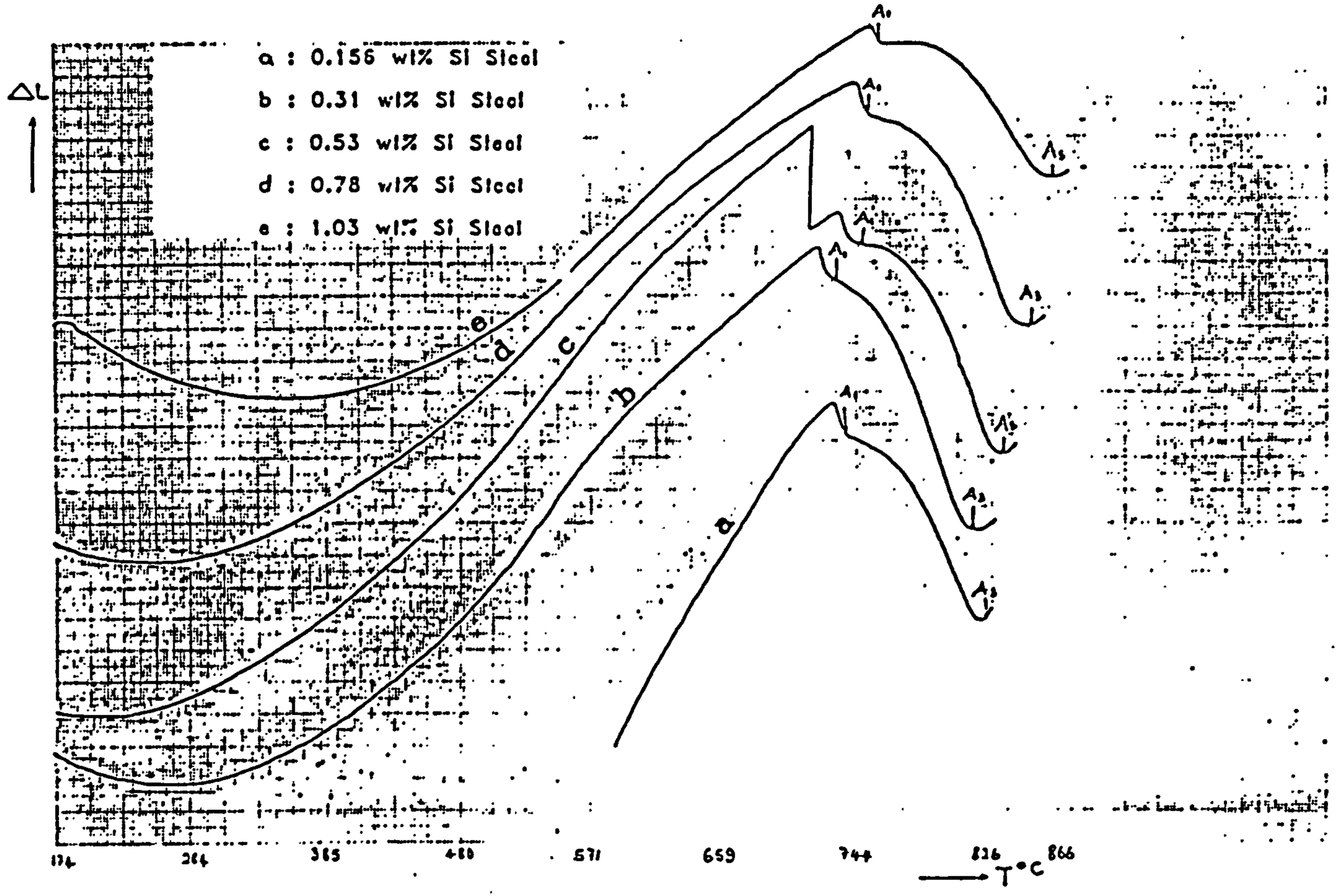

Fig 5.2: Dilatometric curves of steels.

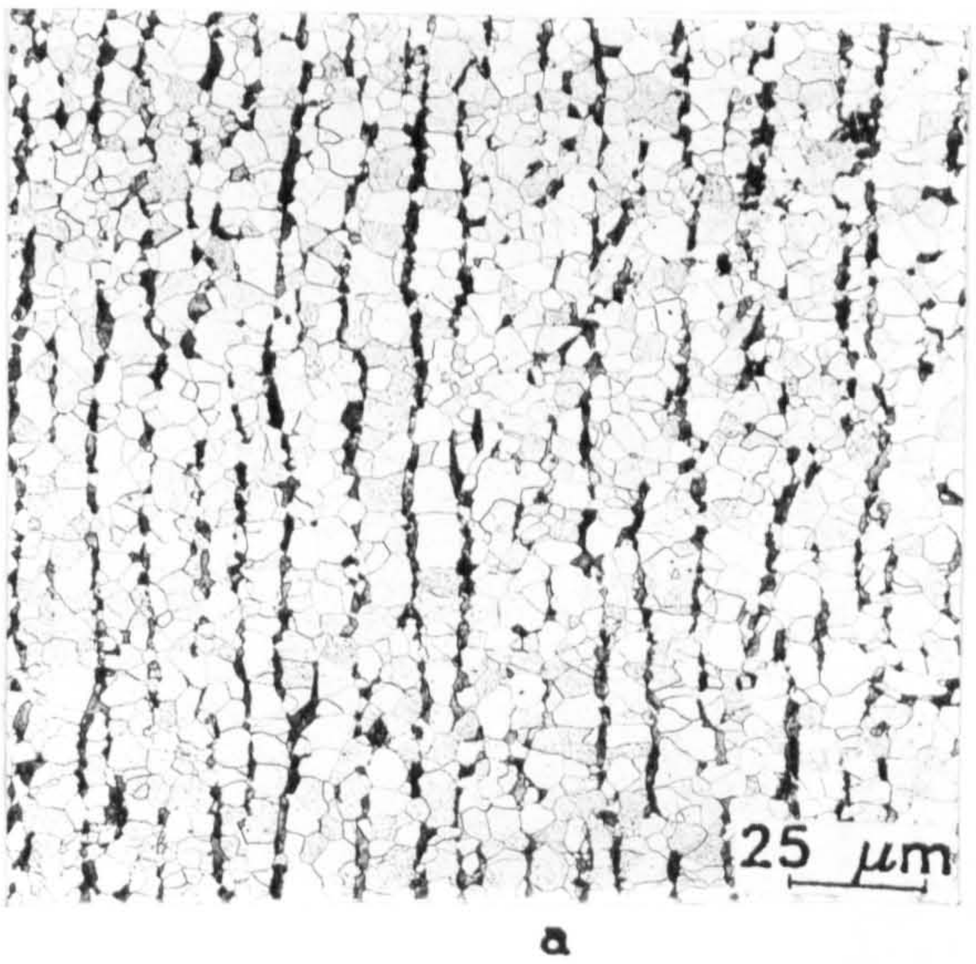

a

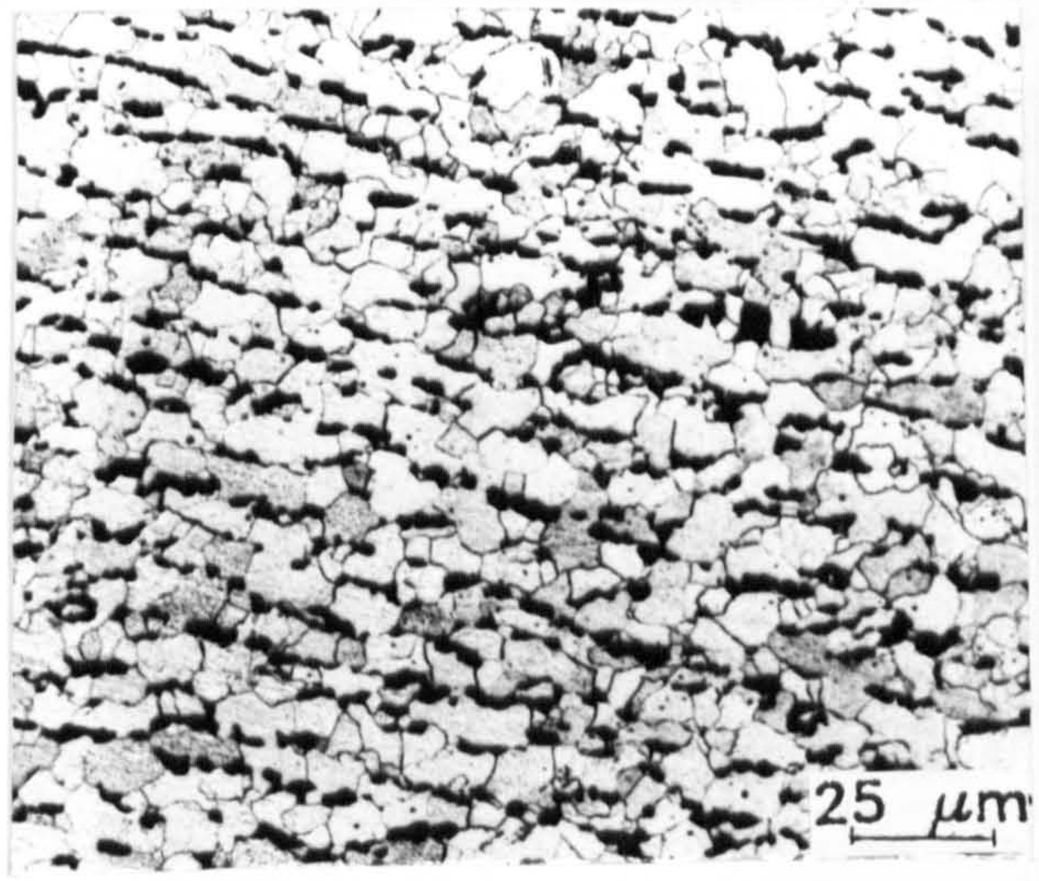

b

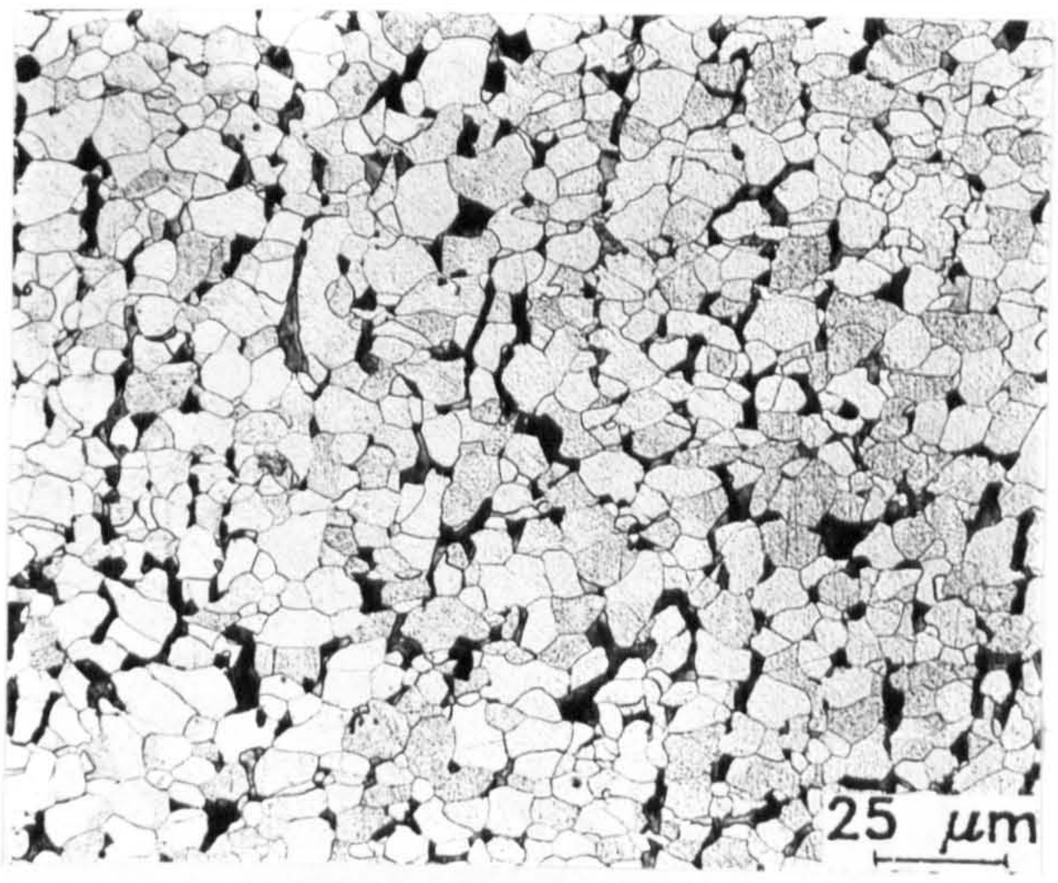

c

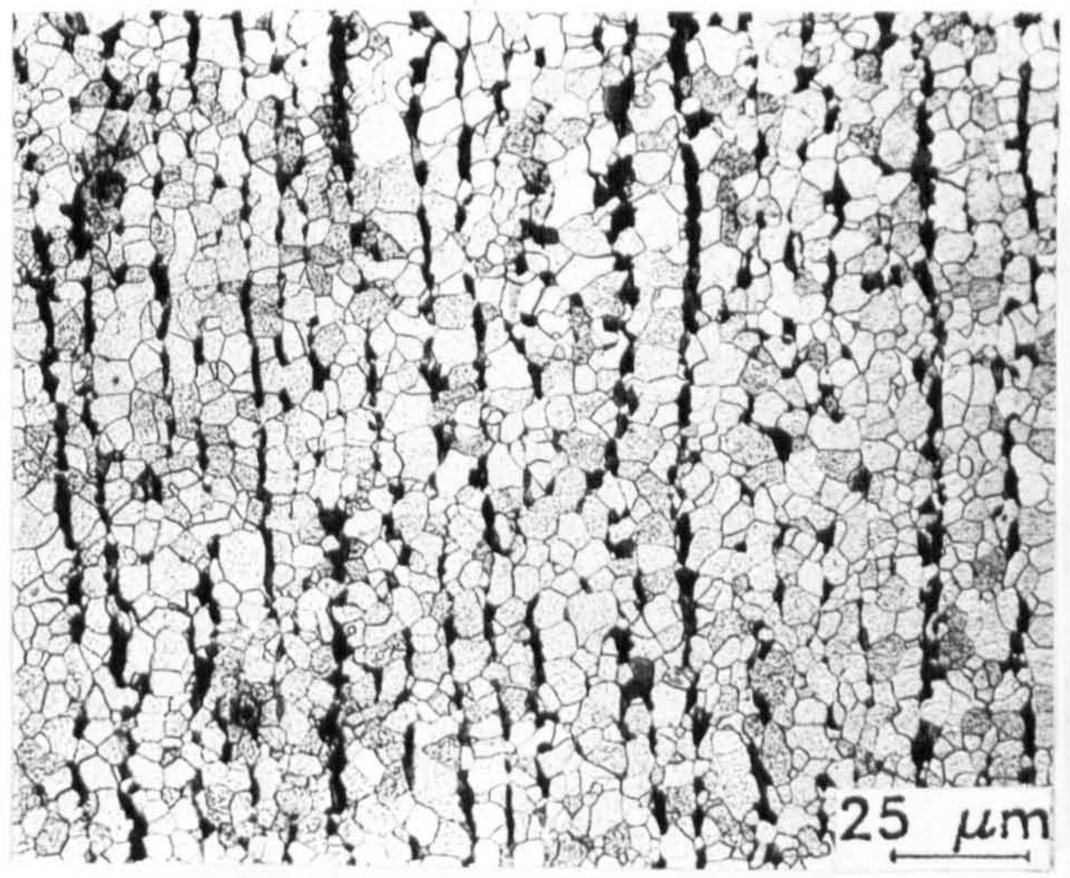

d

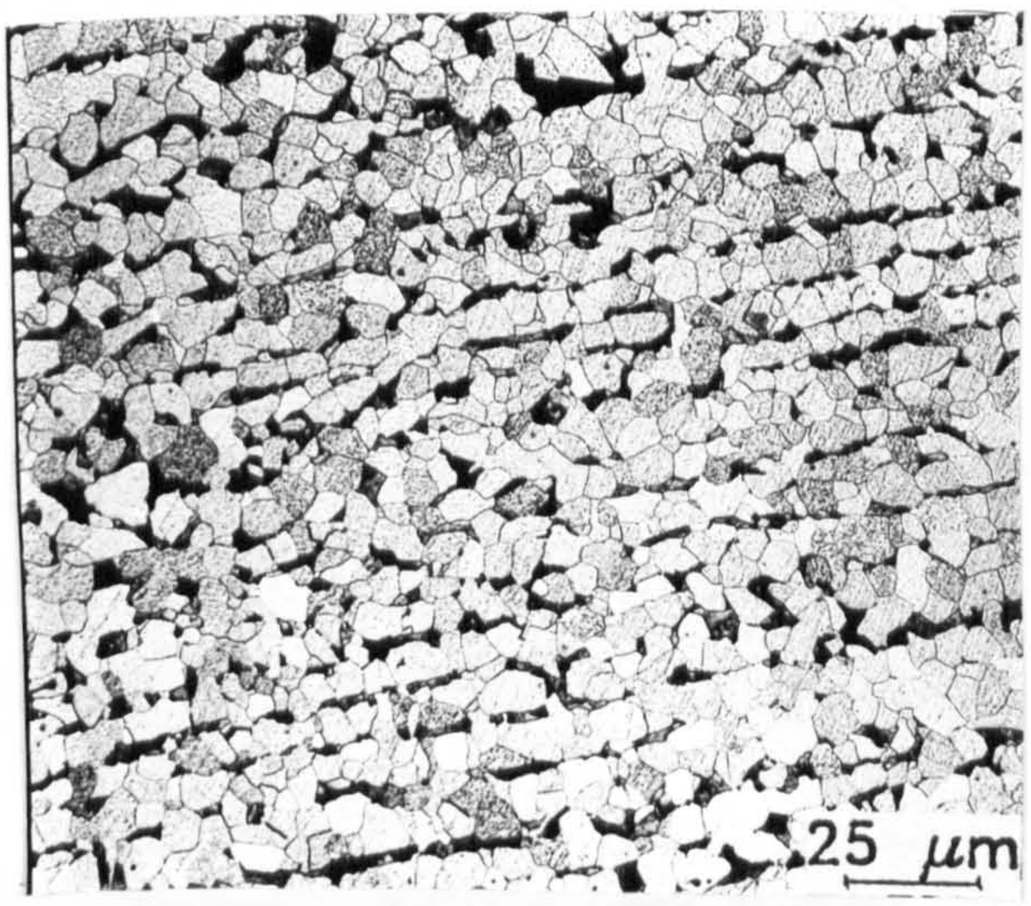

e

Fig 5.3: Optical micrographs, revealing the grain sizes of the as received steel grades typified by the silicon content(wt%):

a), 0.156; b), 0.31; c), 0.53; d), 0.78; e),1.03.

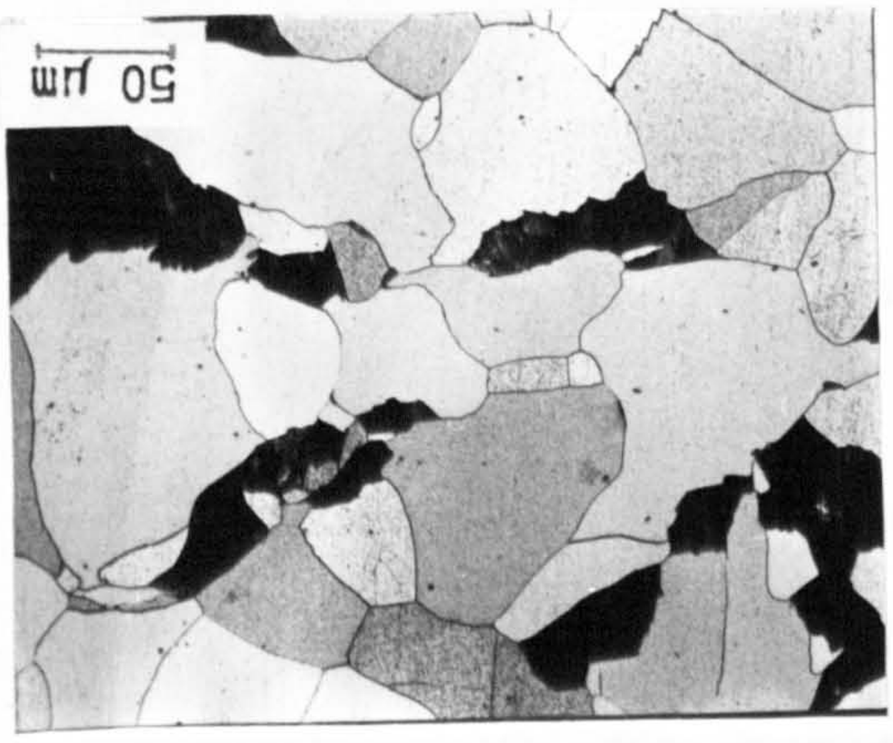

c

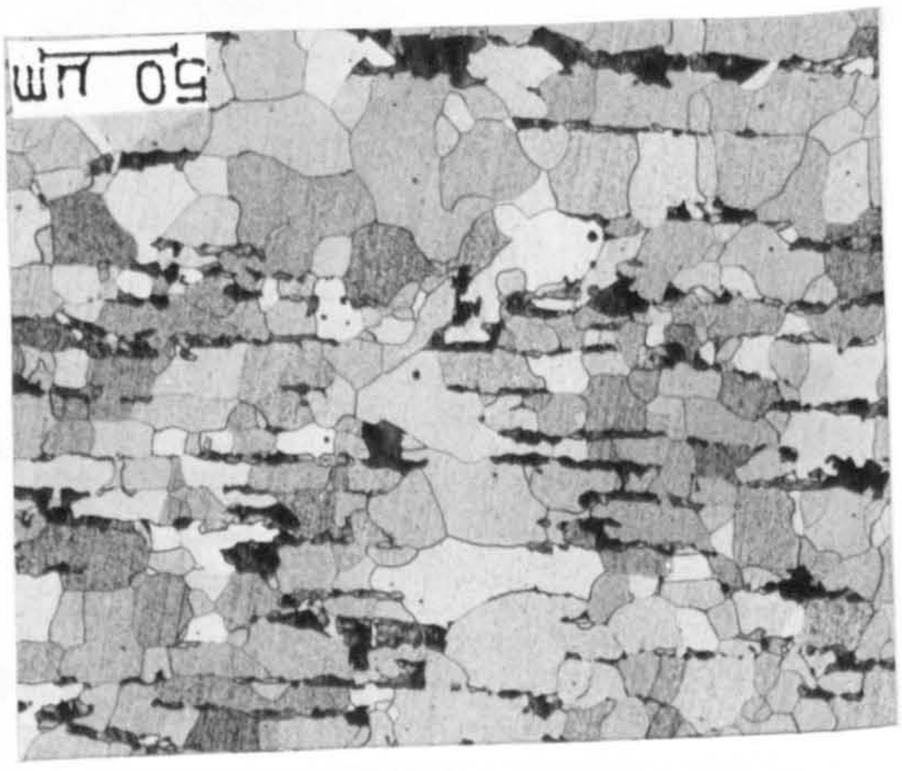

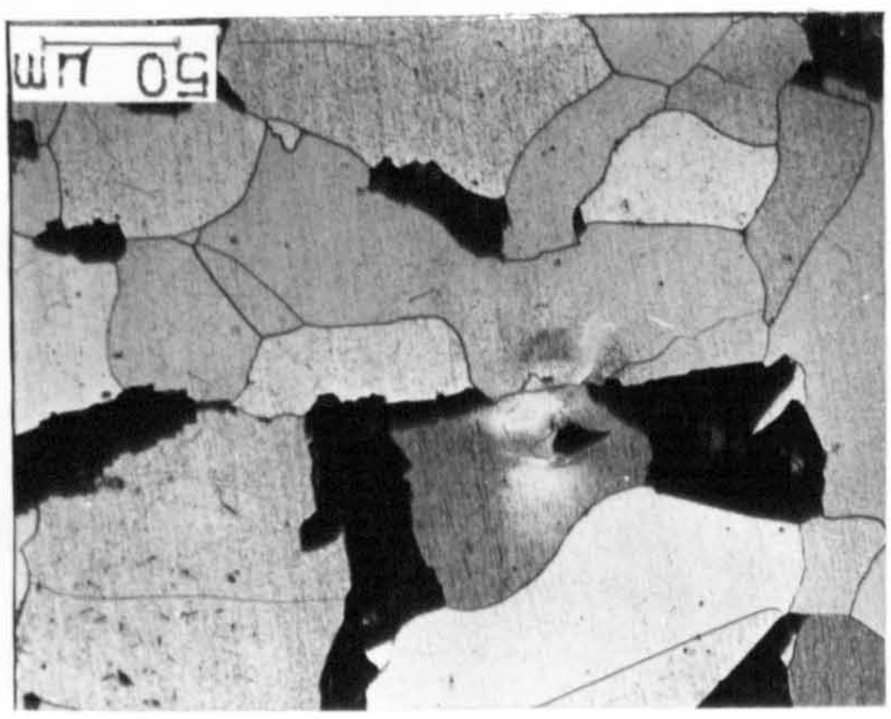

b

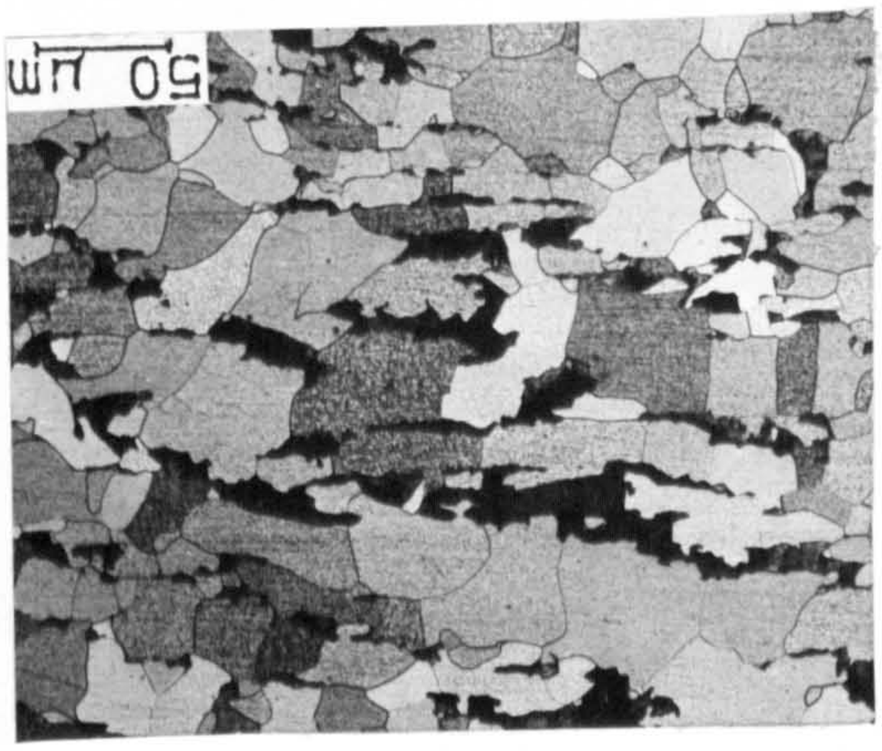

a

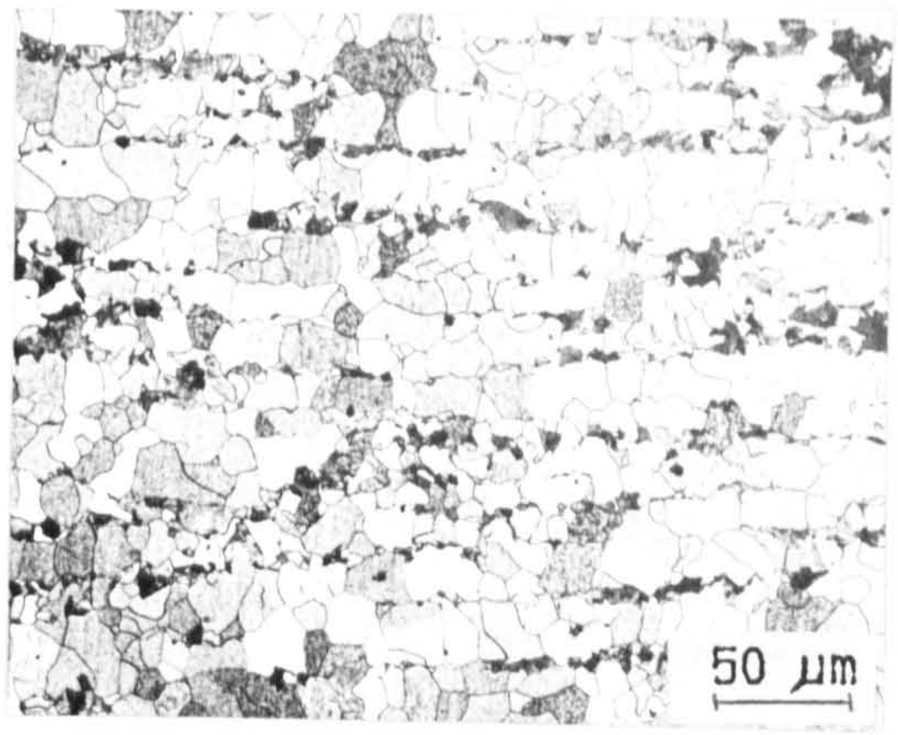

d

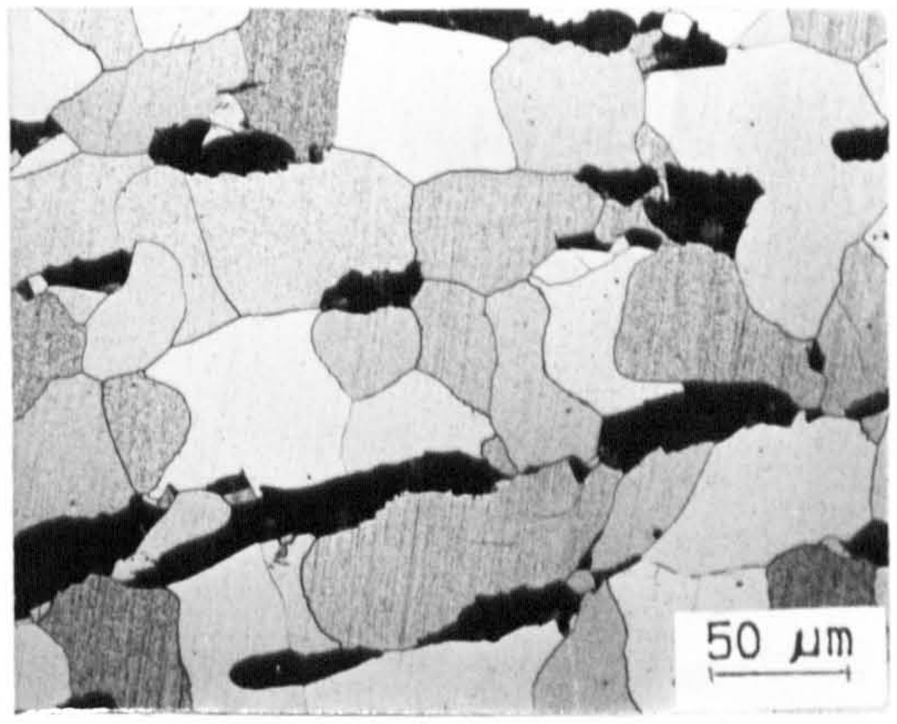

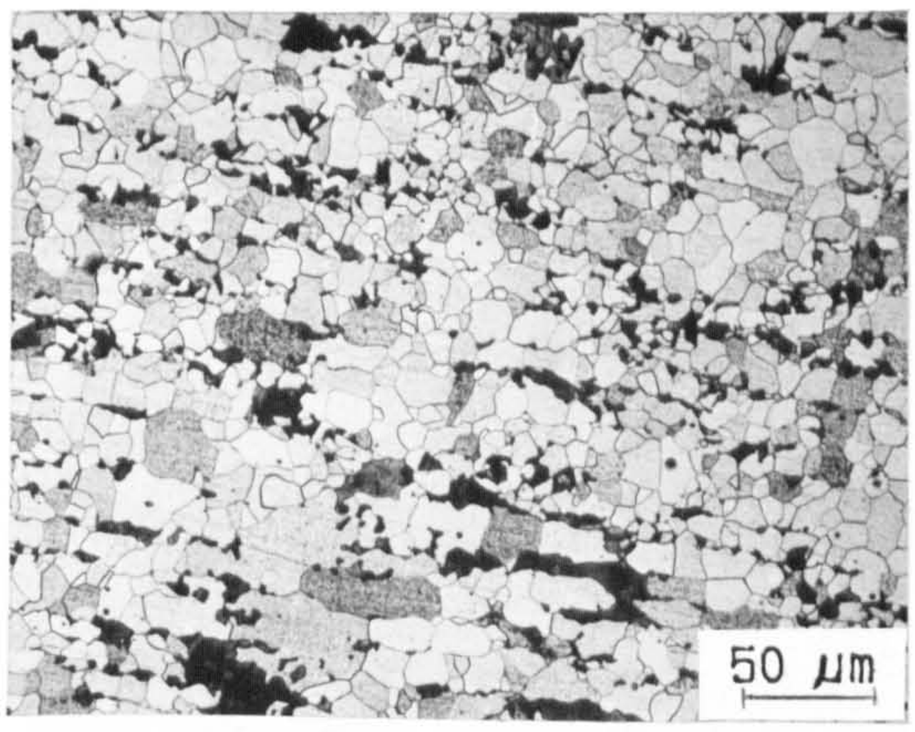

e

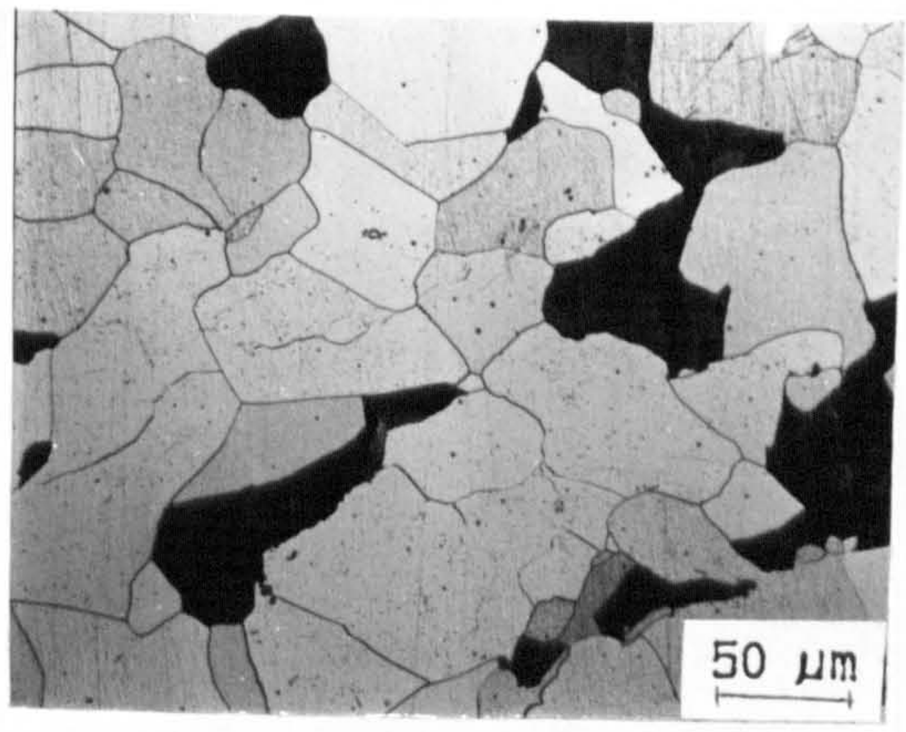

Fig 5.4: Optical micrographs revealing the grain sizes produced from heat treatment codes A (left) and D (right) for steel grades typified by the silicon content (wt%):

a), 0.156; b), 0.31; c),0.53; d),0.78; e),1.03.

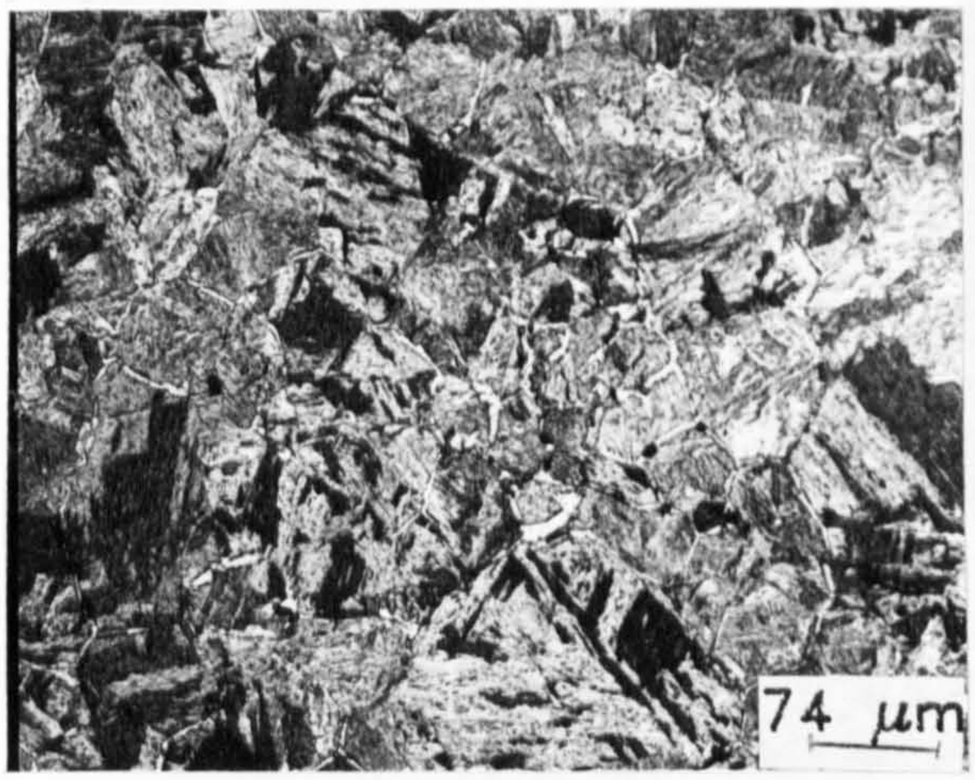

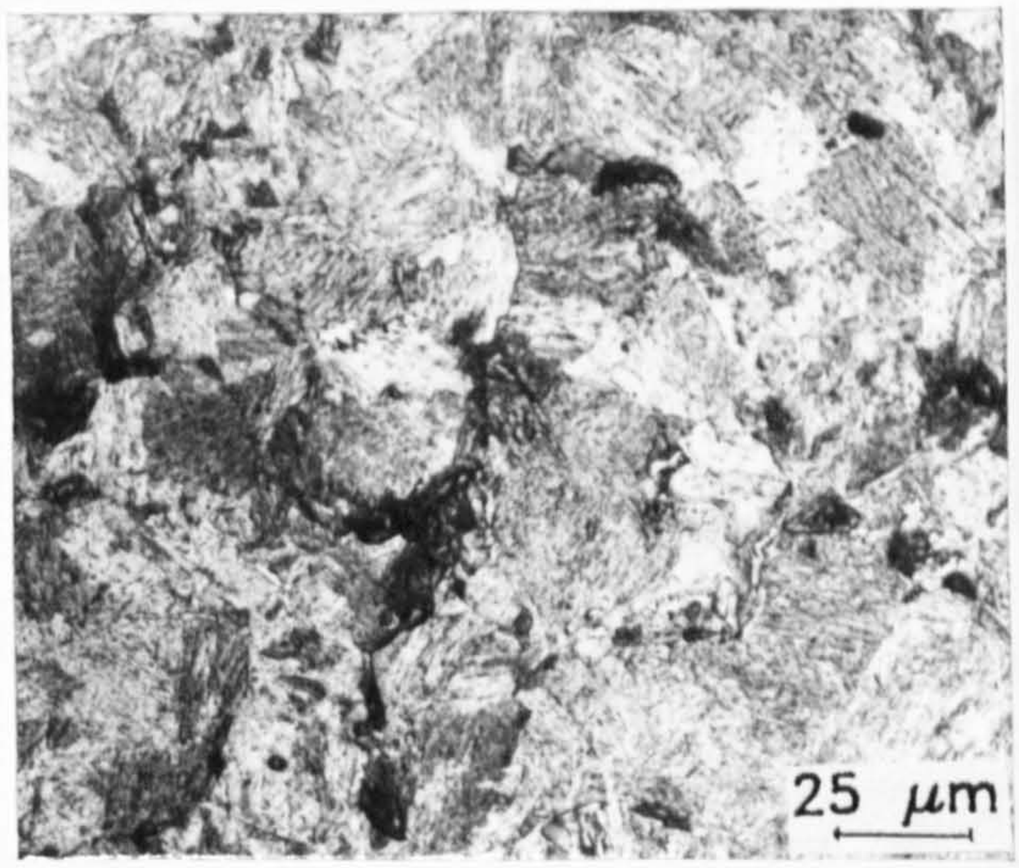

a

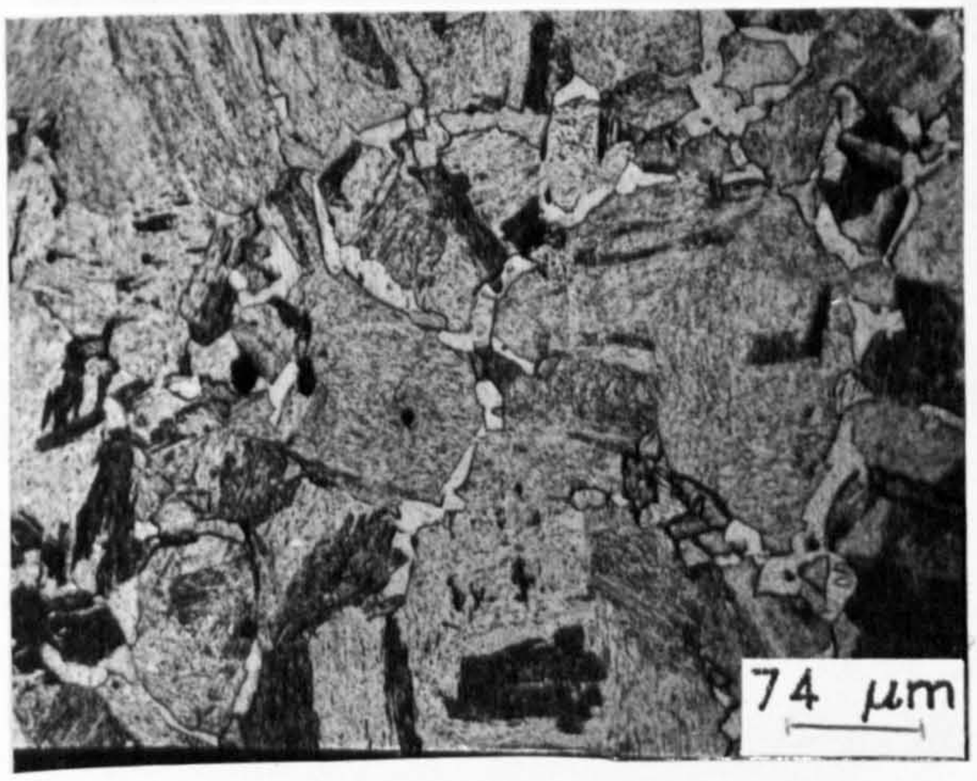

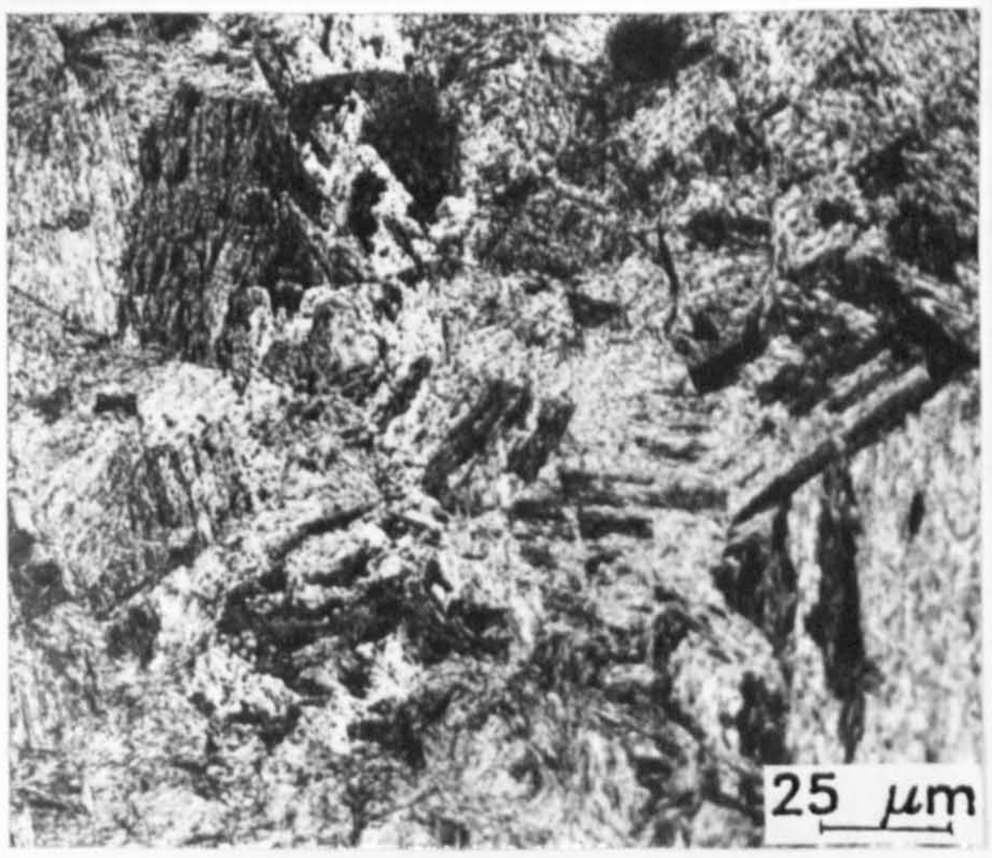

b

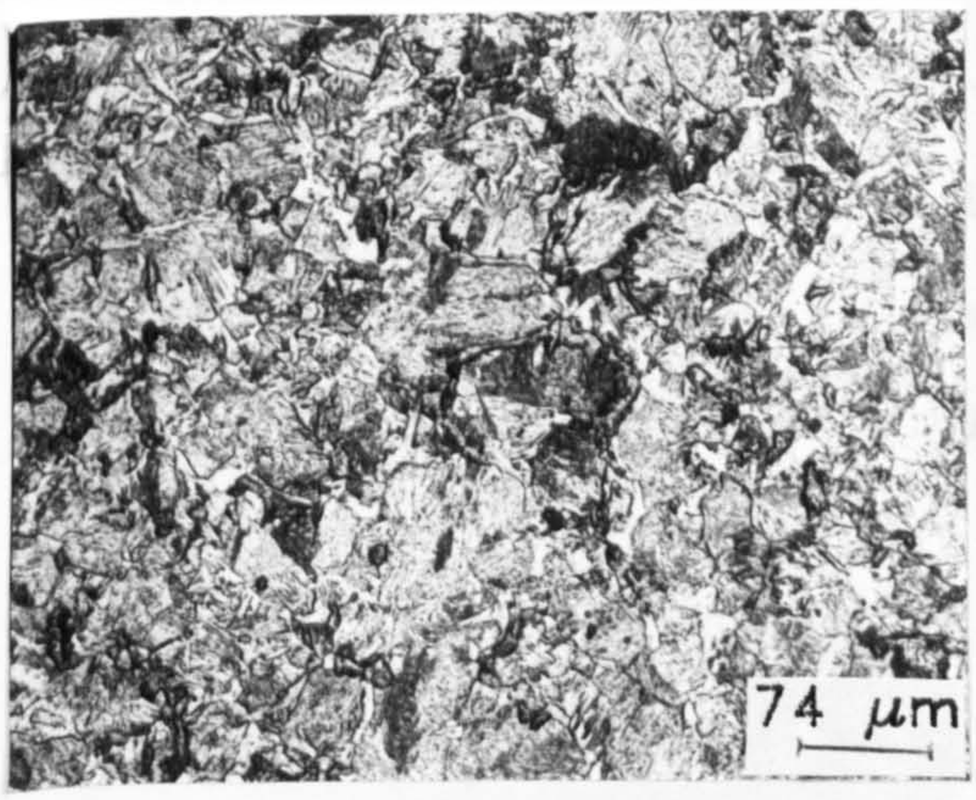

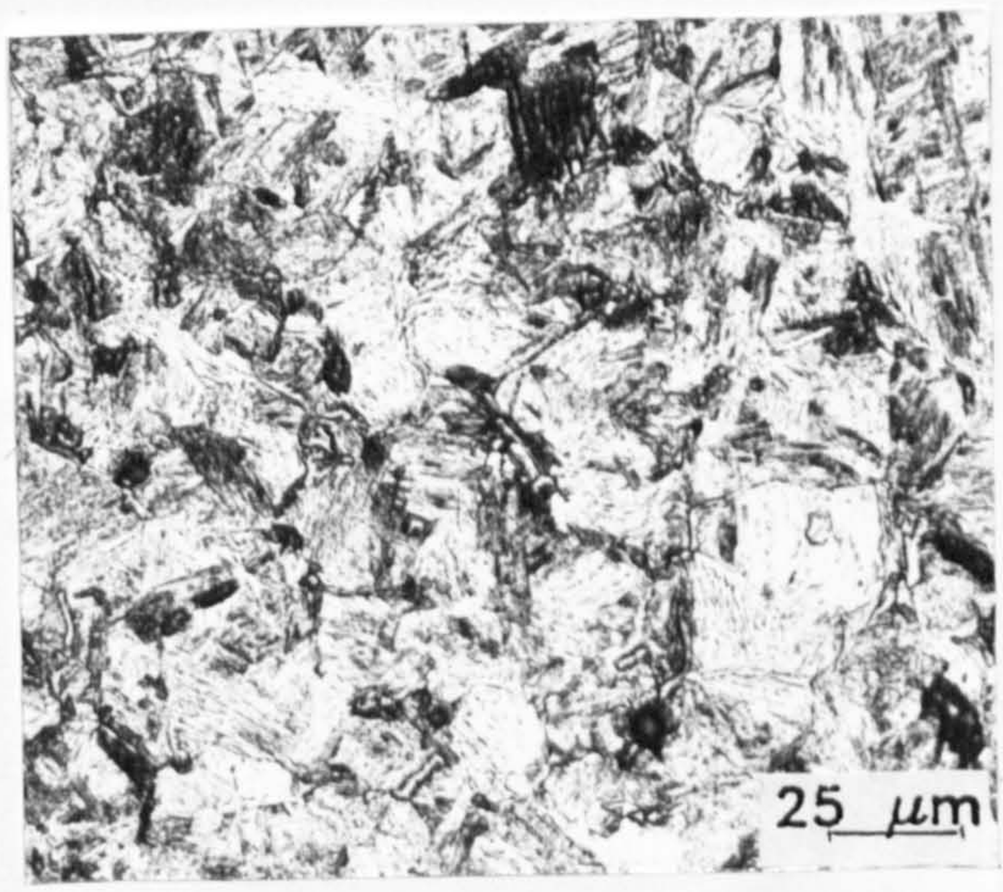

c

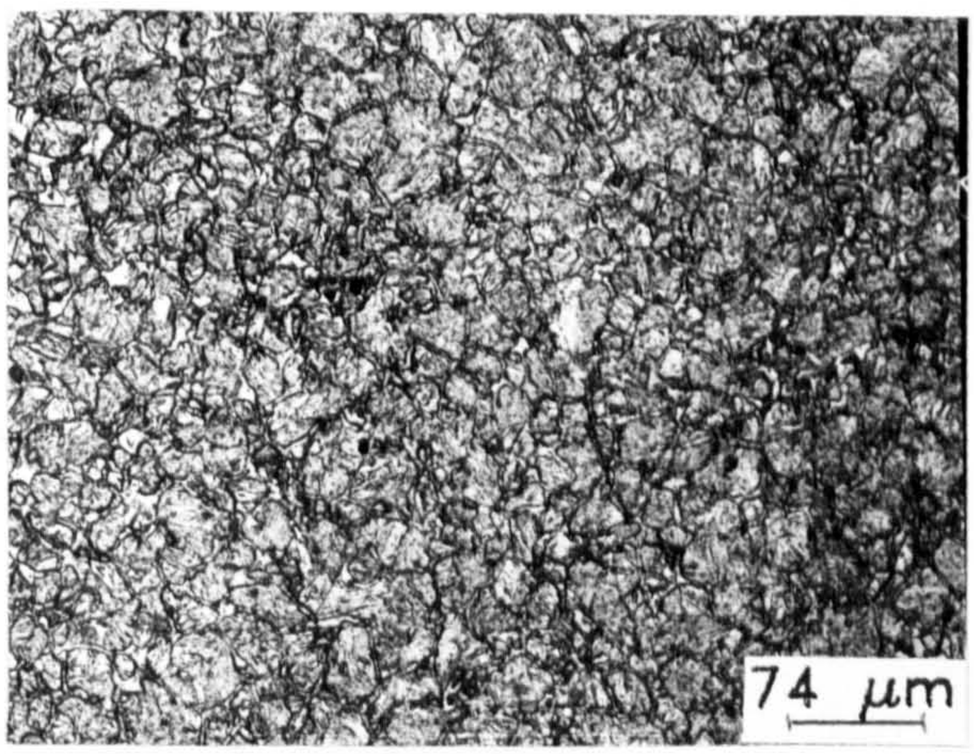

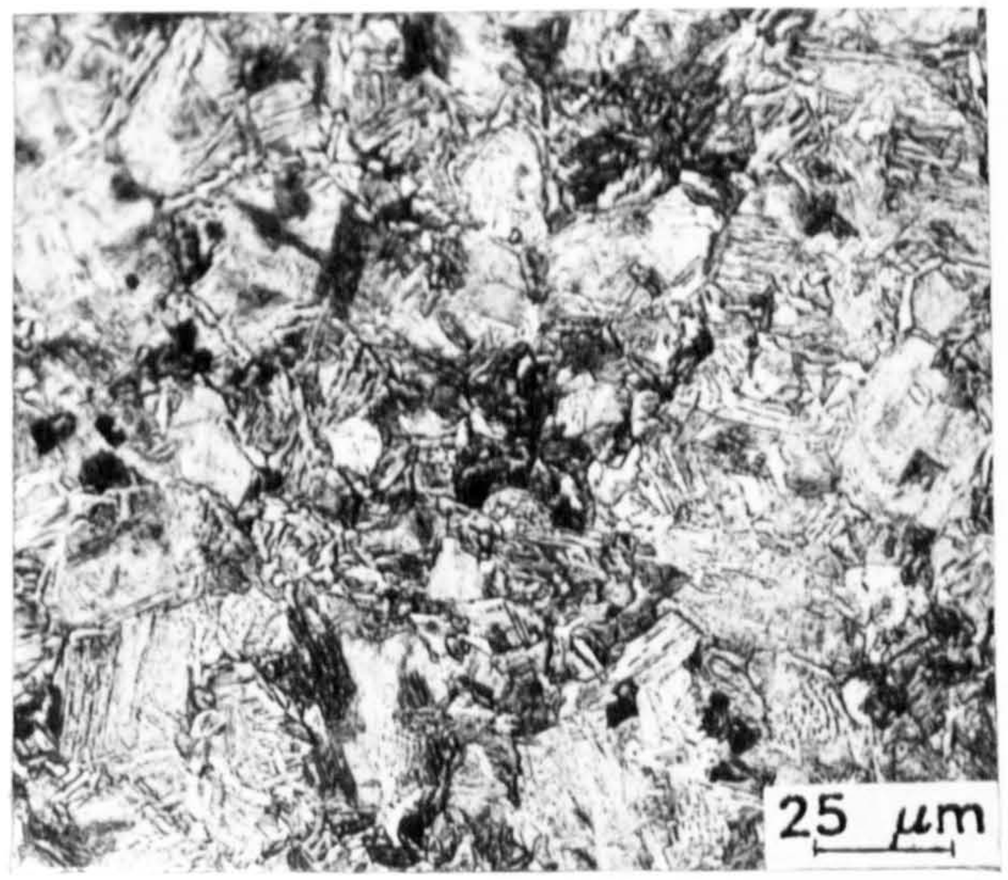

d

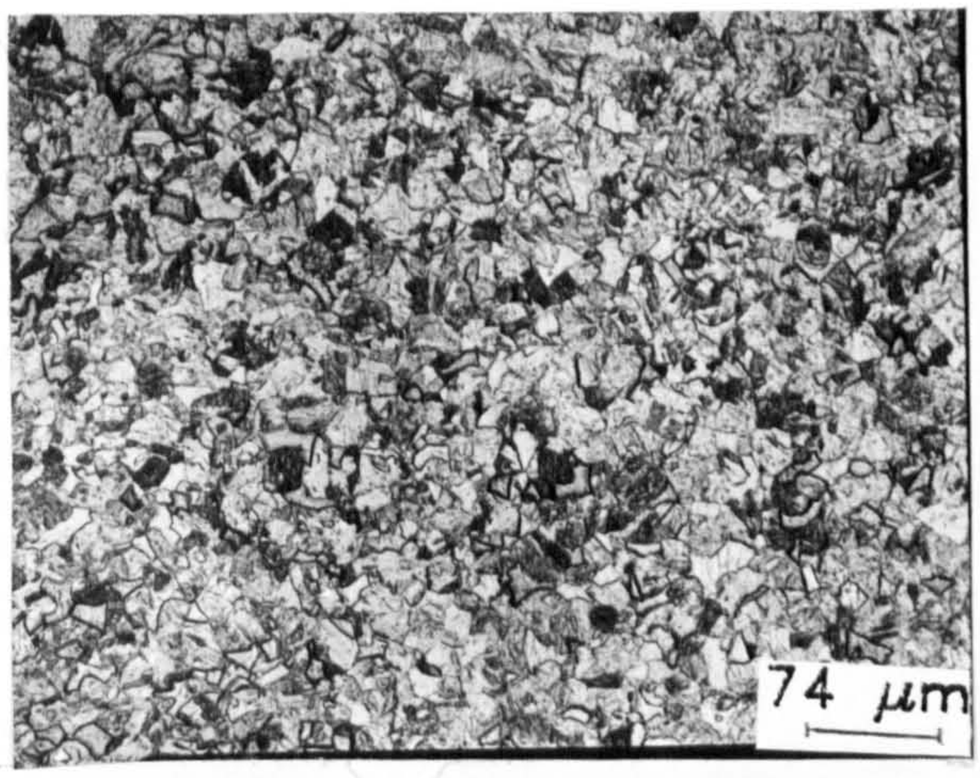

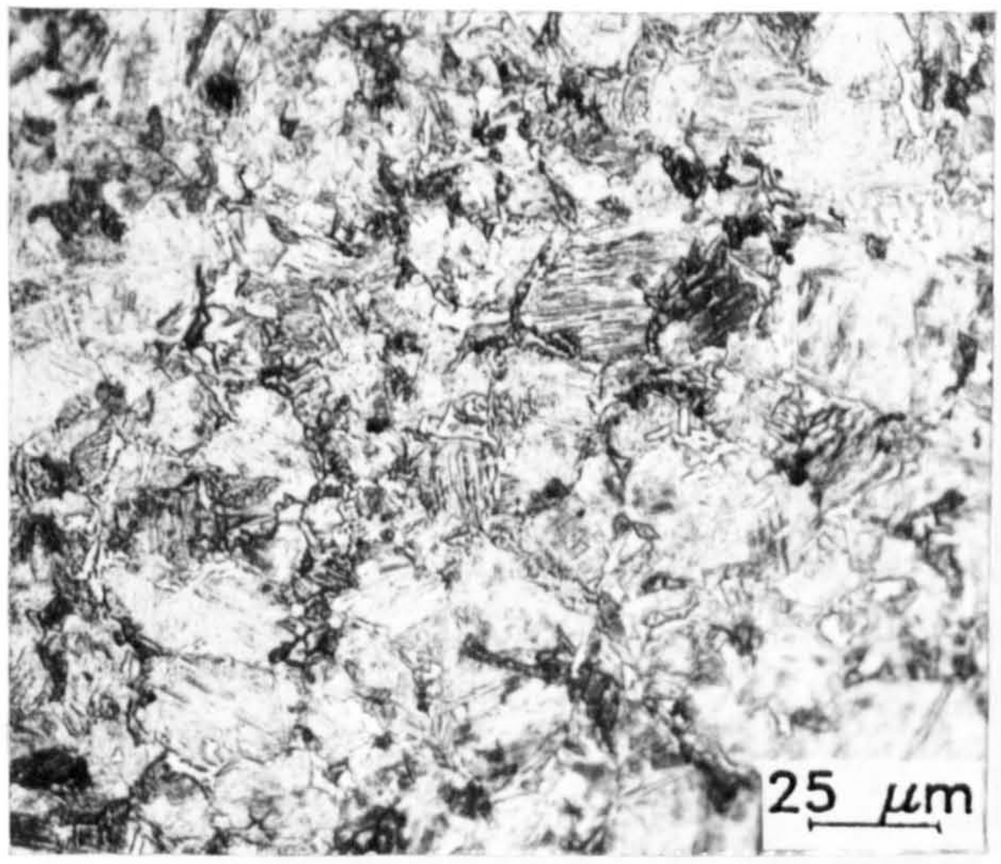

e

Fig 5.5: Prior austenite grain sizes, produced from H.T. codes A, left, and B, right (excluding the cooling times) of steels,typified by wt% Si:

a), 0.156; b), 0.31; c), 0.53; d), 0.78; e), 1.03

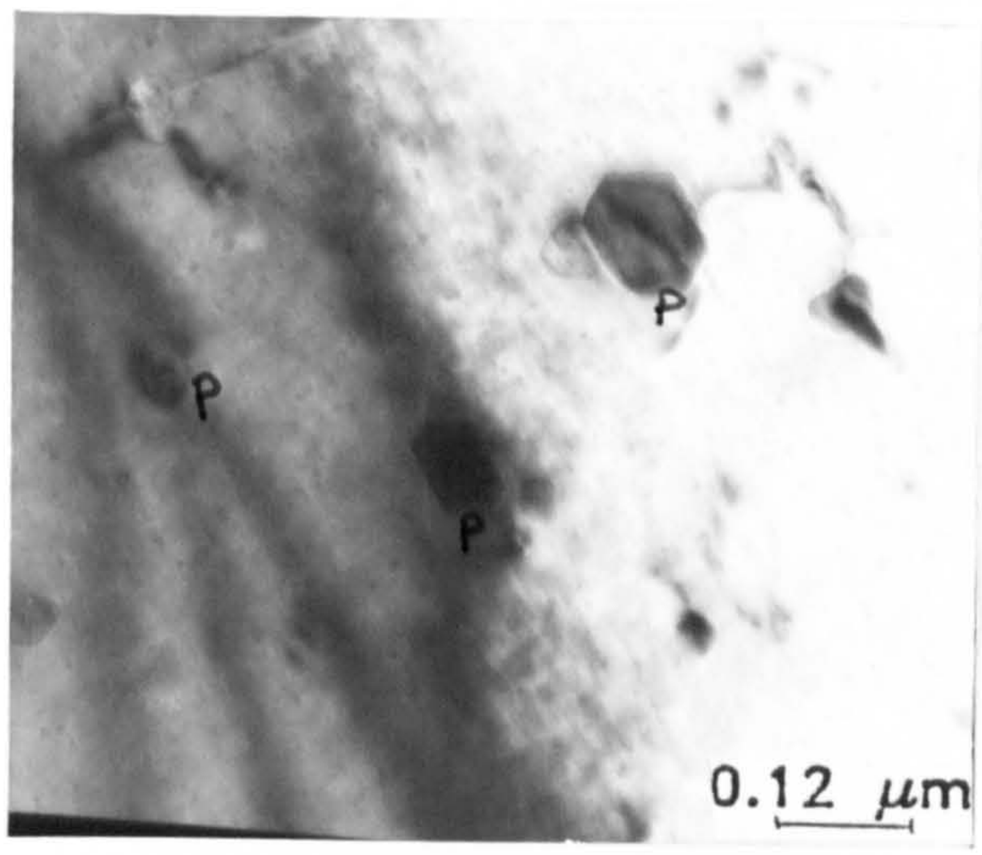

(i)

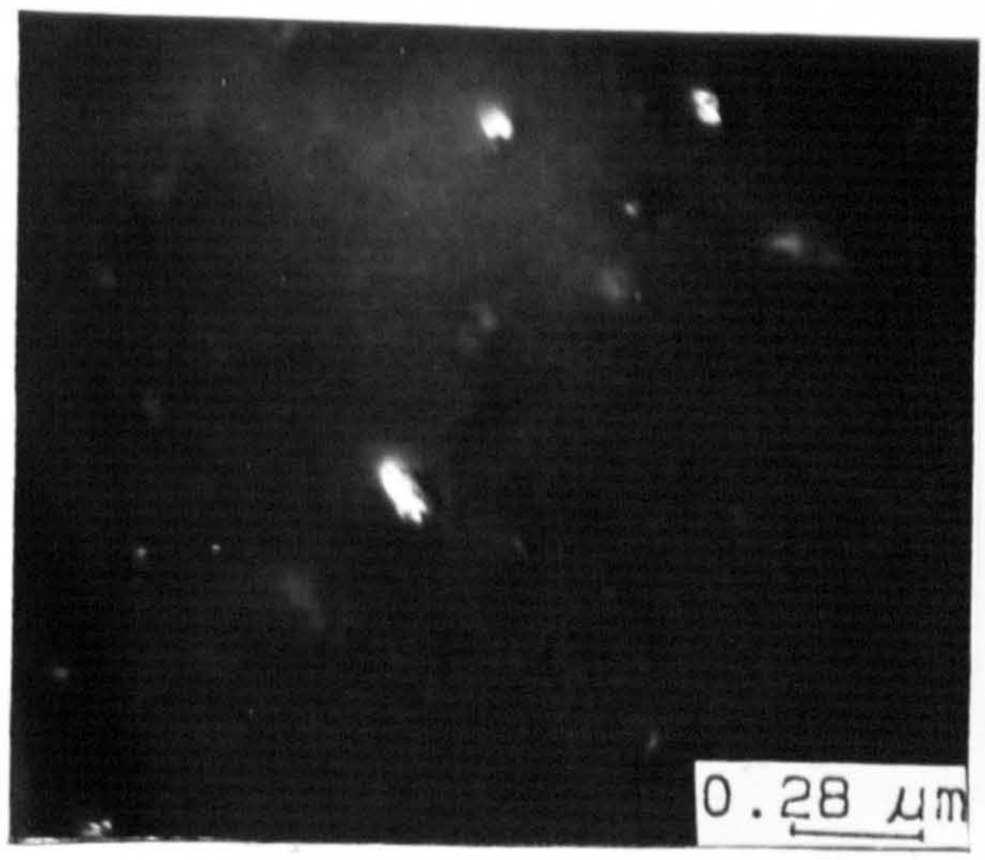

(ii)

a

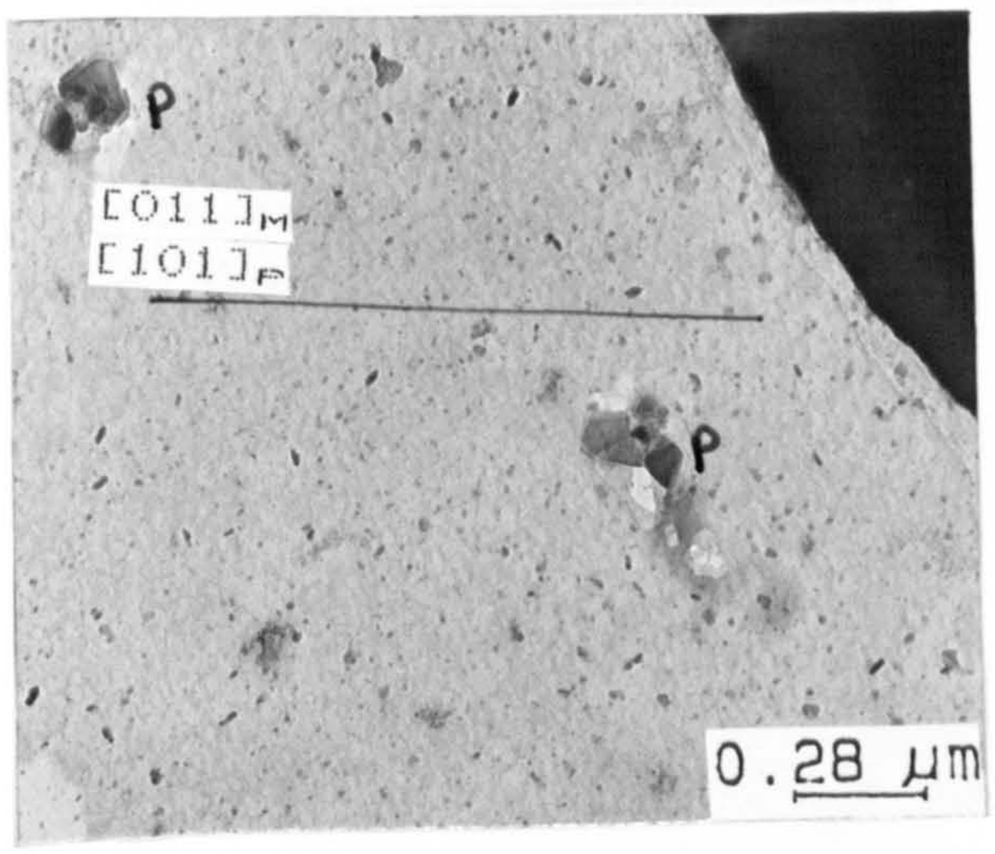

(i)

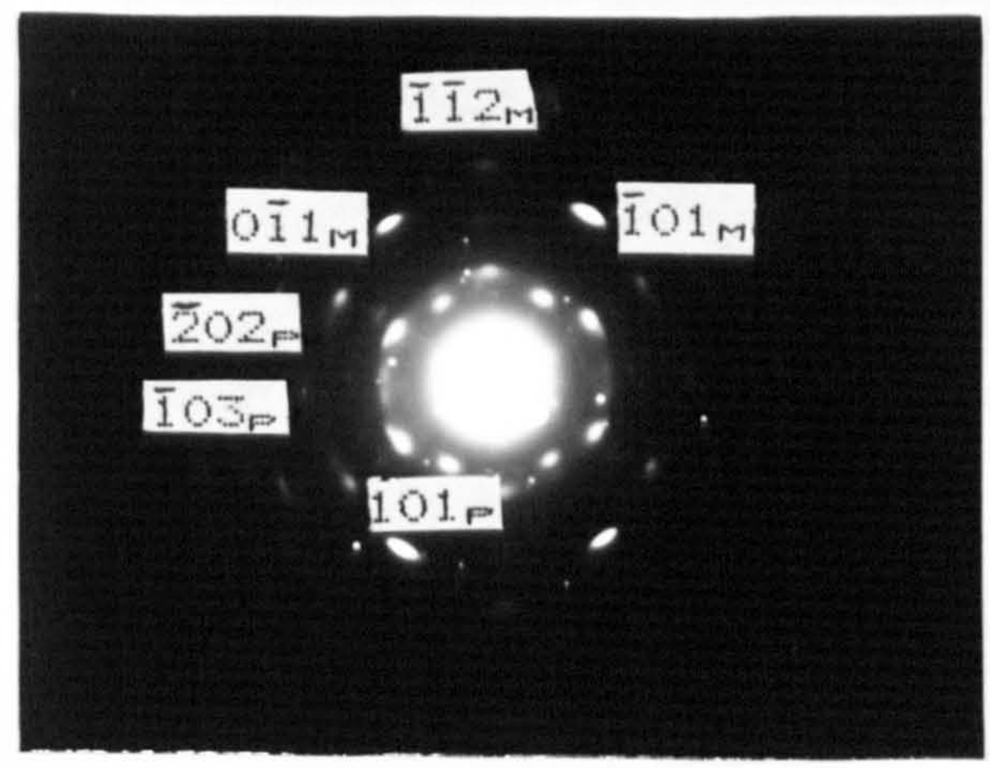

(ii)

b

Fig 5.6: Low temperature (∝) Si_3N_4 precipitates, indicated as P in annealed, a), 0.78 and b), 1.03 % Si steels: (a); i), B.F. image, ii), Dark field to (ai) (b); i), B.F. image, ii), Diffraction pattern of (bi) Note the streaking of the precipitate spots. Annealing conditions are as in code A of H.T.

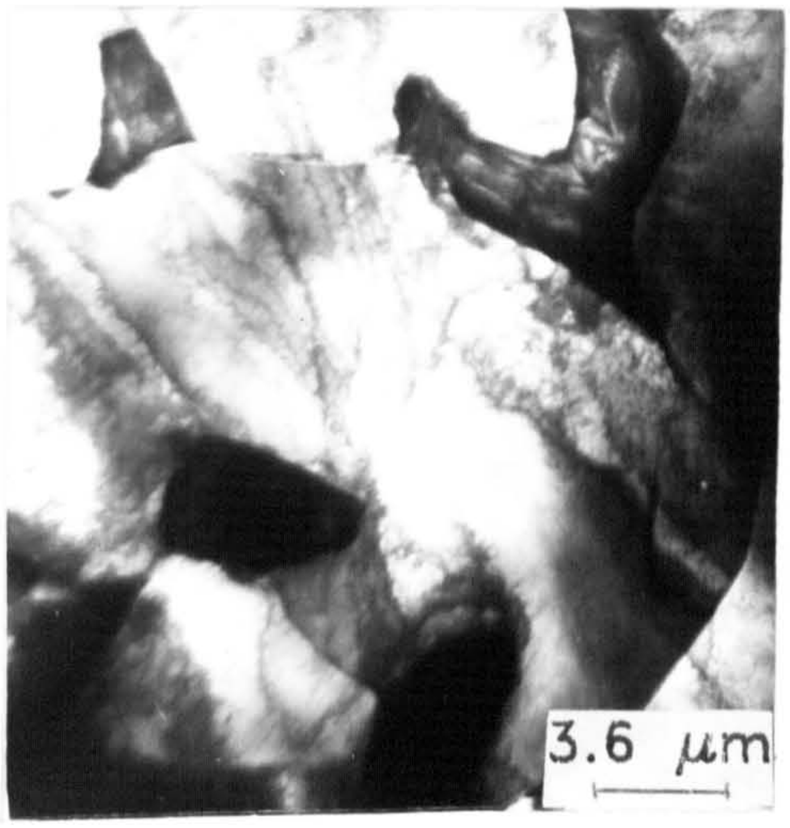

(i)

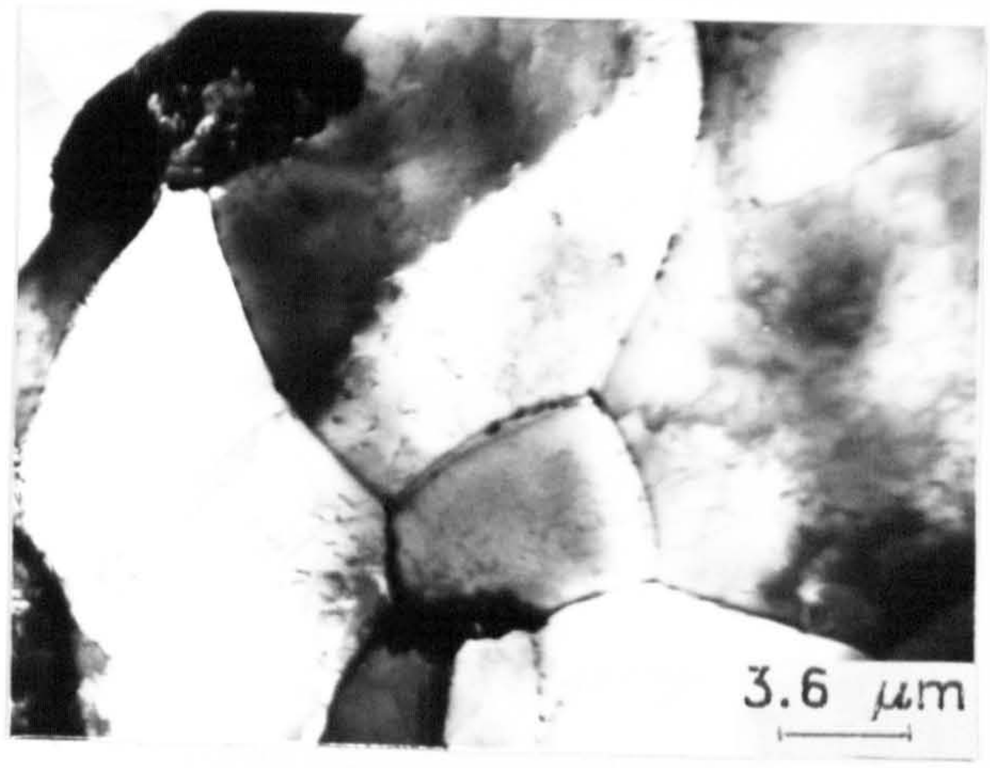

(ii)

a

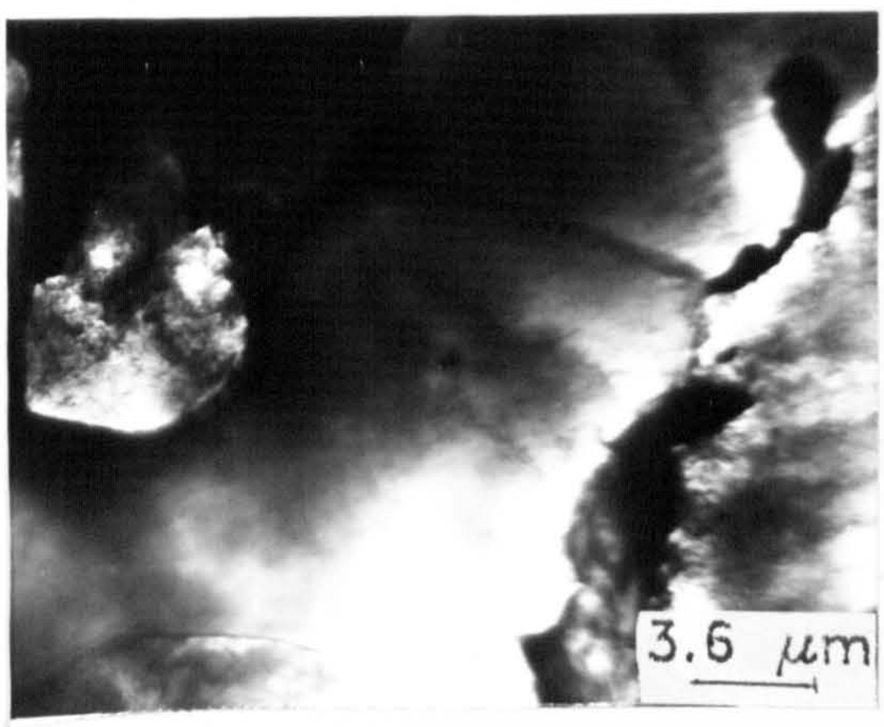

b

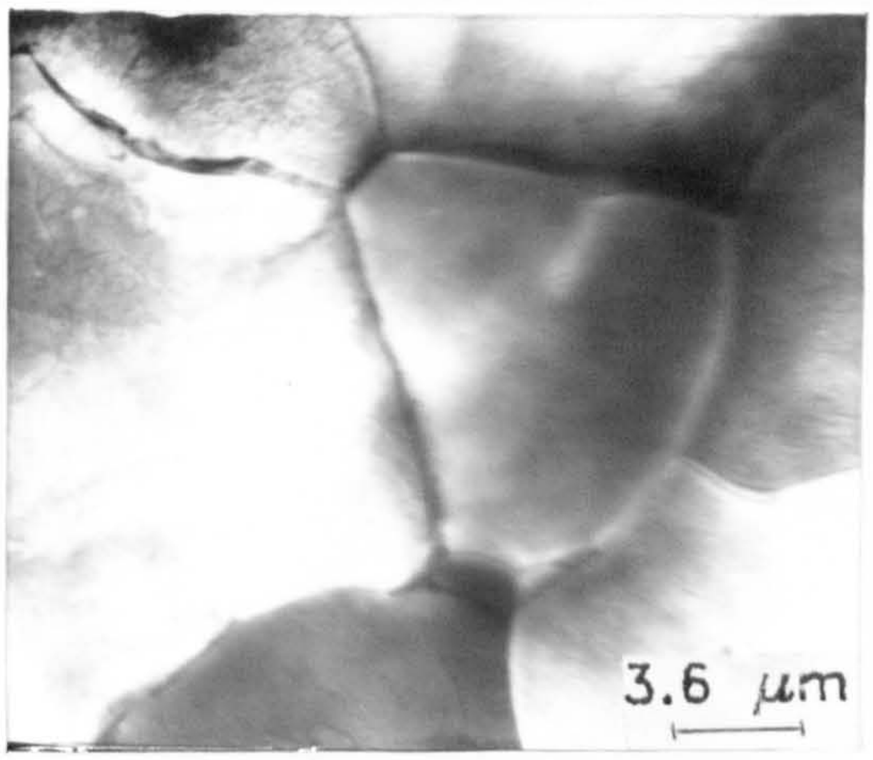

c

Fig 5.7: Electron micrographs of,a),1.03% Si steel: i),unaged, ii),short-aged; b), unaged 0.78% Si and c), unaged 0.31% Si steel grades. Note the presence of micrograins in the 1.03 and 0.78 wt% Si steels.However,such micrograins lack in the rest of the steel grades, example,the 0.31 wt% Si grade(c).

Fig 5.8: Grain size Vs steel strength for different silicon levels, at room temperature tests:

a), Unaged batch; b),same as "a",but with multiple slopes, suggesting that the Hall-Petch equation may not be valid over an infinite range of $d^{-1/2}$;

c), short-aged batch.

a

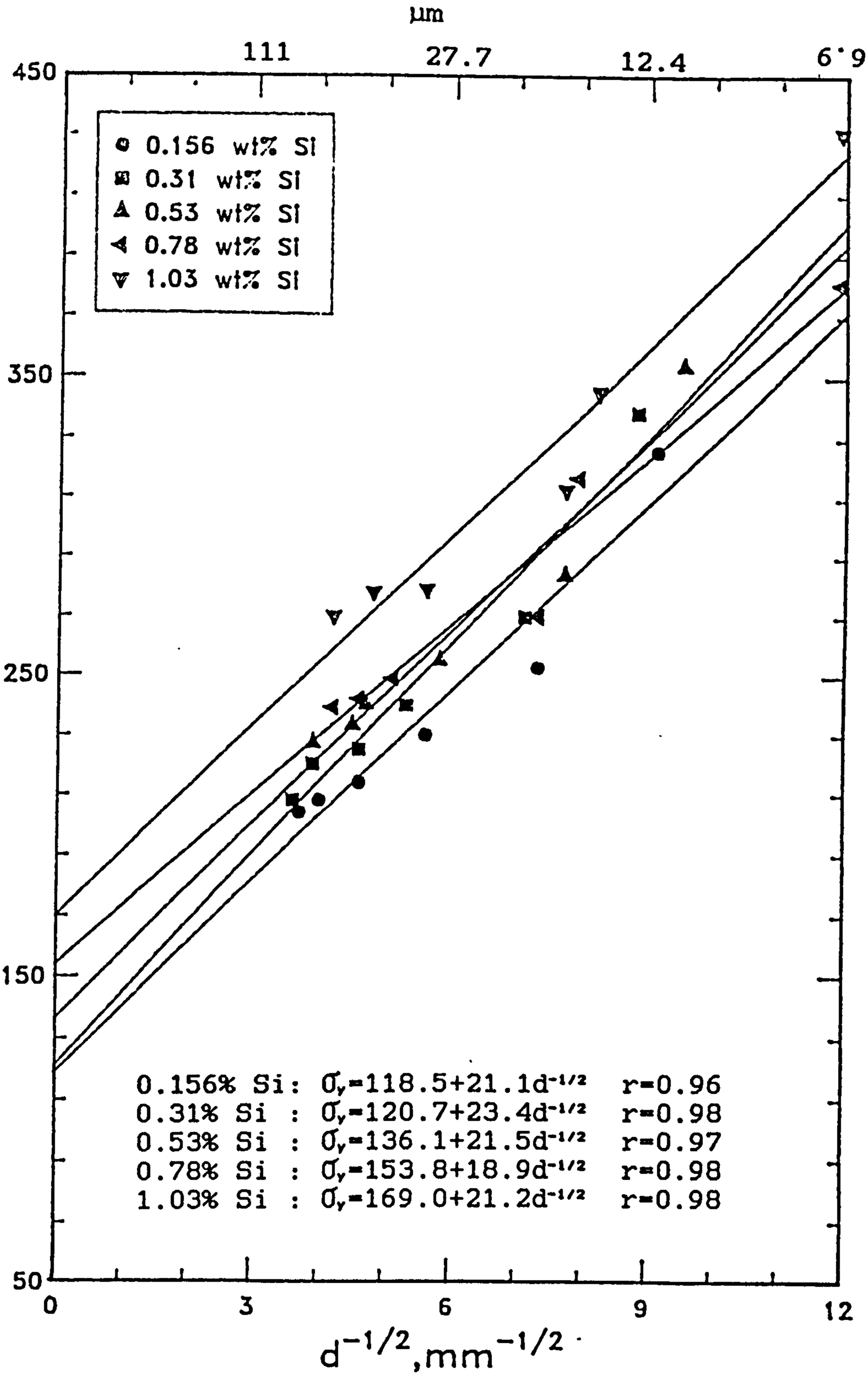

Grain size vs Steel strength for different Si levels.

b

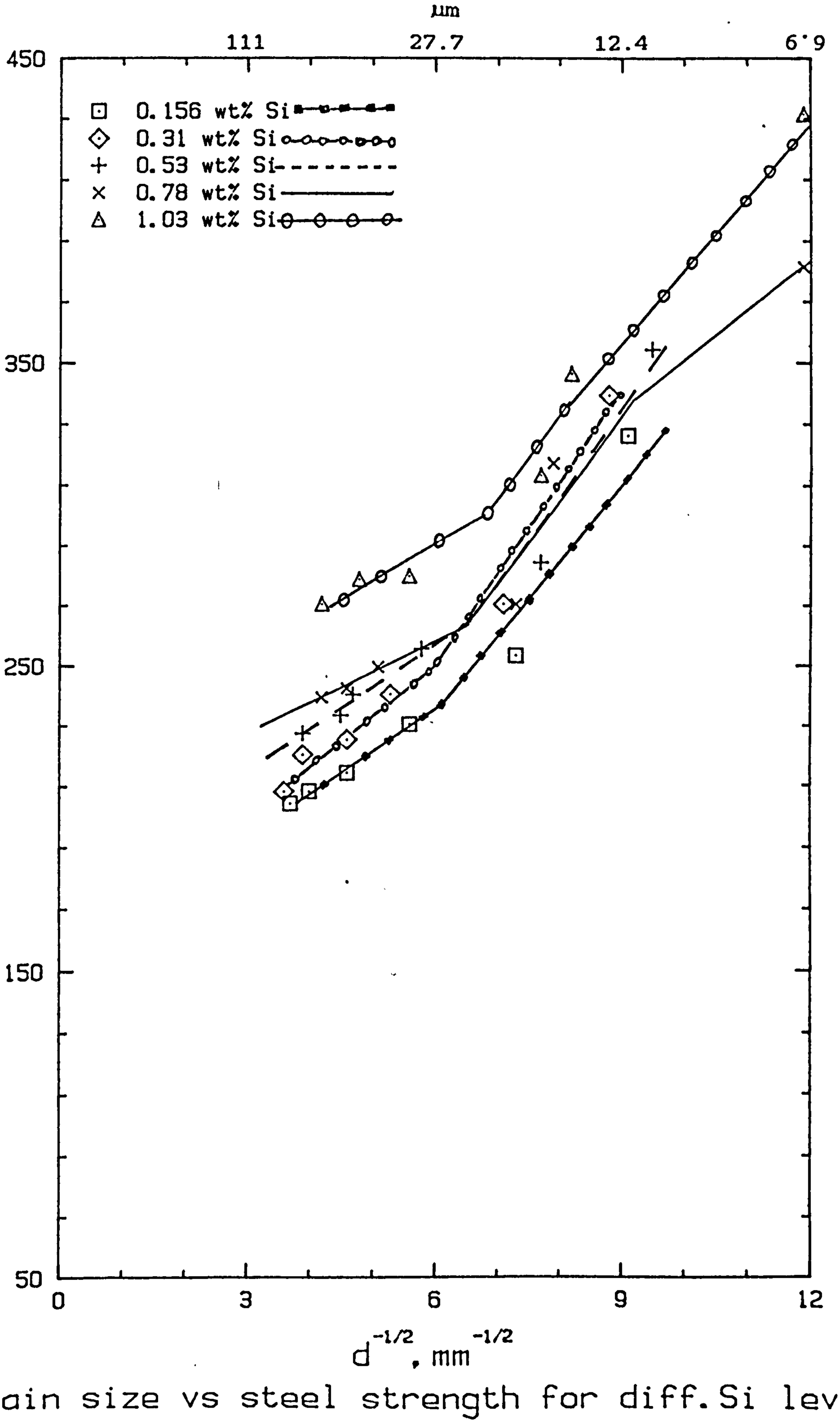

Grain size vs steel strength for diff. Si level

c

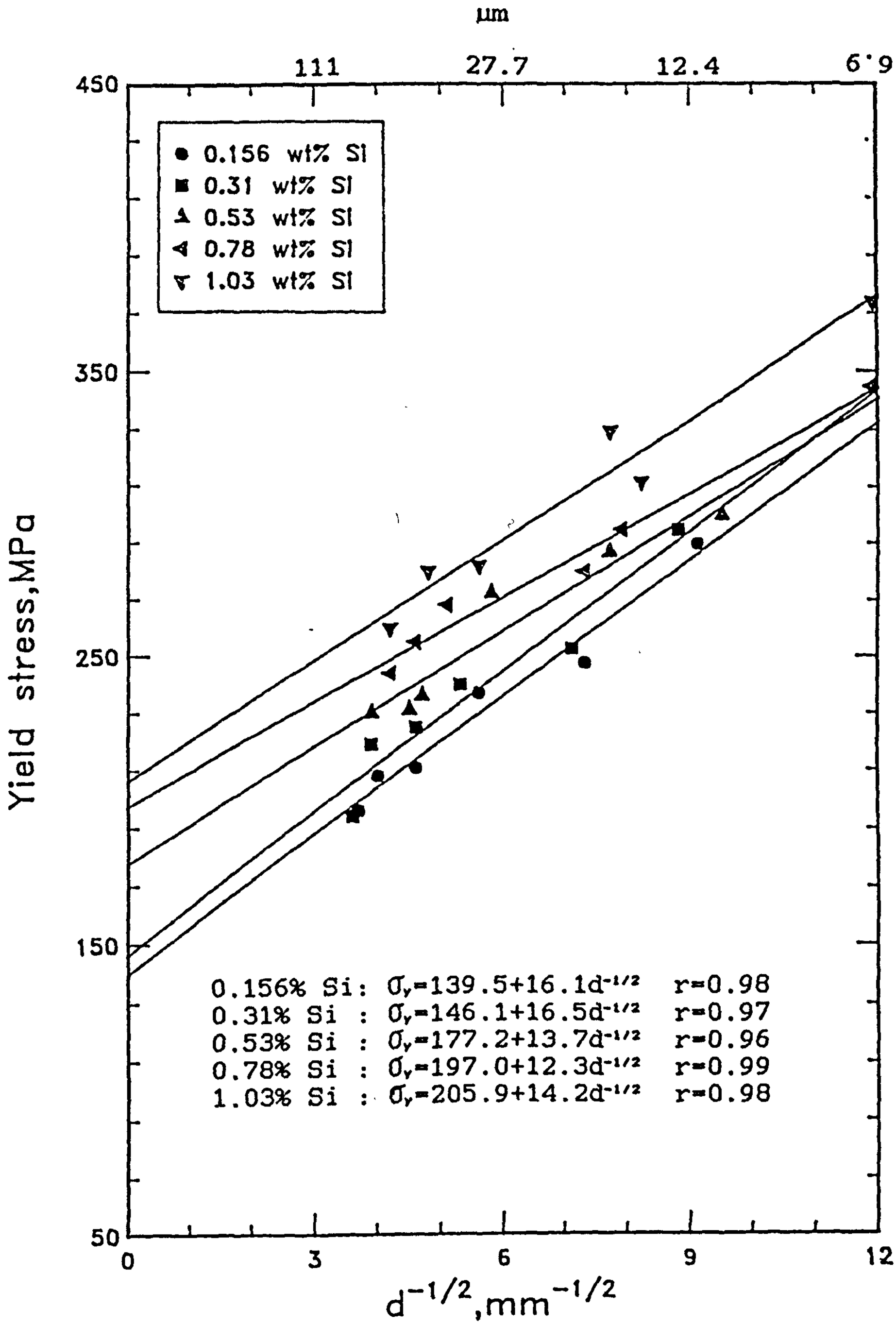

Grain size vs Steel strength for different Si levels.

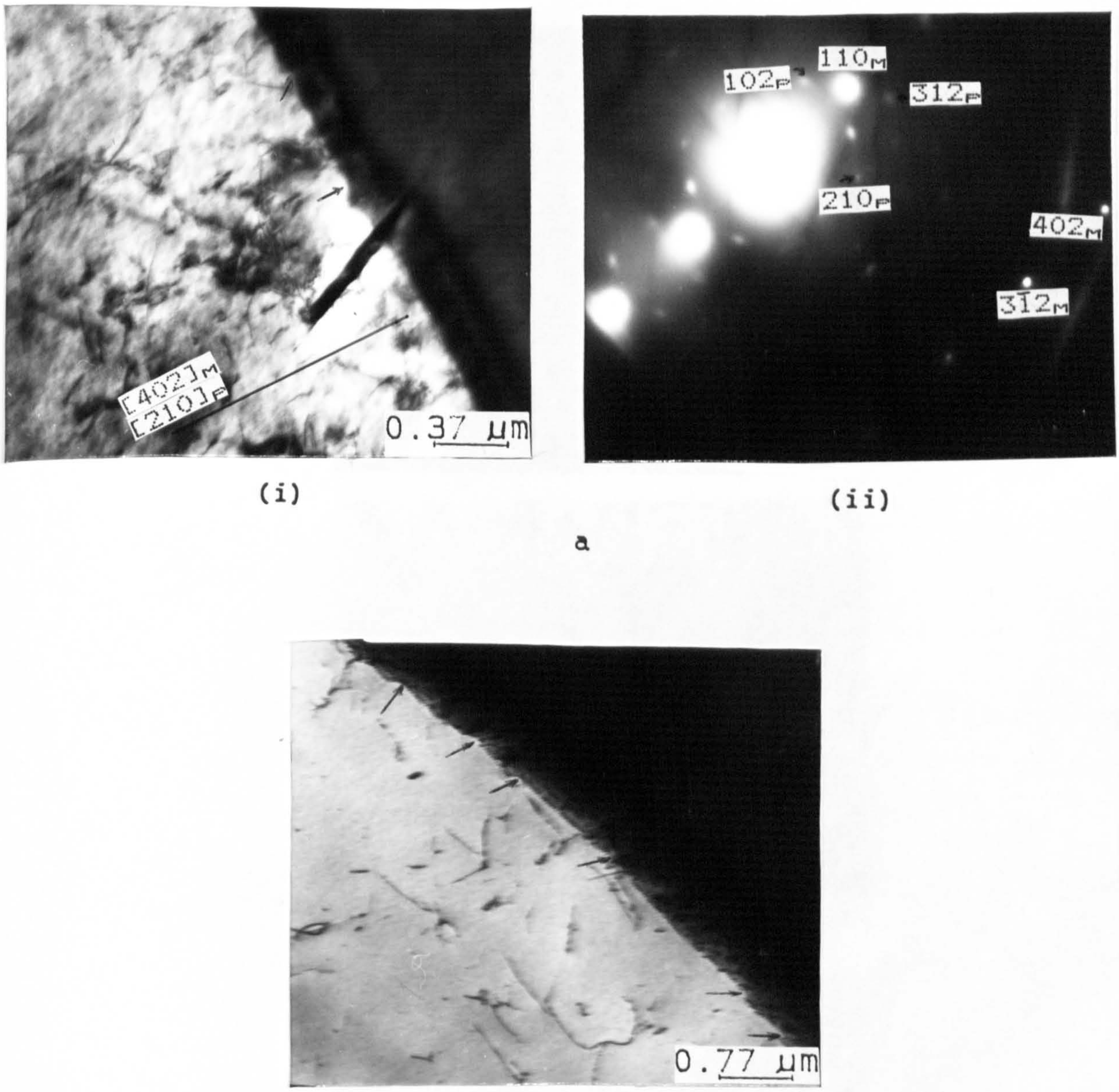

Fig 5.9: Ledge structures,rarely observed in the steels treated according to the A code of the heat treatments:

a); i),0.31% Si steel, ii),the diffraction pattern, revealing the precipitate at the grain boundary in "ai" to be low temperature(α) Si_3N_4,

b); 0.78 % Si steel.

The arrows indicate some of the ledges.

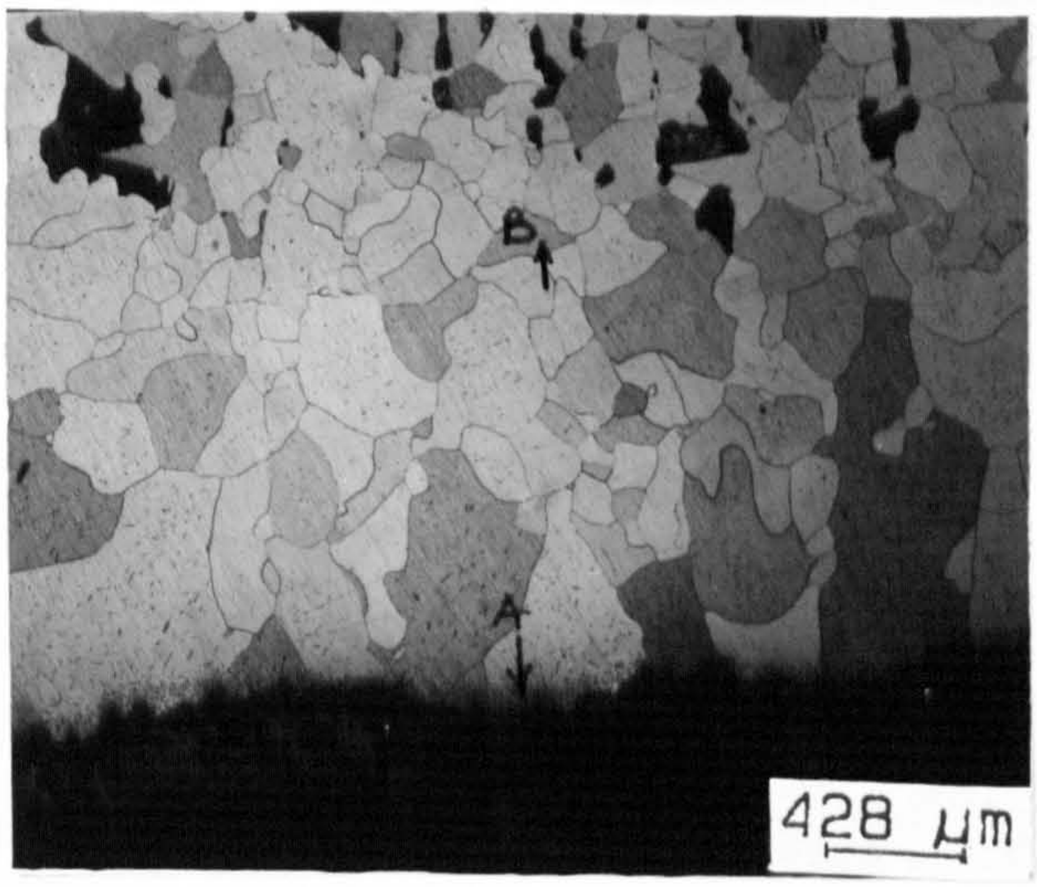

a

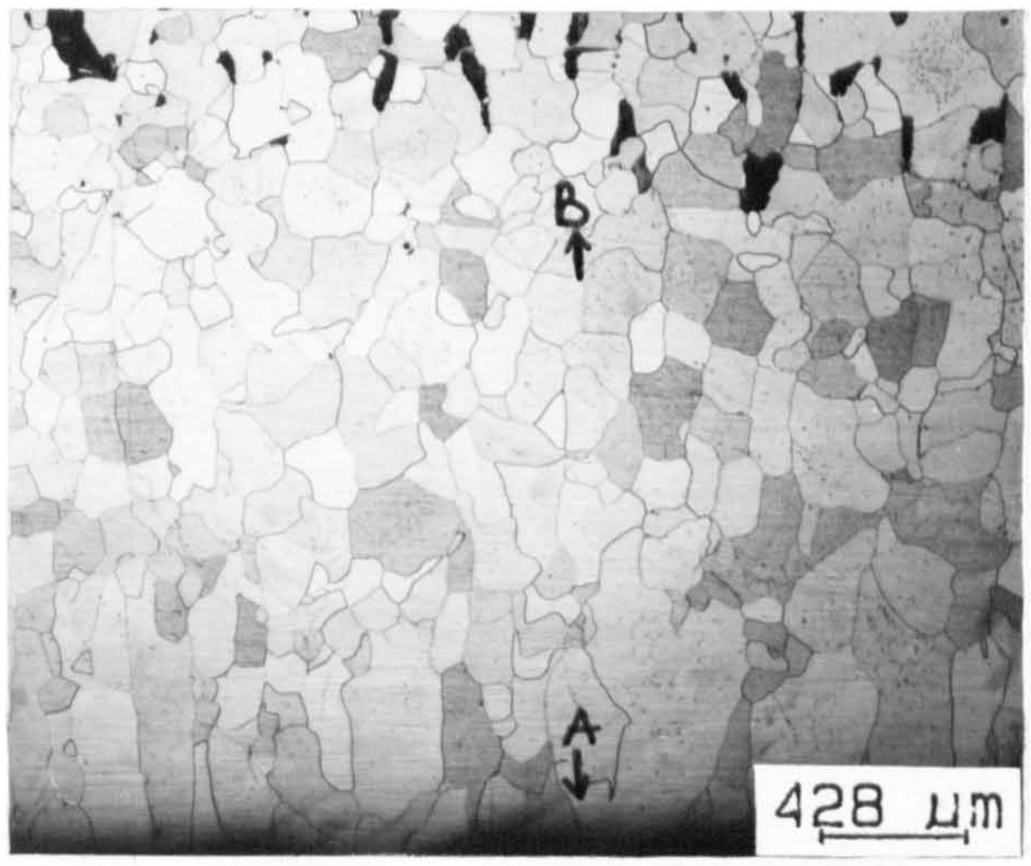

b

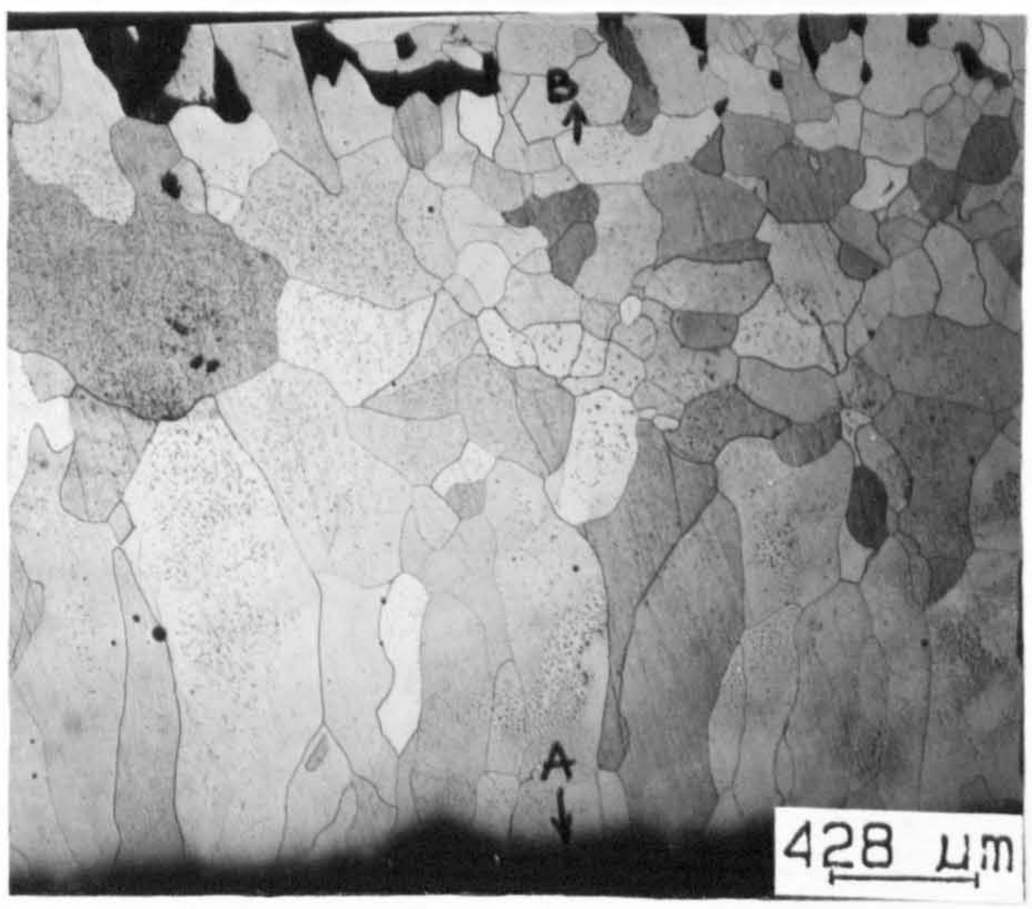

c

Fig 5.10: Optical micrographs of the decarburized layers of the steels:

a), 0.31; b) 0.78 and c),1.03 wt% Si.

Treated according to heat treatment,code D. A–B denotes the decarburized layer.

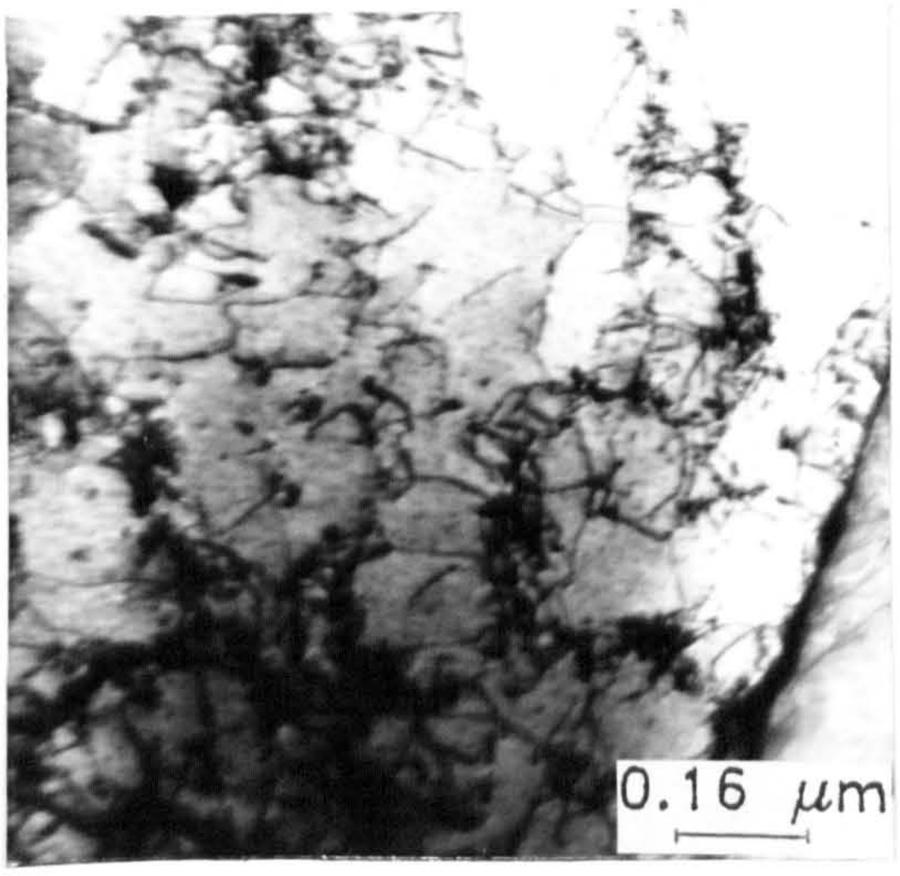

a

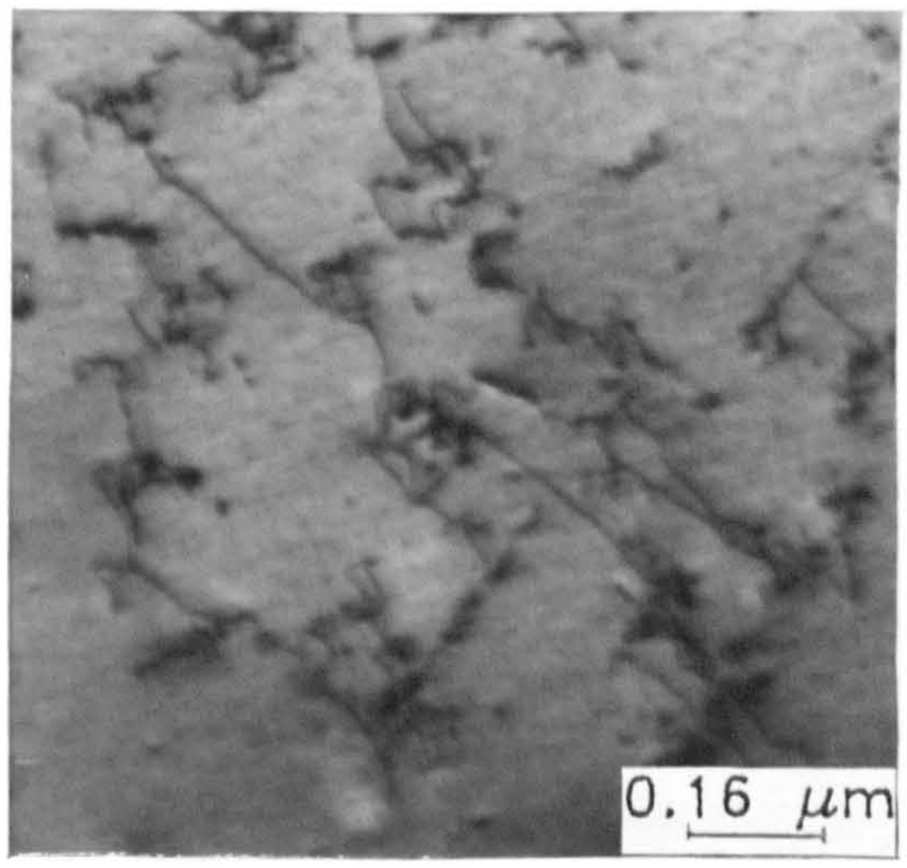

b

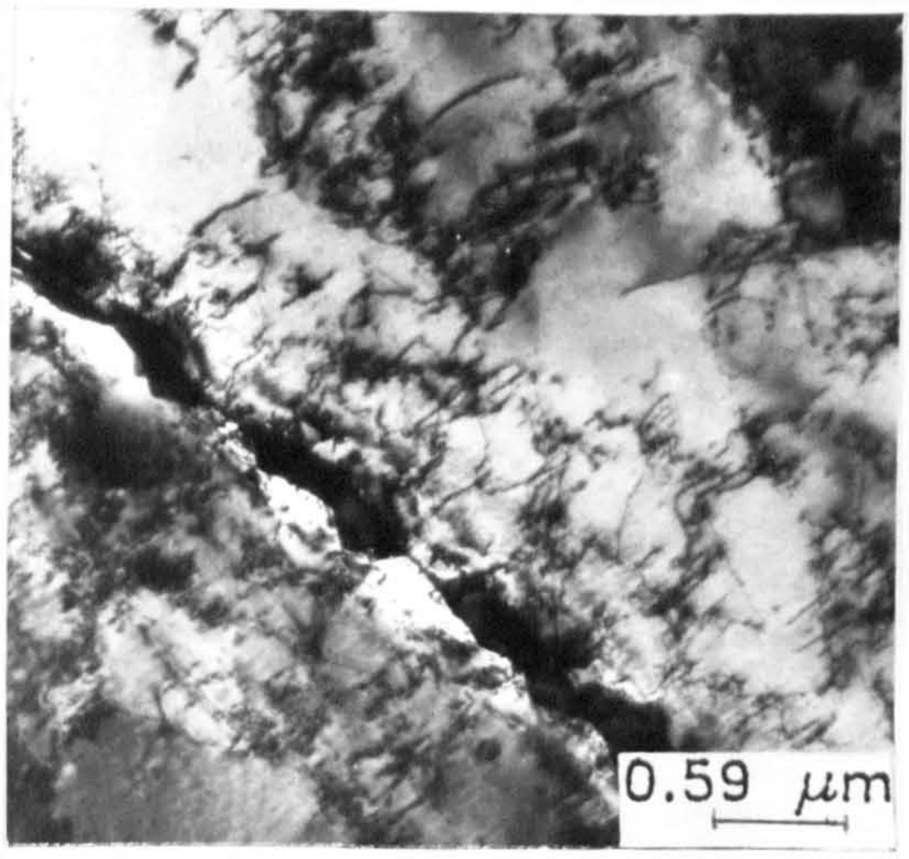

c

Fig 5.11:Electron micrographs of dislocation structures of the smallest(a),and the largest(c) grains; a),unaged 1.03% Si steel treated as in code F b), same as "a",but in short-aged condition c), 0.31% Si steel treated as in code D. Note the similarity in structure,across the grain sizes and conditions.

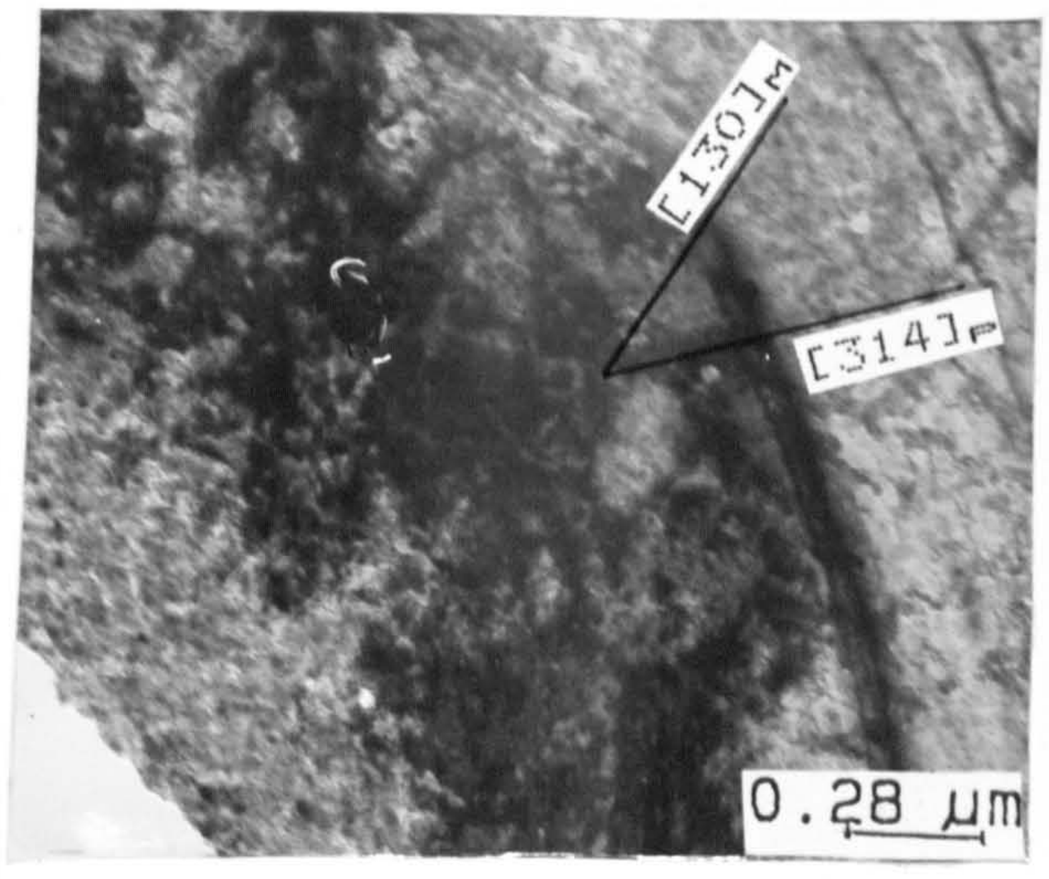
[130]M
[314]P
0.28 μm

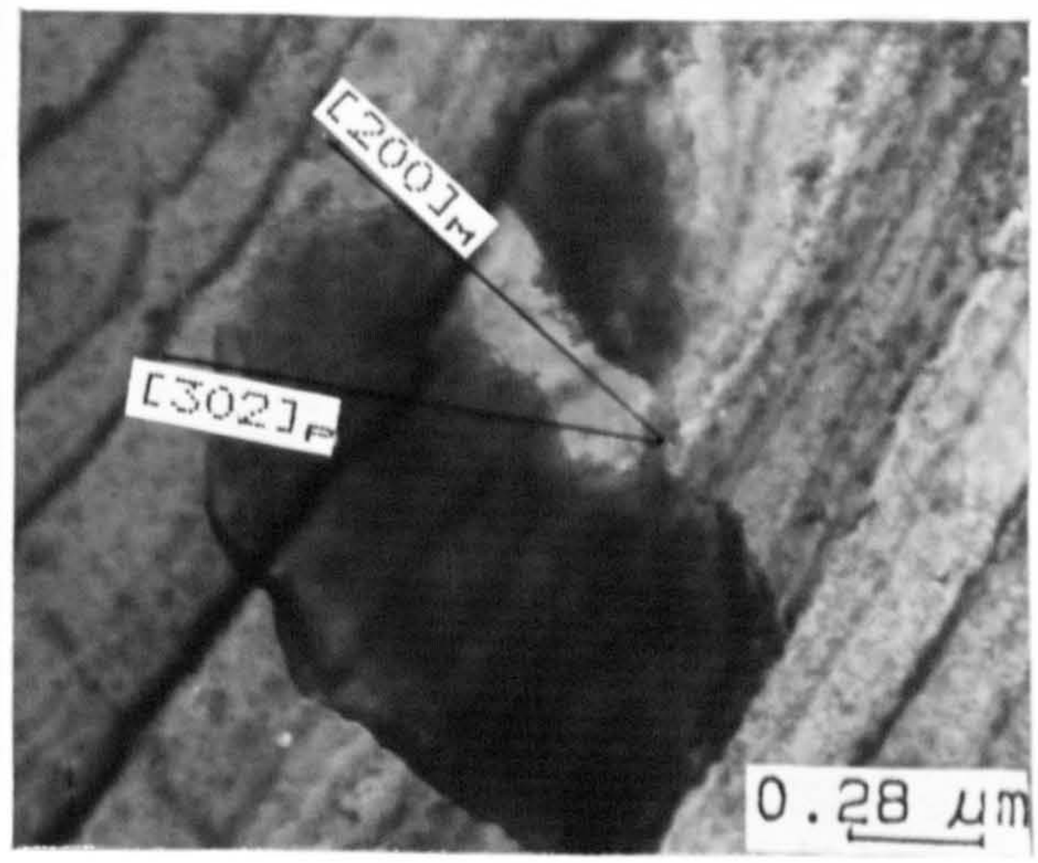
[200]M
[302]P
0.28 μm

(i)

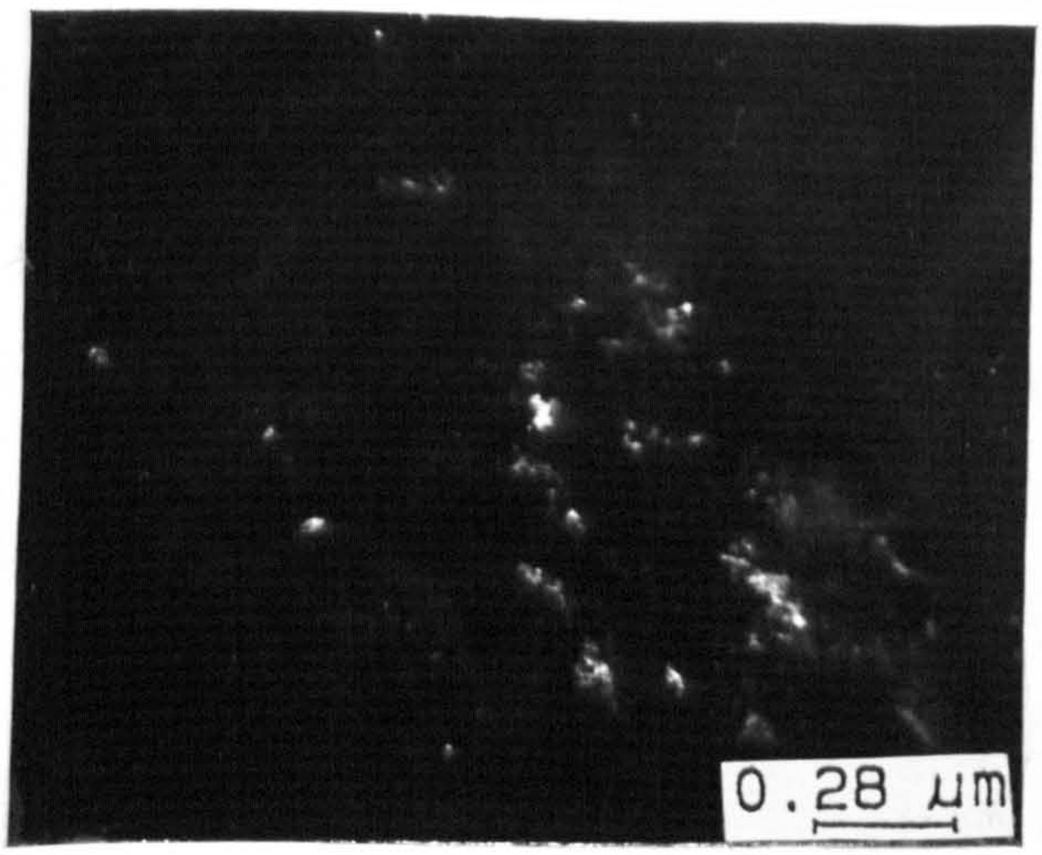
0.28 μm

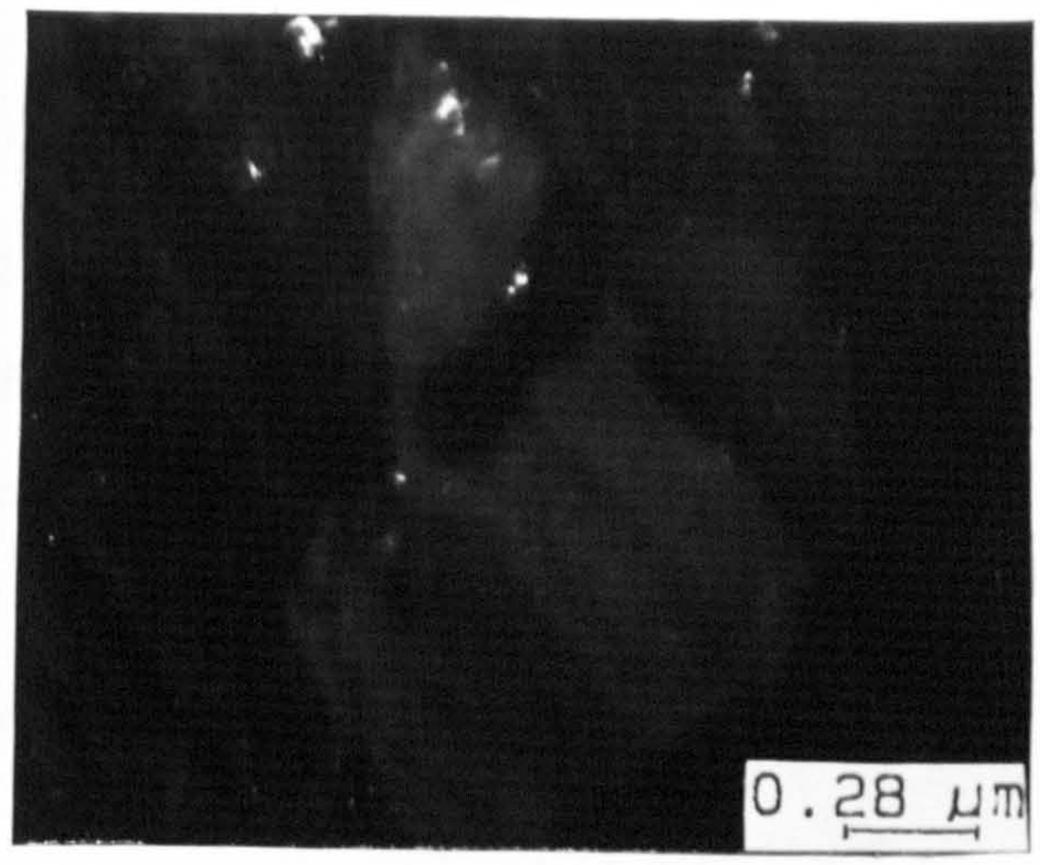
0.28 μm

(ii)

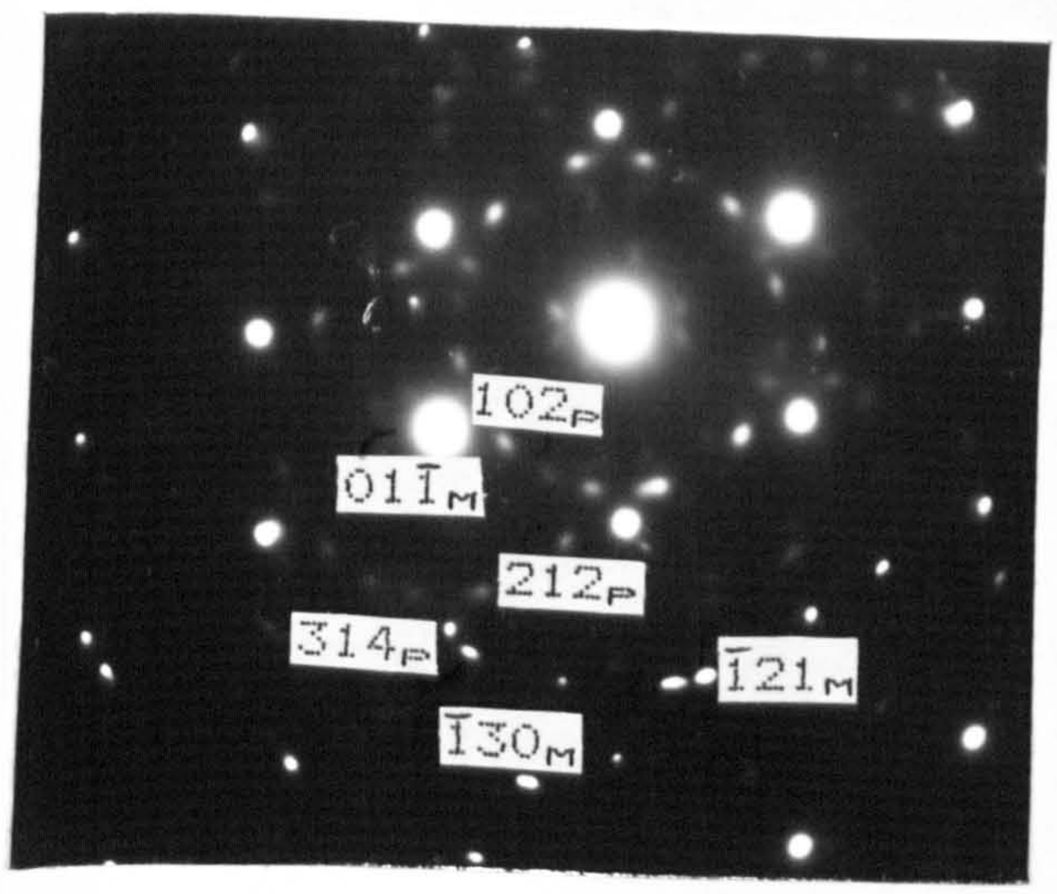
102P
011M
212P
314P
121M
130M

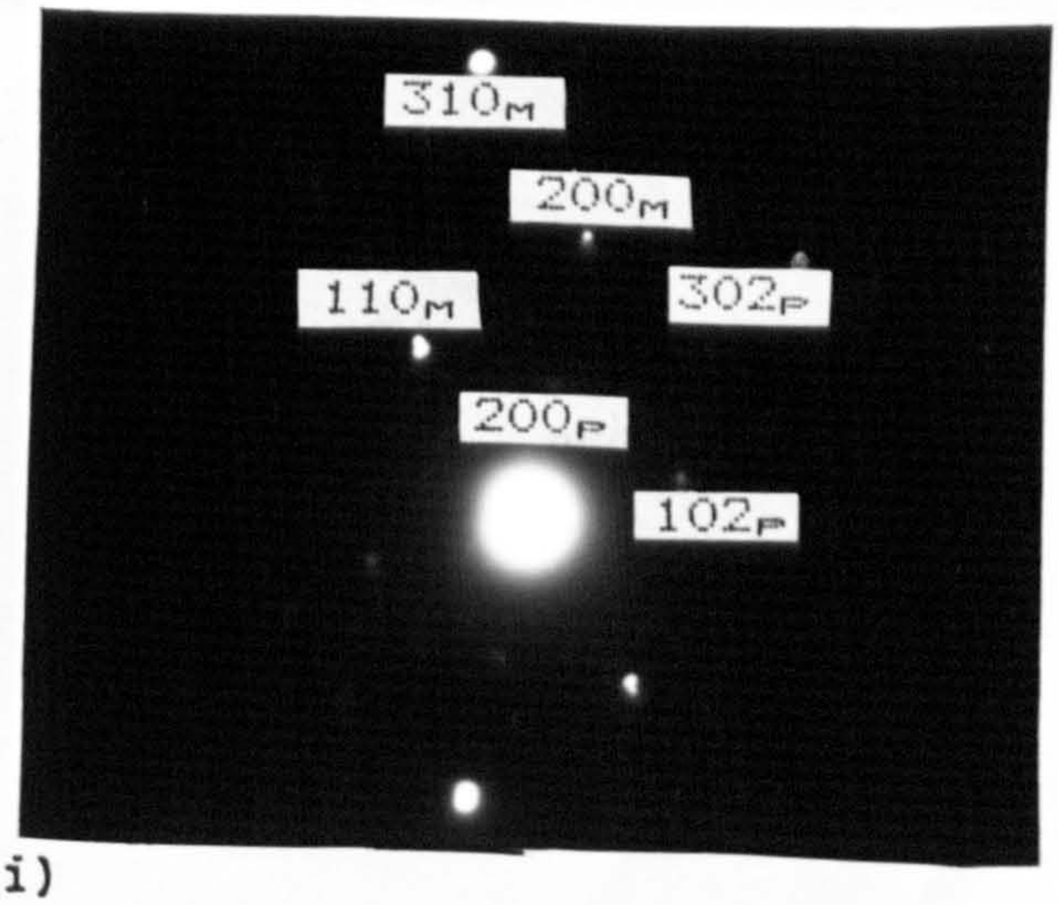
310M
200M
110M
302P
200P
102P

(iii)

a

b

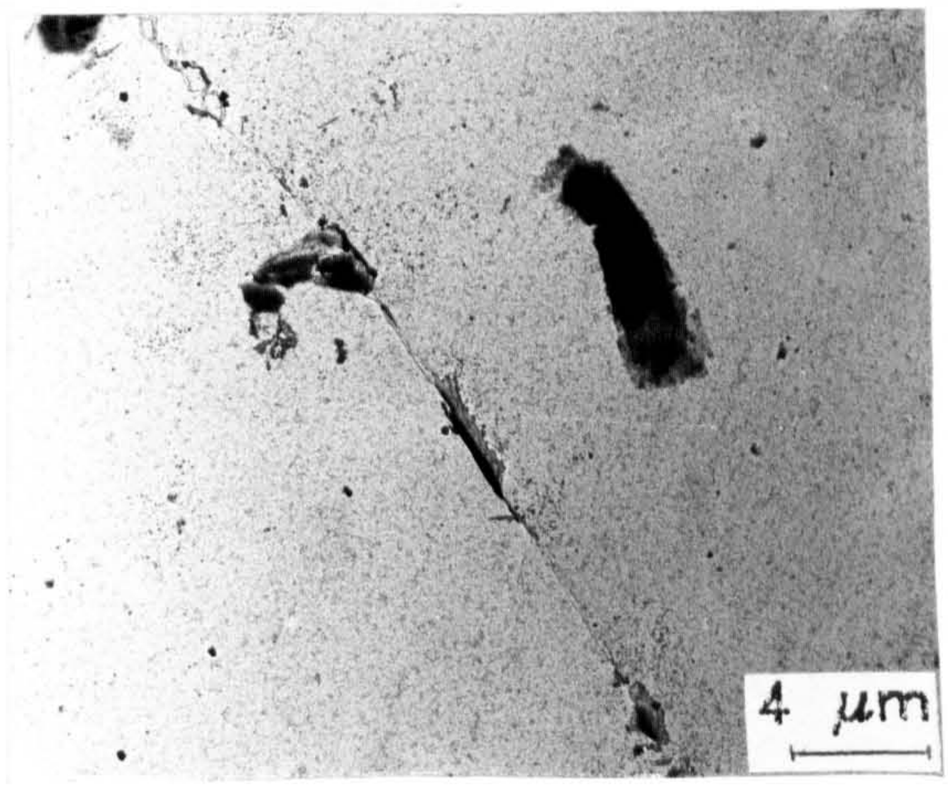

c

Fig 5.12: Low temperature (α) Si_3N_4 precipitates,in the aged(595±10°C for 72 hours under vacuum) prior annealed steels, according to code C:
a), grain boundary region of the 0.31% Si steel, i),B.F.image;ii),D.F. from "ai";iii),D.P.of "ai", b),grain interior of the 0.31% Si steel, i),B.F.image;ii),D.F. from "bi";iii),D.P.of "bi", c),0.78% Si steel,bright field(B.F.) image of the precipitates extracted on a replica.

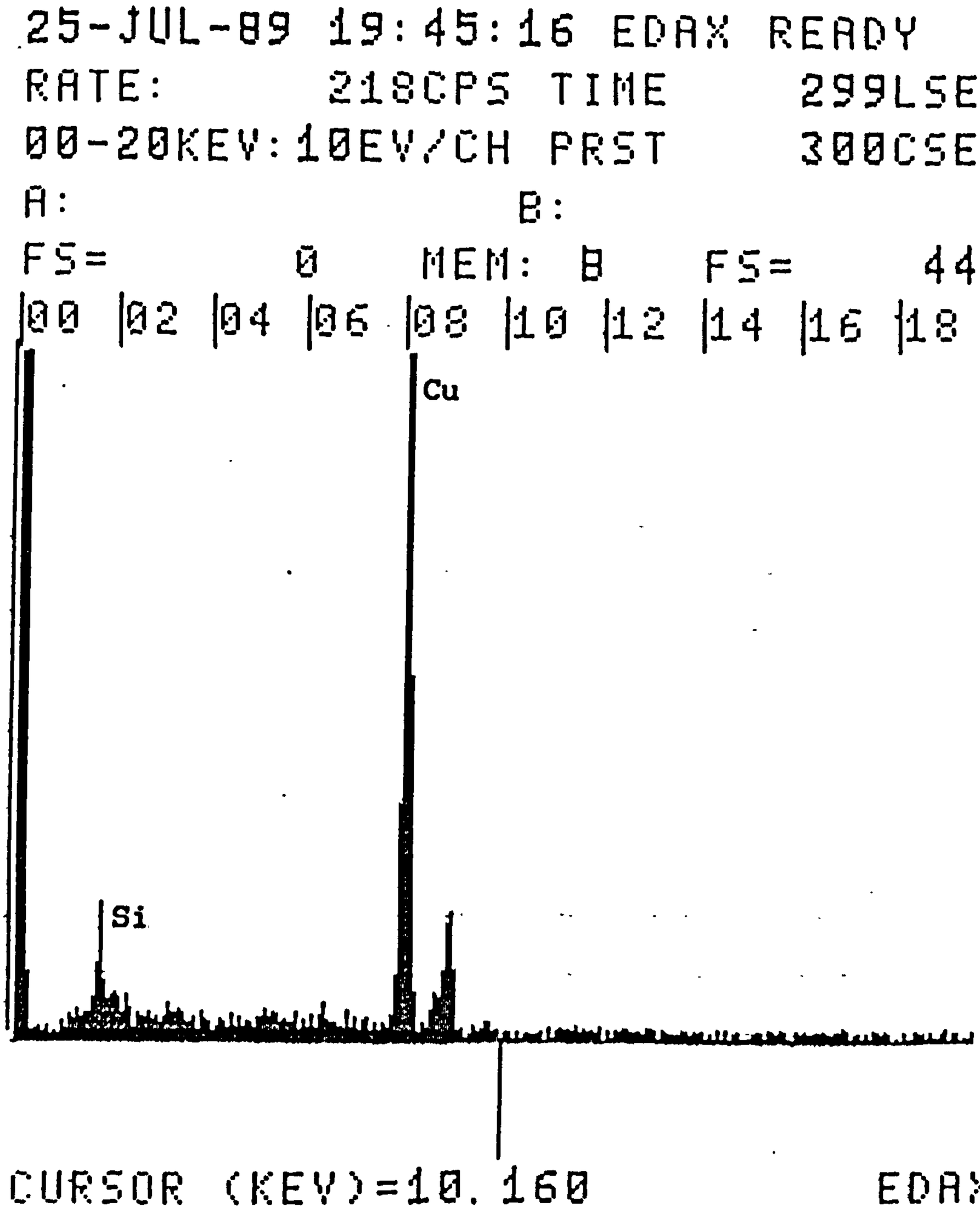

Fig 5.13: EDAX spectra of the extracted precipitates(on a replica) from the aged prior-annealed 0.31% Si steel.

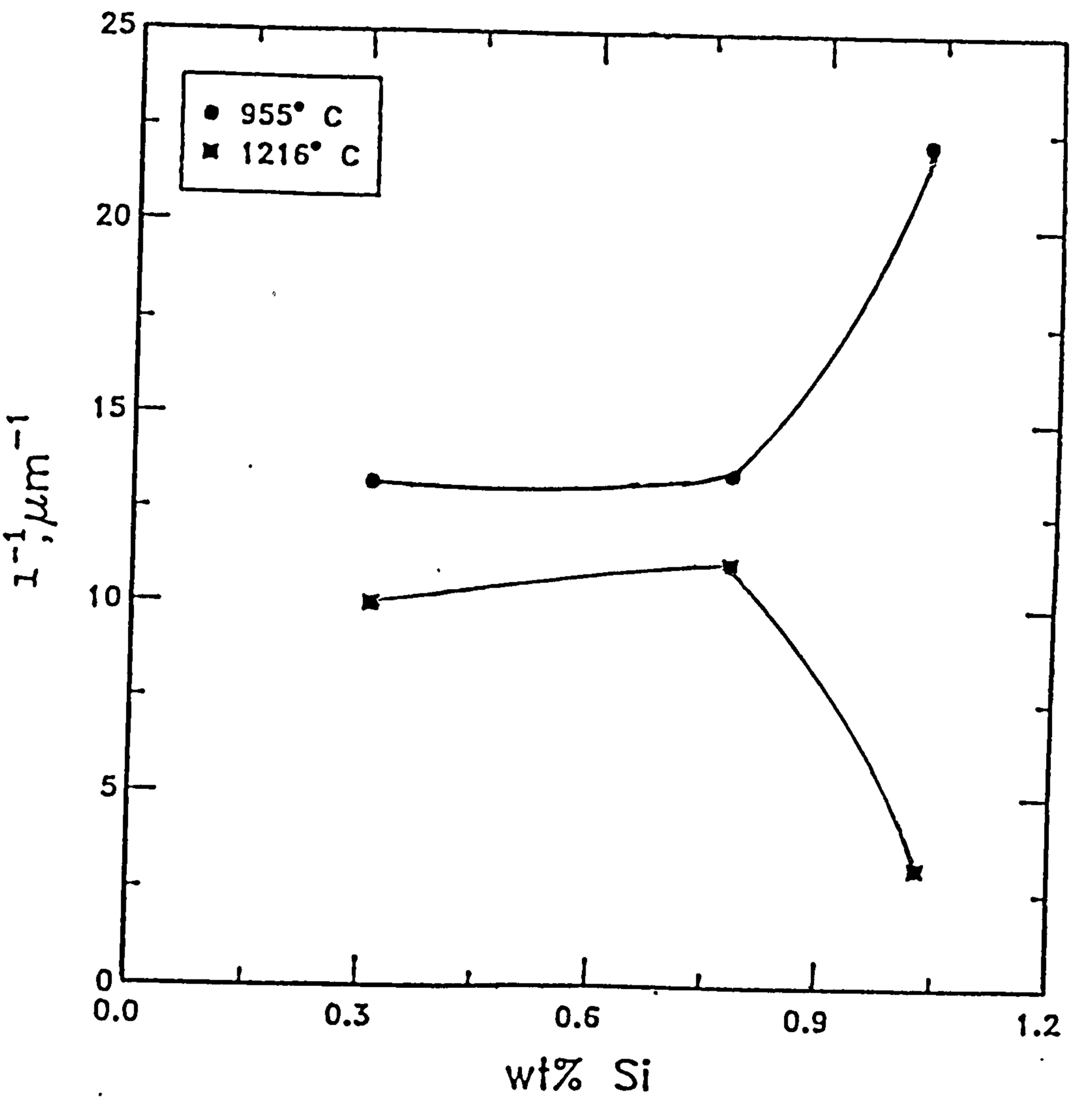

Fig 5.14: Reciprocal interlamellar spacing of pearlite Vs Si content(wt%) in steel at different austenitizing temperatures.

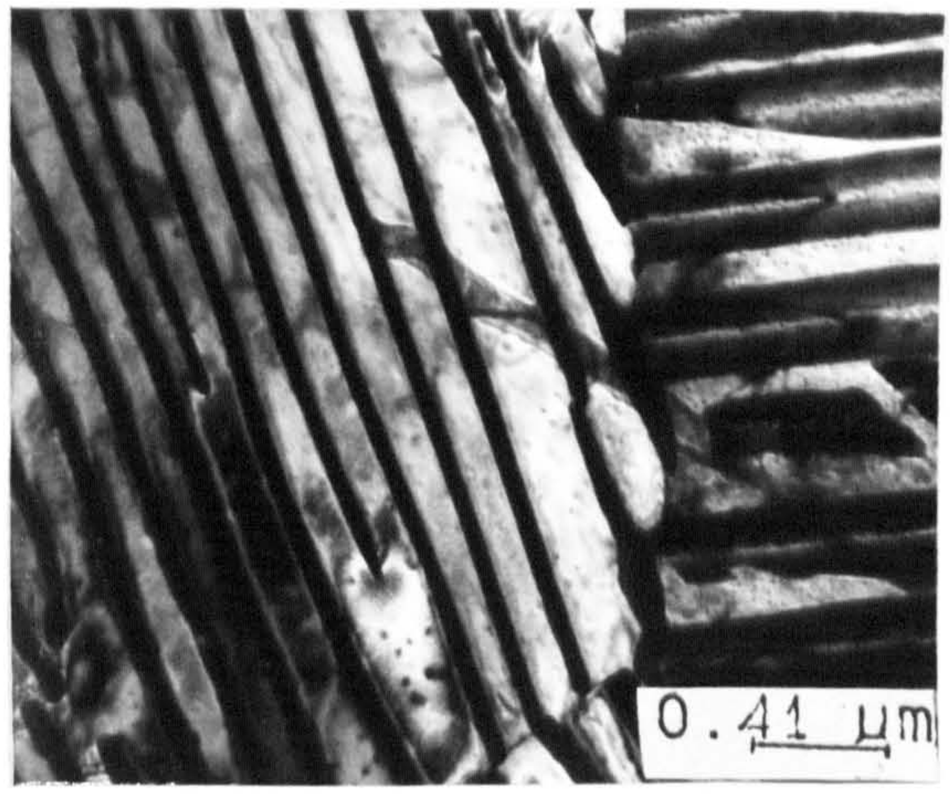

a

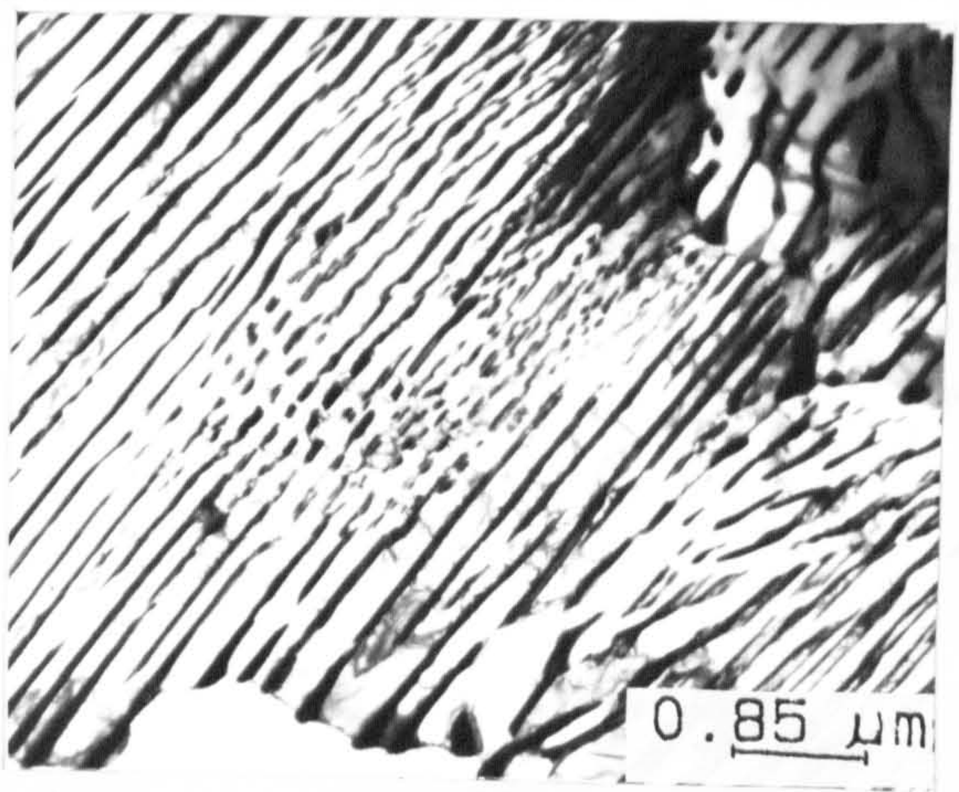

b

c

Fig 5.15: Typical structures of pearlite in the respective steels, treated as per code D:
a),0.31; b), 0.78 and c),1.03 wt% Si steels.Note the fragmentation and the spheroidization of cementite in the 1.03% Si steel.

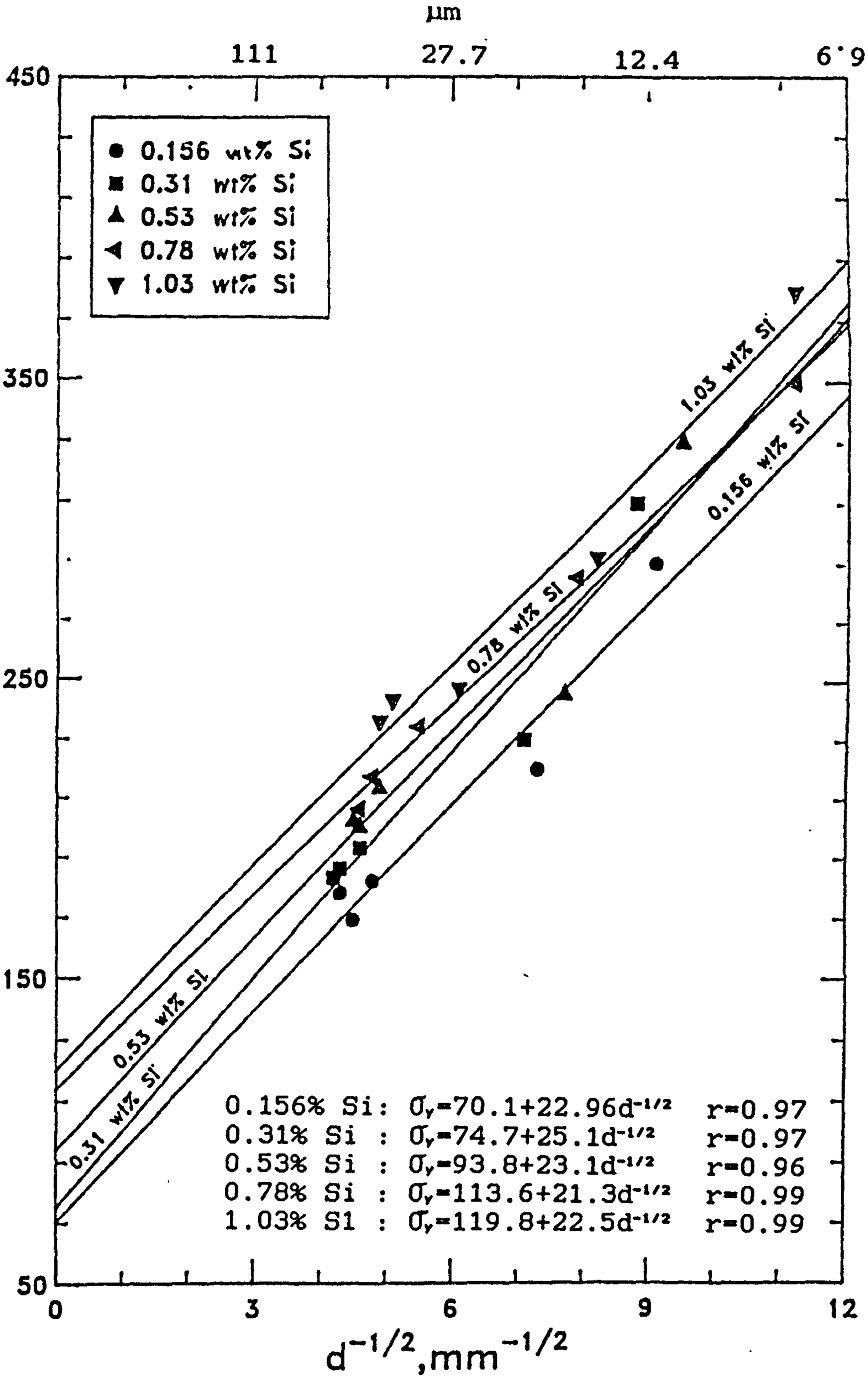

Fig 5.16: Athermal yield stress of steels Vs grain size,from the test at 350 K,with a strain rate of $1.7 \times 10^{-4} s^{-1}$.

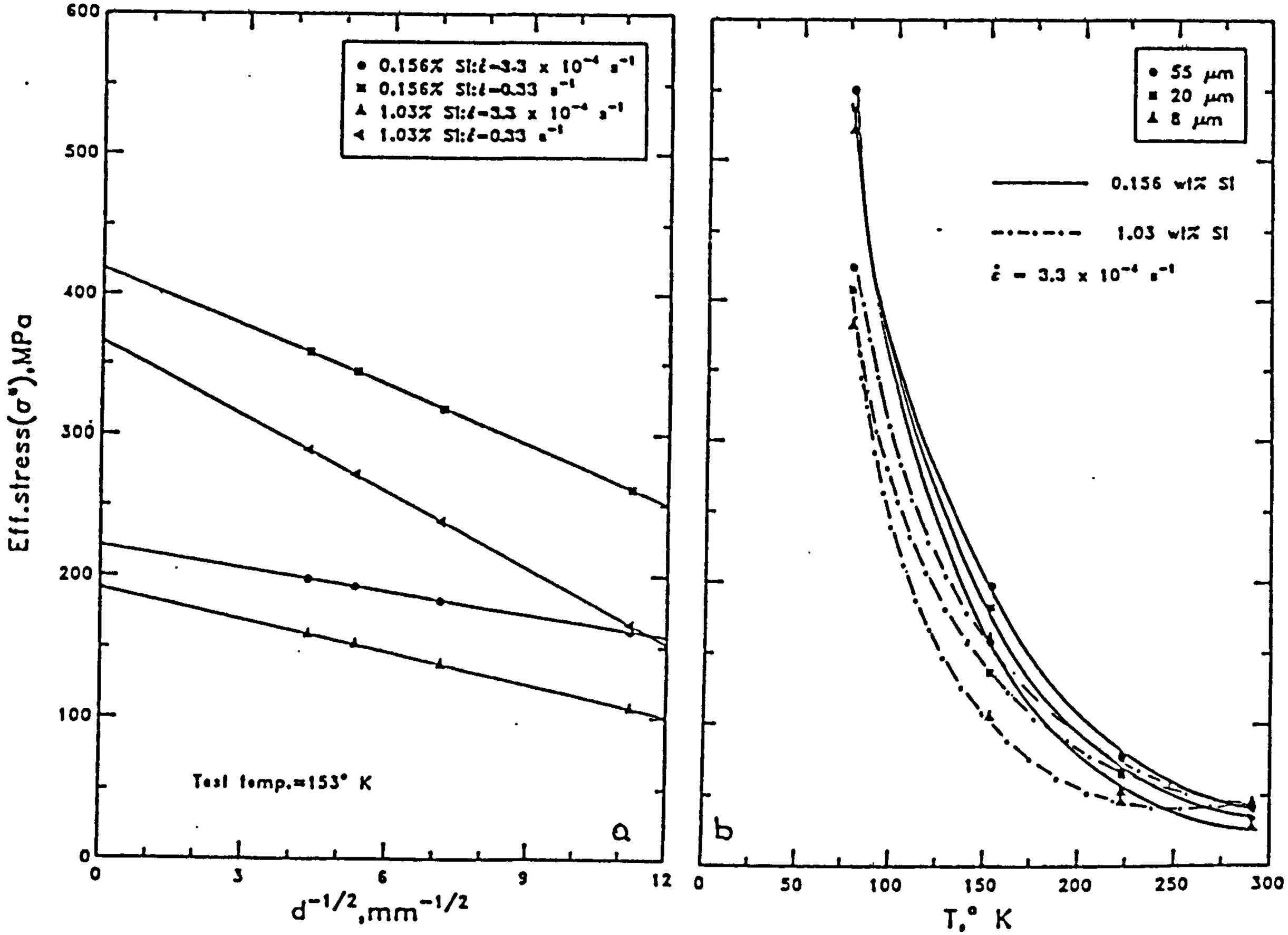

Fig 5.17: Effect of a),grain size and strain rate and b),temperature and grain size on the effective (thermal) yield stress of steels.

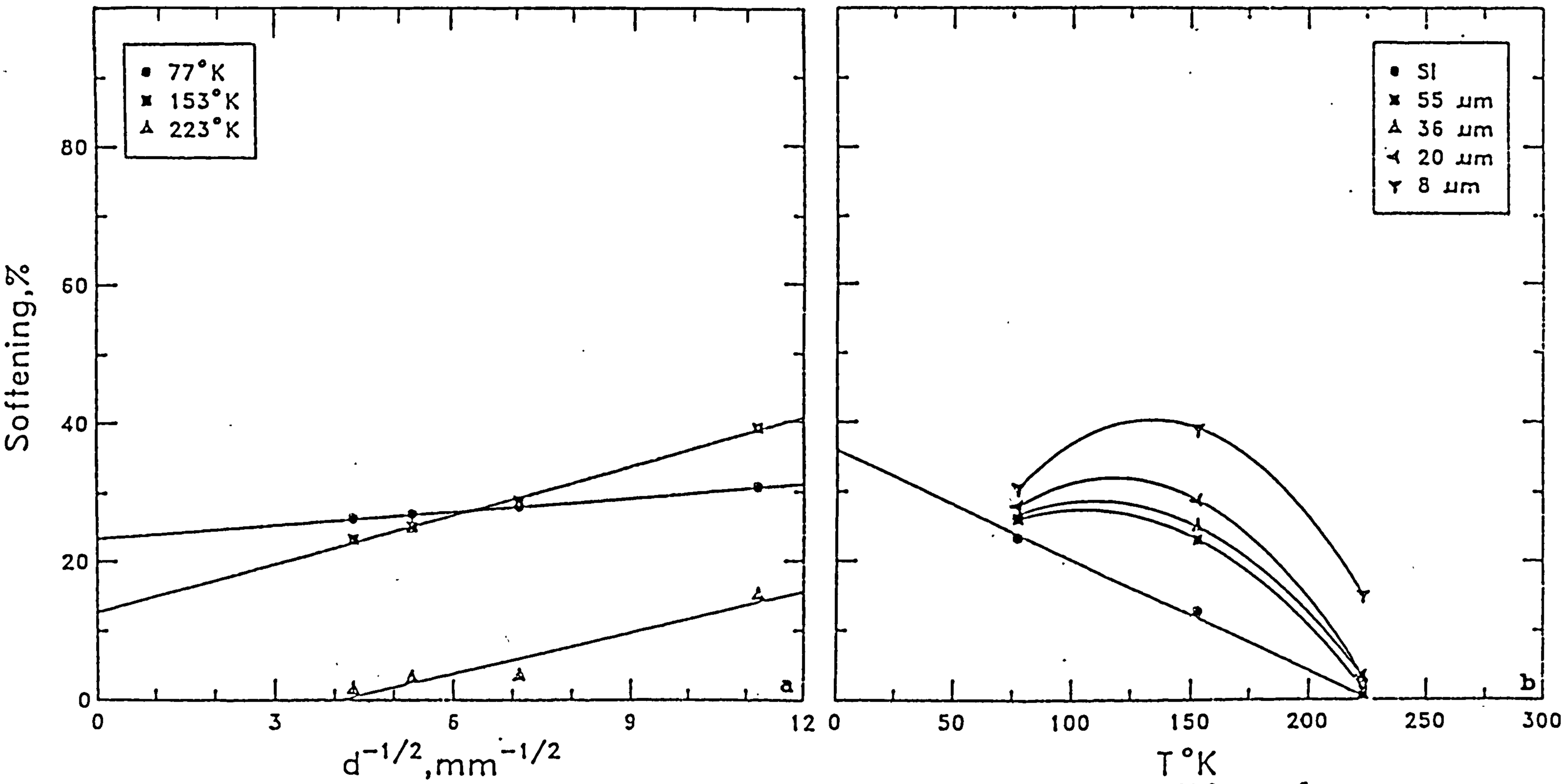

Fig 5.18: Degree of "softening",per one wt% addition of silicon,versus:

a), grain size; b),test temperature at a strain rate of $3.3\times10^{-4}s^{-1}$.

Fig 5.19: Effect of temperature on the lower(total) yield strength of steels at a given grain size with a strain rate of $3.3 \times 10^{-4} s^{-1}$:

a), 55 μm; b), 36 μm; c), 20 μm; d), 8 μm.

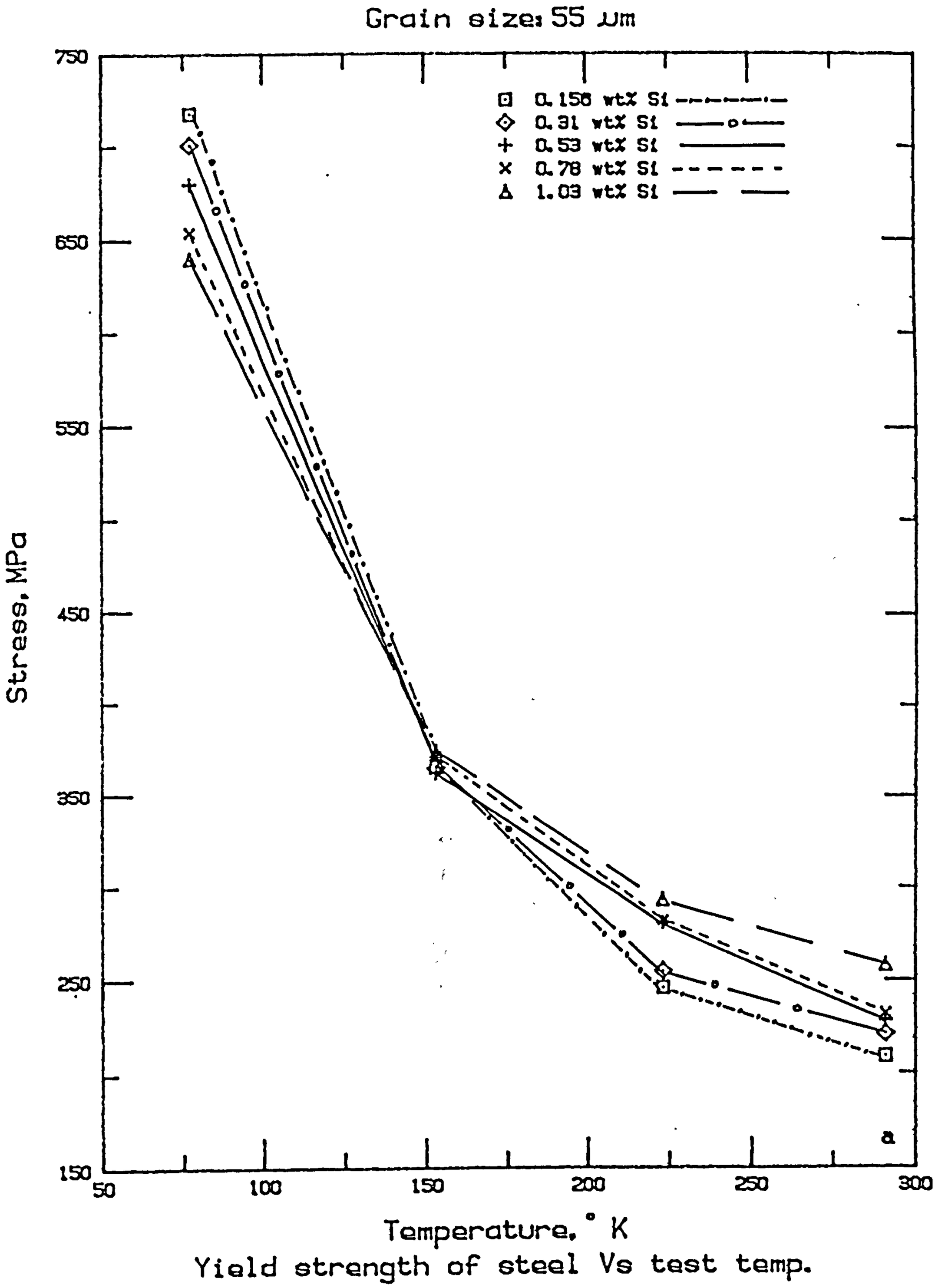

Temperature, ° K

Yield strength of steel Vs test temp.

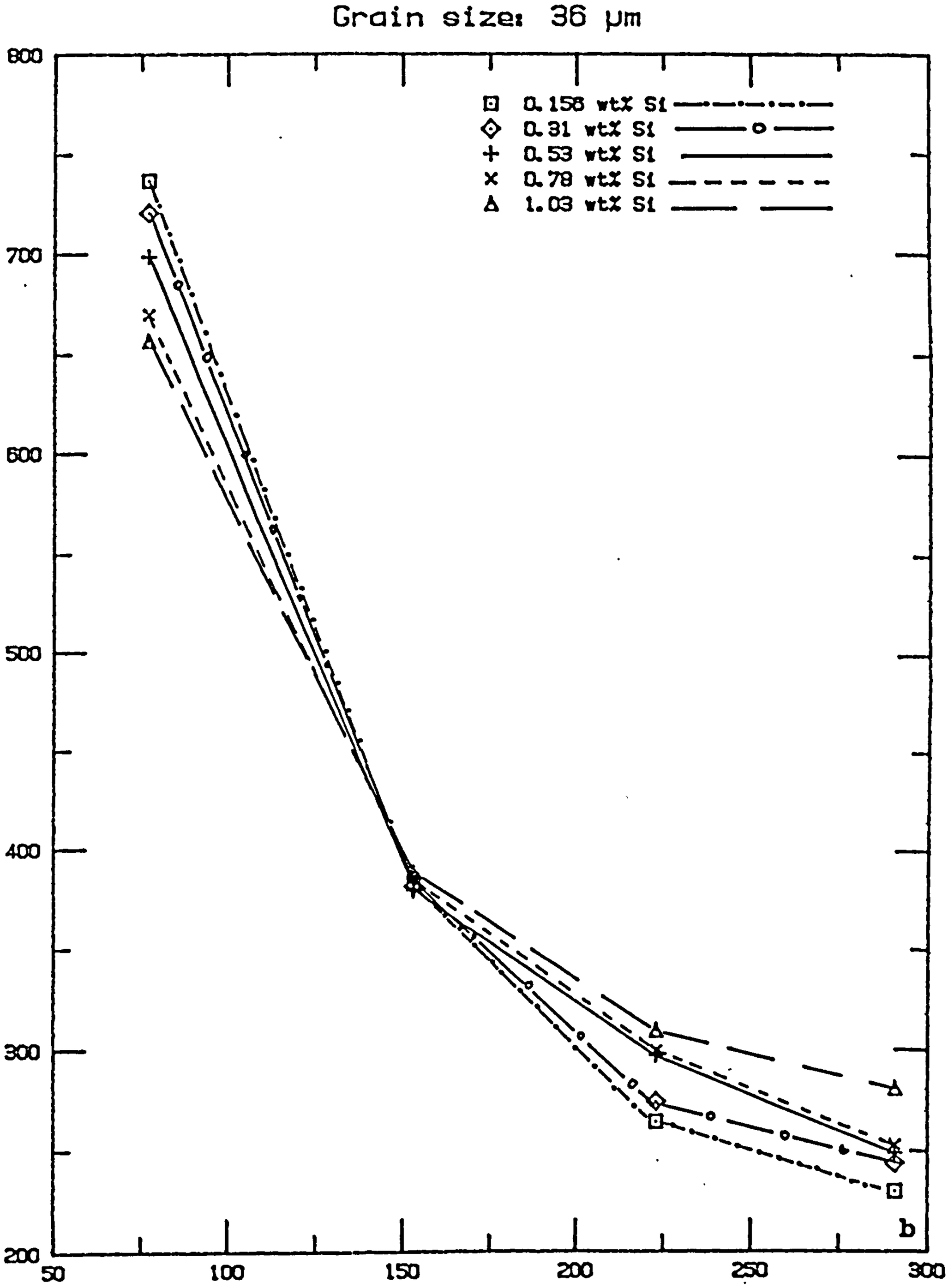

Temperature, ° K

Yield strength of steel Vs test temp.

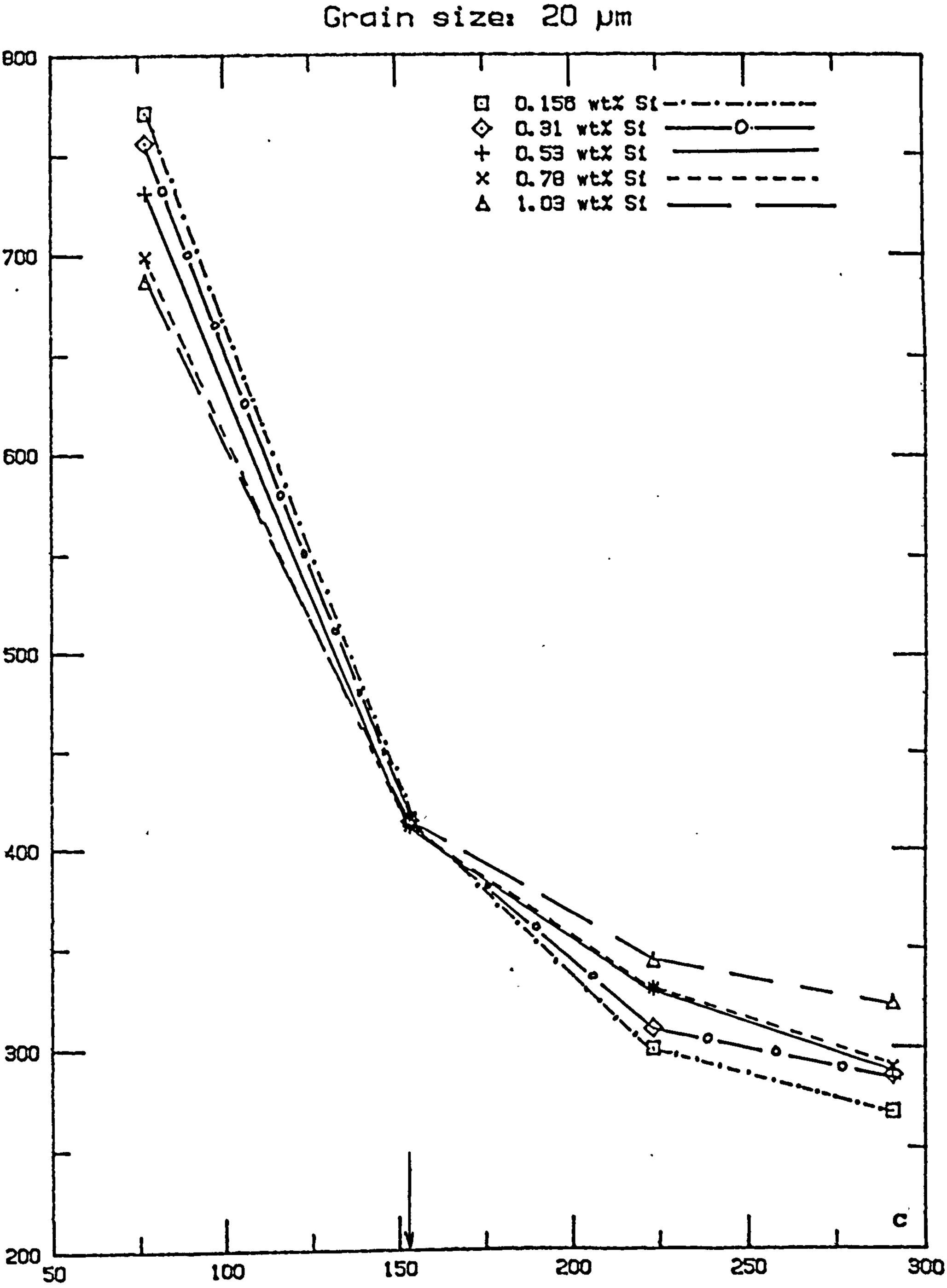

Temperature, ° K

Yield strength of steel Vs test temp.

⟶ : Apparent "softening" start Temp.

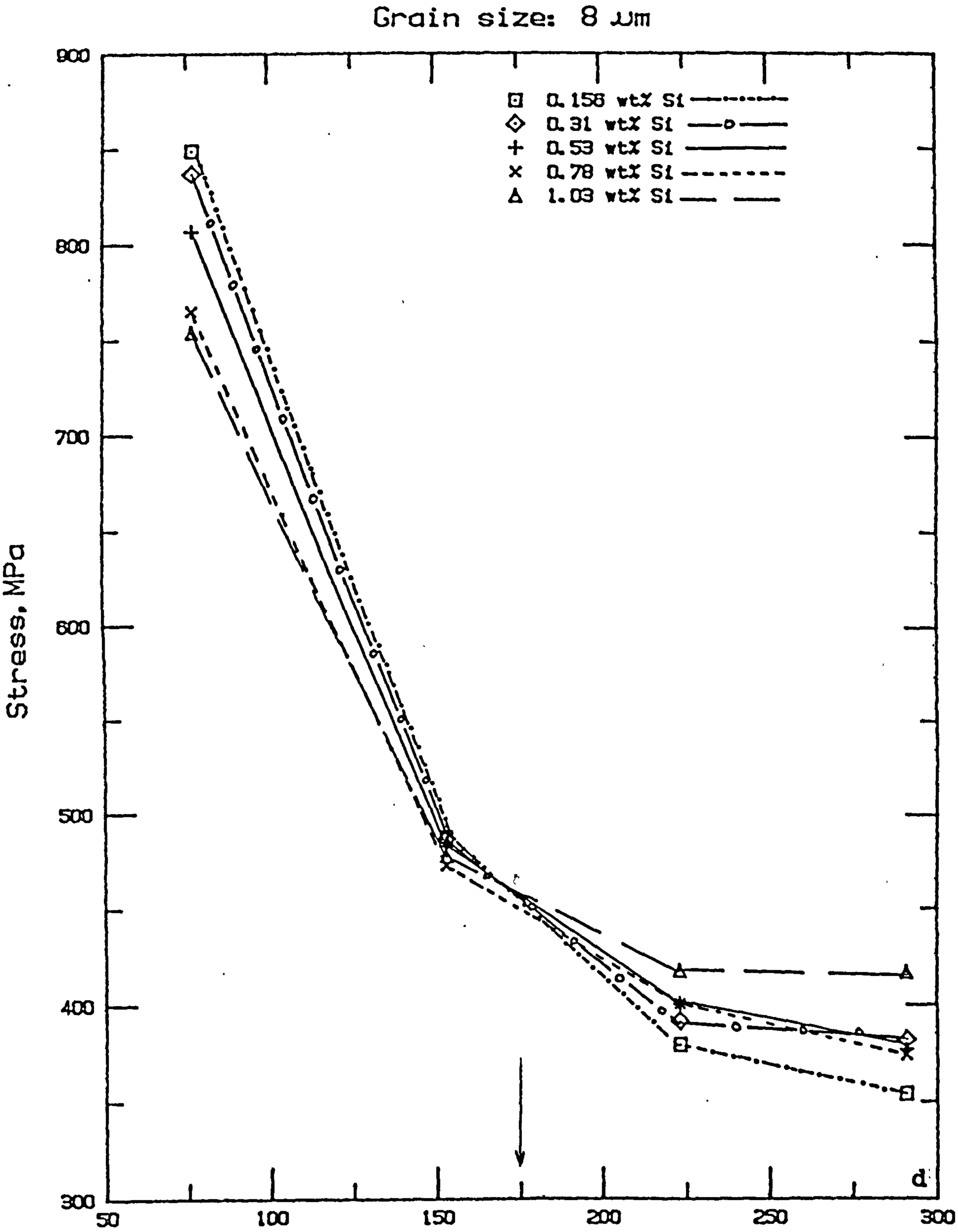

Yield strength of steel Vs test temp.

⟶ : Apparent "softening" start Temp.

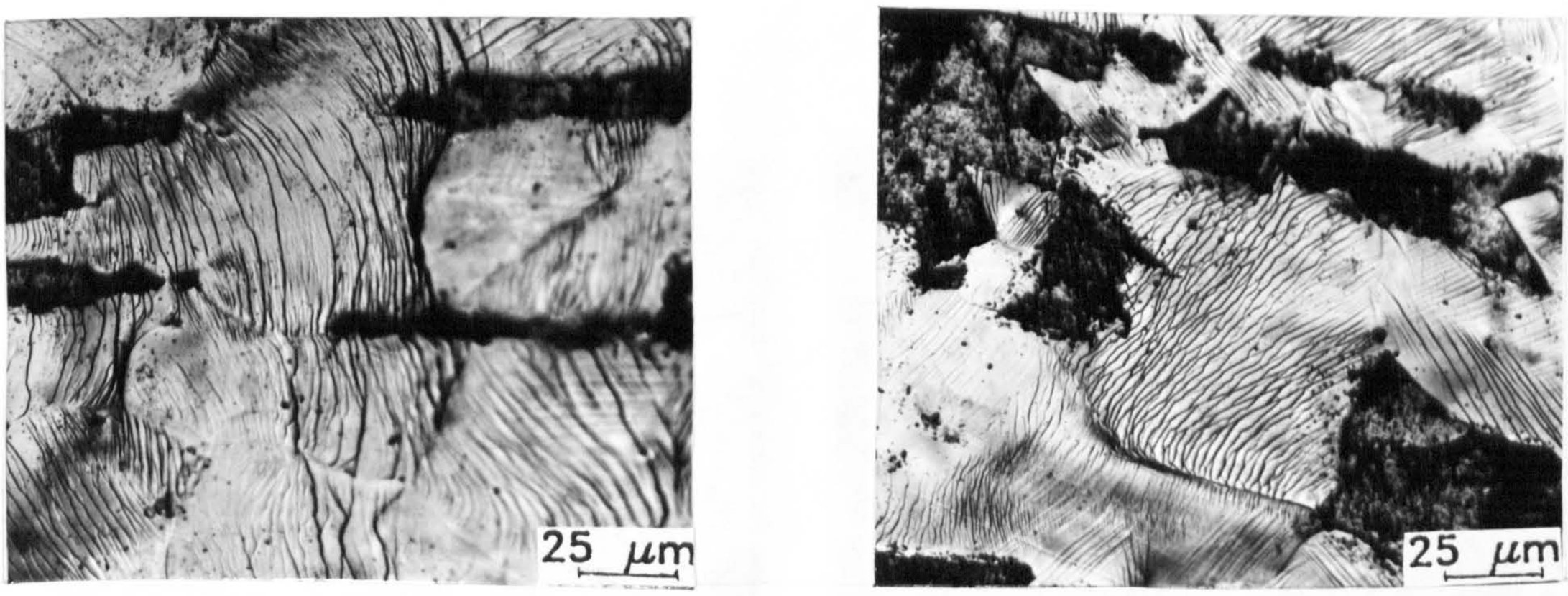

a b

Fig 5.20: Slip lines(bands) presented by the large-grained specimens,8% tensile strained with a strain rate of $3.3x10^{-4}s^{-1}$:a),0.156 and b),1.03 wt% Si steels at room temperature.

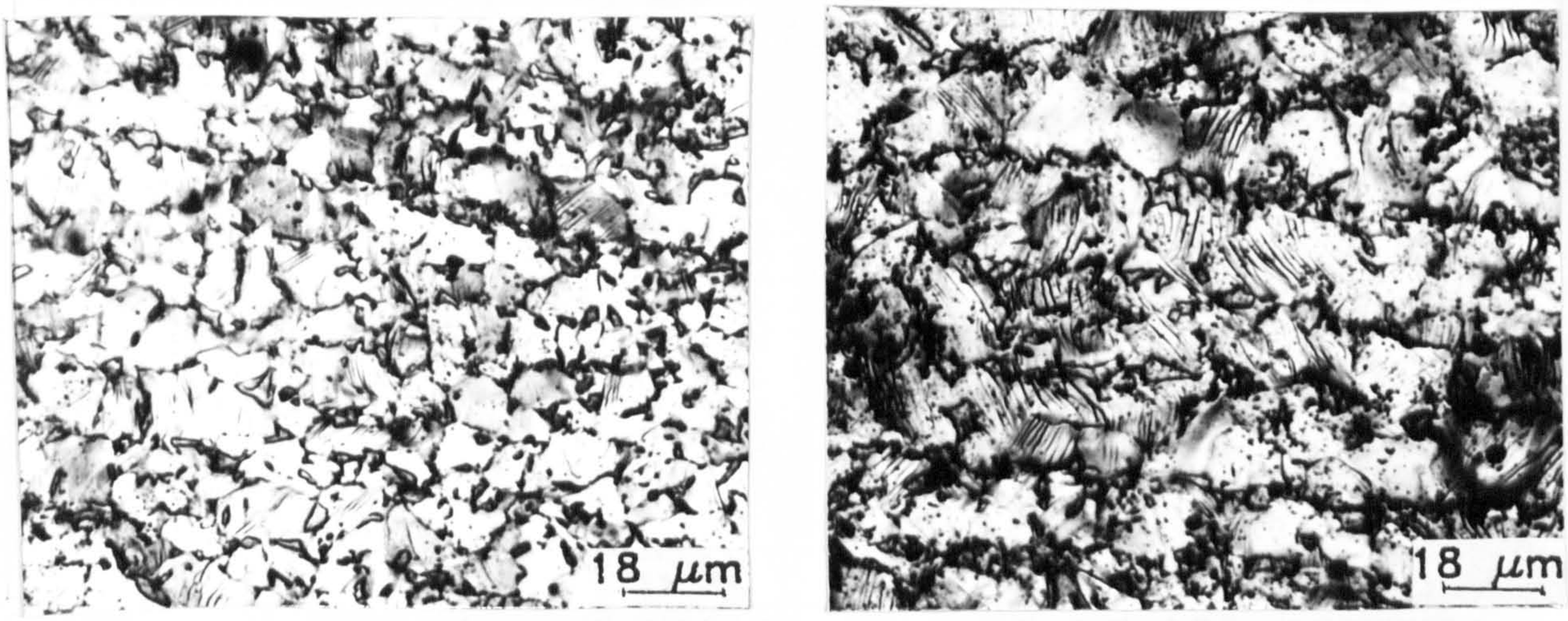

a b

Fig 5.21: Slip lines showed by the small-grained specimens, 8% tensile strained, with a strain rate of 3.3x $10^{-4}s^{-1}$ at:

a), room temperature, b), 77 K.

The structure for both steel grades is the same.

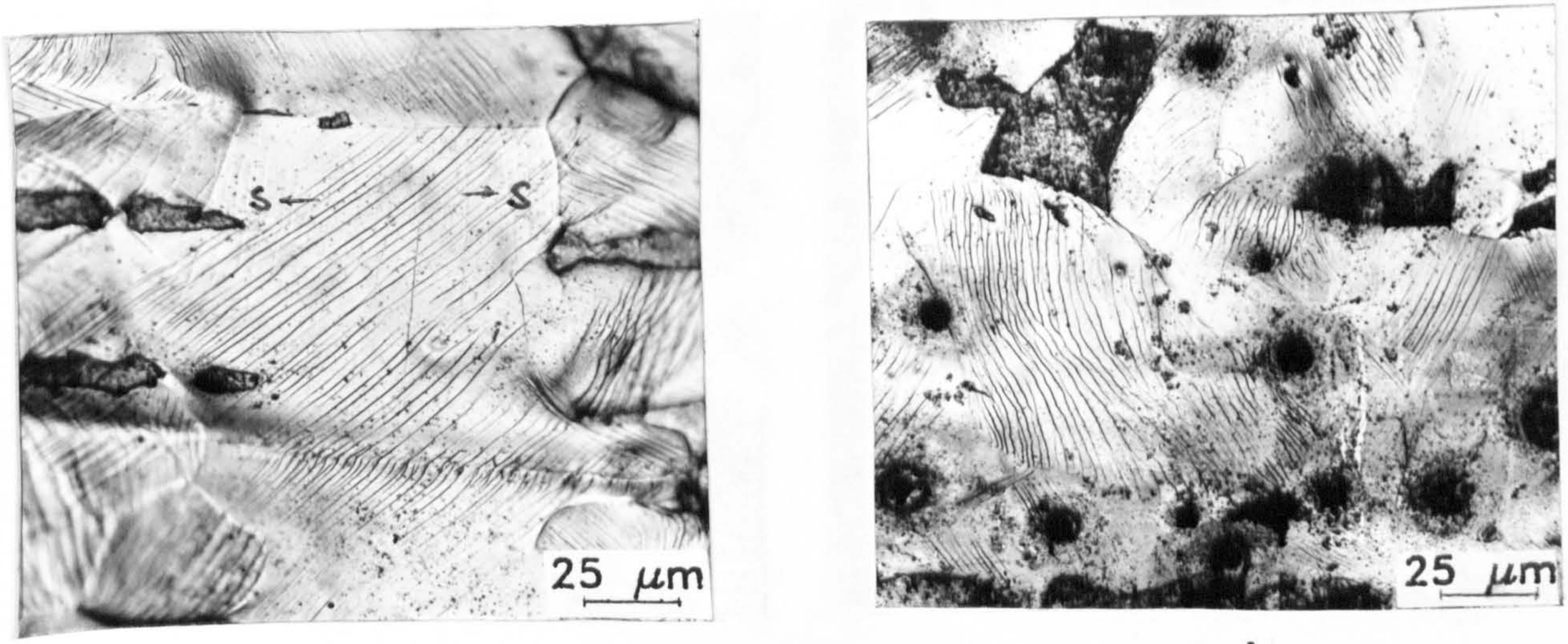

a b

Fig 5.22: Slip lines showed by the large-grained specimens, 8% tensile strained at 77 K,with a strain rate of $3.3x10^{-4}s^{-1}$: a),0.156 and b),1.03 wt% Si steels.

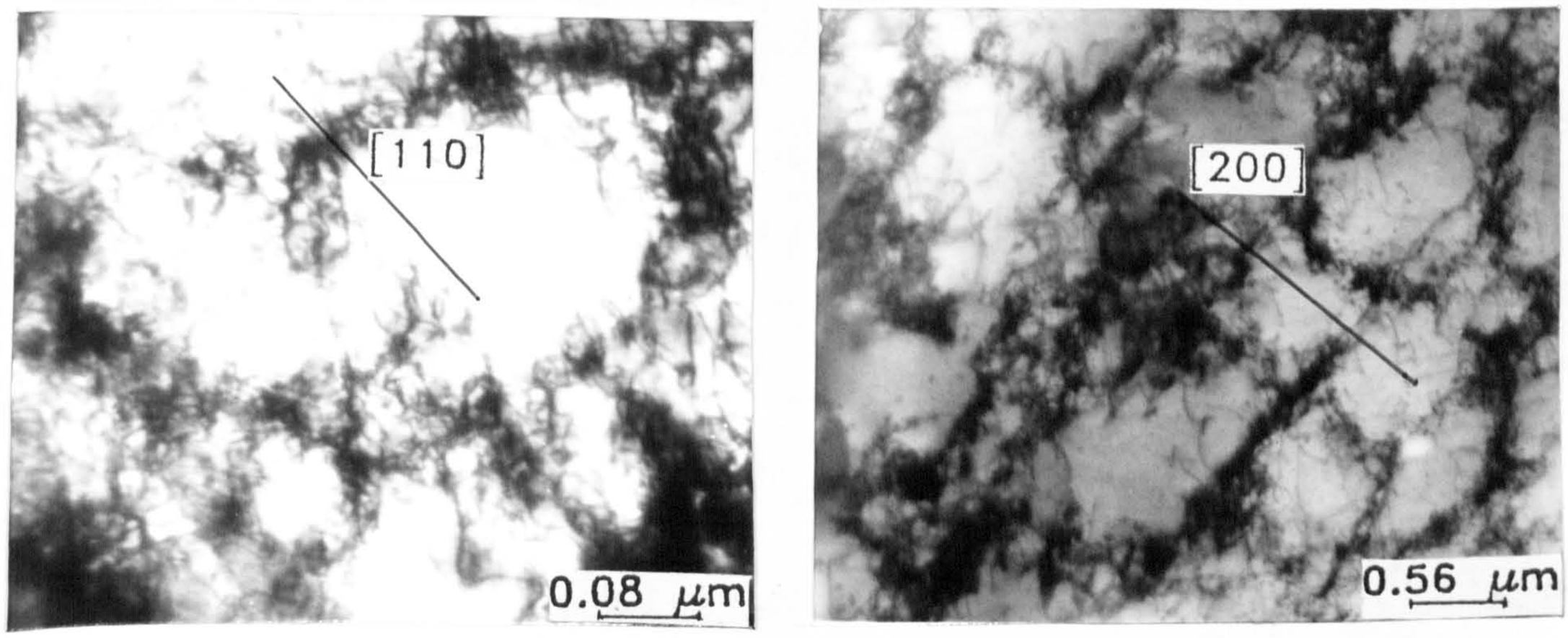

a b

Fig 5.23: Cellular dislocation structure of both small and large-grained specimens,8% tensile strained at room temperature,with a strain rate of 3.3 $x10^{-4}s^{-1}$:

a), 1.03 wt% Si steel, small-grained group,

b), 0.156 wt% Si steel, large-grained group.

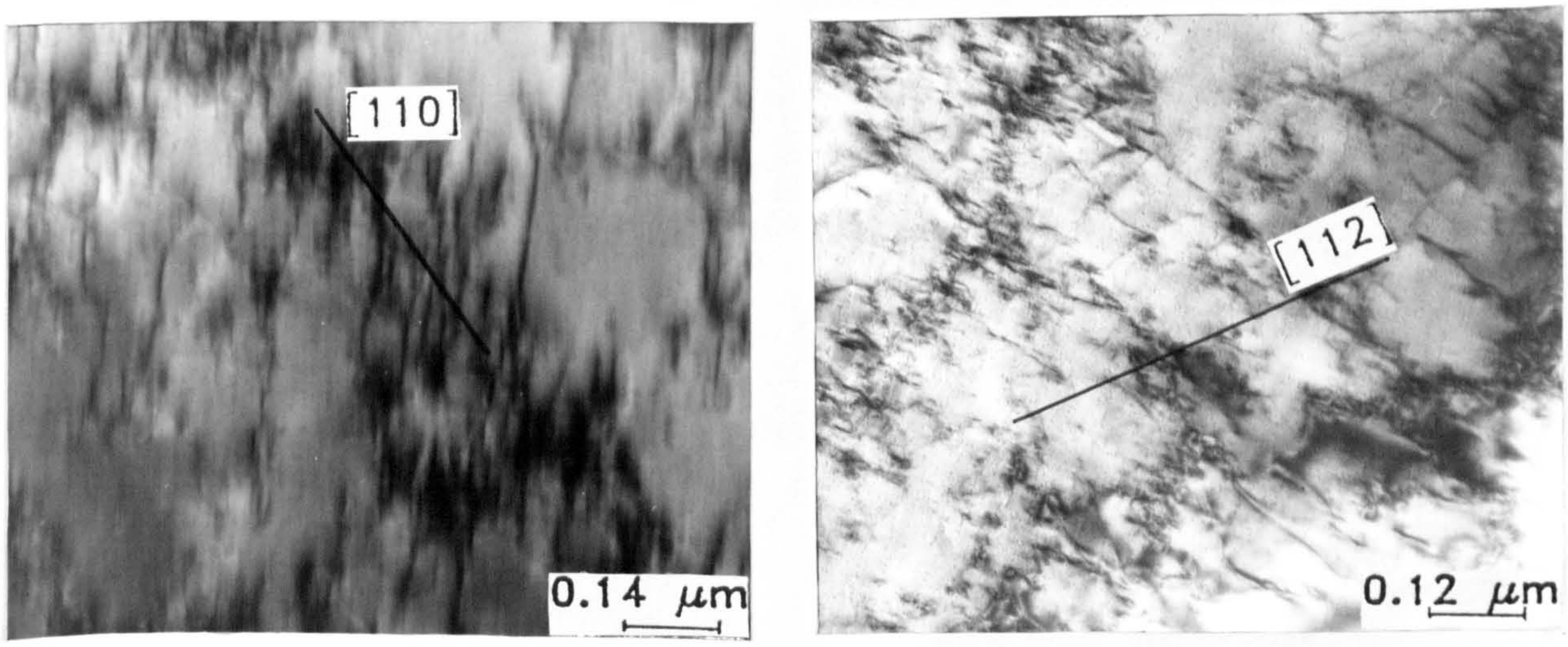

a b

Fig 5.24: Dislocation structures of both small and large-grained specimens, 8% tensile strained at 77 K, with a strain rate of $3.3\times10^{-4}s^{-1}$:
a), 1.03 wt% Si steel,small-grained group
b), 0.156 wt% Si steel,large-grained group.

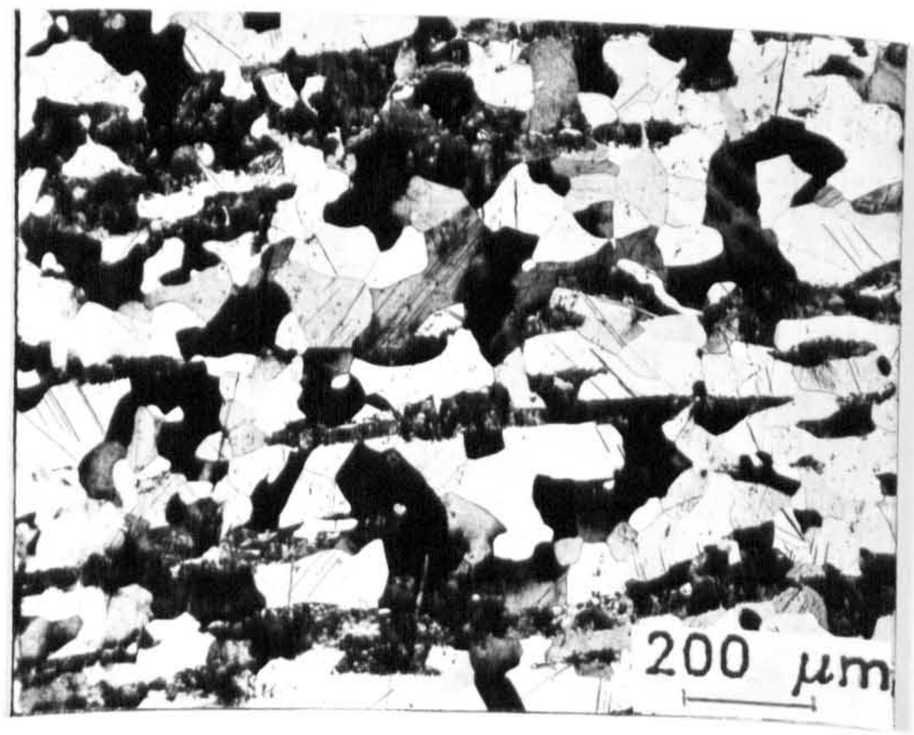

(i)

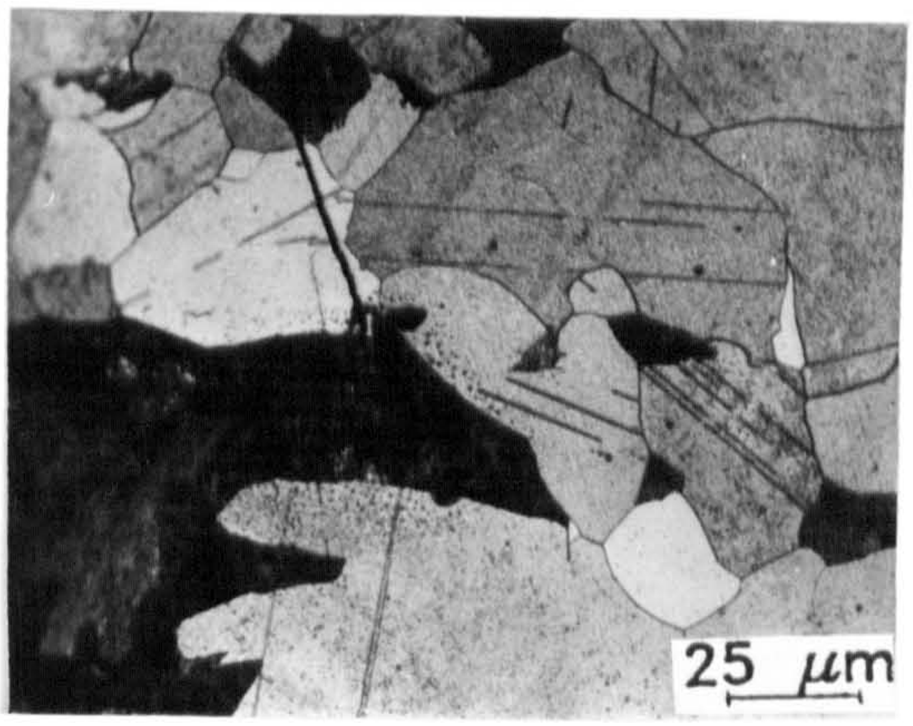

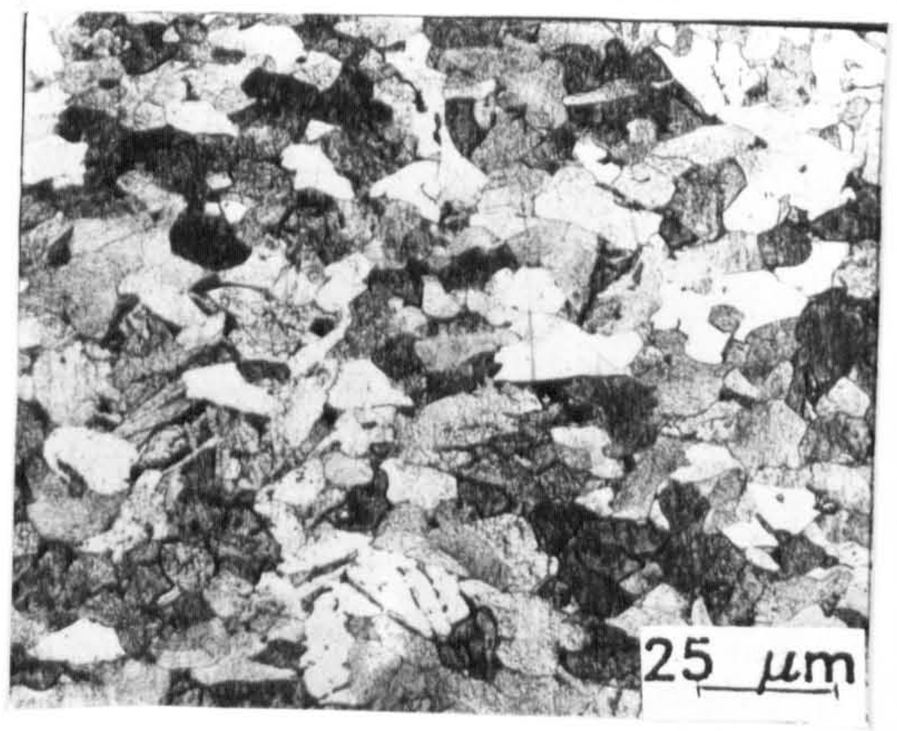

(ii)

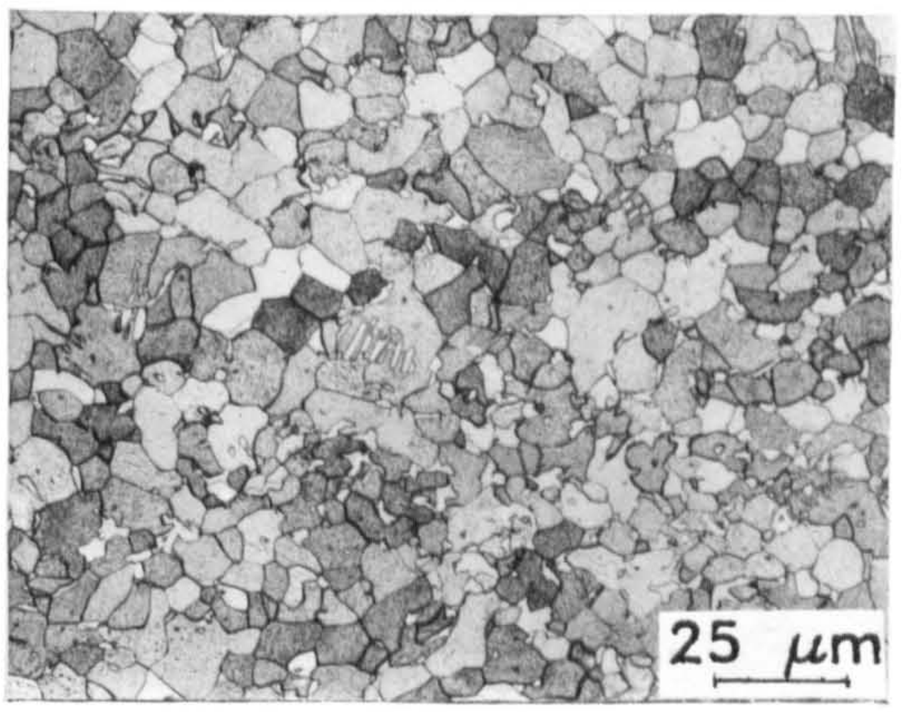

a b

Fig 5.25: Longitudinal sections of fractured round tensile specimens at 77 K, showing the extent of twinning in, a), 0.156; b),1.03 wt% Si steels:
i), large-grained,ii), small-grained groups.
Note the absence of twins in the small-grained group.

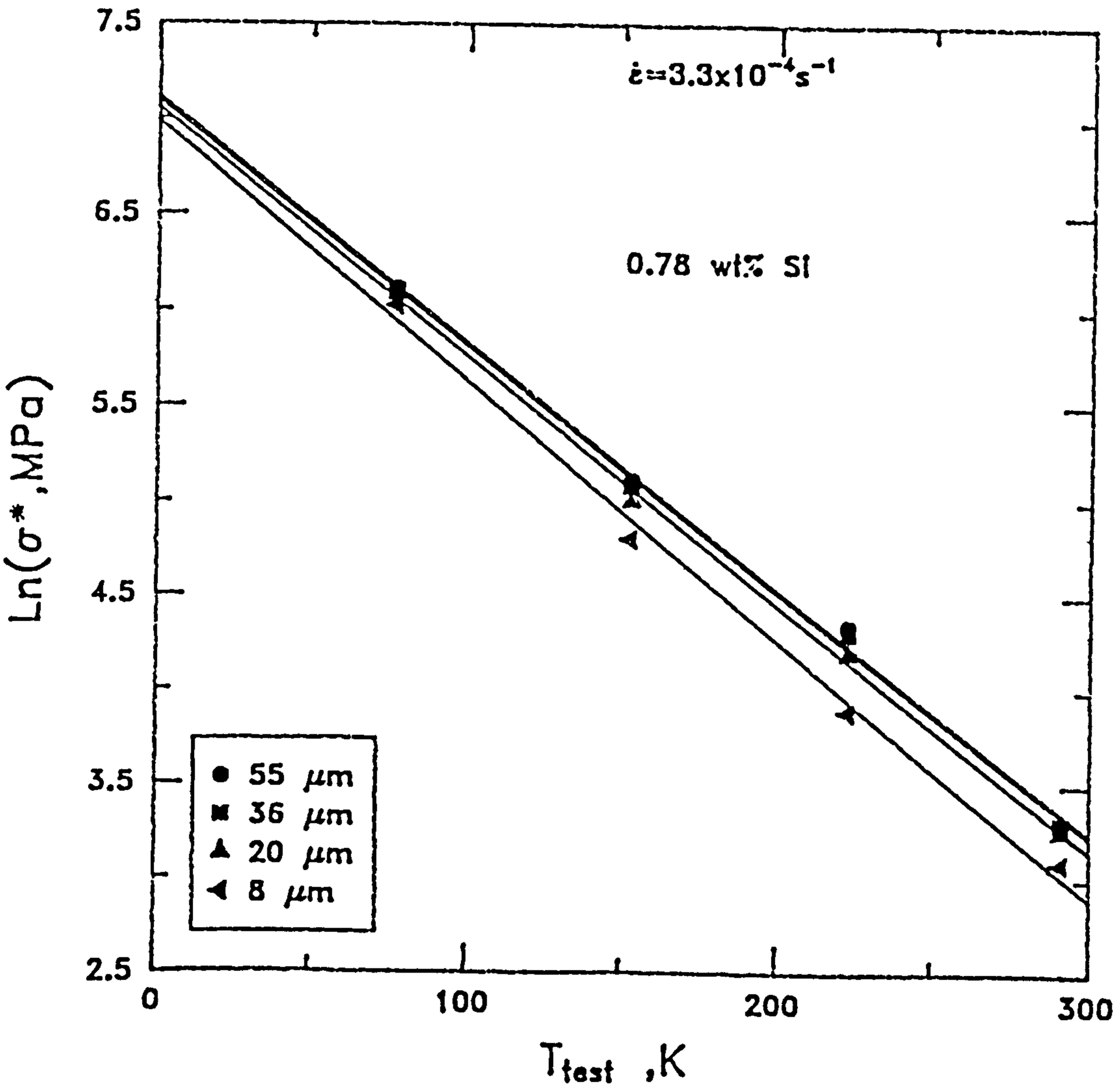

Fig 5.26: Effective stress Vs test temperature, for the 0.78 wt% Si steel,tensile tested with a strain rate of $3.3x10^{-4}s^{-1}$.

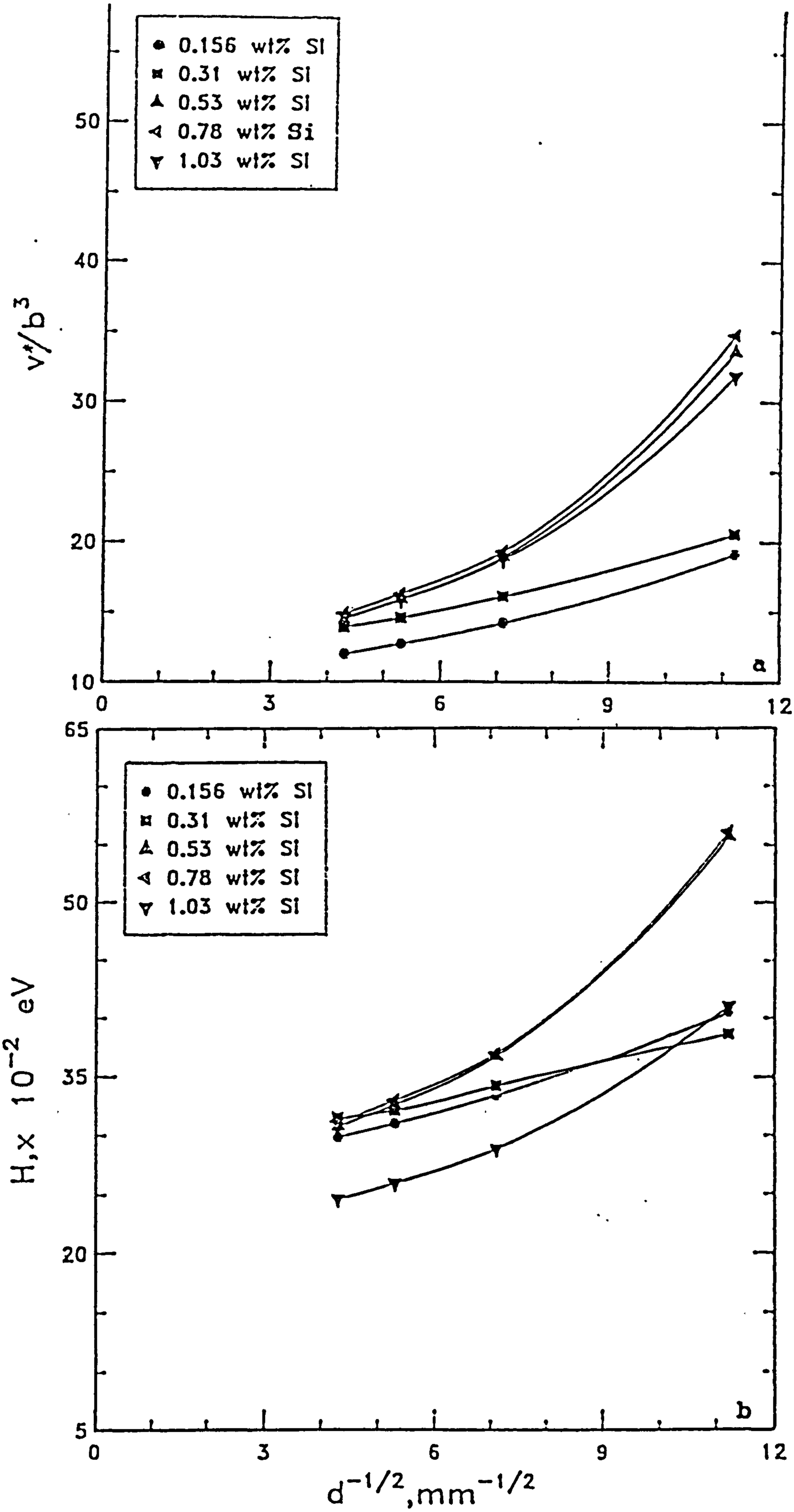

Fig 5.27: Activation a).volume; b).energy versus the grain size of steels at 153 K

CHAPTER SIX

DISCUSSION OF RESULTS

In this chapter, any figure or table newly refered to (the figures and tables compare the results from this work with those of other researchers), would be found in the page immediately after that in which either the figure or Table is mentioned.

6.1 Grain Refinement

The measured ferrite and prior austenite grain sizes (Tables 5.1 and 5.2) suggest that silicon additions may be inhibiting grain growth.

The ratios of austenite to ferrite grain sizes have been plotted against the silicon contents of the steel, Fig 5.1. The ratio becomes smaller as the silicon content in the steel is increased. This result is in disagreement with the work of Cochrane and Morrison[150].

The dilatometric study, Fig 5.2 and Table 5.3 revealed that the initial additions of silicon, up to 0.31 wt%,decreased the transformation temperatures,subsequent to which further additions of silicon increased them.

To rationalize (from the foregoing) the inhibition of grain growth by silicon additions, it is worth mentioning that the materials in the as-received condition had the same grain size of 15±2 μm, Fig 5.3, thus facilitating a comparison. The as-received steel

grades were vacuum-melted and controlled-rolled. Controlled-rolling normally implies a low finished rolling temperature, relative to that used in a conventional rolling[151]. This low finished rolling temperature can lead to a fine uniform grain size[4]. The steel grades were controlled-rolled to about the same finished rolling temperature (except for the 0.31 wt% Si steel), Table 3.1. Since all the processing parameters were about the same, and considering the facts[4,151] mentioned above, it is understandable that the steels in the as-received state had about the same grain size.

6.1.1 Grain Boundary Migration

The optical micrographs reveal that silicon additions do inhibit both austenite and ferrite grain growth, Figs 5.4 and 5.5. Grain growth inhibition is most usually associated with the formation of hard precipitates, like carbides and nitrides, among others, that would inhibit grain boundary migration. Low temperature ($\propto$) Si_3N_4 precipitates were identified in this work, and those observed in the annealed specimens are shown in Fig 5.6 The volume fraction, f, of these precipitates was stoichiometrically calculated to be 5.8×10^{-3}, on the assumption that the entire silicon (of 1.03 wt%) and nitrogen (of 0.0023 wt%) participate in the reaction, see Appendix B. The precipitates, in Fig 5.6, measured 0.035 ± 0.02 μm in radius. Estimates were made of the equilibrium grain size, R attributable to these precipitates, using Zener's equation of

the form:

$$R = (4/3)(r/f), \quad \ldots\ldots\ldots\ldots\ldots\ldots\ldots\ldots 6.1$$

where r is the average radius of these precipitates. An equilibrium grain size of 805 μm was obtained. In the recent review by Rios[152] on the grain boundary pinning by particles, the theoretical equilibrium grain size that fitted into experimental observations was found to be eight times less than that given by Zener's equation. Thus, the 805 μm should be about 101 μm equilibrium grain size. This equilibrium grain size is by far above the 17 μm grain size observed for this sample treated according to code A, or even the maximum grain size of 58 μm obtained for the 1.03 wt% Si steel grade with code D of heat treatments.

Thus, it follows that the grain growth inhibition can not satisfactorily be attributed to the formation of these nitrides, at the level of silicon and nitrogen present in the steels. It therefore does seem that an intrinsic characteristic of silicon in iron is responsible for the inhibition of grain growth.

6.1.2 Nucleation Kinetics

Aaronson et al[50] related the nucleation and growth rates of ferrite allotriomorphs to the effect an alloying element could exert on the A_{r3}. Kinsman and Aaronson[51] showed that silicon additions raise the A_{r3}, and therfore increases the rates of nucleation and growth of ferrite. Further, Irvine and Pickering[44] in their studies on low carbon steels, with $0.42 \leqslant Si \leqslant 2.93\%$

confirmed that silicon additions increased the transformation temperatures (at $0.6 \leqslant Mn \leqslant 1.6\%$).

In the light of the foregoing evidence, it can be said that the addition of silicon inhibits grain growth by its capacity to increase the nucleation rate of ferrite allotriomorphs. The nucleated ferrite would also grow, but the rate of growth would depend on the extent to which the nucleation sites were saturated. Cahn[153] showed that the necessary conditions for nucleation sites' saturation are energy, accessibility of these sites at an early time of reaction and the number of atoms associated with each type of nucleation site. Since silicon additions raise the A_{c3}, for two steels with different silicon contents, at a given temperature, the steel with higher silicon would have a smaller prior austenite grain size. While the lower silicon grade steel reached its A_{c3}, the higher silicon grade may just be about or below its A_{c3}. Thus, the higher silicon grade would possess a smaller austenite grain size, as was found in this work, Fig 5.5. Only smaller austenite grains can satisfy the three conditions suggested by Cahn[153], and hence saturate their nucleation sites faster than the coarse austenite grains. Site saturation implies a reduced ability for growth before impingement. Thus, high silicon grade steels, with small austenite grains, would favour the formation of small ferrite grains, Fig 5.4.

This result is in disagreement with the suggestion made by Phillips and Chapman[154], which concluded that more ferrite grains per austenite grain should be

expected, as the latter increases in size. However, the fact that a small austenite grain size leads to a small ferrite grain size has been implied in many other studies[4,30,155].

6.1.3 Ratios of Austenite to Ferrite Grain Sizes

As was mentioned in the introductory section of this grain refinement discussion, the austenite to ferrite grain size ratio was found to be lowered by silicon additions; a result in disagreement with the work of Cochrane and Morrison[150]. Assuming that a coarse austenite has more ability to nucleate ferrite, they found the ratio to increase with transformation temperature (which in this work would equate with an increase in the silicon content of the steel). However, from the kinetics point of view, it is reasonable to assume that a fine austenite grain saturates its nucleation sites faster than a coarse austenite grain. It seems therefore unreasonable to expect that the growing grains nucleated from coarse austenite would consume the grain surfaces, suppressing further nucleation, as argued by Cochrane and Morrison[150]. Definitely, consumption of some sort takes place in grain growth, but the fine austenite (high silicon grade steels) that had far more nucleation sites saturated than the coarse austenite (low silicon grade steels), would have more small grains unconsumed. Small grains can be seen in Fig 5.7 (a and b) and they were absent in the steels (silicon content) that showed coarse prior austenitic grains, for example, the

0.31 wt% Si grade steel, Fig 5.7c.

When the oxidation technique[154] is used to reveal the surface prior austenite grain size, it has been claimed that a smaller grain size than that in the interior, is found. However, the report[154] added that in the presence of grain growth inhibitors, this dissimilarity disappears. Hence, with the observation that silicon additions (greater than 0.31 wt%) do inhibit grain growth, through silicon's effect on the nucleation kinetics (see section 6.1.2), it is concluded that the oxidation technique used here revealed the true prior austenite grain size. Nevertheless, the oxidation technique has the limitation that above 1000°C, the preferential oxidation of the grain boundaries, the principle on which the technique is based, partially diffused with the oxidation of the main grain, Fig 5.5B. Using pure oxygen to oxidize the steel after removing it from the argon filled furnace, Bepari[130] made a similar observation.

All the work reported previously on the effect of silicon on transformation temperatures used silicon contents greater than or equal to 0.42 wt% Si. This might explain the paucity of reports showing that silicon additions initially reduce the transformation temperatures, as was observed in this work, Fig 5.2 and Table 5.3. However, this trend has been reported[156] for constructional steels (up to 0.3% Si), which coarsen on normalizing.

6.2 Strengthening

The room temperature tensile properties of the steels are given in Table 5.1. To illustrate the variation of the lower yield stress, σ_y, with the grain size, ($d^{-1/2}$) and the importance of the range of grain sizes used for this analysis, the room temperature values of σ_y have also been plotted against the grain size, $d^{-1/2}$, Fig 5.8. A lot of work has been done by researchers on the variation of σ_y with $d^{-1/2}$.However, not much has been reported about the importance of the range of grain sizes used to analyze this variation.

6.2.1 Lattice (Frictional) Stress, σ_o

The solution hardening effect of silicon in steels is already well established, with reports[24,44-46,157] of an increase of frictional stress, σ_o (the intercept of the σ_y axis of a σ_y vs $d^{-1/2}$ graph), of as low as 25 to as high as 117 MPa per one wt% Si. Such a wide variation may not be unconnected with the diversity of base compositions used in these investigations, of which the role of carbon and nitrogen in solution strengthening is not fully defined. In this work, the short-aged batch showed an increase in σ_o of 76 MPa per one wt% Si. This compares well with some other results[44,45] that gave values of 77 MPa per one wt% Si. The unaged batch in this work, however showed an increase in σ_o of 59 MPa per one wt% Si.

6.2.2 Lower Yield Stress, σ_y

Silicon does increase the lower yield stress, σ_y, and many authors have given the level of strength increase, which is brought about by the addition of silicon. However, an important factor that is frequently left out in the discussion is the grain size at which such a level of strength increase was determined. For instance, in the work of Sibley and Breyer[26], at $d^{-1/2} = 5\ mm^{-1/2}$, σ_y would increase by 90.7 Mpa per one wt% Si. But if $d^{-1/2} = 10\ mm^{-1/2}$, the increase would be 64.9 MPa per one wt% Si. In this work, it was found that σ_y, at $d^{-1/2} = 5\ mm^{-1/2}$ for the unaged batch, increases by 59 MPa per one wt% Si, and at $d^{-1/2} = 10\ mm^{-1/2}$, this was unchanged. For the short-aged batch, per one wt% Si, σ_y increases by 65 MPa at $d^{-1/2} = 5\ mm^{-1/2}$, while at $d^{-1/2} = 10\ mm^{-1/2}$, it decreases to 54 MPa.

It would seem, therefore, that if the base composition is kept about the same for all the grades, and using a wide enough range of grain sizes, as used in this work, within a given study, the difference in the increase of the lower yield stress per 1 wt% Si, from one grain size to another would be minimal, as was found in the present investigation.

The two conditions, a wide range of grain sizes, and a similarity of the base compositions of the steel grades under analysis,should be met for the last suggestion to hold.

The same suggestion holds for the absolute increase of the lower yield stress, brought about by 1 wt%

Si addition, for a given grain size. For example, Mintz[15], using a fairly uniform base composition, but a relatively narrow range of grain sizes of $d^{-1/2}$ = 4 to 9.7 $mm^{-1/2}$, found an increase in lower yield stress of 77 MPa per 1 wt% Si at $d^{-1/2}$ = 8 $mm^{-1/2}$. Similarly, Preston's[47] work showed an increase of 97 MPa per 1 wt% Si addition. In the latter, neither of the two conditions were met. But in the present work, where these two conditions are met, the increase in the lower yield stress per 1 wt% Si at $d^{-1/2}$ = 8 $mm^{-1/2}$, was found to be about 57 and 59 MPa for the unaged and the short-aged batches respectively.

In this work, it was generally observed that the smaller the grain size, the less the degree of strengthening by silicon (within the content under study), Table 5.4. A similar trend has been reported by Preston[47], who for silicon increments of 0.2 to 0.5 wt%, observed a change in the yield stress of 34 MPa for $d^{-1/2}$ = 7 $mm^{-1/2}$ and of 18 MPa for $d^{-1/2}$ = 10 $mm^{-1/2}$. The consequence of this is that, between 0.31 and 0.78 wt% Si in the steel, the high silicon steel shows a lower yield strength than low silicon steels, at grain sizes below 13 μm(8.8 $mm^{-1/2}$) and 8 μm (11.2 $mm^{-1/2}$) in Fig 5.8 (a and c respectively).

6.2.3 Hall-Petch Slope, k_y

Of all the tensile properties, that most influenced by the base composition and by the range of grain sizes used for study is k_y, the stress intensity at the tip of the deformation band. It has always been assumed that it

is markedly influenced by carbon and nitrogen, and thus any element that is being considered for its effect on k_y is directly related to carbon and nitrogen. However, it should be noted that the effect of some elements is affected by the presence of others, even when the latter may or may not directly react with carbon or nitrogen. In Fig 6.1 are plotted the values of k_y, resulting from this work, and those of other authors for comparison, from which, support for the last point is made.

The trend in Fig 6.1 is the same for this work and that of Sibley and Breyer[24]. The errors, within 95% confidence limit, in all the various aspects of this work (wherever error margins are given), have been calculated, using estimation theory[138]. However, the trend of the k_y variation found in this work differed from that reported by Preston[46].

The mechanism which gives rise to, or affects, the magnitude of k_y has attracted different views. Most of these have already been reviewed in chapter one of this work. The pile-up theory proposed by Hall[12] and Petch[13] is deficient, because direct observations of pile-ups, in this grade of steels, are rarely made; infact, no such pile-ups were observed in this work. If dislocations pile up at the grain boundary, the implication would be that the slip lines originate from the grain interior. However, studies on silicon steels[19,20], with $3.65\% \leqslant Si \leqslant 4\%$, and 9.8% Mn-titanium alloy[21] have shown that on the contra-ry, the slip lines originate from the grain boundary areas

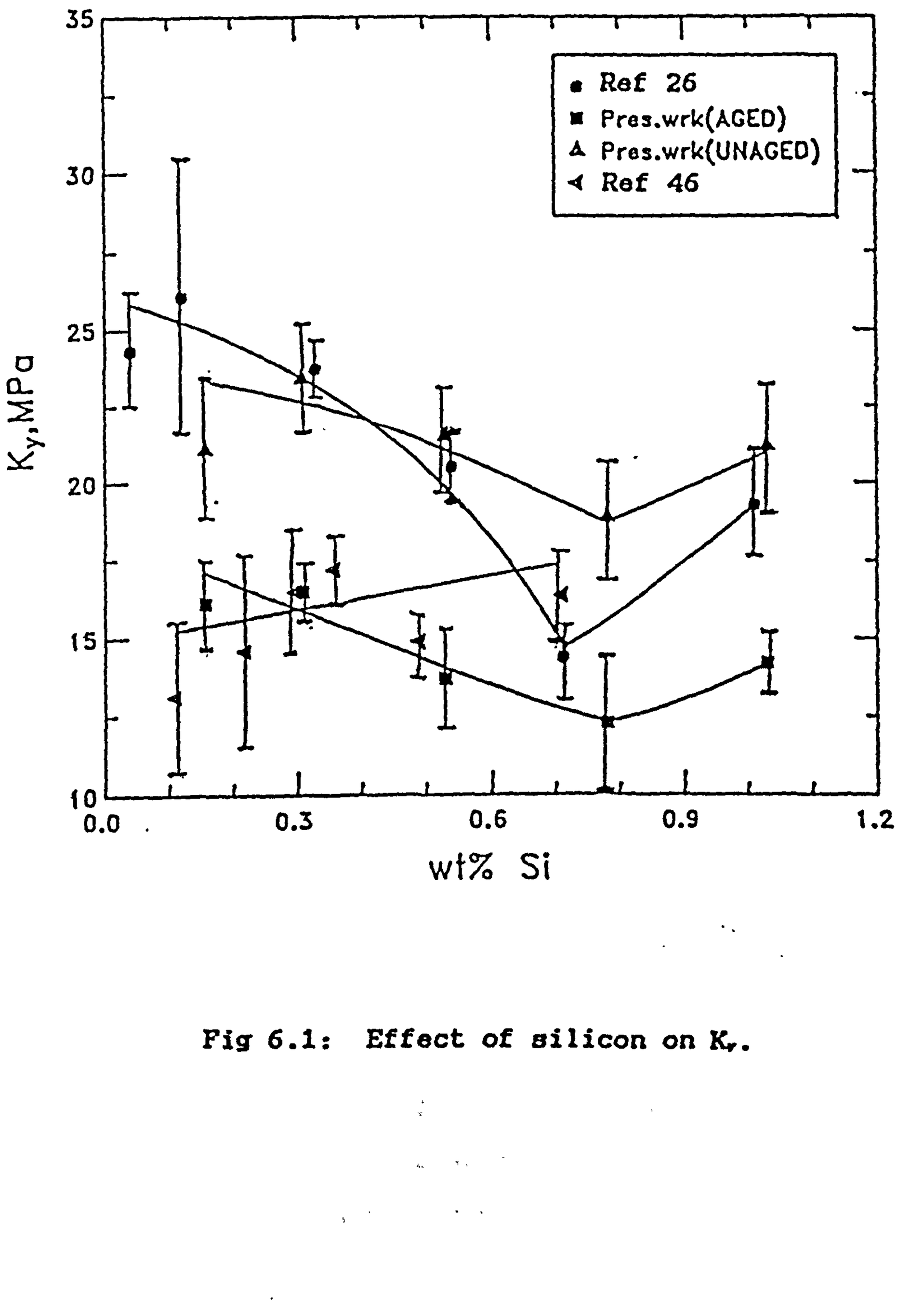

Fig 6.1: Effect of silicon on K_y.

and move to the interior. A Similar observation was made in this work, and will be discussed later.

6.2.3.1 Ledges

Ledged boundaries were very rarely observed in this work, but those observed are shown in Fig 5.9. From Fig 5.9b, it is evident that grain boundaries are "sinks" for dislocations, thus the consequent emission source of dislocations (as proposed by Li[22]) being these boundaries can be understood. Table 5.5 gives the data determined for these ledges. It can be seen from the Table that the low silicon steel showed a lower incidence of resolvable ledges than did the high silicon steel. This, infact, is in agreement with Li's[22] theory of the stability of ledges by impurities (section 1.3.3). But the thermodynamic relationship between K_v and ledge stability (impurities), as proposed by Li[22], appears less strongly supported, because the high silicon steels (up to 0.78 wt% Si) show lower k_v, as observed in this work and others[24,47,48,139]. Mintz et al[37] reported of this non-conformity in the relationship between k_v and the observed ledge structure. This apparent contradiction in Li's thermodynamic relationship may be due to the poor resolution[40] of features like ledges in transmission electron microscopes.

The incidence of pile-ups is very rare. Also the poor resolution of ledges by transmission electron microscopes makes the observation of ledges rather of chance. Therefore, a more consistent mechanism to explain

the variation of k_y should be sought.

6.2.3.2 Segregation and Precipitation

Wilson[33] explained the variation of k_y using the theory of interstitial-solute segregation to grain boundary regions. Mintz and Turner[172], using atom probe and strain-ageing data gave some support to the theory of segregation of nitrogen interstitial atoms to the grain boundaries, in the presence of silicon. However, in a later study on low carbon steels, Mintz[150] suggested that the effect of slow cooling, which leads to more segregation of interstitial atoms to the grain boundaries, did not always lead to a reduction of the k_y values, for example, in the 0.045% C steel. Nonetheless, as the carbon content in the steels of the present study is more than the 0.045%, the level for which this suggestion may be applicable, and on the basis of the identified Si_3N_4 precipitates from this work (which will be discussed in later sections), it is rational to infer that the segregation and precipitation of the interstitials led to the reduction of k_y.

However, there has not been any report, substantiated by micrographic evidence, as to which interstitial, or in support, as to how the interstitial at the grain boundary, affects k_y.

Studies on the interactions of silicon and nitrogen[160,161], as well as on the interactions of silicon and carbon[162,163], in the Fe-Si-N or C system abound, though

all the reports deal with relatively high silicon contents of $\geq$ 2%. There is also a report[192] of silicon reacting with carbon and nitrogen in the Fe-Si-N or carbon system, to produce carbo-nitrides. Such interactions have been used to explain the reduction of the solubility of nitrogen[164], of carbon[165] or a repulsion[192] of interstitial atoms from the grain boundaries in alpha-iron, in the presence of silicon. By this reasoning, both carbon and nitrogen can be said to have equal chances of affecting k_v.

Reduction in solubility however, does not accurately reflect how these interstitials affect k_v, because Petch[32] has pointed out that the locking of dislocations is energy related rather than concentration related. Therefore, a full reflection of the interstitial's effect on the dislocations should be quantified in terms of the magnitude of the interaction energy. Depriving the dislocations of the interstitial atoms with a higher locking energy, would result in the lowering of k_v. Such a deprivation, with such an effect, should be more readily guaranteed by the interstitial that has a higher interaction energy with silicon. Further, a high interaction energy between the interstitial atoms and the silicon atoms would be expected to lead to the precipitation of the interstitial from the solid solution.

Leslie et al[144] observed a non-identified carbide precipitate in a 3.25% Si steel (stating that the carbide was neither cementite nor $Fe_{2.4}C$, ξ-carbide). Harry[147] has reported that silicon carbide precipitates

as a grain boundary film and that carbon segregates to the specimen surface in 4% Si steels.However,there has not been any evidence that the present author has found in the literature for silicon carbide precipitation, particularly at levels of silicon below 2 wt%. However, it was observed in this work, that higher silicon additions lead to thicker decarburized layers, Fig 5.10. The value of the thickness of each layer is given in Table 5.6. Birks[45] has suggested (based on the effect of silicon on the activity of carbon) that the presence of silicon in the steel increases the outward diffusion of carbon to the scale/metal interface. Thus, he concluded, the general effect expected of silicon is to increase decarburization. Hence, with this argument, higher silicon contents in the steel, implies a greater degree of segregation, or repulsion, of carbon to the surface of the specimen; the carbon in turn reacts with the oxygen in the furnace atmosphere, leading to thicker decarburized layers.

The thermodynamic data of silicon[46] indicate that at any temperature (more so at lower temperatures), it is much easier to form nitrides than carbides. It has been demonstrated[29] that nitrogen atoms prefer to lodge at the grain boundary sites. The dislocations (which abound) at grain boundaries would therefore be locked by these nitrogen atoms. However, if the silicon-nitrogen interaction is strong enough, nitrogen should be precipitated out as silicon nitride, provided the solubility concentration of the silicon nitride in alpha iron is exceeded.

Irvine et al[37] suggested that Si_3N_4 is precipitated in silicon-killed mild steels from the annealing process (at zero hour tempering), but the work did not identify the precipitates to be Si_3N_4, or what type of Si_3N_4 the precipitates were. Precipitates were observed and identified (see Appendix C) as low temperature (α) Si_3N_4 (with c = 5.617 Å and a = 7.748 Å) from the annealed steels of this work, Fig 5.6. Thus, in the absence of any silicon carbide precipitates, it can rightly be said that silicon-nitrogen interaction is stronger than the silicon-carbon interaction. In agreement with thermodynamic data[44], the precipitation of these nitrides is more extensive in the short-aged batch (due to the lower temperature used, relative to the annealing temperatures); this led, it is argued, to more dislocations being unlocked, leading to a greater reduction in k_y, Fig 5.8c.

6.2.3.3 Effect of Grain Size Range and Base Composition of Steel on k_y

Manganese has been shown[170] to slow down the diffusion of nitrogen. Ubhi and Baker[171], working on the precipitation of vanadium carbide in steel observed that manganese decelerates the rate of this precipitation.

In low carbon structural steels,the main alloying elements include manganese and silicon. It was decided to evaluate from other studies, how much silicon and manganese individually reduce the k_y value, and to compare the two rates.It was necessary, however that for a reasonable

comparison to be made, the base compositions of the steels of such studies should be about the same, with the element for which its rate of k_y reduction was to be determined (i.e. manganese or silicon) being kept constant for the different steel grades within a study. Also it was assumed that the relationship between the concentration of the elements and the k_y values was inversely linear down to the minimum k_y, which may vary in the studies.

The work of Heslop and Petch[28], with a constant silicon level of about 0.12 wt% and other elements(wt%) being 0.04 C, 0.025 Al and 0.006 N, and that of Sibley and Breyer[24], met these conditions. The steels in the latter had a constant manganese level of 0.6 wt%; other elements(wt%) were, 0.05 C, 0.04 Al,and 0.006 N. The rate of reduction of k_y by manganese was found to be 0.5 $MPamm^{1/2}$/0.1 wt% Mn addition[28], while for silicon[24], it was found to be 1.7 $MPamm^{1/2}$/0.1 wt% Si addition, i.e. about three times more than the rate achieved by manganese additions.

From Mintz's[174] work, in which the base compositions for two low carbon (0.04 wt%) steels of 0.6 and 1.2 wt% Mn, were similar, with 0.03 wt% Si and 0.004 wt% N, a k_y reduction rate of 1.3 $MPamm^{1/2}$/0.1 wt% Mn was obtained. In the same work by Mintz[174], however, this high reduction rate of k_y by manganese, at a constant silicon level, decreased sharply to just 0.08 $MPamm^{1/2}$ when he[194] varied the silicon content (wt%) from 0.15 to 0.3.

This underlines the importance of keeping the base compositions of steels being analyzed for the effect of a particular element on the k_y values, within a study, about constant, if the true effect is to be revealed.

It can therefore be concluded that silicon has a higher k_y reduction rate than manganese has, and when silicon is present with manganese, the latter reduces the effectiveness of the former as a k_y reducer.

Thus,it is considered that had Sibley and Breyer[26] maintained a constant manganese level for the entire series of their steels, with the relatively high amounts of Al present ($0.02 \leqslant Al \leqslant 0.06$) in the steels, and also used a wider range of grain sizes, the values of their k_y (Fig 6.1) may have been lower.

Preston[46] found a linear relationship for k_y with silicon content. His experimental points are in fairly good agreement with the short-aged batch of this work, with the exception of the 0.71 wt% Si steel. This is not unexpected, because his steels contained 0.03 wt% Al (which would equate in effect with the short-ageing of the specimens in this work), and he used a relatively wider range of grain sizes ($d^{-1/2}$ = 4.07 to 9.77 $mm^{-1/2}$) than did Sibley and Breyer[26], who used a range of $d^{-1/2}$ = 3.8 to 8.5 $mm^{-1/2}$

However, owing to the variation of manganese in Preston's work (particularly for the 0.71 wt% Si steel which had a high manganese level of 1.23 wt%), the full effect of the 0.71 wt% Si addition was masked by the manganese effect, as discussed above, thus leading to his linear

relationship.

Table 6.1 is a summary of the tensile properties for a given silicon content of 0.71 and 0.78 wt%, tested at room temperature, from this work and others, related to the composition of the steels studied. These silicon levels were chosen, because most[24,47,48] of the studies on the effect of silicon, at levels greater than 0.5 wt%, on the tensile properties of low carbon steels, have indicated that about these levels, a critical concentration of silicon is reached, at which the k_y values assume a minimum.

From the table, it can be seen that the effect of nitrogen concentration on the lattice friction stress (σ_i) is not well defined, though generally, it does seem that it has no effect. This discrepancy may be due to a suggestion made by Mintz[157] to the effect that it may be incorrect to extrapolate the Hall-Petch line to an infinite grain size to obtain the friction stress term. Another possibility may be that the role of the interstitials in the solid solution is mostly that of locking the dislocations, since it has been argued[2] that through this locking, a minimum energy state is obtained in the interstitial-dislocation system (see section 1.1). Basing on this argument therefore, the nitrogen concentration variation probably would affect only the term $k_y d^{-1/2}$ term in the Hall-Petch equation.

However, from the table, it can be said that a lower nitrogen concentration seems to reduce the stress necessary for yielding. Hence the reduced concentration of

Table 6.1: Room temperature tensile properties, related to the composition of low carbon steels

K_y	σ_y*	σ_o	Si	Mn	Al	N	
MPamm$^{1/2}$	MPa	MPa	wt%	wt%	wt%	wt%	Ref.no
18.9	335	170	0.78	0.83	0.005	0.0023	Pres,Unaged
12.3	315	197	0.78	0.83	0.005	0.0023	Pres,Aged
16.4	324	173	0.71	1.23	0.032	0.009	46
14.4	313	174	0.71	0.64	0.042	0.008	26
14.4	324	185	0.71	1.23	0.043	0.007	47

* Yield stress at $d^{-1/2}$=9.64 mm$^{-1/2}$

nitrogen, achieved either by ageing or the high aluminium content, through the precipitation of nitrides, leads to more dislocations being unlocked. The ease of motion of these unlocked dislocations would therefore reduce the yield stress.This,however, is the case only when the volume fraction of the nitrides formed by the nitrogen removal from solid solution is insignificant, as in this study.

Mintz[170] has suggested that a high value of k_y generally leads to a low σ_o, and vice versa, which normally could cancel out the overall effect of the variation of these two terms on the yield stress. However, from Table 6.1, the percentage reduction of k_y values from the present work (from the unaged to the short-aged batch) was evaluated to be 35%. The associated increase of the value of σ_o was found to be about 16%. Similarly, comparing the two studies by Sibley and Breyer[26] and Preston[44], it can be seen that a reduction in the k_y value of about 12% led only to about a 0.6% increase in the value of σ_o. Thus, the inverse interrelationship of these two properties is not entirely self-compensating.

Despite the importance of the grain size used in the study of k_y, caution should be exercised when very fine grains are present. Anderson et al[172], working on Armco steel and using a grain size range as wide as $d^{-1/2}$ from 2.3 to 16.76 $mm^{-1/2}$, obtained a quadratic fit, the σ_y–$d^{-1/2}$ curve being concave towards the $d^{-1/2}$ axis. Unfortunately, however, they did not undertake any microstructural study of their specimens. As was stated in chapter five, to

ascertain that the microstructures of the specimens being tested in this study were similar for all the steel grades in every respect, the dislocation structures were also studied for the largest and smallest grain sizes, Fig 5.11. They all had ferrite/pearlite structure, with a non cellular dislocation structure. It is not unlikely that the processes through which Anderson et al[172] obtained such fine grains could influence the yielding behaviour. To illustrate this, in Table 5.4 is included the degree of strengthening by silicon at $d^{-1/2}$ = 16.7 $mm^{-1/2}$. Thus k_y could change from being positive to being less positive; a trend which is at its inception in the very fine grain size region ($d^{-1/2}$ > 9.5 $mm^{-1/2}$) of the steels in this study, Fig 5.8b. However, plotting their[172] data from $d^{-1/2}$ = 2.3 to 12.4 $mm^{-1/2}$ gave the equation:

$$\sigma_y = 79.2 + 17.3d^{-1/2} \quad \text{.....6.2}$$

The correlation factor is 0.94

This may therefore suggest that the Hall-Petch equation cannot be applied to an infinite range of $d^{-1/2}$.

Nevertheless, in the present work, as well as in Sibley and Breyers's[24], k_y was observed to attain a minimum value at 0.78 and 0.71 wt% Si in the steel respectively,beyond which it started to increase again. Like any other solid state transformation,as in the precipitation of silicon nitride from ferrite, there should be a thermodynamic equilibrium silicon concentration,whereby a higher silicon addition does not remove any further nitrogen. Thus, the minimum k_y value may coincide with this equilib-

rium silicon concentration. However, the observed increase in k_v after these silicon levels seems to negate the argument about the existence of an equilibrium silicon content. Nonetheless, Morrison and Leslie[48] showed k_v to be constant beyond 1.43% Si.

6.2.4 Nature, Stability and the Identification of the Precipitates

The precipitation of "SiN" isomorphous with AlN has been reported[34,35] in aged 0.25% Si low-carbon steels. α-Si_3N_4(c = 5.617 Å and a = 7.748 Å) is normally refered[49] to as a low temperature form of Si_3N_4, because it is firstly formed at temperatures less than 1450°C. Roberts et al[34] objected to the term, "low temperature" being ascribed to α-Si_3N_4, because as they argued, the precipitation of the so called high temperature (β, with c = 2.91 Å and a = 7.608 Å) or α-Si_3N_4 depends not on the temperature, but rather on the oxygen potential in the steel. They suggested therefore, that the formation of α-Si_3N_4 is favoured by low oxygen potential, while high oxygen potential favours the formation of β-Si_3N_4, which could be precipitated at low temperatures. However, they did not give a threshold for such an oxygen potential. There are also reports of manganese-silicon nitrides (cited in Robert et al[34]) and the presence of manganese[34] in the "SiN" precipitated in commercial low-carbon steels. All these reports leave the impression, that depending on the environment, the low temperature silicon nitride could

exist in different forms, infact, Goldschmidt[173] even made a suggestion to that effect.

Most of the reports[34-36] on the existence of these other forms of silicon nitride at low temperatures were based on an ageing (long ageing) treatment. However, in this work, α-Si_3N_4 precipitates were identified straight from the annealing stage; a similar observation of Si_3N_4 from an annealing treatment had been made by Irvine et al[37], though they did not show the identification procedure. Therefore, an ageing treatment was carried out to investigate if any modification to the precipitates formed during annealing occured.

In Fig 5.12 are the electron micrographs of the precipitates produced by the ageing treatment. These were also identified to be low temperature (α) Si_3N_4. The precipitates in both aged and annealed (Fig 5.6) steels were always found to be partially coherent with the alpha-iron matrix (by virtue of the observed colinearity of the precipitate's and the matrix's spots). The morphology of the precipitates at the grain boundary seems to differ from that in the grain interior; a similar observation was made by Arrowsmith[35].

The study of partially coherent precipitates by electron diffraction is quite difficult[144], because the streaking of the precipitate's spots (suggestive of the extreme thinness of the particles) and the presence of many orientations increase the complexity of the pattern. The ageing treatment, however, increased the volume fraction of

the precipitates. Some of the observed crystallographic relationships between the precipitates and the alpha-iron matrix are:

$$(10\bar{1}1)Si_3N_4 \;//\; (011)Fe$$

$$(21\bar{3}2)Si_3N_4 \;//\; (130)Fe$$

$$(10\bar{1}0)Si_3N_4 \;//\; (100)Fe$$

From the stereogram (Fig 4.1) prepared and rotated (100_{cub} to coincide with $10\bar{1}0_{hex}$, as in the last relation above), it was considered that if the relationships were consistent, then the respective angles between pairs of cube poles should be the same as the corresponding pairs of hexagonal poles. For example, $0\bar{1}1_{cub} \wedge \bar{1}30_{cub}$ is 26° and $10\bar{1}1_{hex} \wedge 12\bar{3}2_{hex}$ is 29°; $110_{cub} \wedge 1\bar{1}2_{cub}$ is 55° and $11\bar{2}2_{hex} \wedge 22\bar{4}0_{hex}$ is 54°. Four such pairs, out of the five pairs verified, were found to agree within 3°, which was regarded as the experimental error; the fifth, $100_{cub} \wedge 0\bar{1}1_{cub} = 45°$ and $10\bar{1}0_{hex} \wedge 10\bar{1}1_{hex} = 50°$ was just outside the error, and the discrepancy was thought to be due to the strain in the lattices arising from the partially coherent nature of the precipitates.

Table 5.7 is the summary of the diffraction data of the identified precipitates and the identification procedure of a pattern is in Appendix C.

The extracted precipitates (on to a carbon replica) from the aged prior annealed 0.31 % Si steel were analyzed qualitatively with the EDAX machine. The spectra show that silicon is the only substitutional element in

this precipitate (the copper peaks are from the copper grids on which the replica was collected), Fig 5.13.

6.2.5 Effect of Silicon on the Ratio of Lower Yield Stress to Ultimate Tensile Strength (LYS/UTS)

Design engineers are always in favour of the reduction of lower yield to ultimate tensile strengths, LYS/UTS ratio, particularly with a simultaneous increase in both the lower yield and the ultimate tensile strengths. This is because it implies a higher capacity of the material to absorb more plastic work; i.e. strain harden[178]. The condition for reducing this ratio, but at the same time increasing the respective values of the LYS and UTS, can only be met if the latter is to increase more rapidly than the former.

An increase in UTS with silicon content was evaluated in this work for the specimens of allthe steel grades showing about the same grain size of 45±2 μm. For the short-aged batch, the UTS increased by 105 MPa per one wt% Si, while for the unaged, the increase was 95 MPa per one wt% Si. A common feature was that the UTS increased faster than the LYS up to 0.78 wt% Si. A similar trend has been reported by others[45,47,174]. This is given in Fig 6.2, where the values of the ratio, σ_y to σ_{UTS} have been plotted against the silicon content (wt%) in the steels. The results of other authors have been included in the figure for a comparison.

The reason for such a variation of this ratio with silicon content may be found in the study of the role

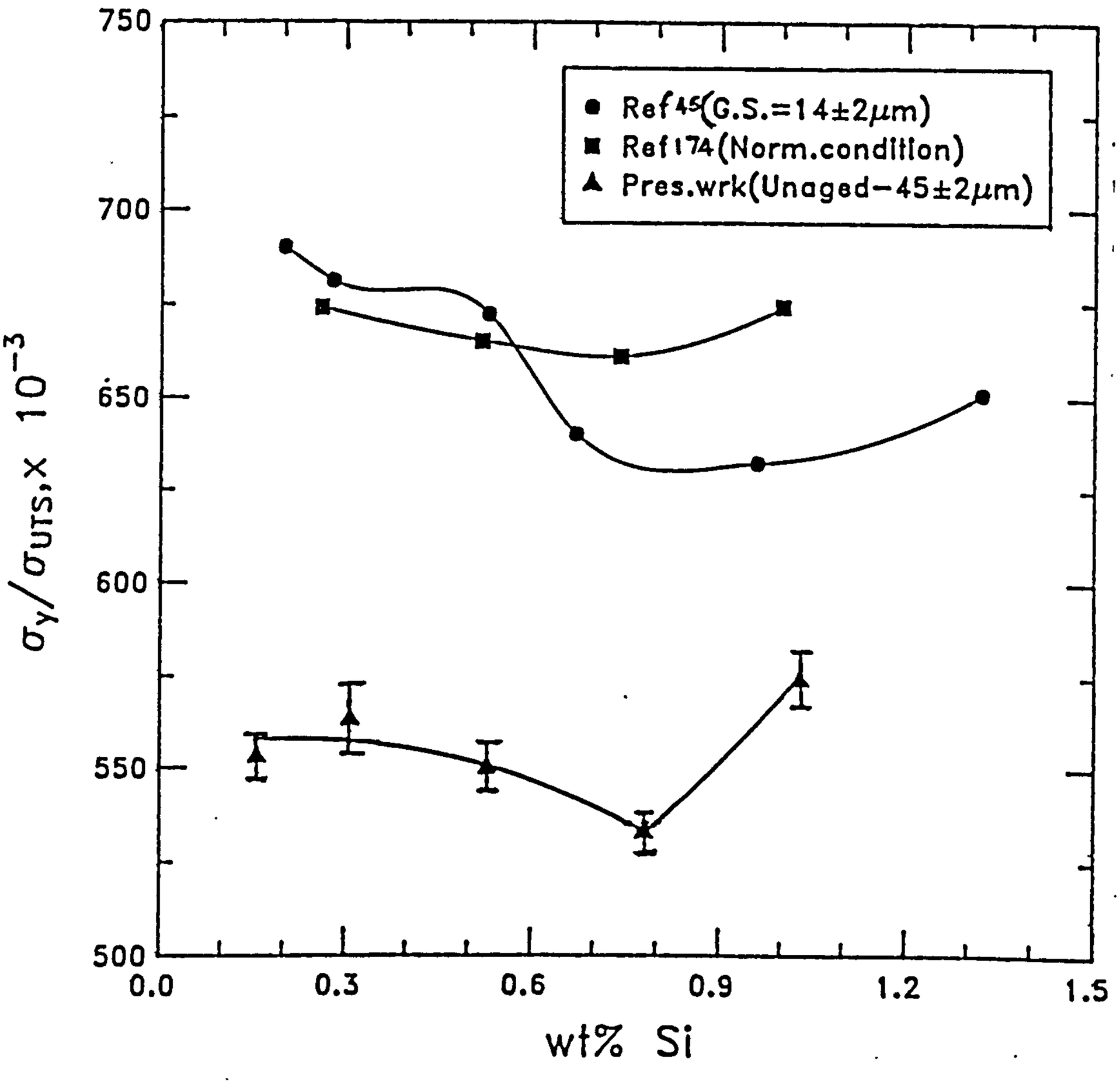

Fig 6.2: Effect of silicon on the lower yield stress(σ_y) to ultimate tensile strength(σ_{UTS}) ratio.

of pearlite in the steels, which was partly reviewed in chapter one.

Mehl and Hagel[179] showed that alloying elements can change l, the interlamellar spacing in pearlite. They related l to the degree of undercooling from the A_{e1}, to the respective cooling temperature, T (below A_{e1}) to which the steel is brought, and gave the relationship:

$$l(A_{e1}-T) = 8.5 \times 10^{-4} \quad cm/^{o}C \quad \ldots\ldots\ldots\ldots\ldots 6.2$$

Thus, equation 6.2 indicates that the higher the A_{e1} (for a given cooling temperature, T), the smaller the interlamellar spacing would be. Irvine and Pickering[44] observed that the greater the degree of undercooling, the smaller the interlamellar spacing. It was observed in this work that silicon additions increase both the A_{e1} and the A_{e3} for a silicon content above 0.31 wt% (see section 6.1, Fig 5.2 and Table 5.3) in the steel. A similar observation was made by Irvine and Pickering[44] for a silicon content above 0.42 wt% in a low-carbon steel, with manganese level less than 1.6 wt%. Therefore, it is understandable why in Fig 5.14 the reciprocal of the interlamellar spacing (1/l) was on the increase with the silicon content,particularly from 0.78 wt%,as the steel was intercritically annealed from the relatively lower temperature of 955°C.

At the same time, the partitioning effect of silicon, at a critical concentration,as the steel is intercritically annealed from higher temperatures, and its consequent effect on the pearlite interlamellar spacing, through the spheroidization of the cementite are establis-

hed (reviewed in section 1.5.1)[4]. Thus, in Fig 5.15 this spheroidization of the cementite is manifest in the 1.03 % Si steel, annealed at the highest temperature of 1216°C (code D). This has led to the rather large interlamellar spacing of the 1.03 wt% Si steel seen in Fig 5.14 at the highest solutionizing temperature. The spheroidization also led to the 1.03 wt% Si steel showing a lower volume fraction of pearlite, Table 5.6.

Gladman et al[41] observed that pearlite does not have any effect on the lower yield stress (σ_y). It has also been shown[13,42] in steels , with less than 0.16% C, that the initial yielding in a ferrite-pearlite steel is confined to the ferrite, though Preston[43] found a slight increase of σ_y, through the increase of k_y, on increasing the volume fraction of pearlite, by varying the carbon content of the steel from 0.067 to 0.21 wt%. Since the steels in the present study have about 0.13 wt% C, the modifications of the properties of pearlite in the present study would not be expected to affect the σ_y. However the amount of pearlite present in the steel does affect the tensile strength, due to the greater[41,44] work-hardening of the pearlite relative to the ferrite. Again, it has been argued[44] that a decreasing interlamellar spacing leads to a pronounced increase in tensile strength, though in low-carbon steels, this effect is expected to be relatively small (see section 1.4).

Thus, prior to the fragmentation of the cementite phase, silicon additions to the steel would lead to a more

rapid increase of the tensile strength, relative to the increase of the σ_y, due to the decrease of the interlamellar spacing. This would therefore explain the observation made in this study and in others[45,174], relating to the reduction of this ratio. This trend should discontinue when the silicon concentration level and the solutionizing temperature are such to destabilize the cementite, as was found in this work, where the reduction of the ratio held up only to a silicon content $\leqslant$ 0.78 wt% in the steels, Fig 6.2

The practical advantage of this more rapid increase of UTS relative to LYS is that the cold workability of these steels, with up to 0.78 wt% Si, could be improved.

6.3 "Softening"

The "softening" aspect of this work borders mainly on explaining how refined grains, brought about by silicon additions (see section 6.1), favour "softening". The discussion therefore does not essentially cover the primary "softening" effect of silicon which has been reviewed in chapter 2.

6.3.1 Low Temperature Tensile Tests. Athermal Yield Stress

In Table 5.8 are given the linear regression equations of the variation of σ_y with the grain size ($d^{-1/2}$), produced from the low temperature tests. It is well established from this work and others[24,44-46,137] that normally, additions of silicon increase the lattice frictional stress, σ_o of the steel. However, from Table 5.8, it is evident that below a critical test temperature and silicon content, the high silicon steels gave lower values of σ_o. A similar observation has been reported by other authors[53,54]. It is known[53] that the Hall-Petch equation can be given as:

$$\sigma_y = \sigma_i + \sigma^* + k_y d^{-1/2} \quad \text{.....6.3}$$

$$\text{i.e.} \quad \sigma_o = \sigma_i + \sigma^* \quad \text{.....6.3a}$$

Thus, the frictional stress consists of an athermal component, σ_i and a thermal (effective) component, σ^*. When the test temperature is such that the thermal component becomes zero (at T_c, Fig 2.1b, section 2.1), the yield stress of the material becomes entirely athermal, noted as σ_c (see equation 4.12, section 4.6).

A possible explanation to the decrease of σ_o below a critical test temperature at higher silicon levels was offered by Anderson and Spreadborough[34]. They suggested that the stress necessary to overcome the athermal (temperature independent) frictional stress, σ_i, being already so high due to solid solution strengthening, in the high silicon steels, at such low temperatures, a smaller increment of stress would be required for the dislocations to surmount their obstacles.

The athermal yield stress, σ_c, determined with the special tensile test (section 4.6) is plotted against grain size ($d^{-1/2}$) in Fig 5.16. As would be expected, the reduction of grain sizes led to an increase of σ_c for all the steels.

6.3.2 Effective (Thermal) Stresses

While the reduction of grain sizes increases the athermal stresses, Fig 5.16, it reduces the effective (thermal) stresses of the steel grades. The reduction of the effective stress is not so obvious at small strain

rates and large grain sizes. For instance, in Fig 5.17a, at a test temperature of 153 K and a strain rate of 3.3 x 10^{-4} s^{-1}, only a 13 % reduction of the effective stress was observed after reducing the grain size from 55 to 20 μm. However, this reduction increased to 33 % on reducing the grain size from 55 to 8 μm, at the same strain rate. But on increasing the strain rate to 0.33 s^{-1}, the 13% merely increased to 17 % (for the 55 to 20 μm reduction) and the 33 % increased to 43 %, for the 55 to 8 μm reduction.

This may be why some authors[42,180], using grain sizes $\geq$ 23 um and a strain rate[42] of 4.2 x 10^{-4} s^{-1}, suggested that the contribution of grain size to the yield stress is only athermal, thereby obtaining a single curve in a graph of σ^* versus test temperatures for different grain sizes. But with the reduced grain sizes and the higher strain rate used in this work, it can be seen in Fig 5.17b that the grain size very much affects the yield stress, by reducing the effective stress.

A thorough appraisal of the grain size effect on "softening" can only be made if the grain size effect can be separated from the silicon (concentration) effect, and if this grain size effect is brought to a common base for all the steel grades (typified by their silicon content). Such a common base would be the "softening" adduced by a silicon addition of one weight %, for a given grain size, at the various test temperatures. This procedure was followed in this work, and is shown in Fig 5.18a. Thus, grain sizes greater than 58 μm would not even show a pseudo

"softening", except when the test temperature was less than 223 K. In agreement with earlier work[53,54] on "softening", the reduction of test temperatures increases the "softening" due to silicon alone, but of interest in Fig 5.18a is that at 77 K, the change in the degree of "softening" with the change in grain size is the smallest.

This drop in the degree of "softening", which was also discussed in the reports of other authors[43,125,181,182], tends to suggest that alloy "Softening" in iron-based alloys may disappear below 100 K. However, this work shows that "softening" never vanishes, Fig 5.18b. Nevertheless, there is a critical temperature, where the "softening" is maximum. Below this temperature, the degree of "softening" is reduced. In the present work, with a strain rate of 3.3×10^{-4} s^{-1}, this critical temperature was found to be higher for the smaller-grained samples; 135 K for the 8 μm, and 120 K for the 20 μm. The implication is that an apparent "softening" (see section 2.1) could be simulated at much higher temperatures, using fine grains. Leslie[125] found a maximum "softening" temperature of 150 K with a 0.7 wt% Si steel. Another fact emerging from Fig 5.18b is that the degree of decrease of "softening" seems to be higher for the small grains, though they still maintain the highest level of "softening". This observation was also present in Leslie's[125], where a 1.5 wt% Mn iron, with a grain size of between 20 and 28 μm showed a much faster decrease than the 0.7 wt% Si iron, with a grain size of about 40 μm. However, it is not

possible to attribute this observation in Leslie's work entirely to grain size, since there were two different elements involved, which , through their intrinsic nature and concentration, may have influenced the results.

The role that the grain size can play in simulating an apparent "softening" is shown in Fig 5.19. The solution hardening effect of silicon is quite strong. But in the presence of the smaller grains, the 0.78 wt% Si steel apparently "softened" at a relatively high temperature of 175 K, and even the 1.03 % Si steel did apparently "soften", though not appreciably, Fig 5.19d. If a comparison is made with Nune's[53] work, where the grain sizes ranged between 30 and 70 μm, except for the 0.2 wt% Si steel (others were: 0.4, 0.6 and 1.5 wt% Si steel grades), there was virtually no apparent "softening". In other words, all these other steel grades; 0.4, 0.6 and 1.5 wt% Si steel grades, showed a higher value of σ_i with a higher silicon content in the steel, down to about 90 K. Thus, it is concluded from these mechanical tests that the grain size (among the other factors: temperature, concentration of the alloying element and strain rate) determines the appearance of an apparent "softening".

6.3.3 Microstructural Features of "Softening"

It was necessary to rationalize why refined grains would promote "softening": hence the need to study the slip lines or bands presented by the flat specimens, after being strained 8% in tension.

It has been suggested[101] that wavy slip lines result when the cross-slip mechanism is present, as would be the case in a room temperature test. Hence, wavy slip lines predominated in all the steels at the room temperature tests, Fig 5.20. (Note that the slip lines originate from the grain boundary areas, as was discussed in section 6.2.3, relating to k_y). It was also suggested that the planar slip lines result from the motion of edge dislocations[101].

Tuominen and Goss[67], working on a Si-Ti, b.c.c. system considered that at low temperatures, only screw dislocations control deformations. Keh and Weismann[103] have suggested that in low temperature tests of iron, the screw dislocations dominate the edge dislocations. The self energy of screw dislocations is lower than that of edge or mixed dislocations[74]. All these facts therefore indicate that the role the screw dislocations play at low temperature deformations can determine the dependence of the yield stress on temperature.

Li and Chou[15] derived equations 1.4, 1.4a and 1.4b (see section 1.2.1) from which a relationship between the grain size and the type of dislocations predominating in such a grain, can be deduced. From equation 1.4 therefore, if n and σ are constant, it can be seen that small-grain sizes favour the preponderance of screw dislocations.

In Fig 5.21, it is seen that the slip lines are wavy and very short for the small-grained samples in both

tests at the room temperature and 77 K.

However, the large-grained samples (Fig 5.22a), in the tests at 77 K showed principally long planar slip lines, with the incidence of secondary slip lines, the S-S zone in the micrograph. The slip lines also crossed the grain boundaries, unlike the slip lines in the small-grained samples. But the relatively smaller grains of the 1.03 % Si steel (within the large-grained group) still maintained fairly, the wavy and short nature of the slip lines in the tests at 77 K, Fig 5.22b.

Johnston and Gilman[184] have demonstrated that under the normal dislocation velocity range (< 10^3 cm s^{-1}), as experienced in tests with a strain rate of up to 10^2 s^{-1}, the edge dislocations are fifty times faster than the screw component. Ogilvie[185] has suggested that slip lines cross the boundaries when the latter are straight. Straight boundaries should therefore be found more frequently in the large-grained specimens than in the small-grained specimens. Thus, with the high speed of the edge dislocations in the large-grained specimens, it is understandable why the slip lines cross the grain boundaries in Fig 5.22a. This fast motion of the edge dislocations (dislocations start to move right from the microstrain region[20,184]) at such a low temperature of 77 K, where the relaxation of the material is not possible, would lead to the hardening of the steel. This hardening coincided with the appearance of the secondary slip lines, which it has been suggested[21], appear at the instance of higher stresses.

It has been shown[21,140] that the average slip line spacing per grain, S_{Av} decreases with an increasing stress. This was confirmed in this work, Table 5.9, where the small-grained specimens showed larger slip line spacings.

Dislocation cell formation has been proposed[107] to be a result of an intense cross-slip of dislocations during room temperature deformation. It is also known that the multiplication of screw dislocations is essentially through the cross-slip mechanism[74].Irrespective of grain-group, at the room temperature tests, the dislocation structure was cellular, Fig 5.23. This confirms the waviness of the slip lines of these specimens viewed under the optical microscope. However, the small-grained specimens showed smaller cell sizes. Swann[108], modelling the f.c.c. structure, showed that harder metals present smaller cell sizes, and suggested that the cell size is independent of the grain size of the material. The first conclusion of Swann is in agreement with the finding in this work, Fig 5.23a. In this work, at the room temperature tests, the harder specimens were those with higher silicon content. A higher silicon content in the steels also led to smaller grain sizes. Therefore, the latter suggestion by Swann[108] is unconfirmed in this work. Generally, in b.c.c. alloys, small-grained specimens, tested at room temperature are always harder than the large-grained. Since in this work, the small-grained samples contained smaller cell sizes, the second suggestion by Swann[108] may not hold for

alpha-iron.

It is generally accepted that dislocation tangles and cells, with associated wavy slip lines when viewed under the optical microscope, are the main features of a cross-slip mechanism[101]. Spitzig and Leslie[97], basing on an earlier work by Barrett et al[124] regarding the effect of silicon on the formation of slip lines (section 2.5), argued that a cross-slip mechanism is insignificant in alloy "softening" by silicon.

Nevertheless, it was observed in this work that the small-grained samples, irrespective of steel composition, which showed more "softening", had a higher dislocation density, and maintained a fairly cellular dislocation structure, with long dislocation segments, in the tests at 77 K, Fig 5.24a (see the associated wavy slip lines observed under the optical microscope in Fig 5.21b). In contrast, the large-grained samples showed short segments with a relatively lower dislocation density, Fig 5.24b.

It has been shown by Jolley[101], that cross-slipping could still occur without tangles and cells being present. His samples contained long dislocation segments, which are indicative of a lower mobility of the jogged screw dislocations[103]. Screw dislocations jog after being multiplied through the cross-slip mechanism[104]. Later on in this work, it will be shown that one of the most probable rate-controlling mechanisms was cross-slip. Michalak[104] has also suggested that the longer the

dislocation segments, the more the dislocations can participate in the thermal activation process (TAP), but that the reduced density or lack of tangles, and the short dislocation segments would require a higher stress for the dislocations, so characterized, to be moved (see section 2.3.2). Dislocation cutting should be expected in the large-grained specimens, Fig 5.24b, where the predominating edge dislocations are calculated to move about fifty times faster than the screw component.

It was earlier mentioned in section 2.3.2 about the various[54,101,104-108] views relating the incidence of twinning to the lower yield stress of a material, particularly with respect to the decrease of the latter. However, the work of Anderson and Spreadborough[54] tends to suggest that alloy "softening" may not be related to twinning. This was confirmed in this work, whereby the large grained specimens, irrespective of steel grade, showed a very high incidence of twins, Fig 5.25a, but in the small-grained samples of all the steel grades, there was a virtual absence of twins, Fig 5.25b. This may suggest that twinning in alpha iron is strictly dependent on grain size.

Some reports[113,114] made a fairly similar observation (section 2.3.2), and related the incidence of twinning to the existence of a critical grain size. If the grain size is less than this critical value, it was suggested, twinning can only occur if there are inhomogeneities in the grain size distribution. Since the grain size distribution is fairly uniform in this work, it is

understandable why the small-grained samples showed no twins. Thus, it is concluded that twinning does not have any effect on the "softening" of low-carbon steels. Since most of the earlier work on "softening" used grain sizes of between 23 and 500 μm[53,54,56,62,97,110], where actually the twinning incidence could be high, it was impossible to separate the twinning incidence from the "softening" phenomenon.

Nevertheless, recently it has been shown[18], using a 20/25 austenitic steel that profuse twinning led to a reduction in the value of the Hall-Petch slope, k_y, with a consequent reduction in the value of the flow stress in the tests at room temperature. In this work, it was observed that the k_y values in the low temperature tests (see Table 5.8) were smaller than those observed at the room temperature tests (0.156 % Si had a k_y value of 21.1 MPamm$^{1/2}$, 0.31 had 23.4, 0.53 had 21.5, 0.78 had 18.9 and 1.03 % Si had a k_y value of 21.2 MPamm$^{1/2}$. It may be that twins do reduce just the athermal component of the total lower yield stress. If the effective (thermal) yield stress, which constitutes the major part of the total σ_y at low temperature tests, is not reduced, it is rational to assume that the degree of reduction of the "minor" athermal component, brought about by the incidence of twins, may not be enough to lead to a "softening" of the alloy, particularly as "softening" is mainly manifest through the effective stress.

Jolley[101] argued that if a material showed wavy

slip lines after room and low temperature tests, that the k_y values should be expected to be the same. This argument was based on the work by Armstrong et al[190], who showed that k_y could be a function of the number of slip systems available. Thus, waviness in the specimens tested at both the room and low temperatures would imply the same number of slip systems operating. However, the k_y values of specimens that showed waviness at both the low and room temperature tests of this work did not confirm this hypothesis.

6.3.4 Consistency of the Scavenging (Extrinsic) and the Intrinsic Theories of Alloy "Softening"

It is hard to rationalize the results of the"softening" study of this work in terms of extrinsic theory (the scavenging model), see section 2.2.6. This theory proposes the reduction of the frictional stress, which leads to the "softening" phenomenon, when the interstitial atoms are scavenged by the substitutional atoms[82]. Assuming that this theory is consistent, following the argument for the precipitation of nitrides (which led to the reduction of k_y), "softening", irrespective of grain size should have ceased at the maximum precipitation level. This is because, it was argued in section 6.2.3.3, the precipitation of nitrides from ferrite should have an equilibrium point. Thus, the moment a further precipitation of nitrides stops, and "free" residual nitrogen atoms abound, there should be no "softening". Nevertheless, the "softe-

ning" did not in the least decrease beyond the 0.78 wt% Si level, a level at which it was argued could be the maximum nitride precipitation level (see section 6.2.3.3); but rather the "softening" increased. It could be argued that the "softening" is brought about by the effect the substitutional element has on the carbon atoms, which in this work was found to be that of decarburization, while other researchers[142,143] reported a reduction of the solubility of carbon in the presence of silicon. However, those[42,88] who investigated specifically the "softening" of steels based on the scavenging of interstitial atoms, demonstrated the inconsistency of this model.

If the scavenging model were to be consistent, in view of the time used in this work to produce the small grains, relative to that used for the large grains, the latter should be expected to have far more precipitates and thus, should have showed a higher tendency to "softening". However, this was not the case. Similarly, the intrinsic theories that involve solute interaction with dislocations or stress fields do not fit into this work. The present results do suggest that the most probable theories explaining the "softening" phenomenon in dilute solid solutions are those which invoke changes in the deformation mechanism[44,47] and the increase in thermal activation parameters[43,75,77].

6.4 Thermal Activation Parameter Studies

From Fig 5.26, the effective stress at 0 K, σ_i^*, of the 0.78 % Si steel was obtained. Similar graphs, for the other steel grades were used to obtain all values of σ_i^*. These values , the values of the dislocation velocity-exponent, m' and those of the dislocation frequency factor, υ are given in Table 5.10.

Campbell and Ferguson[91], using a 0.1 % Si-0.62 % Mn alpha-iron, estimated σ_i^* to be at least 1100 MPa (i.e., τ_i^* = 550 MPa). Sandström and Bergström[93], using a 0.39 wt% Si - 1.32 wt% Mn steel, obtained a σ_i^* of 1000 MPa. Thus, the values obtained in this work are reasonable, if allowances are made for the difference in compositions. From Table 5.10, it can also be seen that the values of m' and υ very much depend on the degree of "softening".

Some authors have suggested that m' increases[54,97] with the addition of silicon and varies[148] with 1/T. The m' values in this work were generally found to increase with silicon content and grain size reduction, but only if an appreciable apparent "softening" was present, for example, in Fig 5.19, at 20 μm, where there was not yet an appreciable apparent "softening" for any of the steels at 153 K, the m' value was about constant at 13 ± 1, for all the steels. By comparison at 8 μm, where there was quite an appreciable apparent "softening" for the 0.78 % Si, relative to the 0.31 or the 0.156 wt% Si steel grades, the m' value of the former was higher than those of the latter two steel grades. However, the 1.03 % Si steel

that had not yet shown an appreciable apparent "softening", relative to the 0.78 and the 0.53 wt% Si steel grades, with a grain size of 8 μm, had a lower value, relative to the values of the latter two, but a value higher than those of the 0.31 and 0.156 wt% Si steels. The room temperature values of m' for a 0.39 wt% Si-Mn steel[53] were reported to be 8.7, and for 2.5 to 4.5 wt% Si steels[54] they were 4.3 ± 0.7 to 10.6 ±1. The room temperature values in this work were evaluated from equation 4.14 and found to range from 6 to 11, but from Table 5.10, it can be seen that in the large-grained samples of the 1.03 % Si steel, where there was no apparent "softening", the values remained low. The same argument holds for the υ values of the steels.

Using these values, the thermal activation parameters were obtained and plotted against grain size ($d^{-1/2}$), Fig 5.27. It is evident, particularly in the activation energy (H) - grain size curve, how the H-value of the 0.78 % Si steel matches that of the 0,53 wt% Si steel, the current maximum silicon content permitted in these steels.

To test the validity of the approach used in this study of the activation parameters, the H and activation volume (V^*/b^3) values of the respective grain sizes used in this work were compared with the activation volume and energy values of the effective shear stresses given in the work of Conrad and Frederick[52], which matched the effective shear stresses showed by the grain sizes used in this work. Fig 6.3. There is a satisfactory agreement.

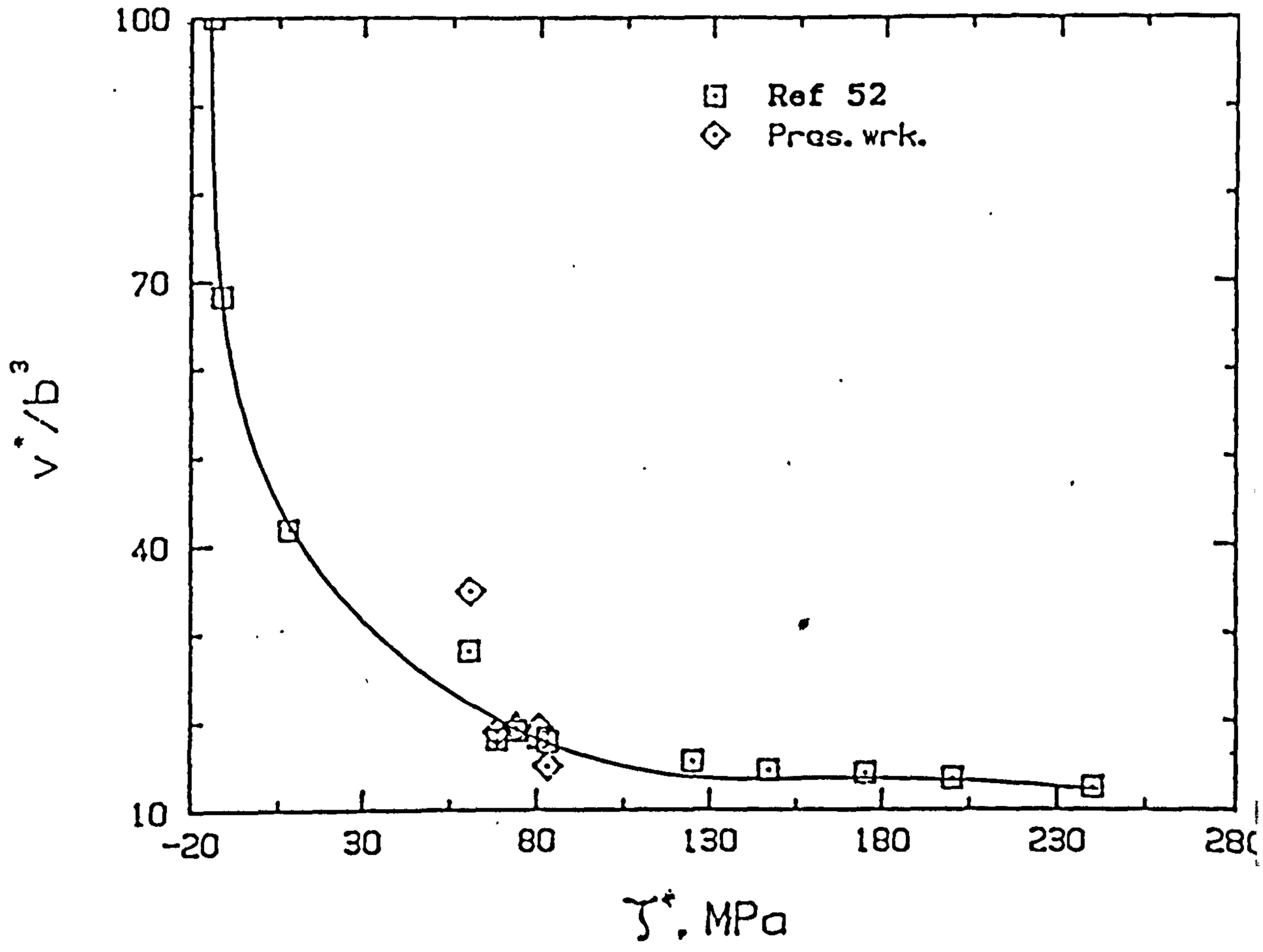

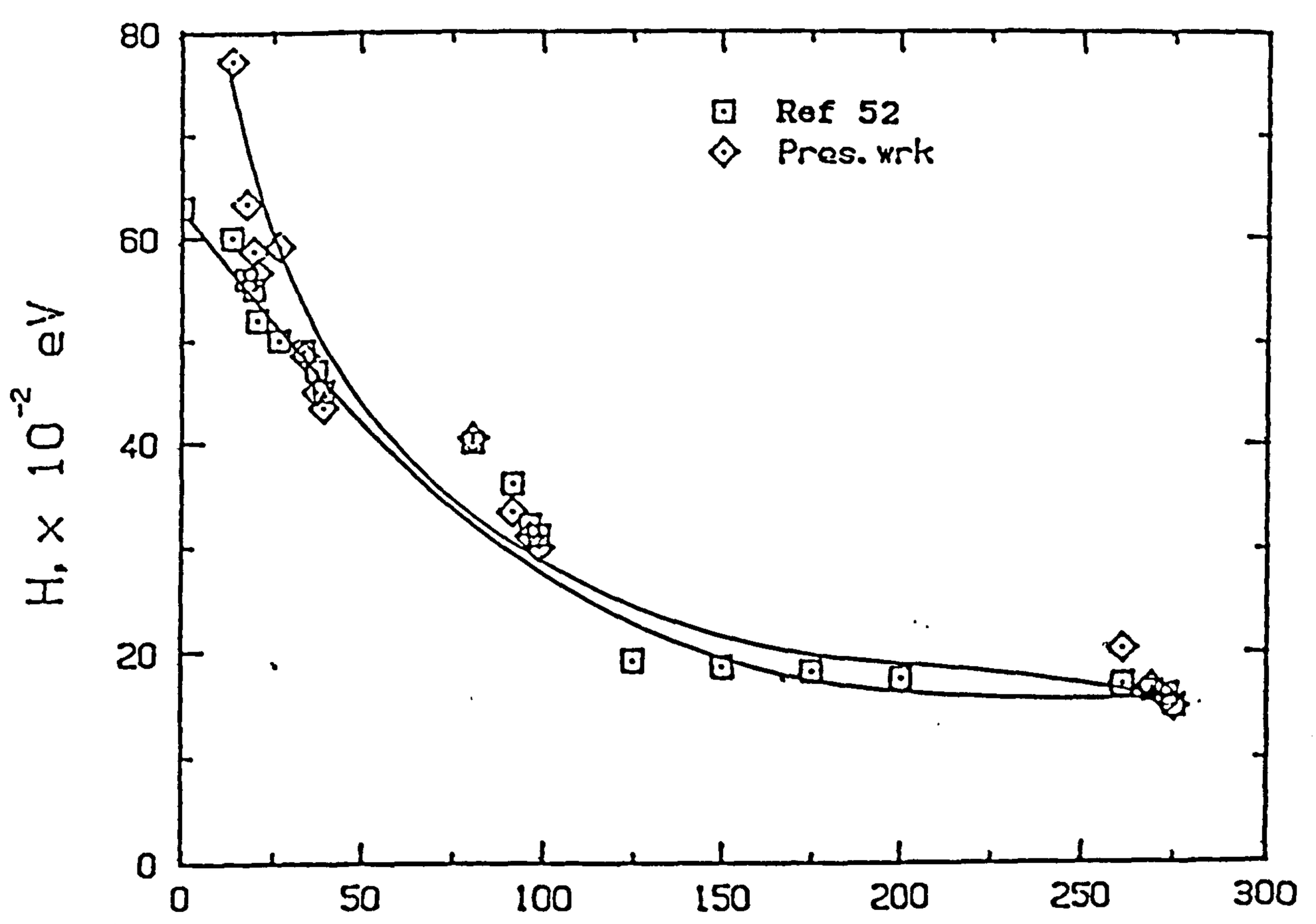

Fig 6.3: Comparison of the values of the activation parameter of this work, with those of the work of Conrad and Frederick[52]

It has been suggested[58] that the typical value of activation volume (V^*/b^3) for a cross-slip mechanism is 10 to 10^2. It is evident from Fig 5.27 (V^*/b^3 vs $d^{-1/2}$), that the activation volume values fall within the range of 10 to 10^2. Thus the rationalization achieved in the dislocation/slip line structure study was indeed upheld. The cross-slip mechanism is only the most probable; other mechanisms can equally be operative at low temperature testing[58]

6.5 "Softening" and Impact Behaviour

Studies of the impact behaviour of low-carbon steels, with a silicon content in the steel above 0.7 wt% are very few. One such report[154], with limited measurements of the impact transition temperature, T_c vs grain size ($d^{-1/2}$) showed that a 0.9 wt% Si steel had a better impact behaviour, relative to a 0.2 wt% silicon steel, at reduced grain sizes. Sibley and Breyer[24] have shown that silicon additions, up to 0.7 wt%, improve the impact behaviour of low-carbon steels, at small grain sizes, and that a 25% reduction in grain size decreases T_c by 14 to 17°C. Abramowitz and Moll[43] found the T_c of a 0.67 wt% Si low carbon steel, with a grain size of about 12.5 μm to be -84°C and that for a 0.96 wt% Si steel, with a grain size of about 16 μm, to be -69°C. This implies that the latter steel is about 28 % larger in grain size than the former, which could also account for the difference of 15°C in their T_c values.

From this work, it has been observed that silicon additions do reduce the grain size, Fig 5.4. The previous work[24,156] showed an improvement of impact behaviour simultaneously with reduced grain sizes and increased silicon content. Nevertheless, there has not been any suggestion that this improved behaviour could be due to the effect of silicon on grain size. Rather, theories[24,45] of silicon-carbon interaction are favoured. As already mentioned in section 6.2.3.2, it is evident that if interstitial (carbon and nitrogen) - silicon interactions were responsible for the improved impact behaviour, the interstitial would primarily be nitrogen.

Abramowitz and Moll[45] used the reduction in hardness, associated with the initial additions of silicon, as an index to substantiate the silicon-carbon interaction. It has been reported[40] that a reduction in hardness is equally present in alloy "softening", Fig 2.2. It was found in this work, and reported by other authors[53,54] that silicon additions "soften" low carbon steels. Thus, the improved impact behaviour observed with silicon additions may well be partly due to alloy "softening". But silicon-carbon interaction theory (scavenging model) has been found unsatisfactory[42] in explaining the "softening" phenomenon. Mintz and Turner[192] also have used internal friction measurements to show that the improvement in the impact properties of low-carbon steels by silicon additions is not due to the depletion of interstitial atoms.

It was suggested[125] that the advantages of

"softening" are lost during cold deformations, and therefore, their gainful tapping is unlikely. However, such a suggestion may have been arrived at because the work did not consider the "apparent" aspect of alloy "softening".

Pink and Arsenault[57] have argued that "softening" may favour the reduction of the impact transition temperature, T_c, only if the "softening" is apparent (true) and the fracture stress of the alloy is not lowered by the impurities in the alloy (see section 2.4). Consequent upon this suggestion, the facts emerging from figures 5.18b and 5.19d with regard to the simulation of apparent "softening" at higher temperatures could point to the possibility of permitting higher silicon levels in these steels, provided the grain size is tailored. This is more so, because the modern steel-making processes would make it possible to reduce the level of impurities in the steels.

From the activation studies of this work, it is evident how the activation energy, for all the steels, and particularly for the 1.03 wt% silicon steel, appreciated in the small-grain region, Fig 5.27b. This improvement in the activation parameters, resulting from the apparent "softening" of the higher silicon steels, could be extended to the impact behaviour, since both the "softening" and the impact behaviour are controlled by the same thermally activated processes.

A rough calculation, based on the prices of ferroalloys alone, indicates that two pounds (sterling) per

tonne of steel is accruable as savings, with improved strength and T_c values of the steels, if low-carbon structural steels, presently with (wt%) 0.5 Si - 1.2 Mn are changed to 0.7 Si - 0.8 Mn, although Mintz and Campbell[177] have shown that about 1 wt% Mn in low carbon steels, improves their T_c by refining the carbide thickness.

6.6 Future Work

Low carbon structural steels very often contain aluminium (including manganese and silicon). In view of the strong interrelationship, observed and discussed in this work, between silicon and manganese, in the variation of k_y, a future study on k_y would investigate the type of interrelationship that exists between aluminium and silicon. Such a study should use a range of grain sizes as wide as possible, and the low carbon steels under analysis should have about the same base composition.

On the effect of silicon upon the impact behaviour of low carbon steels, concentration should be on small grain sizes (less than 10 μm). Most importantly, the analyses across the steel grades (silicon content) should be for a constant ferrite grain size.

CHAPTER SEVEN

CONCLUSIONS

The conclusions from this investigation are as follow:

A Strengthening

1) Silicon does refine grains by its effect on the prior austenite grain size; the fine austenite grain size obtained by silicon additions leads to a fine ferrite grain size.

2) Low carbon steels are strengthened by silicon, not only by solution hardening, but also by grain refining; the latter becoming less efficient at grain sizes less than 14 um, within 0.31 to 0.78 wt% Si.

3) The rate of increase of σ_y with silicon content depends on the grain size;the smaller the grain size,the lower the rate of increase.Hence,the degree of strengthening (σ_y) of low carbon steels by silicon is more noticeable in coarse-grained than in fine-grained specimens.

4) In low carbon steels, the value of the Hall-Petch slope,K_y,at room temperature is reduced up to 0.78 wt% Si, after which it starts to appreciate again. The reduction is such that within 0.31 and 0.78 wt% Si content in the steel, low silicon steels may possess higher strength than the high silicon steels, at grain sizes less than about 14 μm.

Neither pile-ups nor sufficient ledges were

observed to satisfactorily explain the variation of K_y. On the basis of the identification of partially coherent Si_3N_4 precipitates, even from the annealing treatment, it is suggested that a more satisfactory theory to explain the variation of K_y in these steels would be the segregation of the interstitial nitrogen atoms to the grain boundary.

Nitrogen seems to have little effect on solid solution hardening, but its removal by precipitation may be favourable to yielding.

5) The inverse inter-relationship of the lattice frictional stress, σ_o and K_y is not entirely self compensating. For a fairly representative K_y value, the base composition of the steels under study should be maintained (about the same) for all the grades, and a wide range of grain sizes is also necessary. However, it does seem that the Hall-Petch equation can not be applied to an infinite $d^{-1/2}$

6) Silicon addition, up to 0.78 wt%, increases the ultimate tensile strength (UTS) faster than the lower yield stress (LYS), thus reducing the ratio, LYS/UTS up to about this silicon level in the steels. The reduction of the ratio is attributed to the reduction of the interlamellar spacing of cementite in the pearlite colony, which starts to spheroidize at high austenitizing temperatures, from about 1 wt% Si.

7) Silicon additions increase the decarburization tendency in these steels.

8) In both the annealed (continuously cooled) and

the aged conditions, low temperature (∝) Si_3N_4, precipitates (with c=5.617 Å and a=7.748 Å),partially coherent with alpha iron, were identified. After ageing for 72 hours at 595±10°C in vacuum, no transformation of the ∝-Si_3N_4 was observed, strongly suggesting that the precipitates are very stable.

B "Softening"

9) Reduced grain size appreciably increases the "softening" potential of silicon in low carbon steels; the smaller grain sizes most probably favour the abundance of screw dislocations, which on multiplying by the cross-slip mechanism, participate more effectively in thermally activated processes.

10) There is a critical temperature for maximum "softening", and it was found to increase with a reduction in grain size. The implication of a higher critical temperature for a maximum "softening" is that an apparent "softening" can set in at higher temperatures. For a strain rate of 3.3×10^{-4} s^{-1}, the range of the critical temperature was 120 to 135 K. Below these temperatures for maximum "softening", the degree of "softening" is reduced to a minimum "softening" determined solely by the silicon concentration in the steel.

11) Apparent (true) "softening" of steels results only when all the parameters, grain size, test temperature, strain rate and silicon content are correlated. Provided

there is an appreciable apparent "softening", a higher silicon content in the steel (implying refined grains) leads to larger values of thermal activation parameters. Since "softening" and impact behaviour are similar, in terms of activation processes, it is suggested that refining the grains further could permit a higher silicon content in low carbon structural steels.

APPENDIX A

GRAIN SIZE ESTIMATION, USING THE TRANSMISSION ELECTRON MICROSCOPE (TEM), "PHILIPS" 400T

From the manual of the microscope, the screen has a diameter of 155 mm, and the image projected on it is of a true magnification (T.M.) of 0.915 times the magnification reading on the microscope.

Twenty fields of view, i, each with a number of grains, n contained in it, were taken from the sample under study.

For each field of view, the average grain size, $\bar{x}_i$ was determined with the equation:

$$\bar{x}_i = 155/n \times T.M \quad \ldots\ldots\ldots\ldots\ldots\ldots\ldots\ldots 1$$

Therefore, for the entire sample, the average grain size, $\bar{d}$ was determined with the equation:

$$\bar{d} = \sum_{i=1}^{i=20} x_i/20 \quad \ldots\ldots\ldots\ldots\ldots\ldots\ldots\ldots 2$$

APPENDIX B

STOICHIOMETRIC CALCULATION OF THE MAXIMUM VOLUME FRACTION OF Si_3N_4 PRECIPITATES POSSIBLE IN THE STEELS UNDER STUDY

With maximum contents of 1.03 wt% Si and 0.0023 wt% N in the steels, if it is assumed that all the silicon and the nitrogen react to form Si_3N_4, the latter should constitute at most the sum of the two reactants; i.e. only 1.0323 wt% of the steel.

The equilibrium reaction is:

$$3\,Si + 2\,N_2 \longrightarrow Si_3N_4$$

i.e 84 parts Si + 56 parts N_2 ---> 140 parts Si_3N_4

Thus, 1 part Si + 0.667 Parts ---> 1.667 parts Si_3N_4

Since there is 1.03 wt% Si, it means that 0.687 wt% N_2 is required to yield 1.7167 wt% Si_3N_4.

However, there is only 0.0023 wt% N_2, therefore the percentage of nitrides formed in the steel would be:

$$(1.7167/0.687)\ 0.0023 = 0.0058 \text{ wt\%}$$

Consequently, the volume fraction, f, of the nitrides in the steel is 5.8×10^{-3}

APPENDIX C

PROCEDURE OF IDENTIFYING THE PRECIPITATES

Let n represent $(h_i^2 + k_i^2 + l_i^2)^{1/2}$, ...1

where i is the reflecting plane. From the diffraction pattern (see the insert), the following data were obtained for the matrix alpha-iron and the precipitates:

	Alpha-iron, mm	Precipitates, mm
D_1	31	24.8
D_2	54	33.6
D_3	70	54.5

where D is the ring diameter of the reflecting family of planes:

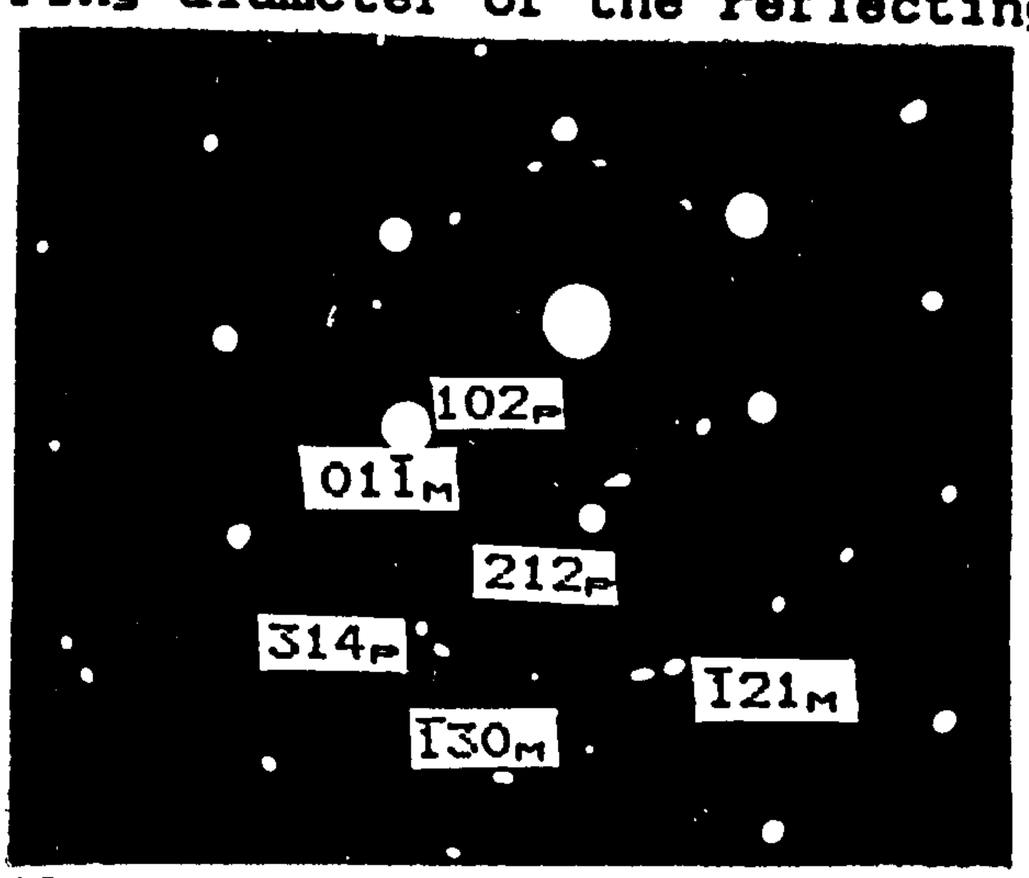

From the crystallographic relationship[144] of the cubic system, it is known that,

$$1/d^2 = n_i/a^2 \quad \text{.....2}$$

where "d" is the interplanar spacing of the crystal and "a" is the crystal constant.

From equation 2, it results that for a system with a constant crystal lattice, such as the cubic system,

$$d_i/d_{i+1} = n_{i+1}/n_i \quad \text{.....3}$$

However, the camera constant is given[144] as:

$$D_i d_i \quad \ldots\ldots\ldots\ldots\ldots\ldots\ldots\ldots 4$$

Therfore, equation 3 can be rewritten as:

$$D_i/D_{i+1} = d_{i+1}/d_i = n_i/n_{i+1} \quad \ldots\ldots\ldots\ldots\ldots 5$$

Hence,

$$D_1/D_2 = 0.574 = 2^{1/2}/6^{1/2}; \equiv (011)/(121)$$

$$D_1/D_3 = 0.443 = 2^{1/2}/10^{1/2}; \equiv (011)/(130)$$

It therefore follows that $D_2/D_3 = 0.771$. The interplanar distances were then chosen from the Standard Diffraction Data Book[149] to correspond with these planes.

Thus, $d_1 = 2.03$ Å, $d_2 = 1.17$ Å, $d_3 = 0.91$ Å. Hence the average camera constant is = 63.27 mmÅ.

<u>Verification:</u>

Using the geometric interrelationship[144] of cubic crystal planes:

$$\cos\theta = (h_1h_2+k_1k_2+l_1l_2)/[(h_1^2+k_1^2+l_1^2)(h_1^2+k_1^2+l_1^2)]^{1/2},$$

the respective angles were measured and calculated:

Planes (Rings)	Measured angles,°	Calcted. angles,°
D_1/D_2	73.0	73.2
D_1/D_3	48.0	47.9
D_2/D_3	25.0	25.3

<u>For the Precipitates,</u>

the interplanar distances were obtained using the ring diameters of the reflecting families of planes and equation 4. Thus,

$$d_1 = \text{Camera constant}/D_1 = 2.55 \text{ Å}$$

d_2 = Camera constant/D_2 = 1.88 Å

d_3 = Camera constant/D_3 = 1.16 Å

From the Standard Data Book[49], these "d" values correspond with those of low temperature (∝) Si_3N_4 (c=5.617 Å, a=7.748 Å), having

d_1 = 2.6 Å, which corresponds to (102)

d_2 = 1.88 Å, which corresponds to (212)

In the Standard Data Book[49], the "d" values extend down to 1.155 Å, however,the corresponding planes are given only down to a "d" value of 1.213 Å.

Therefore, the vector addition principle of Miller indices[44] was used to obtain the corresponding plane to the "d_3" of the precipitate. This is (314), and it was verified to be correct.

Verification of the Identification Procedure

Again, using the geometric interrelationship[44] of crystal planes, for the hexagonal system,

$$\cos\theta = [h_1h_2+k_1k_2+1/2(h_1k_2+h_2k_1)+(3a^2l_1l_2)/4c^2]/[[h_1^2+k_1^2+$$

$$+h_1k_1+(3a^2l_1^2)/4c^2][h_2^2+k_2^2+h_2k_2+(3a^2l_2^2)/4c^2]]^{1/2},$$

the respective angles were measured and calculated:

Planes (Rings)	Measured angles,°	Calcted.angles,°
D_1/D_2	27.5	27.2
D_2/D_3	11.0	11.4
D_1/D_3	16.5	15.8

REFERENCES

1 R.W.K. Honeycombe, "Steels, Microstructures and Properties", Edward Arnold, London (1987)

2 A.H. Cottrell and B.A. Bilby, Proc. Phys. Soc. Vol A62, 49 (1949)

3 S. Takeuchi, J. Phys. Soc. Japan Vol 27, 929 (1969)

4 W. C. Leslie, "The Physical Metallurgy of Steels", O Hemisphere (McGraw Hill Books Coy) Publishers, New-York/London (1981)

5 L. Zwell, G.R. Speich and W.C. Leslie, Metall. Trans. Vol 4, 1990 (1973)

6 P.M. Tennent, "Science Data Book", Oliver and Boyd (Longman Group Ltd), Edinburgh, 57 (1973)

7 J.L. Snoek, Physica Vol 8,711 (1941)

8 W.C. Leslie and R.J. Sober, Trans. ASM Vol 60,459 (1967)

9 D. Mclean, "Grain Boundaries in Metals", Clarendon Press, Oxford (1957)

10 J. Gouzou, Acta Metall. Vol 12 785 (1964)

11 D. Mclean, J. Inst. Metals Vol 74 95 (1948)

12 E.O. Hall, Proc. Phys. Soc. London Vol B64, 747 (1951)

13 N.J. Petch, J. Iron Steel Inst. Vol 174, 25 (1953)

14 A.H. Cottrell, Trans. TMS-AIME Vol 212, 192 (1958)

15 J.C.M. Li and Y.T. Chou, Metall. Trans. Vol 1, 1145 (1970)

16 Y.T. Chou, J. Appl. Phys. Vol 38, 2080 (1967)

17 A.A. Johnson, Phil. Mag. Vol 7, 177 (1962)

18 Y.T. Chou and N. Louat, J. Appl. Phys. Vol 33, 3312 (1962)

19 P.J. Worthington and E. Smith, Acta Metall. Vol 12, 1277 (1964)

20 W.E. Carrington and D. Mclean, Acta Metall. Vol 13, 493 (1965)

21 H. Margolin and M.S. Stanescu, Acta Metall. Vol 23, 1411 (1975)

22 J.C.M. Li, Trans. TMS-AIME Vol 227, 239 (1963)

23 A.N. Stroh, Acta Metall. Vol 9, 315 (1961)

24 A.W. Cochardt, G. Schock and H. Wiedersich, Acta Metall. Vol 3, 533 (1955)

25 I. Codd and N.J. Petch, Phil. Mag. Vol 5, 30 (1960)

26 K.D. Sibley and N.N. Breyer, Metall. Trans. Vol 7A, 1602 (1976)

27 G.V. Smith, P.M. Kranzelin and M.S. Burton, Trans. AMS Vol 56, 701 (1963)

28 J. Heslop and N.J. Petch, Phil. Mag. Vol 2, 649 (1957)

29 E.D. Hondros, Metal Sc. J. Vol 1, 36 (1967)

30 D.A.Porter and K.E. Easterling, "Phase Transformations in Metals and Alloys" Von Nostrad Reinhold, London (1986)

31 R.W. Cahn, "Physical Metallurgy" North Holland Publishers, 595 (1970)

32 N.J. Petch, in "Fracture" (Eds.: B.L. Averbach, D.K. Felbeck, G.T. Hahn and D.A. Thomas), John Wiley, New-York/London, 54 (1959)

33 D.V. Wilson, Metal Sc. J. Vol 1, 40 (1967)

34 T.N. Baker, J. Iron Steel Inst. Vol 205, 315 (1967)

35 J.M. Arrowsmith, J. Iron Steel Inst. Vol 201 699 (1963)

36 W. Roberts, P. Grieveson and K.H. Jack, J. Iron Steel

Inst. Vol 210, 931 (1972)

37 K.J. Irvine, J.D. Murray and F.B. Pickering, Iron Steel Inst. Spec. Rep. No. 70, 246 (1961)

38 J.C.M. Li, J. Appl. Phys. Vol 32, 525 (1961)

39 B. Mintz, R.C. Cochrane and J.D. Baird, Scand.J. Metall.

40 Y. Ishida, T. Hasegawa and F. Nagata, J Appl. Physics Vol 40, 2182 (1969)

41 T. Gladman, B. Holmes and F.B. Pickering. J. Iron Steel Inst. Vol 208, 172 (1970)

42 B. Karlson, G. Lindon and K.E. Easterling, Jernkon. Ann. Vol 155, 413 (1971)

43 R.R. Preston, in "Yield Flow and Fracture in Polycrystals" (Ed.: T.N. Baker), Applied Sc. Publ., London/New-York, 199 (1983)

44 K.J Irvine and F.B. Pickering, J. Iron and Steel Inst. Vol 201, 944 (1963)

45 P. Abramowitz and R.A. Moll, Metall. Trans. Vol 1, 1774 (1970)

46 R.R. Preston, "Factors Controlling Yield and Tensile Strengths of Ferrite/Pearlite Steel", Ph.D. Thesis, Univ. Coll. Cardiff, 90 (1984)

47 R.R. Preston, in "Strength of Metals and Alloys", Proc. 5th Int. Conf. (Eds.: P.Haasen et al), Aachen, Vol 2, 1025 (1979)

48 W.B. Morrison and W.C. Leslie, Metall. Trans. Vol 4, 379 (1973)

49 H.M. Howe, in "Metallurgy of Steel" 2nd edn., Scientific Publ., New York/London, 36 (1891)

50 H.I. Aaronson, H.A. Domain and G.M. Pound, Trans. TMS-AIME Vol 236, 768 (1966)

51 K.R. Kinsman and H.I. Aaronson, Metall. Trans. Vol 4, 959 (1973)

52 H.Conrad and S. Frederick, Acta Metall. Vol 10, 1013 (1962)

53 J. Nunes, J. Iron Steel Inst. Vol 204, 371 (1966)

54 E. Anderson and J. Spreadborough, J. Iron Steel Inst. Vol 206, 1223 (1968)

55 R. Sandström and Y. Bergström, Metal Sc. Vol 18, 177 (1984)

56 B. Aaronson and L. Gränäs, Metall. Trans. Vol 2, 1087 (1971)

57 E. Pink and R.J. Arsenault, Prog. Mats. Sc. Vol 24, 1 (1979)

58 H. Conrad, J. of Metals Vol 16, 582 (1964)

59 J. Diehl, M. Schreinder, S. Staiger and S. Zwiesele, Scr. Metall. Vol 10, 949 (1976)

60 J.R. Stephens and W.R. Witzke, J. Less-common Metals, Vol 23, 325 (1971)

61 D. Mills, Scr. Metall. Vol 2, 311 (1968)

62 T. Tanaka and S. Watanabe, Acta Metall. Vol 19, 991 (1971)

63 Y. Nakada and A.S. Keh, Acta Metall. Vol 16, 903 (1968)

64 B.W. Christ, R.P. Gamble and G.V. Smith, Scr. Metall. Vol 3, 521 (1969)

65 W. Frank and B. Šestak, Scr. Metall. Vol 4, 451 (1970)

66 L.M. Brown and R.K. Ham, in "Strengthening Methods in

Crystals" (Eds.: A. Kelly and R.B. Nicholson), Appl. Sc. Publ, London, 9 (1971)

67 S.M. Tuominen and D.A. Koss, Mats. Sc. Engrg. Vol 21, 71 (1975)

68 S. Takeuchi, Scr. Metall. Vol 4, 73 (1970)

69 R.J. Arsenault and J.C.M. Li, Phil. Mag. Vol 16, 1307 (1967)

70 W. Roberts and Y. Bergström, Scand. J. Metall. Vol 1, 265 (1972)

71 W.G. Johnston and J.J. Gilman, J. Appl. Physics Vo 131, 632 (1960)

72 B.W. Christ, Acta Metall. Vol 17, 1317 (1969)

73 J.R. Low and R.W. Guard, Acta Metall. Vol 7, 171 (1959)

74 H. Conrad, J. Iron Steel Inst. Vol 198, 364 (1961)

75 J.R. Stephens, Metall. Trans. Vol 1, 1293 (1970)

76 T. Sakuma and S. Karashima, Trans. Iron Steel Inst. Japan Vol 11, 240 (1971)

77 E. Pink, Phys. Status Solidi (a) Vol 11, 87 (1972)

78 B.C. Allen and R.I. Jaffee, Trans. ASM Vol 56, 387 (1963)

79 W.P. Rees, B.E. Hopkins and H.R. Tipler, J. Iron Steel Inst. Vol 177, 93 (1954)

80 C.A. Edwards, D.L. Phillips and H.N. Jones, J. Iron Steel Inst. Vol 142, 199p (1940)

81 K.V. Ravi and R. Gibala, Scr. Metall. Vol 3, 547 (1969)

82 A.A. Sagues and R. Gibala, Scr. Metall. Vol 5, 689 (1971)

83 C.D. Statham and J.W. Christian, Scr. Metall. Vol 5, 399 (1971)

84 A.A. Sagues and R. Gibala, Acta Metall. Vol 22, 1423 (1975)

85 Z.S. Basinski and J.W. Christian, Aust. J. Physics Vol 13, 299 (1960)

86 R. Burbach, B.L. Mordike and P. Haasen, J. Iron Steel Inst. Vol 204, 390 (1966)

87 D.F. Stein, in "Dislocation Dynamics" (Ed.: A.R. Rosenfield et al), McGraw-Hill, New York, 453 (1968)

88 C.R. Crowe and R.J. Arsenault, Acta Metall. Vol 24, 925 (1976)

89 R.B. Roy, Scr. Metall. Vol 3, 531 (1969)

90 M.G. Ulitchny, A.K. Vasudevan and R. Gibala, in 3rd Int. Conf."Strength of Metals and Alloys", Cambridge Vol 1, 505 (1973)

91 R.J.Arsenault, in "Microplasticity" (Ed.:C. H.J. Mcmahon), Intersc., New York, 91 (1968)

92 C.D. Statham and J.W. Christian, Scr. Metall. Vol 5, 399 (1971)

93 J.R. Stephens and W.R. Witzke, J. Less-common Metals Vol 48, 285 (1976)

94 J. Weertman and J.R. Weertman, "Elementary Dislocation Theory", Macmillan, New York (1964)

95 P. Dubots and G. Cizeron, Acta Metall. Vol 23, 703 (1975)

96 T. Tanaka, Scr. Metall. Vol 7, 97 (1973)

97 W.A. Spitzig and W.C. Leslie, Acta Metall. Vol 19, 1143 (1971)

98 R.J. Arsenault, Acta Metall. Vol 15, 501 (1967)

99 A. Urakami and M. Fine, Scr. Metall. Vol 4, 667 (1970)

100 J.P. Hirth and J. Lothe, "Theory of Dislocations", McGraw Hill (1968)

101 W. Jolley, Trans. AIME Vol 242, 306 (1968)

102 U. Hildebrandt and W. Dickenscheid, Acta Metall. Vol 19, 49 (1971)

103 J.L. Jellison and N.S. Stoloff, Mats. Sc. Engrg. Vol 13 231 (1974)

104 J.T. Michalak, Acta Metall. Vol 13, 213 (1965)

105 J.R. Low and A.M. Turkalo, Acta Metall. Vol 10, 215 (1962)

106 R.E. Reed-Hill, in "Deformation Twinning" (Eds.: R.E. Reed-Hill et al), Gordon and Breach, New York/London, 295 (1963)

107 R. Priestener, ibid, 321 (1963)

108 R.W. Armstrong, ibid, 356 (1963)

109 M.J. Kelley and N.S. Stoloff, Metall. Trans. Vol 7A, 331 (1976)

110 G.E. Lakso and M.J. Marcinkowski, Metall. Trans. Vol 5, 839 (1974)

111 P.J. Worthington and E. Smith, Acta Metall. Vol 14, 35 (1966)

112 F.M. Hamer and D. Hull, Acta Metall. Vol 12, 682 (1964)

113 P.B. Price, Proc. Roy. Soc. Vol A 260, 251 (1961)

114 R.L. Bell and R.W. Cahn, ibid, Vol A 239, 494 (1957)

115 G.T. Horne, R.B. Roy and H.W. Paxton, J. Iron Steel Inst. Vol 201, 161 (1963)

116 A.S. Keh, W.C. Leslie and D.L. Sponseller, in "Precipitation from Iron-base Alloys" (Eds.: G.R.Speich and J.B. Clark), Gordon and Breach, New York/London, 281 (1965)

117 W.A. Spitzig, Metall. Trans. Vol 3, 1183 (1972)

118 W.C. Leslie, R.J. Sober, S.G. Babcock and S.J. Green, Trans. ASM Vol 62, 690 (1969)

119 G.E. Dieter, "Mechanical Metallurgy", McGraw Hill, New York (1961)

120 H.J. Rack, Metall. Trans. Vol 3, 1667 (1972)

121 H.T. Green and R.M. Brick, Trans. AIME Vol 200, 906 (1954)

122 C.R. Austin, Trans. ASM Vol 31, 321 (1943)

123 L. Gränäs and B. Aaronson, Scr. Metall. Vol 2, 541 (1968)

124 C.S. Barrett, G.Ansel and R.F. Mehl, Trans. AMS Vol 25, 702 (1937)

125 W.C. Leslie, Metall. Trans. Vol 3, 5 (1972)

126 N. Zarubova and B.Šestak, Phys. Status Solidi (a) Vol 30, 365 (1975)

127 P.G. Shewmon, "Transformation in Metals", McGraw-Hill, New York/London (1969)

128 E.C. Bain and H.W. Paxton, in "Alloying Elements in Steel", 2nd edt., (ASM) 3rd Rev Printing Ohio (1966)

129 ASTM, "Std. Methods for Estimating Av. Grain Size of Metals", Designation E 112-84

130 M.D. Mohar Ali Bepari, Metall.Trans. Vol 20 A, 13 (1989)

131 J.I. Goldstein and D.B. Williams, in "Quantitative Microanalysis with High Spatial Resolution", Metals Soc, London, 5 (1981)

132 G. McIntosh, "Silicide Precipitation in the Commercial near-alpha Titanium base Alloy, IMI 829", Ph.D. Thesis, University of Strathclyde, 165 (1986)

133 K. Farrell and B.T.M. Lah, J. Iron Steel Inst. Vol 209, 915 (1971)

134 A.J. Lapointe,"Microstructure and Strength of Continuously Cooled Low Alloy Vanadium and Niobium Steels", Ph. D. Thesis, University of Strathclyde, 75 (1975)

135 A.W. Thompson, Metallography Vol 5, 366 (1972)

136 E.E. Underwood, "Quantitative Stereology", Addison-Wesley, London, 80 (1970)

137 Abrams, Halle, Metallography Vol 4, 59 (1971)

138 C. Chatfield, "Statistics for Technology", Chapman and Hall, London, 117 (1975)

139 J.E. Hilliard and J.W. Cahn, Trans. TMS-AIME Vol 221, 344 (1961)

140 F.D. Rosi and C.H. Mathewson, Trans. AIME Vol 188, 1159 (1950)

141 B.E. O'Donnelly, "The Correlation of Microstructure with the Strength and Fracture Toughness of Pearlitic Steels", Ph.D. Thesis, University of Strathclyde (1984)

142 A.W. Agar, British J.Appl. Phys. Vol 11, 185 (1960)

143 R. Phillips, ibid Vol 11, 504 (1960)

144 P.B. Hirsch, A. Howie, R.B. Nicholson, D.W. Pashley and M.J. Whelan, "Electron Microscopy of Thin Crystals",

Butterworths, London (1965)

145 R.H. Alderson and J.S. Halliday, in "Techniques for Electron Microscopy", 2nd edt. (Ed.: D.H. Kay), Blackwell, Oxford, 503 (1965)

146 M.J.C. De Jong, in "Proc. 9th European Congress on Electron Microscopy" Vol 1, Inst Phys., York, 141 (1988)

147 H. Conrad and W. Hayes, Trans. ASM Vol 56, 249 (1963)

148 H.L. Prekel, A. Lawley and H. Conrad, Acta Metall. Vol 16, 337 (1968)

149 Metals and Alloys Data Book, "Selected Powder Diffraction Data", International Centre for Diffraction Data, Cards 6-696 and 9-250 (1978)

150 R.C. Cochrane and W.B. Morrison, in "Phase Transformation" Vol 2, Inst. Metallurgists, York, 77 (1979)

151 G.R. Speich and D.S. Dabkowski, in "Hot Deformation of Austenite" (Ed.: J.B.M. Ballance), AIME, New York, 557 (1977)

152 P.R. Rios, Acta Metall. Vol 35, 2805 (1987)

153 J.W. Cahn, Acta Metall. Vol 4, 449 (1956)

154 R. Phillips and J.A. Chapman, Iron Steel Inst. Spec. Rep. No 81, Iron Steel Inst, London, 60 (1963)

155 R. Millsop, in "Hardenability Concepts with Application to Steel" (Eds.: D.V. Doare and J.S. Kirkaldy), AIME, Chicago, 316 (1977)

156 N.J. Petch, Acta Metall. Vol 35, 2027 (1987)

157 N.S. Stoloff, Fundamental Phenomena Mats. Sc. Vol 4, 197 (1967)

158 B. Mintz, Metal Technol. Vol 11, No 2, 52 (1984)

159 B. Mintz, J. Iron Steel Inst. Vol 211, 433 (1973)

160 D.A. Leak, W.R. Thomas and G.M. Leak, Acta Metall. Vol 3, 501 (1955)

161 R. Rawlings and P.M. Robinson, Acta Metall. Vol 7, 659 (1959)

162 P. Stark, B.L. Averbach and M. Cohen, Acta Metall. Vol 4, 91 (1956)

163 C.A, Wert, J. Met. Vol 188, 1242 (1950)

164 N.S. Corney and E.T. Turkdogan, J. Iron Steel Inst. Vol 180, 344 (1955)

165 E.F. Petrova, M.I. Lapshina and L.A. Shvartsman, Metalloved Edenie I Term Obrabotka, No 4 (English Translation: Henry Butcher), 22 (1960)

166 W.C. Leslie, R.M. Fisher and N. Sen, Acta Metall. Vol 7, 632 (1959)

167 E.D. Harry, J. Iron Steel Inst. Vol 167, 241 (1951)

168 N. Birks, in "Decarburization", Iron Steel Inst. Spec. Rep., No 133, 1 (1969)

169 J.F. Elliott, "Thermochemistry for Steelmaking" Vol 1, Pergamon Press, Sect.3, 143,156 (1960)

170 B. Mintz, Met. Tech. Vol 11, 265 (1984)

171 H.S. Ubhi and T.N. Baker, Mats. Sc. Engrg. Vol A111, 189 (1989)

172 E.Anderson, B.Law, W. King and J.Spreadborough, Trans. AIME Vol 242, 115 (1968)

173 H.J. Goldschmidt, "Interstitial Alloys", Butterworths, London, 249 (1967)

174 H.G. Lapwood and R.R. Preston, Private Communication, (1987)

175 ASTM "Standard Methods of Tension Testing of Metallic Materials" Designation E8-1986

176 B. Mintz, Metal Technol. Vol 1, 226 (1974)

177 B. Mintz and P. Campbell, Mats. Sci. Technol. Vol 5 155 (1989)

178 W. Johnson and P.B. Mellor, "Engineering Plasticity", 2nd edt., Van Nostrand, London, 84 (1975)

179 R.F. Mehl and H.C. Hagel, Prog. Met. Phys. Vol 6, 74 (1956)

180 H. Conrad and G. Schoeck, Acta Metall. Vol 8, 791 (1960)

181 W.A. Spitzig, Mats. Sc. Engrg. Vol 16, 169 (1974)

182 K.V. Ravi and R. Gibala, Acta Metall. Vol 18, 623 (1970)

183 A.S. Keh and S. Weismann, in Conf Proc."Electron Miicroscopy and Strength of Crystals" (Eds.: G. Thomas and J. Washburn), Intersc., New York/London, 231 (1963)

184 W.G. Johnston and J.J. Gilman, J. Appl. Phys. Vol 30, 129 (1959)

185 G.J. Ogilvie, J. Inst. Met. Vol 81, 491 (1953)

186 N.J. Petch, Acta Metall. Vol 12, 59 (1964)

187 N.S. Stoloff, R.G. Davies and K.C. Ku, Trans. TMS-AIME Vol 233, 1500 (1965)

188 P.R. Swann, in Conf. Proc. "Electron Microscopy and Strength of Crystals" (Eds.: G. Thomas and J. Washburn), Intersc. New York/London, 131 (1963)

189 E.C. Ogu, in Conf. Proc. "7th Polish Conf. on Electron Microscopy" (Eds.: S. Gorczyca et al), Krakow-Poland, 301 (1989)

190 R.W. Armstrong, I Codd, R.M. Douthwaite and N.J. Petch, Phil. Mag. Vol 7, 194 (1962)

191 J.D. Campbell and W.G. Ferguson, Phil. Mag. Vol 21, 63 (1970)

192 B. Mintz and P.J. Turner, Metall. Trans. Vol 9A, 1611 (1978)

193 Metal Bulletin, No 7374, 30 (1989)